

GROMACS

分子动力学模拟 —程序拓扑

李继存

北京

2017年8月7日

GROMACS

- 简介 安装 版本异同
- 运行流程
- 辅助工具软件
 - VMD: 构型/轨迹查看
 - GaussView: 分子结构建模
 - PackMol: 复杂结构建模
 - SPDBV: 蛋白处理
 - AmberTool+acpype: 基于amber的建模, 拓扑创建
 - Notepad2: 文本文件编辑查看
 - qtgrace: xvg图形文件查看
 - msys2: windows下的Linux bash模拟环境,
- 文件格式:gro, top, mdp, ndx, xvg
- 简单模拟:He, H₂O, 尿素水溶液,石墨烯,小肽²

GROMACS简介

- 开源,自由免费的MD程序包
- 支持多种力场
- 100多种分析工具
- 主要用于化学生物领域
- C语言,一些汇编
- CPU, GPU
- MPI并行,线程并行
- 集群,多核
- ...

3

安装: Linux

- 管理员权限,个人机器
 - 二进制安装 `sudo apt-get install gromacs`
 - 编译
- 非管理员权限,远程机器
 - 编译: `cmake`, 编译器, `fftw`, `mpi`, `CUDA`

建议安装Intel Parallel Studio:
编译器+mkl(fftw)+impi(MPI)

4

Linux下编译

1. 下载 `wget gromacs-5.1.4.tar.gz`
2. 解压 `tar xvf gromacs-5.1.4.tar.gz`
3. 切换路径 `cd gromacs-5.1.4`
4. 创建目录 `mkdir build`
5. 进入目录 `cd build`
6. 配置 `cmake ..`
`-DCMAKE_INSTALL_PREFIX=/安装/路径/gromacs-5.1.4`
`-DGMX_FFT_LIBRARY=fftw3`
`-DFFTWF_LIBRARY="/opt/fftw-3.3.4/lib/libfftw3f.so"`
`-DFFTWF_INCLUDE_DIR="/opt/fftw-3.3.4/include/"`
`-DCMAKE_C_COMPILER=/opt/gcc-4.8.2/bin/gcc`
`-DCMAKE_CXX_COMPILER=/opt/gcc-4.8.2/bin/g++`
`-DGMX_MPI=on -DGMX_DOUBLE=on -DGMX_GPU=on`
7. 创建安装 `make -j4`
8. 安装 `make install`

5

安装: Windows

- Visual Studio 编译
 - cmake 创建解决方案
 - 直接编译
- CygWin 编译(不建议)

6

新旧版本

- 4.x 多个可执行文件 g_*
- 5.x 单个可执行文件 gmx **推荐**
- 最新 2016 暂不建议

7

运行

- 版本
 - 4.x: g_*
 - 5.x: gmx * 或 gmx_d/gmx_mpi_d *
- 路径
 - 全路径
 - 加入 **path** 环境变量
- 并行 mpirun -np x gmx_mpi mdrun ...
- PBS 参考机器说明

8

运行流程

- 准备输入文件
 - 初始结构 gro, pdb
 - 力场拓扑 top, itp
 - 参数控制 mdp
 - 原子组索引 ndx 可选,更多时候用于分析
- **grompp** 打包整合二进制输入文件 tpr
- **mdrun** 运行
- 分析结果
 - 能量 edr
 - 轨迹 trr(坐标+速度+力), xtc(坐标)

9

Path环境变量

<https://jerkwin.github.io/2016/08/23/Windows>
下的bash环境及path环境变量设置/

- Windows CMD: **echo %path%**
 - 右键我的电脑→属性→高级→环境变量
 - path: 盘符:/添加/路径/;
- Linux bash: **echo \$PATH**
 - /home/用户名/.bashrc
 - export PATH=\$PATH:/添加/路径/

10

运行环境配置: gmx, VMD

- 将gmx5.1.4和VMD1.9.2添加到CMD和msys2的path环境变量，保证在CMD和msys2命令行中都可以使用gmx和VMD
- 将msys2的`\usr\bin`路径添加到CMD的path环境变量，保证在CMD中能调用bash命令

11

配置qtgrace

- 设定xvg文件的打开方式为
qtgrace.bat
- 双击xvg文件， 使用qtgrace打开图形

12

运行环境配置: Notepad2

- 右键管理员权限运行
Notepad2\!设置.bat, 选择3
添加Notepad2到右键菜单
- 保证可以右键打开文件

13

熟悉Notepad2常用功能

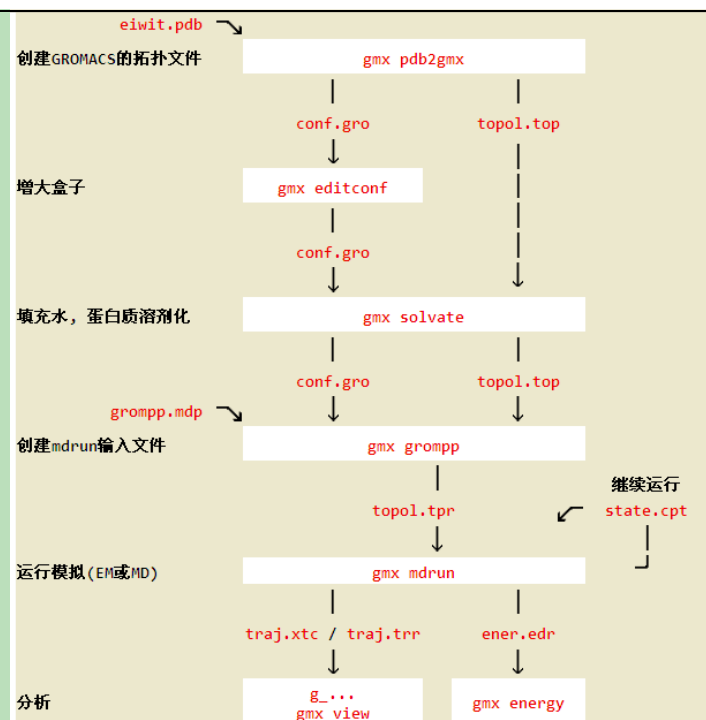
- 文件
 - 启动运行→运行外部命令
 - 编码,换行符
- 编辑
 - 追加复制
 - 文本块: 移除行尾空白符, 合并空行, 移除空行, 修改行, 排序行
 - 查找, 替换
- 查看
 - 代码折叠, 切换折叠
- 列操作: Alt, Shift+Alt

14

运行简单实例

<code>./GMX/_Day1/He216</code>	单原子体系	
<code>Wat216</code>	单分子体系	
<code>UreaWat</code>	尿素水溶液	<code>gmx grompp</code>
<code>MeOH</code>	甲醇盒子	<code>gmx mdrun</code>
<code>MeOHWat</code>	甲醇水两相	
<code>Ice</code>	晶体	
<code>GraWat</code>	周期性分子	
<code>C20C60</code>	碰撞	
<code>NanoCar</code>	好玩	
<code>peptide</code>	小肽	<code>bash _gmxpep.bsh</code>

蛋白模拟基本流程



建模

- 建模工具的使用

- Gauss View

- PackMol

- 在线服务器

- 不同体系的建模

- 有机小分子

- 生物大分子

- 固/晶体

- 复杂体系的构建

- 溶剂盒子

- 多相体系

- 蛋白配体复合物

- 膜蛋白

模拟三部曲

- 前处理

- 建模准备输入文件

- 运行

- 耗时最长,但参与最少

- 后处理

- 分析,处理输出文件

建模工具

- 工具繁多,根据个人喜好,实验室传统,方便程度选择
- 第三方工具
 - ChemOffice, GaussView, Packmol, VMD
 - Material Studio, Discovery Studio, Schrodinger, Chimera
- GMX自带工具
 - editconf genconf
 - solvate insert-molecules
- 自写/网络脚本程序

19

配置GaussView

- 双击运行
`\Gview5_G09view_Win64.reg`
导入设置
- 运行 `\Gview5\gview.exe`

20

GaussView

- 小分子
- 简单生物分子
- 晶体(建议MS)
- 晶面(建议MS)

元素 自定义片段
环状 官能团 生物

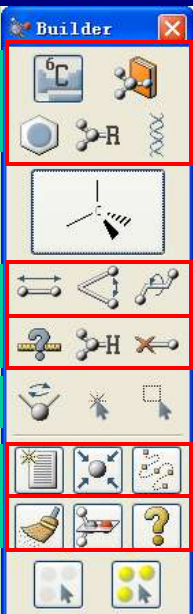
键长 键角 二面角

测量 加氢 删除

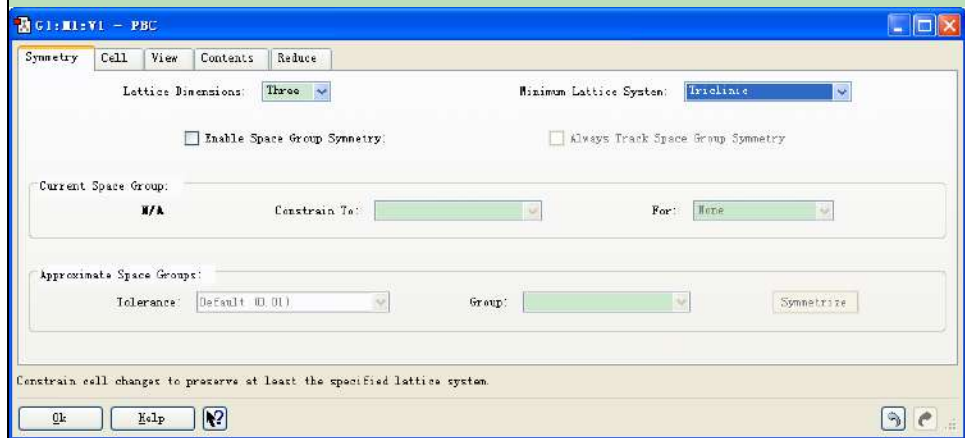
选择

新建 居中 成键

优化 对称性



GaussView: Edit → PBC

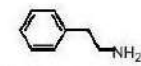


22

爱情化学中的小分子

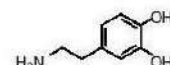
2003年5月，美国著名的科普杂志《发现》月刊发表了一篇关于破解爱情秘密的文章。该文章说，像所有情感一样，爱情也源于大脑，我们之所以能感受到爱的激情，是因为大脑中特定的神经化学体系使然。

爱情化学



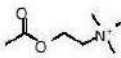
2-phenylethanamine

苯乙胺



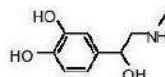
4-(2-aminoethyl)benzene-1,2-diol

多巴胺



2-acetoxy-*N,N,N*-trimethylethanaminium

胆碱



4-(1-hydroxy-2-(methylamino)ethyl)benzene-1,2-diol

肾上腺素

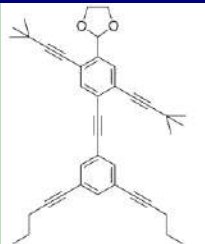


3-(2-aminoethyl)-1*H*-indol-5-ol

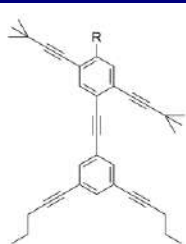
五羟色胺

23

纳米小人Nanoputian



二步
微波炉辐射 1-16 min



R = 纳米小人的缩略名称与符号



纳米运动员
NanoAthlete



纳米朝圣者
NanoPilgrim



纳米绿色贝雷帽
NanoGreenBeret



纳米丑匠
NanoJester



纳米君王
NanoMonarch



纳米德州小人
NanoTexan



纳米学者
NanoScholar



纳米面包师
NanoBaker

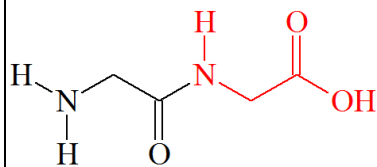


纳米厨师
NanoChef

24

小肽/多肽

Dipeptide

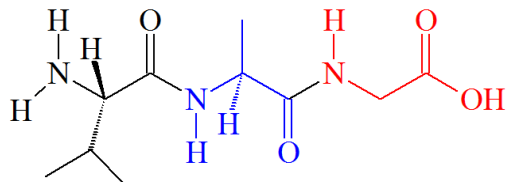


Gly-Gly

GG
 $\text{C}_4\text{H}_8\text{N}_2\text{O}_3$
 132.11
 132.053492

C 36.36% H 6.10% N 21.20% O 36.33%

Tripeptide



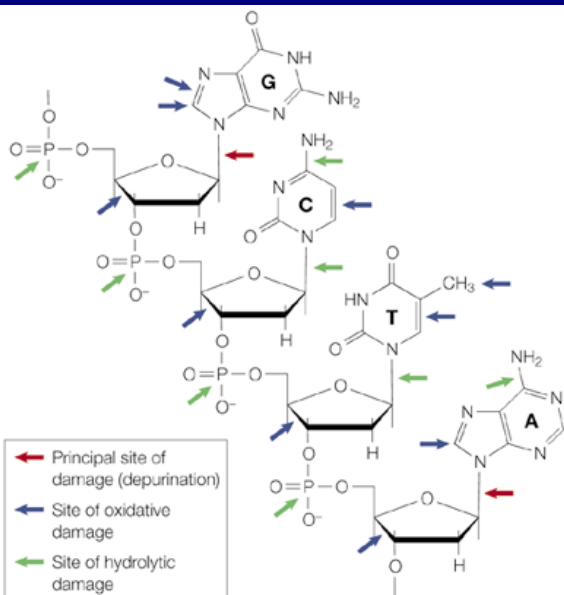
Val-Ala-Gly

VAG
 $\text{C}_{10}\text{H}_{19}\text{N}_3\text{O}_4$
 245.27
 245.137556

C 48.97% H 7.81% N 17.13% O 26.09%

25

DNA短链



26

周期性体系: 石墨烯

将石墨烯分解为含有四个C原子的基本单元在二维平面中排布

以C-C键长 a (1.4 Å)为单位

基本单元的长宽分别为 $\sqrt{3}a, 3a$

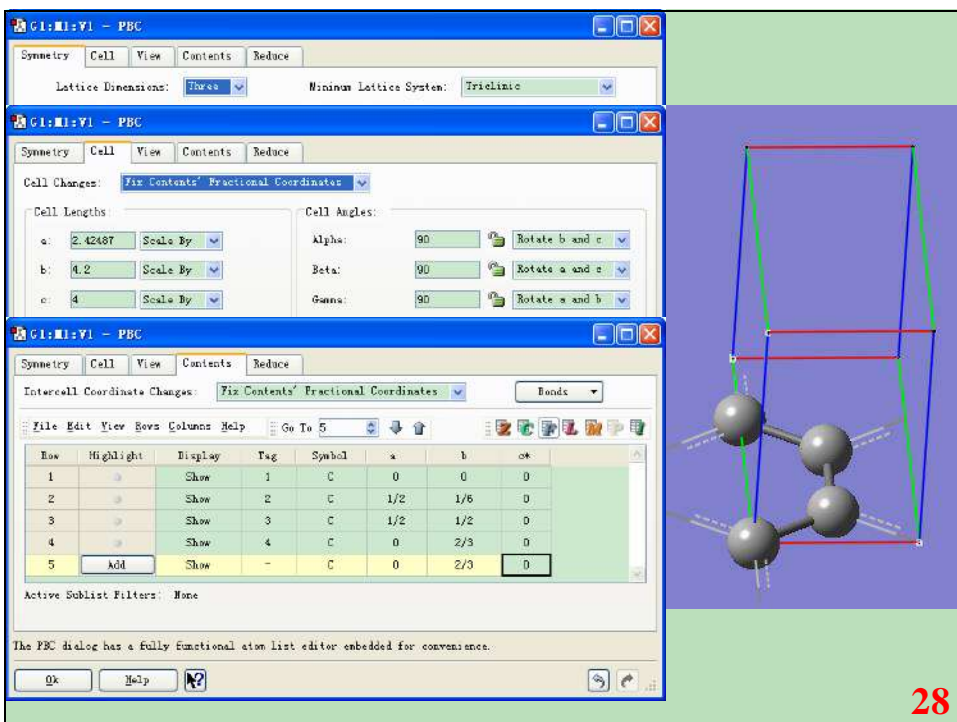
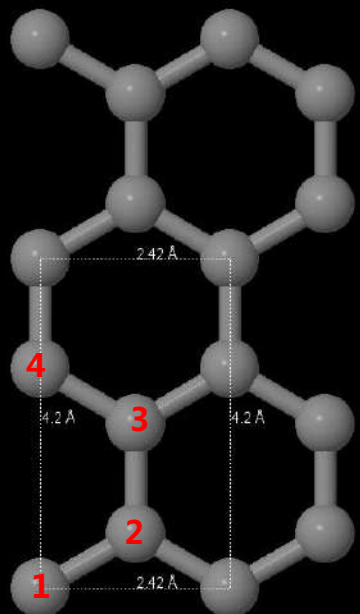
四个碳原子分数坐标分别为:

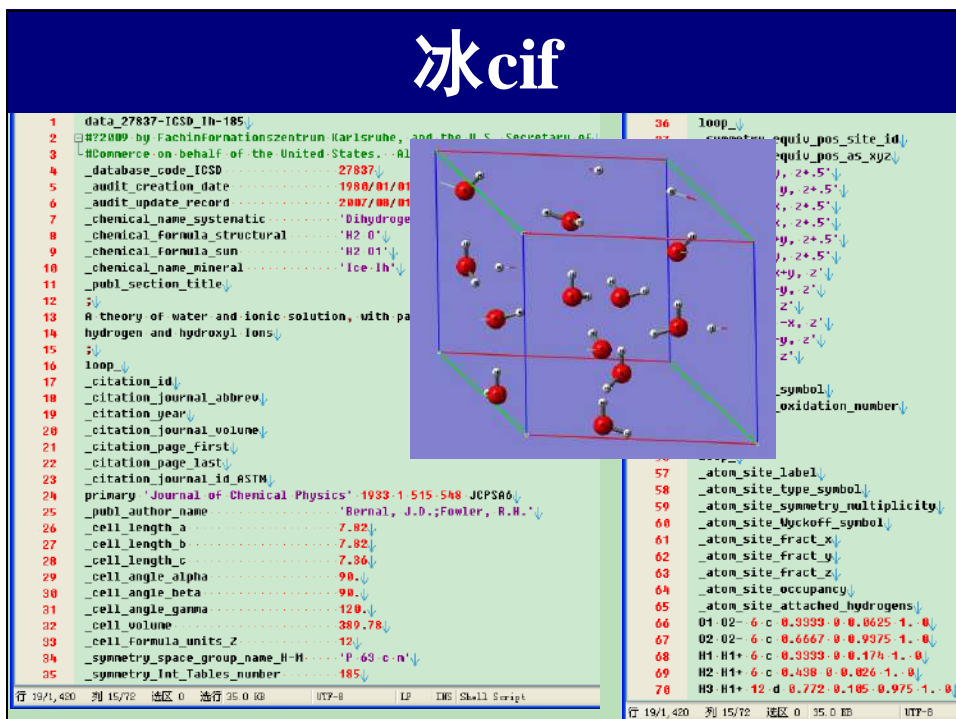
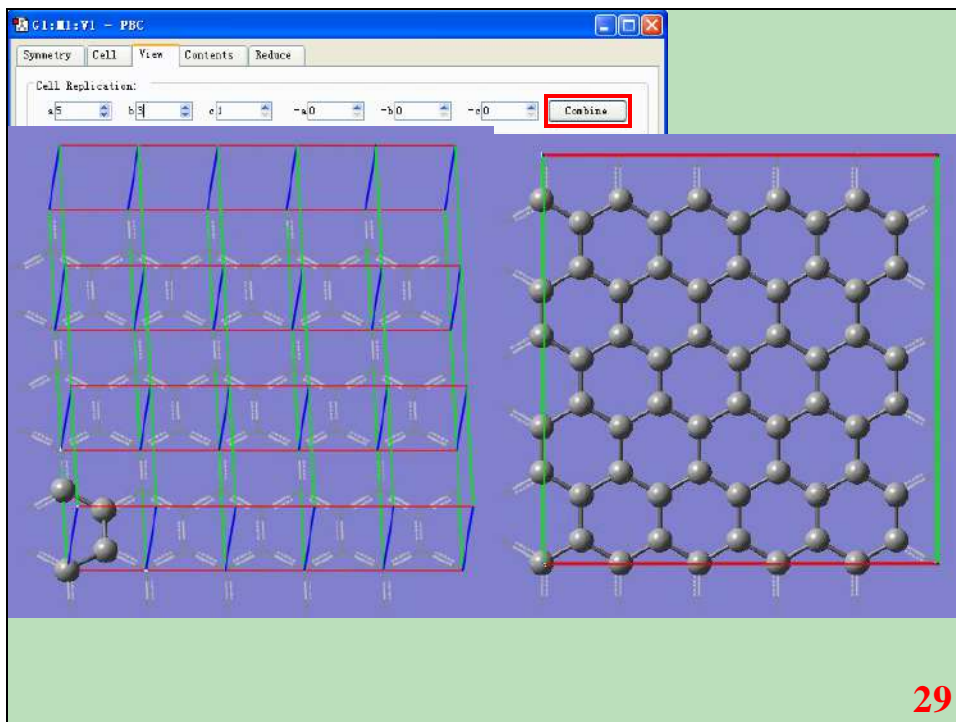
1: (0,0)

2: (1/2, 1/6)

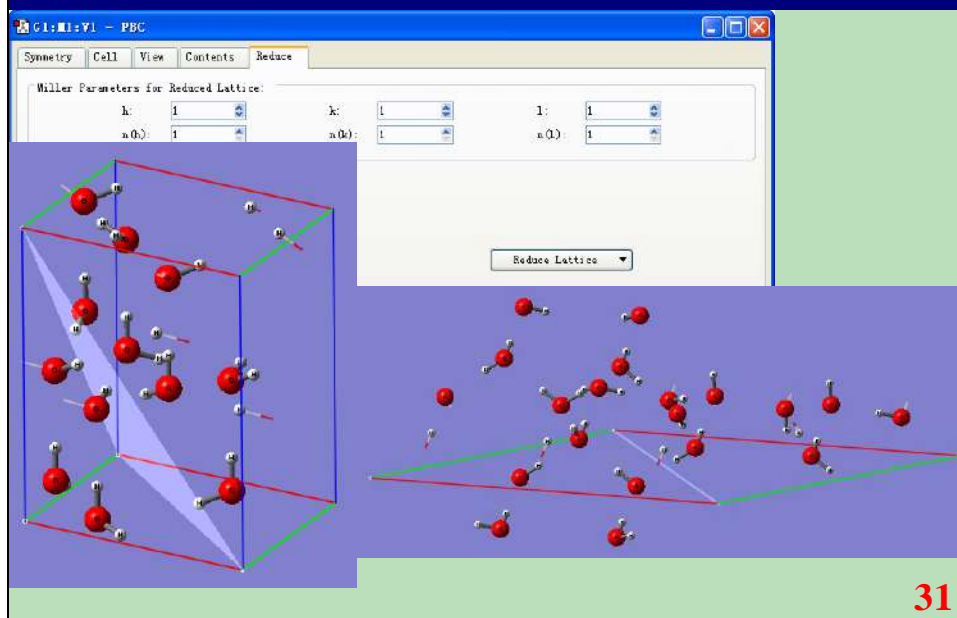
3: (1/2, 1/2)

4: (0, 2/3)





冰 111面



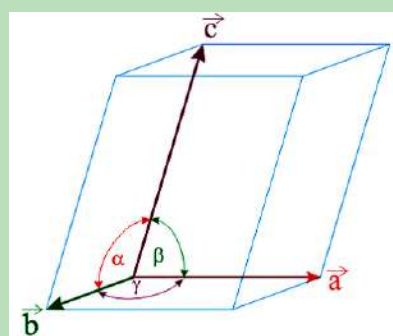
gmx editconf

<code>-bt <enum></code>	<code>triclinic</code>	用于 <code>-box</code> 和 <code>-d</code> 的盒子类型: <code>triclinic</code> , <code>cubic</code> , <code>dodecahedron</code> , <code>octahedron</code>
<code>-box <vector></code>	<code>0 0 0</code>	盒向量长度 (a, b, c). 即自定义的盒子大小
<code>-angles <vector></code>	<code>90 90 90</code>	盒向量之间的角度 ($\text{bc}, \text{ac}, \text{ab}$)
<code>-d <real></code>	<code>0</code>	溶质分子与盒子之间的距离

选项`-angles`只能与选项`-box`和三斜盒子一起使用才有意义, 而且不能和选项`-d`一起使用.

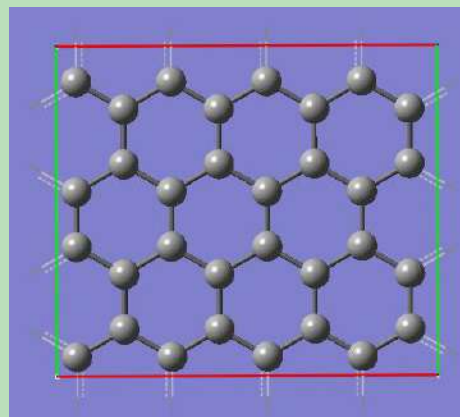
●长方盒子 指定间距 -d

●精确盒子 指定晶格参数 -box a b c -angles α β γ



示例

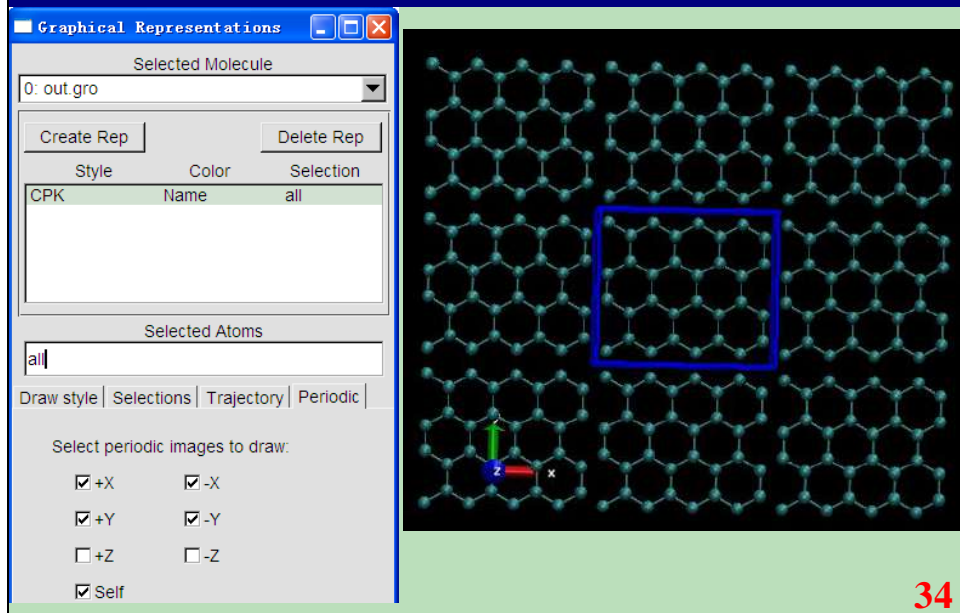
将创建的石墨烯放入准确的盒子，确保周期性正确



```
gmx editconf -f gra.pdb -box .969948 .84 .84
```

33

VMD查看周期性



34

gmx editconf

-[no]c	no	使分子在盒子内居中 (-box 和 -d 选项暗含此选项)
-center <vector>	0 0 0	几何中心的坐标
-aligncenter <vector>	0 0 0	平齐的旋转中心
-align <vector>	0 0 0	与目标向量平齐
-translate <vector>	0 0 0	平移
-rotate <vector>	0 0 0	绕x, y和z轴的旋转角度, 单位为度
-[no]princ	no	使分子取向沿其主轴
-scale <vector>	1 1 1	缩放因子
-density <real>	1000	通过缩放使输出盒子的密度(g/L)为指定值
-[no]pbc	no	移除周期性(使分子保持完整)

-rotate 选项可以对坐标和速度进行旋转. 如 -rotate 0 30 0 表示将体系绕Y轴沿顺时针方向旋转30度.

-princ 选项将体系(或体系某一部分)的主轴与坐标轴平齐, 并且最长的轴沿z轴方向. 这可以减小盒子的体积, 特别当分子为长条形时. 但是注意分子在纳秒的时间尺度内可能发生明显的旋转, 所以使用时要小心.

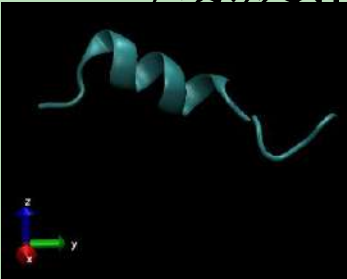
选项-align 可以将特定组的主轴与给定的向量平齐. -aligncenter 选项指定可选的旋转中心.

缩放会在任何其他操作之前进行. 可以对盒子和坐标进行缩放以得到一定的密度(选项-density).

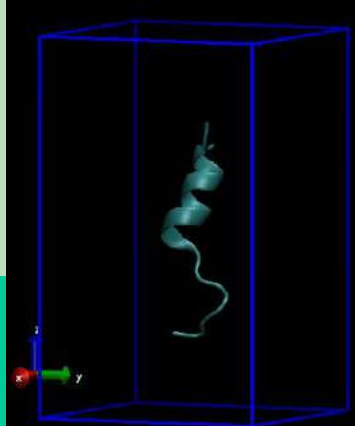
35

示例

- 将小肽放入盒子, 距盒子边缘1 nm, 螺旋沿z轴



```
gmx editconf -f peptide.pdb  
-d 1 -princ -rotate 0 90 0  
-o pep_box.gro
```



gmx genconf

`gmx genconf` 程序对给定的坐标文件进行简单的堆叠, 就像小孩子玩积木一样. 该程序会根据用户定义的比例(`-nbox`)创建一个网格, 格点间的额外空间由`-dist`指定.

指定`-rot`选项时, 程序不会检查格点上分子之间的重叠. 建议输入文件中的盒子边长至少等于原子坐标与范德华半径之和.

<code>-nbox <vector></code>	1 1 1	盒子数目 将分子像堆积木一样堆积起来, 一般按从小到大的顺序定义x y z方向上的分子数, 否则会出现分子间距离较近的情况. 最后分子的个数为 $x*y*z$
<code>-dist <vector></code>	0 0 0	盒子间的距离
<code>-seed <int></code>	0	随机数发生器的种子, 如果为0, 根据当前时间产生.
<code>-[no]rot</code>	no	随机旋转构象
<code>-[no]shuffle</code>	no	随机混洗分子
<code>-[no]sort</code>	no	根据X方向坐标对分子排序
<code>-block <int></code>	1	根据此CPU数将盒子划分为块
<code>-nmolat <int></code>	3	每个分子的原子数, 假定从0开始. 如果设置错误, 体系可能完全不对.
<code>-maxrot <vector></code>	180 180 1 80	最大的随机转动
<code>-[no]renumber</code>	yes	重新编号残基

37

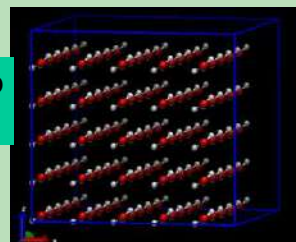
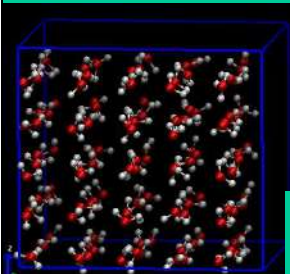
示例

● 创建 $5 \times 5 \times 5$ 的水盒子

- 先获得包含单个分子的最小盒子

```
gmx editconf -f wat.pdb -d 0 -o  
wat.gro
```

```
gmx genconf -f wat.gro -o wat_box.gro  
-nbox 5 5 5 -dist 0.2 0.2 0.2
```



```
gmx genconf -f wat.gro -o wat_box.gro  
-nbox 5 5 5 -dist 0.2 0.2 0.2 -rot
```

gmx solvate

<code>-box <vector></code>	0 0 0	盒子尺寸(单位nm)
<code>-radius <real></code>	0.105	默认的范德华距离
<code>-scale <real></code>	0.57	用于数据文件 <code>share/gromacs/top/vdwradii.dat</code> 中范德华半径的缩放因子。对水中的蛋白质，使用默认值0.57可以得到接近1000 g/l的密度值。
<code>-shell <real></code>	0	溶质周围水层的可选厚度
<code>-maxsol <int></code>	0	加入的最大溶剂分子数。若为零(默认)则忽略此选项。

`gmx solvate`可以为模拟分子添加溶剂环境

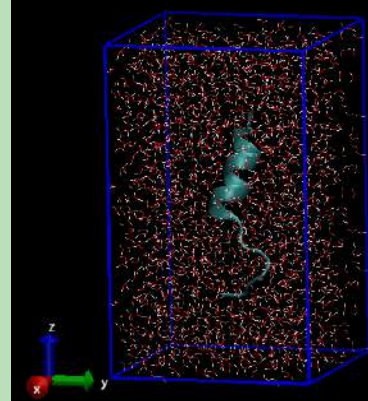
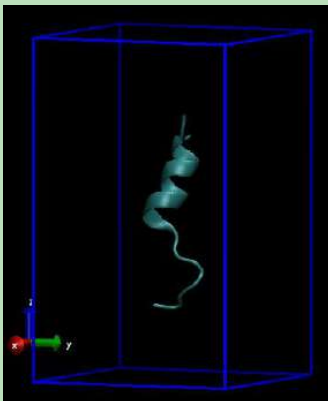
- `-cp`: 带盒子参数的分子坐标文件, 一般是 `editconf` 的输出文件
- `-cs`: 添加的水分子模型, 如 `spc216`, `spce`, `tip3p`, `tip4p` 等
- `-o`: 输出坐标文件, 就是添加水分子之后的分子坐标文件, 默认为 `.gro` 文件, 但也可以为其他格式, 如 `pdb`
- `-p`: 体系拓扑文件, `gmx solvate` 会往里面写入添加水分子的个数。这个不要忘记, 不然在进行下一步计算时, 会出现坐标文件和拓扑文件中原子数不一致的错误

- `-box a b c` 空盒子
- `-cs slv.gro -box a b c` 以slv.gro中分子填充盒子, `-maxsol N`可用
- `-cp slu.gro -box a b c` 指定box, 否则用slu.gro的box
- `-cp slu.gro -cs slv.gro` 以slv填充slu的box
- `-cp slu.gro -cs slv.gro -shell a b` 表面填充
- `-cp slu.gro -cs slv.gro -maxsol N -box a b c`

39

示例

- 向小肽盒子中添加SPC/TIP3P水

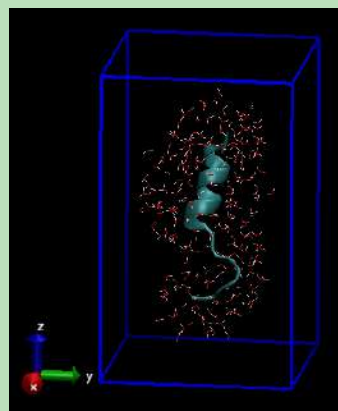
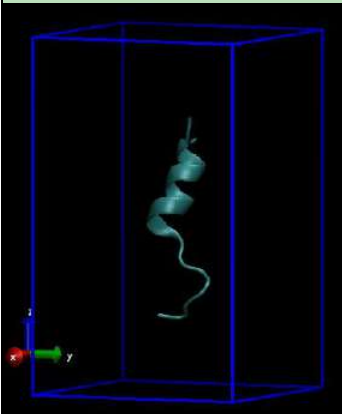


```
gmx solvate -cp pep_box.gro  
-cs spc216.gro -o pep_wat.gro
```

40

示例

- 在小肽表面添加0.5 nm SPC/TIP3P水层



```
gmx solvate -cp pep_box.gro -cs spc216.gro  
-o pep_shell.gro -shell 0.5
```

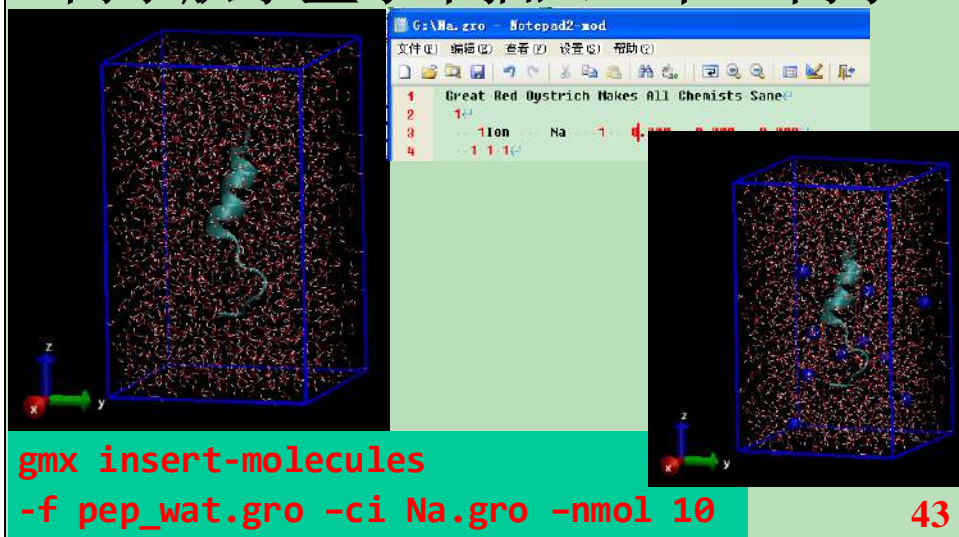
gmx insert-molecules

`gmx insert-molecules`命令可以插入`-nmol`个体系的副本到盒子中，体系由`-ci`输入文件定义。插入的分子可以填充由`-f`指定的溶质分子构型中的空位，或者填充由`-box`指定的空盒子。同时指定`-f`和`-box`选项等同于`-f`，但插入前会在溶质周围放置一个新盒子。该命令运行过程中，坐标文件中的速度不予考虑。

<code>-box <vector></code>	<code>0 0 0</code>	盒子尺寸(nm)
<code>-nmol <int></code>	<code>0</code>	要插入的分子的数目
<code>-try <int></code>	<code>10</code>	尝试插入 <code>-nmol</code> 乘以 <code>-try</code> 次
<code>-seed <int></code>	<code>1997</code>	随机数发生器的种子
<code>-radius <real></code>	<code>0.105</code>	默认的范德华距离
<code>-scale <real></code>	<code>0.57</code>	用于数据文件 <code>share/gromacs/top/vdwradii.dat</code> 中范德华半径的缩放因子。对水中的蛋白质，使用默认值 <code>0.57</code> 可以得到接近 <code>1000 g/1</code> 的密度值。
<code>-dr <vector></code>	<code>0 0 0</code>	相对 <code>-ip</code> 文件中的位置，在x/y/z方向允许的最大偏移位移
<code>-rot <enum></code>	<code>xyz</code>	随机旋转插入分子，可用选项： <code>xyz</code> , <code>z</code> 或 <code>none</code>
<code>-[no]allpair</code>	<code>no</code>	与 <code>-ci</code> 选项同用时避免近邻搜索过程中的内存泄露。对大的体系可能会比较慢。

示例

- 向小肽水盒子中插入10个Na离子



43

PackMol

- 利用堆积优化方法创建分子动力学模拟所需的初始构型

<http://jerkwin.github.io/2016/08/05/Packmol程序资料整理/>

44

配置packmol

- 将**packmol.exe**所在路径添加到CMD的**path**环境变量, 保证可以在CMD中调用**packmol.exe**

45

复杂体系建模: 溶剂盒子

- **gmx**
editconf
solvate
insert-molecules

- **Packmol**
尿素水溶液

mixture.inp

```
1 # 可以使用注释  
2 # 尿素-水混合溶液  
3  
4 # 距离容差, 不同分子中原子间的最小距离2A  
5 tolerance 2.0  
6  
7 # 输入输出文件的格式  
8 filetype pdb  
9  
10 # 输出文件的名字  
11 output mixture.pdb  
12  
13 # 1000个水分子, 400个尿素分子  
14 # 盒子顶点坐标(x,y,z) 最小(0, 0, 0) 最大(40, 40, 40)  
15 # 也即边长为40Å的正方盒子  
16 # 也可使用简单写法 inside cube 0. 0. 0. 40  
17 structure water.pdb  
18   number 1000  
19   inside box 0. 0. 0. 40. 40. 40.  
20 end structure  
21  
22 structure urea.pdb  
23   number 400  
24   inside box 0. 0. 0. 40. 40. 40.  
25 end structure
```

复杂体系建模: 多相体系

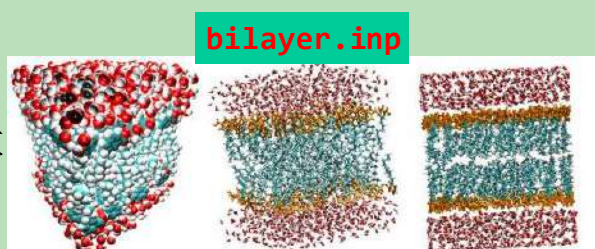
- gmx

- editconf
- solvate
- editconf



- packmol

- 水-四氯化碳界面上的甲状腺激素分子
- 上下有水的双脂层



47

复杂体系建模: 蛋白配体复合物

- PDB中位置

- GaussView

- 手动移动配体
- Shift Alt 中键

- VMD

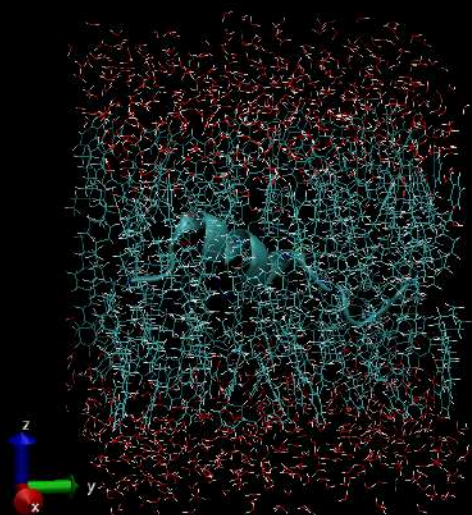
- move

48

复杂体系建模: 膜蛋白

- VMD建膜:
extension → Modeling
- Packmol: 混合膜, 蛋白
- 自编脚本

membrane.inp



Packmol的几点估算

- 蛋白/脂分子自身大小
`gmx editconf -c -d 0.2`
- 盒子大小
- 水分子个数

在线服务器

- CHARMM-GUI

- <http://www.charmm-gui.org/>

- DNA/RNA

- <http://structure.usc.edu/makena/server.html>

- Automated Topology Builder (ATB) and Repository

- <http://atb.uq.edu.au/index.py>

51

大纲

- 力场分类
- GROMACS自带力场
 - AMBER, CHARMM, OPLS-AA
 - GROMOS, Martini
- GROMACS拓扑文件
 - itp, top的结构以及参数说明
- GROMACS拓扑文件的创建
 - pdb2gmx
 - AmberTool+acpype
 - tppmktop
 - x2top
 - ATB/PRODRG
 - Martini

52

力场分类

- 名称
 - AMBER CHARMM
 - GROMOS OPLS
 - CVFF UFF MM3
- 一个原子类型是否包含多个原子
 - 全原子AA
 - 联合原子UA
- 电荷可变与否
 - 极化
 - 非极化
- 适用范围
 - 生物分子:蛋白质, DNA, RNA
 - 有机分子
 - 无机物质

53

力场=原子类型 +势能函数+参数

- 原子类型: 粒子种类
 - 全原子AA, 联合原子UA
 - 质量, 电荷, VDW参数
- 势能函数: 相互作用
 - 成键: 键长, 键角, 二面角
 - 非键: 库伦(静电/长程), 范德华(短程)

54

GMX自带的力场

- AMBER
- CHARMM
- GROMOS
- OPLS-AA

其他力场导入相应的力场文件即可

55

初步认识 力场结构

名称	大小	类型	修改日期	创建日期
amber03.ff		<文件夹>	2015/12/1 22:00:12	2015/12/1 22:00:12
amber94.ff		<文件夹>	2015/12/1 22:00:12	2015/12/1 22:00:12
amber96.ff		<文件夹>	2015/12/1 22:00:14	2015/12/1 22:00:14
amber99.ff		<文件夹>	2015/12/1 22:00:12	2015/12/1 22:00:12
amber99sb.ff		<文件夹>	2015/12/1 22:00:14	2015/12/1 22:00:14
amber99sb-ildn.ff		<文件夹>	2015/12/1 22:00:12	2015/12/1 22:00:12
amberGS.ff		<文件夹>	2015/12/1 22:00:14	2015/12/1 22:00:14
charmm27.ff		<文件夹>	2015/12/1 22:00:12	2015/12/1 22:00:12
gromos43a1.ff		<文件夹>	2015/12/1 22:00:12	2015/12/1 22:00:12
gromos43a2.ff		<文件夹>	2015/12/1 22:00:14	2015/12/1 22:00:14
gromos45a3.ff		<文件夹>	2015/12/1 22:00:14	2015/12/1 22:00:14
gromos53a5.ff		<文件夹>	2015/12/1 22:00:14	2015/12/1 22:00:12
gromos56a6.ff		<文件夹>	2015/12/1 22:00:12	2015/12/1 22:00:12
gromos54a7.ff		<文件夹>	2015/12/1 22:00:14	2015/12/1 22:00:14
oplsaa.ff		<文件夹>	2015/12/1 22:00:12	2015/12/1 22:00:12
atom_nom.tbl	7.8 kB	TBL File	2015/6/22 7:17:54	2015/12/1 22:00:14
atommass.dat	3.6 kB	DAT File	2015/6/22 7:17:54	2015/12/1 22:00:12
bonds.dlg	733 B	DLG File	2015/6/22 7:17:54	2015/12/1 22:00:12
bromacs.dat	1.1 kB	DAT File	2015/6/22 7:17:54	2015/12/1 22:00:14
ca-shift.dat	1.9 kB	DAT File	2015/6/22 7:17:54	2015/12/1 22:00:12
cb-shift.dat	1.9 kB	DAT File	2015/6/22 7:17:54	2015/12/1 22:00:12
co-shift.dat	1.9 kB	DAT File	2015/6/22 7:17:54	2015/12/1 22:00:12
defselection.dat	1003 B	DAT File	2015/6/22 7:17:54	2015/12/1 22:00:12
dgsolv.dat	2.0 kB	DAT File	2015/6/22 7:17:54	2015/12/1 22:00:12
edissoc.dat	138 B	DAT File	2015/6/22 7:17:54	2015/12/1 22:00:12
electroneg.dat	837 B	DAT File	2015/6/22 7:17:54	2015/12/1 22:00:12
elements.dat	3.8 kB	DAT File	2015/6/22 7:17:54	2015/12/1 22:00:12
export.dlg	345 B	DLG File	2015/6/22 7:17:54	2015/12/1 22:00:14
ffG43a1.itp	162 B	ITP File	2015/6/22 7:17:54	2015/12/1 22:00:12
ffG43a2.itp	167 B	ITP File	2015/6/22 7:17:54	2015/12/1 22:00:14
ffG45a3.itp	162 B	ITP File	2015/6/22 7:17:54	2015/12/1 22:00:12
ffG53a5.itp	167 B	ITP File	2015/6/22 7:17:54	2015/12/1 22:00:12
ffG53a6.itp	163 B	ITP File	2015/6/22 7:17:54	2015/12/1 22:00:12

C:\Users\Jicun\Downloads\gromacs-5.1.1\share\top\amber99sb-ilidn.ff					
名称	大小	类型	修改日期	创建日期	注释
aminoacids.amr	2.5 kB	Autoruns Log File	2015/12/2 9:32:32	2015/12/1 22:00:12	氨基酸残基参数文件, 用于构建蛋白质的拓扑
aminoacids.c.tdb	10 B	TDB File	2015/12/2 9:32:32	2015/12/1 22:00:12	氨基酸残基参数文件, 用于构建蛋白质的拓扑
aminoacids.hdb	8.6 kB	HDB File	2015/12/2 9:32:32	2015/12/1 22:00:12	氨基酸残基参数文件, 用于构建蛋白质的拓扑
aminoacids.n.tdb	10 B	TDB File	2015/12/2 9:32:32	2015/12/1 22:00:12	氨基酸残基参数文件, 用于构建蛋白质的拓扑
aminoacids.r2b	849 B	R2B File	2015/12/2 9:32:32	2015/12/1 22:00:12	氨基酸残基参数文件, 用于构建蛋白质的拓扑
aminoacids.rtp	85.5 kB	RTF File	2015/12/2 9:32:32	2015/12/1 22:00:12	氨基酸残基参数文件, 用于构建蛋白质的拓扑
aminoacids.vsd	5.0 kB	Microsoft Visio 绘图	2015/12/2 9:32:32	2015/12/1 22:00:12	氨基酸残基参数文件, 用于构建蛋白质的拓扑
atomtypes.atp	3.6 kB	ATP File	2015/12/2 9:33:48	2015/12/1 22:00:12	原子类型文件, 列出所有用的所有原子类型
dna.amr	116 B	Autoruns Log File	2015/12/2 9:34:14	2015/12/1 22:00:12	DNA参数文件, 用于构建DNA的拓扑
dna.hdb	3.0 kB	HDB File	2015/12/2 9:34:14	2015/12/1 22:00:12	DNA参数文件, 用于构建DNA的拓扑
dna.r2b	145 B	R2B File	2015/12/2 9:34:14	2015/12/1 22:00:12	DNA参数文件, 用于构建DNA的拓扑
dna.rtp	20.9 kB	RTF File	2015/12/2 9:34:14	2015/12/1 22:00:12	DNA参数文件, 用于构建DNA的拓扑
fbonded.itp	35.1 kB	ITP File	2015/12/2 9:38:40	2015/12/1 22:00:12	键合参数文件, 列出与键子类型对应的键、键角、二面角参数以及的伸展信息
ffnonbonded.itp	4.5 kB	ITP File	2015/12/2 9:40:36	2015/12/1 22:00:12	非键合参数文件, 列出每种原子类型的电荷, VDW参数
forcefield.doc	718 B	DOC File	2015/12/2 9:44:16	2015/12/1 22:00:12	该力场的说明
forcefield.itp	951 B	ITP File	2015/12/2 9:43:40	2015/12/1 22:00:12	力场的 default (设置, #include设置
gbsa.itp	1.8 kB	ITP File	2015/12/2 9:44:46	2015/12/1 22:00:12	用于计算GBSA的参数文件
ions.itp	2.1 kB	ITP File	2015/12/2 9:45:14	2015/12/1 22:00:12	带电离子的拓扑文件
ma.amr	116 B	Autoruns Log File	2015/12/2 9:45:50	2015/12/1 22:00:12	RNA参数文件, 用于构建RNA的拓扑
ma.hdb	4.0 kB	HDB File	2015/12/2 9:45:50	2015/12/1 22:00:12	RNA参数文件, 用于构建RNA的拓扑
ma.r2b	145 B	R2B File	2015/12/2 9:45:50	2015/12/1 22:00:12	RNA参数文件, 用于构建RNA的拓扑
ma.rtp	30.3 kB	RTF File	2015/12/2 9:45:50	2015/12/1 22:00:12	RNA参数文件, 用于构建RNA的拓扑
spc.itp	746 B	ITP File	2015/12/2 9:47:00	2015/12/1 22:00:12	各种水模型的拓扑文件
spce.itp	746 B	ITP File	2015/12/2 9:47:00	2015/12/1 22:00:12	各种水模型的拓扑文件
tip3p.itp	802 B	ITP File	2015/12/2 9:47:00	2015/12/1 22:00:12	各种水模型的拓扑文件
tip4p.itp	1.2 kB	ITP File	2015/12/2 9:47:00	2015/12/1 22:00:12	各种水模型的拓扑文件
tip4pew.itp	1.2 kB	ITP File	2015/12/2 9:47:00	2015/12/1 22:00:12	各种水模型的拓扑文件
tip5p.itp	2.0 kB	ITP File	2015/12/2 9:47:00	2015/12/1 22:00:12	各种水模型的拓扑文件
urea.itp	1.2 kB	ITP File	2015/12/2 9:47:20	2015/12/1 22:00:12	尿素分子的拓扑文件
watermodels.dat	301 B	DAT File	2015/12/2 9:47:44	2015/12/1 22:00:12	水模型的说明文件

57

C:\Users\Jicun\Downloads\gromacs-5.1.1\share\top\gromos54a7.ff				
名称	大小	类型	修改日期	创建日期
aminoacids.c.tdb	665 B	TDB File	2015/6/22 7:17:54	2015/12/1 22:00:14
aminoacids.hdb	3.0 kB	HDB File	2015/6/22 7:17:54	2015/12/1 22:00:14
aminoacids.n.tdb	1.2 kB	TDB File	2015/6/22 7:17:54	2015/12/1 22:00:14
aminoacids.r2b	132 B	R2B File	2015/6/22 7:17:54	2015/12/1 22:00:14
aminoacids.rtp	301.9 kB	RTF File	2015/6/22 7:17:54	2015/12/1 22:00:14
aminoacids.vsd	3.5 kB	Microsoft Visio 绘图	2015/6/22 7:17:54	2015/12/1 22:00:14
atomtypes.atp	2.5 kB	ATP File	2015/6/22 7:17:54	2015/12/1 22:00:14
dppc.itp	9.3 kB	ITP File	2015/6/22 7:17:54	2015/12/1 22:00:14
ff_dum.itp	1.1 kB	ITP File	2015/6/22 7:17:54	2015/12/1 22:00:14
ffbonded.itp	13.1 kB	ITP File	2015/6/22 7:17:54	2015/12/1 22:00:14
ffnonbonded.itp	113.5 kB	ITP File	2015/6/22 7:17:54	2015/12/1 22:00:14
forcefield.doc	98 B	DOC File	2015/6/22 7:17:54	2015/12/1 22:00:14
forcefield.itp	176 B	ITP File	2015/6/22 7:17:54	2015/12/1 22:00:14
ions.itp	1014 B	ITP File	2015/6/22 7:17:54	2015/12/1 22:00:14
popc.itp	9.8 kB	ITP File	2015/6/22 7:17:54	2015/12/1 22:00:14
spc.itp	815 B	ITP File	2015/6/22 7:17:54	2015/12/1 22:00:14
spce.itp	815 B	ITP File	2015/6/22 7:17:54	2015/12/1 22:00:14
tip3p.itp	636 B	ITP File	2015/6/22 7:17:54	2015/12/1 22:00:14
tip4p.itp	1.1 kB	ITP File	2015/6/22 7:17:54	2015/12/1 22:00:14
tmcl.itp	21.2 kB	ITP File	2015/6/22 7:17:54	2015/12/1 22:00:14
watermodels.dat	90 B	DAT File	2015/6/22 7:17:54	2015/12/1 22:00:14

58

C:\Users\Jicun\Downloads\gromacs-5.1.1\share\top\oplsaa.ff				
名称	大小	类型	修改日期	创建日期
1propanol.itp	1.9 kB	ITP File	2015/6/22 7:17:54	2015/12/1 22:00:12
aminoacids.c.tdb	1.7 kB	TDB File	2015/6/22 7:17:54	2015/12/1 22:00:12
aminoacids.hdb	3.4 kB	HDB File	2015/6/22 7:17:54	2015/12/1 22:00:12
aminoacids.n.tdb	1.2 kB	TDB File	2015/6/22 7:17:54	2015/12/1 22:00:12
aminoacids.r2b	96 B	R2B File	2015/6/22 7:17:54	2015/12/1 22:00:12
aminoacids.rtp	40.6 kB	RTP File	2015/6/22 7:17:54	2015/12/1 22:00:12
aminoacids.vsd	5.3 kB	Microsoft Visio 绘图	2015/6/22 7:17:54	2015/12/1 22:00:12
atomname2type.n2t	1.4 kB	N2T File	2015/6/22 7:17:54	2015/12/1 22:00:12
atomtypes.atp	36.9 kB	ATP File	2015/6/22 7:17:54	2015/12/1 22:00:12
ethanol.itp	1.4 kB	ITP File	2015/6/22 7:17:54	2015/12/1 22:00:12
ffbonded.itp	214.7 kB	ITP File	2015/6/22 7:17:54	2015/12/1 22:00:12
ffnonbonded.itp	61.4 kB	ITP File	2015/6/22 7:17:54	2015/12/1 22:00:12
forcefield.doc	58 B	DOC File	2015/6/22 7:17:54	2015/12/1 22:00:12
forcefield.itp	882 B	ITP File	2015/6/22 7:17:54	2015/12/1 22:00:12
gbsa.itp	4.3 kB	ITP File	2015/6/22 7:17:54	2015/12/1 22:00:12
ions.itp	2.2 kB	ITP File	2015/6/22 7:17:54	2015/12/1 22:00:12
methanol.itp	868 B	ITP File	2015/6/22 7:17:54	2015/12/1 22:00:12
spc.itp	561 B	ITP File	2015/6/22 7:17:54	2015/12/1 22:00:12
spce.itp	567 B	ITP File	2015/6/22 7:17:54	2015/12/1 22:00:12
tip3p.itp	636 B	ITP File	2015/6/22 7:17:54	2015/12/1 22:00:12
tip4p.itp	1.0 kB	ITP File	2015/6/22 7:17:54	2015/12/1 22:00:12
tip4pew.itp	1.3 kB	ITP File	2015/6/22 7:17:54	2015/12/1 22:00:12
tip5p.itp	1.9 kB	ITP File	2015/6/22 7:17:54	2015/12/1 22:00:12
tip5pe.itp	1.4 kB	ITP File	2015/6/22 7:17:54	2015/12/1 22:00:12
watermodels.dat	319 B	DAT File	2015/6/22 7:17:54	2015/12/1 22:00:12

59

力场拓扑文件

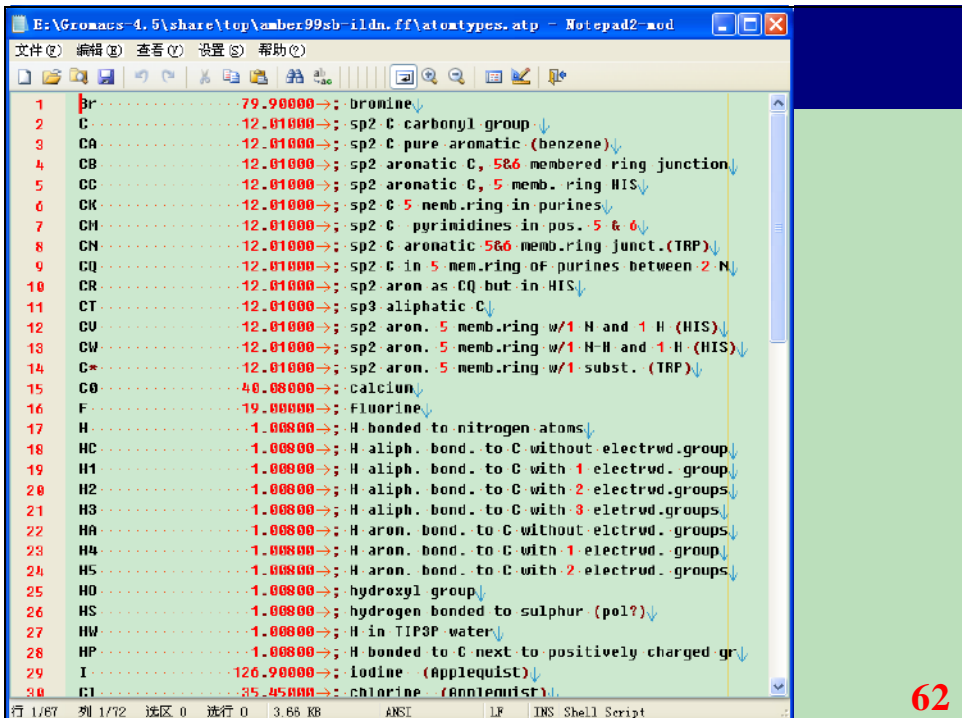
- 总拓扑文件 top
- 可包含拓扑文件 itp, 提高重用性

60

原子类型

- 每个力场都定义了一组原子类型，它们具有特征名称或编号，质量(以a.m.u为单位)
- 这些原子类型的列表可以在 atomtypes.atp (.atp = atom type parameter, 原子类型参数) 文件中找到
- 你可以从这个文件开始修改和/或增加原子类型

61



The screenshot shows a Windows Notepad window titled "E:\Gromacs-4.5\share\top\amber99sb-ildn.ff\atomtypes.atp - Notepad2-mod". The file contains a list of atomic types, each defined by a name and its properties. The properties include a numerical value followed by a colon and a descriptive string. Some entries also have arrows pointing to specific parts of the string. The list includes elements like Br, C, CA, CB, CC, CK, CM, CN, CQ, CR, CT, CU, CW, C*, C0, F, H, HC, H1, H2, H3, HA, H4, H5, HO, HS, HW, HP, I, and Cl.

原子类型	属性
Br	79.90000 : Bromine
C	12.01000 : sp2 C carbonyl group
CA	12.01000 : sp2 C pure aromatic (benzene)
CB	12.01000 : sp2 aromatic C, 5&6 membered ring junction
CC	12.01000 : sp2 aromatic C, 5 memb. ring HIS
CK	12.01000 : sp2 C 5 memb.ring in purines
CM	12.01000 : sp2 C pyrimidines in pos. 5 & 6
CN	12.01000 : sp2 C aromatic 5&6 memb.ring junct.(TRP)
CQ	12.01000 : sp2 C in 5 mem.ring of purines between 2 N
CR	12.01000 : sp2 aron as CQ but in HIS
CT	12.01000 : sp3 aliphatic C
CU	12.01000 : sp2 aron. 5 memb.ring w/1 H and 1 H (HIS)
CW	12.01000 : sp2 aron. 5 memb.ring w/1-H and 1-H (HIS)
C*	12.01000 : sp2 aron. 5 memb.ring w/1-subst. (TRP)
C0	40.08000 : calcium
F	19.06000 : Fluorine
H	1.00800 : H bonded to nitrogen atoms
HC	1.00800 : H aliph. bond. to C without electrwd.group
H1	1.00800 : H aliph. bond. to C with 1 electrwd. group
H2	1.00800 : H aliph. bond. to C with 2 electrwd. groups
H3	1.00800 : H aliph. bond. to C with 3 electrwd. groups
HA	1.00800 : H aron. bond. to C without electrwd. groups
H4	1.00800 : H aron. bond. to C with 1 electrwd. group
H5	1.00800 : H aron. bond. to C with 2 electrwd. groups
HO	1.00800 : hydroxyl group
HS	1.00800 : hydrogen bonded to sulphur (pol?)
HW	1.00800 : H in TIP3P water
HP	1.00800 : H bonded to C next to positively charged gr
I	126.90000 : iodine (Applequist)
Cl	35.45000 : chlorine (Bonnefist)

62

63

```

E:\Gromacs-4.5\share\top\oplsaa.ff\atomtypes.atp -- Notepad2-mod
文件(F) 编辑(E) 查看(V) 设置(S) 帮助(H)
1 ; OPLS atom types and masses.↓
2 ; Atom types are named opls_X, where X is the OPLS number.↓
3 ; The opls_ prefix is to avoid users confusing atom types.↓
4 ; (always prefixed) with atom numbers in molecules (never prefixed).↓
5 ;↓
6 ; Types 1-134 are from the united-atom OPLS, which can be↓
7 ; useful for solvents and/or CH2 optimizations (e.g. in lipids).↓
8 ; Explicit all-atom parameters start with opls_135.↓
9 ; Note: For UNI amide parameters ↓
10 ; NHM - types 1,2,3,4,7,8↓
11 ; Formamide 131,2,12,13↓
12 ; DHF ..... 131,2,3,132↓
13 ; Acetamide 1,2,7,12,13↓
14 ;↓
15 ; Types 1-65 are united-atom parameters for proteins, ↓
16 ; see JACS 110, 1657 (1988).↓
17 ;↓
18 ; opls_001 : 12.01100 ;↓
19 ; opls_002 : 15.99948 ;↓
20 ; opls_003 : 14.00670 ;↓
21 ; opls_004 : 1.00800 ;↓
22 ; opls_005 : 14.02700 ;↓
23 ; opls_006 : 13.01900 ;↓
24 ; opls_007 : 15.00500 ;↓
25 ; opls_008 : 13.01900 ;↓
26 ; opls_009 : 14.02700 ;↓
27 ; opls_010 : 15.00500 ;↓
28 ; opls_011 : 12.01100 ;↓
29 ; opls_012 : 14.00670 ;↓
30 ; opls_013 : 1.00800 ;↓
31 ; opls_014 : 13.01900 ;↓
32 ; opls_015 : 14.02700 ;↓
33 ; opls_016 : 14.02700 ;↓
34 ; opls_017 : 12.01100 ;↓

```

原子参数

原子类型 静态性质(参见表 5.2)的指定基于几个地方的数据. 质量来源于 [atomtypes.atp](#) 文件(参见5.2.1节). 电荷来源于 [*.rtp](#) (*rtp = residue topology parameter, 残基拓扑参数, 参见5.6.1节*)文件. 这就意味着只对构建氨基酸, 核酸的基本单元定义了电荷. 对其他的分子, 用户需要自己定义电荷. 当使用 [pdb2gmx](#) 程序生成一个拓扑文件 ([*.top](#))时, 来自这些文件的信息将被整合在一起.

表 5.2: GROMACS中的静态原子类型性质

性质	符号	单位
类型	-	-
质量	m	a.m.u
电荷	q	e
epsilon	ε	kJ/mol
sigma	σ	nm

64

非键参数

非键参数包括van der Waals参数V(c_6 或 σ ,由组合规则决定)和W(c_{12} 或 ϵ),它们列在ffnonbonded.itp文件中,其中的ptype是粒子类型(参见表5.1).[*type]指令中的条目和键合参数会被应用它们在拓扑文件中的相应部分.除了将在5.3.4节中提到的那些,缺少参数将导致警告.

```
[ atomtypes ]
;name      at.num      mass      charge      ptype      V(c6)      W(c12)
O          8       15.99940    0.000        A     0.22617E-02   0.74158E-06
OM         8       15.99940    0.000        A     0.22617E-02   0.74158E-06
.....
[ nonbond_params ]
; i      j      func      V(c6)      W(c12)
O      O      1     0.22617E-02   0.74158E-06
O      OA     1     0.22617E-02   0.13807E-05
.....
```

65

键参数

键参数(如原子类型,键参数都用到相同的键参数)

```
[ bondtypes ]
; i      j      func      b0      kb
C      O      1     0.12300    502080.
C      OM     1     0.12500    418400.
.....
[ angletypes ]
; i      j      k      func      th0      cth
HO     OA     C      1     109.500    397.480
HO     OA     CH1    1     109.500    397.480
.....
[ dihedraltypes ]
; i      l      func      q0      cq
NRS*   NRS     2     0.000    167.360
NRS*   NRS*    2     0.000    167.360
.....
[ dihedraltypes ]
; j      k      func      phi0      cp      mult
C      OA     1     180.000    16.736     2
C      N      1     180.000    33.472     2
.....
[ dihedraltypes ]
; Ryckaert-Bellemans Dihedrals
;
; aj      ak      funct
CP2    CP2     3     9.2789   12.156   -13.120   -3.0597   26.240   -31.495
```

66

top文件: 参数

表5.4: 拓扑(*.top)文件

参数					
相互作用类型	指令	原子数	函数类型	参数	自由能
必需	defaults			非键函数类型; 组合规则 c^r ; 生成对(no/yes); fudge LJ(); fudge QQ()	
必需	atomtypes			原子类型; 质量 $m(u)$; 电荷 $q(e)$; 粒子类型; V^{cr} ; W^{cr}	
	bondtypes			(参考表 5.5 bonds 指令)	
	pairtypes			(参考表 5.5 pairs 指令)	
	angletypes			(参考表 5.5 angles 指令)	
	dihedraltypes*			(参考表 5.5 dihedrals 指令)	
	constrainttypes			(参考表 5.5 constraints 指令)	
LJ	nonbond_params	2	1	V^{cr} ; W^{cr}	
Buckingham	nonbond_params	2	2	$a(kJ mol^{-1})$; $b(nm^{-1})$; $c6(kJ mol^{-1} nm^6)$	

67

top文件: 分子系统

分子定义

相互作用类型	指令	原子数	函数类型	参数	自由能
必需	moleculename			分子名称; n_{ex}^{mrexcl}	
必需	atoms	1		原子类型; 残基编号; 残基名称; 原子名称; 电荷组编号; 电荷 $q(e)$; 质量 $m(u)$	类型, q , m
分子内相互作用和几何构型定义见表 5.5					
系统					
相互作用类型	指令	原子数	函数类型	参数	自由能
必需	system			系统名称	
必需	molecules			分子名称; 分子数	

68

表 5.5: [moleculetype] 指令详解							
相互作用名称	拓扑文件指令	原子数	参数类型	参数顺序及其单位	用于自由能计算?	交叉参考(节)	
键	bonds ^{§,¶}	2	1	b_0 (nm); k_b (kJ mol ⁻¹ nm ⁻²)	所有	4.2.1	
G96键	bonds ^{§,¶}	2	2	b_0 (nm); k_b (kJ mol ⁻¹ nm ⁻²)	所有	4.2.1	
Morse键	bonds ^{§,¶}	2	3	b_0 (nm); D (kJ mol ⁻¹); β (nm ⁻¹)	所有	4.2.2	
立方键	bonds ^{§,¶}	2	4	b_0 (nm); $C_{i=2,3}$ (kJ mol ⁻¹ nm ⁻²)		4.2.3	
连接	bonds [§]	2	5			5.4	
简谐势	bonds	2	6	b_0 (nm); k_b (kJ mol ⁻¹ nm ⁻²)	所有	4.2.1, 5.4	
FENE键	bonds [§]	2	7	b_m (nm); k_b (kJ mol ⁻¹ nm ⁻²)		4.2.4	
表格键	bonds [§]	2	8	表号(z0); k (kJ mol ⁻¹)	k	4.2.14	

69

表格键 [¶]	bonds	2	9	表号(z0); k (kJ mol ⁻¹)	k	4.2.14, 5.4
约束势	bonds	2	10	下限,上限1,上限2(nm); k_{dr} (kJ mol ⁻¹ nm ⁻²)	所有	4.3.5
额外LJ或库仑	pairs	2	1	V**; W**	所有	5.3.4
额外LJ或库仑	pairs	2	2	fudge QQ(λ ; q _i , q _j (e); V; W)		5.3.4
额外LJ或库仑	pairs_nb	2	1	q _i , q _j (e); V*; W*		5.3.4
键角	angles [§]	3	1	θ_0 (deg); k_θ (kJ mol ⁻¹ rad ⁻²)	所有	4.2.5
G96键角	angles [§]	3	2	θ_0 (deg); k_θ (kJ mol ⁻¹)	所有	4.2.6
键-键交叉项	angles	3	3	r_{1e}, r_{2e} (nm); $k_{rr'}$ (kJ mol ⁻¹ nm ⁻²)		4.2.9
键-角交叉项	angles	3	4	r_{1e}, r_{2e}, r_{3e} (nm); $k_{r\theta}$ (kJ mol ⁻¹ nm ⁻²)		4.2.10
Urey-Bradley键角	angles [¶]	3	5	θ_0 (deg); k_θ (kJ mol ⁻¹ rad ⁻²); r_{13} (nm); k_{UB} (kJ mol ⁻¹ nm ⁻²)	所有	4.2.8
四次键角	angles [¶]	3	6	θ_0 (deg); $C_{i=0,1,2,3,4}$ (kJ mol ⁻¹ rad ⁻¹)		4.2.11
表格角	angles	3	8	表号(z0); k (kJ mol ⁻¹)	k	4.2.14
限制弯曲势	angles	3	10	θ_0 (deg); k_θ (kJ mol ⁻¹)		4.2.7

70

正常二面角	dihedrals	4	1	$\phi_s(\text{deg})$; $k_\phi(\text{kJ mol}^{-1})$; 多重数	ϕ, k	4.2.13
异常二面角	dihedrals	4	2	$\xi_0(\text{deg})$; $k_\xi(\text{kJ mol}^{-1} \text{ rad}^{-2})$	所有	4.2.12
Ryckaert-Bellermans二面角	dihedrals	4	3	$C_0, C_1, C_2, C_3, C_4, C_5(\text{kJ mol}^{-1})$	所有	4.2.13
周期异常二面角	dihedrals	4	4	$\phi_s(\text{deg})$; $k_\phi(\text{kJ mol}^{-1})$; 多重数	ϕ, k	4.2.12
傅立叶二面角	dihedrals	4	5	$C_0, C_1, C_2, C_3, C_4(\text{kJ mol}^{-1})$	所有	4.2.13
表格二面角	dihedrals	4	8	表号(≥ 0); $k(\text{kJ mol}^{-1})$	k	4.2.14
正常二面角(多重)	dihedrals	4	9	$\phi_s(\text{deg})$; $k_\phi(\text{kJ mol}^{-1})$; 多重数	ϕ, k	4.2.13
限制二面角	dihedrals	4	11	$\phi_0(\text{deg})$; $k_\phi(\text{kJ mol}^{-1})$		4.2.13
结合弯曲扭转势	dihedrals	4	10	$a_0, a_1, a_2, a_3, a_4(\text{kJ mol}^{-1})$		4.2.13

71

排除	exclusions	1		一个或多个原子索引号		5.4
约束	constraints [§]	2	1	$b_0(\text{nm})$	所有	4.5, 5.5
约束	constraints	2	2	$b_0(\text{nm})$	所有	4.5, 5.5, 5.4
SETTLE	settles	1	1	$d_{\text{oh}}, d_{\text{HH}}(\text{nm})$		3.6.1, 5.5
二体虚拟站点	virtual_sites2	3	1	$a()$		4.7
三体虚拟站点	virtual_sites3	4	1	$a, b()$		4.7
三体虚拟站点占 (fd)	virtual_sites3					
三体虚拟站点 (fad)	virtual_sites3	4	3	$\theta(\text{deg})$; $d(\text{nm})$		4.7
三体虚拟站点 (out)	virtual_sites3	4	4	$a, b(); c(\text{nm}^{-1})$		4.7
四体虚拟站点 (fdn)	virtual_sites4	5	2	$a, b(); c(\text{nm})$		4.7
N体虚拟站点 (COG)	virtual_sitesn	1	1	一个或多个构建原子索引号		4.7
N体虚拟站点 (COM)	virtual_sitesn	1	2	一个或多个构建原子索引号		4.7
N体虚拟站点 (COM)	virtual_sitesn	1	3	一对或多对构建原子的索引号与权重		4.7

72

位置约束	<code>position_restraints</code>	1	1	$k_x, k_y, k_z (\text{kJ mol}^{-1} \text{ nm}^{-2})$	所有	4.3.1
平底位置约束	<code>position_restraints</code>	1	2	$g, r (\text{nm}), k (\text{kJ mol}^{-1} \text{ nm}^{-2})$		4.3.2
距离约束	<code>distance_restraints</code>	2	1	类型; 标签; 下限, 上限1, 上限2(nm); 权重()		4.3.5
二面角约束	<code>dihedral_restraints</code>	4	1	$\phi_0 (\text{deg}); \Delta\phi (\text{deg})$	所有	4.3.4
方向约束	<code>orientation_restraints</code>	2	1	$\exp.; \text{标签}; \alpha; c(U \text{ nm}^\alpha); \text{obs.}(U); \text{权重}(U^{-1})$		4.3.6
角度约束	<code>angle_restraints</code>	4	1	$\theta_0 (\text{deg}); k_c (\text{kJ mol}^{-1})$; 多重数	θ, k	4.3.3
角度约束(z)	<code>angle_restraints_z</code>	2	1	$\theta_0 (\text{deg}); k_c (\text{kJ mol}^{-1})$; 多重数	θ, k	4.3.3

73



拓扑文件的创建

- 简单的手动,用于理解
- 辅助脚本程序,减轻工作量
- 一些集成的程序网站,仍需检查

75

回答问题

- 什么体系
- 什么力场
- 参数可有
- 若无成键参数
 - 冻结刚性
 - 限制近似刚性
 - 约束构型刚性

76

一些工具

- 生物大分子: pdb2gmx
- 有机小分子
 - AMBER GAFF: AMBER Tool+ACPYPE
 - OPLS: tppmktop
 - GROMOS: ATB/PRODRG
- 无机材料: x2top
- 粗粒化: martini

77

pdb2gmx

- 默认只能用于力场数据库中的分子,主要是生物分子
- 只适用于标准残基
- 扩展到任意分子,非标准残基需要修改残基数据库
- 使用前需要对pdb进行数据清洗

78

pdb数据清洗

- 是否含有杂原子,如何处理
- 是否缺失原子,缺失程度
- 残基是否标准
- 是否包含氢原子,能否忽略
- 残基质子化状态如何,是否考虑
- 二硫键是否特殊处理
- 残基末端是否特殊处理
-

79

示例

- 创建小肽的拓扑

```
gmx pdb2gmx -f peptide.pdb -ignh
```

用于未清洗的PDB，你可能遇到各种错误!!!

用于未清洗的PDB，你可能遇到各种错误!!!

用于未清洗的PDB，你可能遇到各种错误!!!

用于未清洗的PDB，你可能遇到各种错误!!!

用于未清洗的PDB，你可能遇到各种错误!!!

80

AMBER GAFF

- AMBER力场推荐方法
- 电荷
 - RESP 基于其他量化程序
 - AM1-BCC 半经验,自带
- 原子类型,其他参数: GAFF或相应的力场文件

81

AMBER Tool配置

- AMBER 14
- 来源Chimera 1.10.2
- 基于CygWin环境编译
- 未包含所有工具
- 添加自编译的RESP,ACPPPE程序

添加 **AMBERHOME** 环境变量

其值为**amber**的目录

如 **C:/amber14**

注意：使用斜线，否则运行出错

82

GAFF流程

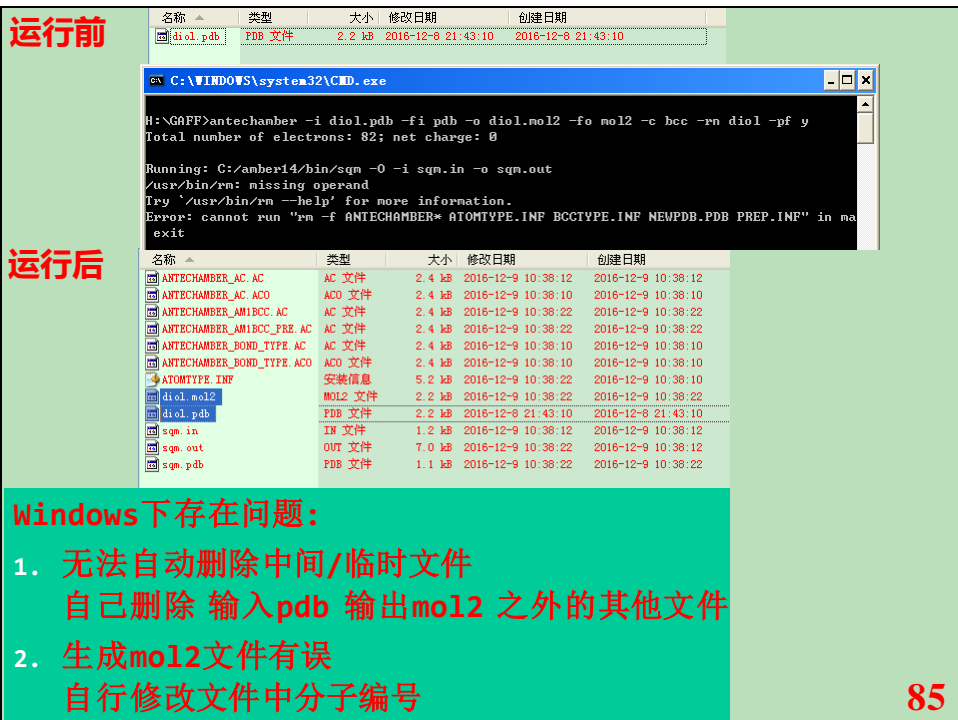


示例: 多巴胺GAFF

antechamber

```
-i diol.pdb -fi pdb      输入构型文件  
-o diol.mol2 -fo mol2    输出构型电荷文件  
-c bcc                    使用AM1-BCC电荷  
-rn diol                  指定分子名称，否则sleap出错  
-pf y                     运行结束后删除中间/临时文件  
                           其他选项根据需要添加
```

84



检查缺失参数

```
parmchk2
```

```
-i diol.mol2 -f mol2
```

输入构型电荷文件

```
-o diol.frcmod
```

输出缺失力场参数文件

根据具体情况决定是否修改

```
H:\GAFF\diol.frcmod - Notepad2-mod
1;#mark line goes here
2 MASS
3;
4 BOND
5;
6 ANGLE
7;
8 DIHED
9;
10 IMPROPER
11 ca-ca-ca-ha      1.1      188.0      2.0
    Using general improper torsional angle
    ca-X-ca-ha, penalty score= 6.0
12 ca-ca-ca-oh      1.1      180.0      2.0
    Using the default value
13;
14 NONBON
15;
```

87

运行leap脚本

```
H:\GAFF\leap.in - Notepad2-mod
1 source leaprc.ff14SB
2 source leaprc.gaff
3;
4 loadamberparams diol.frcmod
5 LIG=loadmol2 diol.mol2
6 check LIG
7 saveamberparm LIG diol.prmtop diol.inpcrd
8 quit
```

sleap -f leap.in

名称	类型	大小	修改日期	创建日期
diol.frcmod	FRCMOD	284 B	2016-12-9 11:14:56	2016-12-9 11:14:56
diol.inpcrd	INPCRD	814 B	2016-12-9 11:27:46	2016-12-9 11:27:46
diol.mol2	MOL2 文件	2.2 kB	2016-12-9 11:14:18	2016-12-9 10:38:22
diol.pdb	PDB 文件	2.2 kB	2016-12-8 21:43:10	2016-12-8 21:43:10
diol.prmtop	PRMTOP	12.2 kB	2016-12-9 11:27:46	2016-12-9 11:27:44
leap.in	IN 文件	160 B	2016-12-9 11:22:40	2016-8-2 13:24:16

88

运行ACPYPE

acpype

-p diol.prmtop 参数文件

-x diol.inpcrd 构型文件

-d 多输出些信息

名称	类型	大小	修改日期	创建日期
diol.pdb	PDB 文件	2.2 kB	2016-12-8 21:43:10	2016-12-8 21:43:10
diol.mol2	MOL2 文件	2.2 kB	2016-12-9 11:14:18	2016-12-9 10:38:22
diol.frcmod	FRCMOD...	284 B	2016-12-9 11:14:56	2016-12-9 11:14:56
leap.in	IN 文件	160 B	2016-12-9 11:22:40	2016-8-2 13:24:16
diol.inpcrd	INPCRD...	814 B	2016-12-9 11:27:46	2016-12-9 11:27:46
diol.prmtop	PRMTOP...	12.2 kB	2016-12-9 11:27:46	2016-12-9 11:27:44
diol_GMX.gro	GRO 文件	1.0 kB	2016-12-9 11:34:16	2016-12-9 11:34:16
diol_GMX.top	TOP 文件	14.2 kB	2016-12-9 11:34:16	2016-12-9 11:34:16
emmdp	MDP 文件	182 B	2016-12-9 11:34:16	2016-12-9 11:34:16
mdmdp	MDP 文件	172 B	2016-12-9 11:34:16	2016-12-9 11:34:16

完整top文件

可修改为itp文件

方便移植

89

几点说明

- 使用不同电荷, 只要修改 antechamber选项即可
- acpype可一步执行所有过程, 但不易理解流程, 排查错误
- 加载不同力场文件, 使用不同参数

90

tppmktop

- 只生成oplsaa力场拓扑文件
- 原子类型判断目前最好
- 对oplsaa原子类型和参数有扩充, 需要下载单独的力场文件
- 服务器少, 可同时提交作业有限

91

Your request is processing at the server in background.

You started local program: [tppmktop](#)

Your process PID: 0

Wait a little and follow this link: [diolpdb_jAJ8dk](#)

ATTENTION! Do not forget to use the proper
of the force field force (not less than re:
Watch for corresponding force field at:
[bitbucket.com/comconl](#)

Please ascertain that the topology is val:
do not guarantee that. If you find that s:
is wrong, please report us to comconad@
[bitbucket.com/comconl](#)

Topology was prepared for use with the fo:
OPLS-AA revision jun16

[moleculetype]
0 3

不要使用IE打开, 乱行
itp中未包含分子名称

Project directory: diolpdb_jAJ8dk

Force field: OPLS-AA

Executed command:

Returned:

Input PDB file: [input000.pdb](#) [2.3 kB]

Output ITP file: [output000.itp](#) [9.8 kB]

Output RTP file: [output000.rtp](#) [2.0 kB]

Parameter lack-file: [lack.itp](#) [0.0 kB]

tppmktop verbose LOG: [log](#) [186.3 kB]

tppmktop console OUTPUT: [pytpp_tppmktop](#) [6.4 kB]
[main page](#)

检查是否缺失参数

92

ATB/PRODRG

- 有限制
- 需注册
- 自行探索

- 要检查得到的力场文件!!!
- 要检查得到的力场文件!!!
- 要检查得到的力场文件!!!

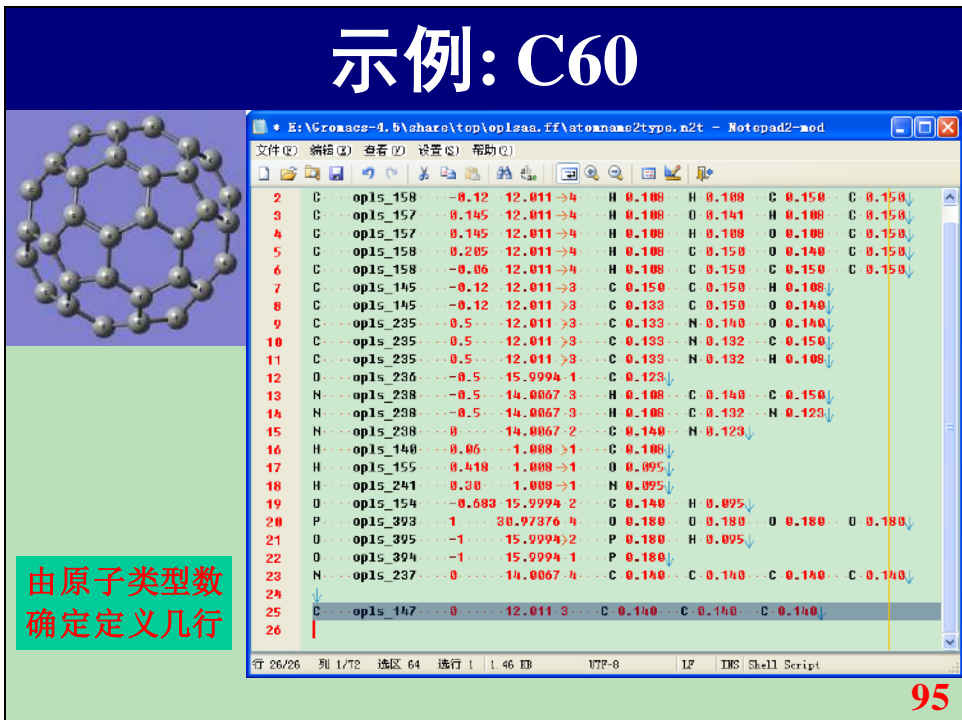
93

x2top

- 用于周期性/规律性体系
- 只生成拓扑文件模板,具体参数需要自己决定

94

示例: C60



执行x2top

```
gmx x2top -f C60.pdb -o C60.top -name C60
```

cmd window showing the execution of gmx x2top command:

```

ex C:\WINDOWS\system32\cmd.exe
-kb      real 400000 Bonded force constant (kJ/mol/nm^2)
-kt      real 400 Angle force constant (kJ/mol/rad^2)
-kp      real 5 Dihedral angle force constant (kJ/mol/rad^2)

WARNING: all CONECT records are ignored
Opening force field file E:/Gromacs-4.5/share/top/oplsaa.ff\atomname2type.n2t
There are 24 name to type translations in file E:/Gromacs-4.5/share/top/oplsaa.ff
Generating bonds from distances...
atom 60
There are 1 different atom types in your sample
Generating angles and dihedrals from bonds...
Before cleaning: 300 pairs
Before cleaning: 360 dihedrals
There are 90 Ryckaert-Belleman dihedrals, 0 impropers, 180 angles
    240 pairs, 90 bonds and 60 atoms
Total charge is 0, total mass is 720.659

Back Off! I just backed up C60.top to ./#C60.top.1#
WARNING: topologies generated by g_x2top can not be trusted at face value.
Please verify atomtypes and charges by comparison to other
topologies.

gcq#65: "Give a Man a Fish" (Arrested Development)

```

96

修改得到的top文件

```
H:\GAFF\C60.top - Notepad2-mod
文件(?) 编辑(?) 查看(?) 设置(?) 帮助(?) 
22 ;@ 
23 @ 
24 ; Include Forcefield parameters@ 
25 #include "oplsaa.ff/Forcefield.itp"@ 
26 @ 
27 [ moleculetype ]@ 
28 ; Name ..... nrexcl@ 
29 C60 ..... 3@ 
30 @ 
31 [ atoms ]@ 
32 [ bonds ]@ 
33 @ 
34 ; ai aj Funct ..... c0 ..... c1 ..... c2 ..... c3@ 
35 1 2 -1 1.460000e-001 4.000000e+005 1.460000e-001 4.000000e+005@ 
36 1 6 -1 1.380000e-001 4.000000e+005 1.380000e-001 4.000000e+005@ 
37 1 7 -1 1.460000e-001 4.000000e+005 1.460000e-001 4.000000e+005@ 
38 2 3 -1 1.390000e-001 4.000000e+005 1.390000e-001 4.000000e+005@ 
39 2 9 -1 1.460000e-001 4.000000e+005 1.460000e-001 4.000000e+005@ 
40 3 4 -1 1.460000e-001 4.000000e+005 1.460000e-001 4.000000e+005@ 
41 3 11 -1 1.460000e-001 4.000000e+005 1.460000e-001 4.000000e+005@ 
42 4 5 -1 1.390000e-001 4.000000e+005 1.390000e-001 4.000000e+005@ 
43 4 12 -1 1.460000e-001 4.000000e+005 1.460000e-001 4.000000e+005@ 
44 5 6 -1 1.460000e-001 4.000000e+005 1.460000e-001 4.000000e+005@ 
45 5 15 -1 1.460000e-001 4.000000e+005 1.460000e-001 4.000000e+005@ 
46 6 17 -1 1.460000e-001 4.000000e+005 1.460000e-001 4.000000e+005@ 
47 7 8 -1 1.460000e-001 4.000000e+005 1.460000e-001 4.000000e+005@ 
行 95/713 列 1/72 选区 0 选行 0 41.9 KB | UTF-8 | CR+LF | INI | Configuration 配置文件 | 97
```

Martini粗粒化

- 用于蛋白时不改变二级结构
- 需要提前知道二级结构: dssp
- 多个版本, 多种分子
- **martinize.py** 脚本或可执行程序
 - 最新版本2.4
 - 支持力场(p用于极化水模型)
martini21/21p
martini22/22p
elnedyn, elnedyn22/22p
martini22dna

蛋白
弹性网
DNA

98

示例: 粗粒化小肽

● `martinize.py` 脚本或可执行程序

- 最新版本2.4
 - 支持力场(p用于极化水模型)

martini21/21p

martini22/22p

elnedyn, elnedyn22/22p

martini22dna

蛋白

弹性网

DNA

- martinize没有考虑在Windows下调用dssp, 直接使用有问题

- #### ■先手动执行dssp生成二级结构文件

99

获取二级结构文件

```
dssp -i peptide.pdb  
-o peptide.ss
```

```

1 === Secondary Structure Definition by the program DSSP, CHBI version by M.L. Hekkelman/2010-10-21
2 REFERENCE W. KABOSCH AND C. SANDER, BIOPOLYMERS 22 (1983) 2577-2637
3
4   19 1 0 0 0 TOTAL NUMBER OF RESIDUES, NUMBER OF CHAINS, NUMBER OF SS-BRIDGES(TOTAL, INTRACHAIN
5 2085.6 ACCESSIBLE SURFACE OF PROTEIN (ANGSTROM<sup>2</sup>)
6   8 2 1 TOTAL NUMBER OF HYDROGEN BONDS OF TYPE O(1)-->H-N(C), SAME NUMBER PER 100 RESIDUES
7   0 0 0 TOTAL NUMBER OF HYDROGEN BONDS IN PARALLEL BRIDGES, SAME NUMBER PER 100 RESIDUES
8   0 0 0 TOTAL NUMBER OF HYDROGEN BONDS IN ANTIPARALLEL BRIDGES, SAME NUMBER PER 100 RESIDUES
9   0 0 0 TOTAL NUMBER OF HYDROGEN BONDS OF TYPE O(1)-->H-N(I-5), SAME NUMBER PER 100 RESIDUES
10  0 0 0 TOTAL NUMBER OF HYDROGEN BONDS OF TYPE O(1)-->H-N(I-4), SAME NUMBER PER 100 RESIDUES
11  0 0 0 TOTAL NUMBER OF HYDROGEN BONDS OF TYPE O(1)-->H-N(I-3), SAME NUMBER PER 100 RESIDUES
12  0 0 0 TOTAL NUMBER OF HYDROGEN BONDS OF TYPE O(1)-->H-N(I-2), SAME NUMBER PER 100 RESIDUES
13  0 0 0 TOTAL NUMBER OF HYDROGEN BONDS OF TYPE O(1)-->H-N(I-1), SAME NUMBER PER 100 RESIDUES
14  0 0 0 TOTAL NUMBER OF HYDROGEN BONDS OF TYPE O(1)-->H-N(I+1), SAME NUMBER PER 100 RESIDUES
15  0 0 0 TOTAL NUMBER OF HYDROGEN BONDS OF TYPE O(1)-->H-N(I+2), SAME NUMBER PER 100 RESIDUES
16  0 0 0 TOTAL NUMBER OF HYDROGEN BONDS OF TYPE O(1)-->H-N(I+3), SAME NUMBER PER 100 RESIDUES
17  -1 5 3 TOTAL NUMBER OF HYDROGEN BONDS OF TYPE O(1)-->H-N(I+4), SAME NUMBER PER 100 RESIDUES
18  -7 36 8 TOTAL NUMBER OF HYDROGEN BONDS OF TYPE O(1)-->H-N(I+5), SAME NUMBER PER 100 RESIDUES
19  0 0 0 TOTAL NUMBER OF HYDROGEN BONDS OF TYPE O(1)-->H-N(I+6), SAME NUMBER PER 100 RESIDUES
20   1 2 3 4 5 6 7 8 9 10 11 12 13 14 15 16 17 18 19 20 21 22 23 24 25 26 27 28 29 30 *** 
21  0 0 0 0 0 0 0 0 1 0 0 0 0 0 0 0 0 0 0 0 0 0 0 0 0 0 0 0 0 0 0 0 0 0 0 0 0 0 0 0 RESID
22  -0 0 0 0 0 0 0 0 0 0 0 0 0 0 0 0 0 0 0 0 0 0 0 0 0 0 0 0 0 0 0 0 0 0 0 0 0 0 0 0 PARAL
23  -0 0 0 0 0 0 0 0 0 0 0 0 0 0 0 0 0 0 0 0 0 0 0 0 0 0 0 0 0 0 0 0 0 0 0 0 0 0 0 0 ANITP
24  0 0 0 0 0 0 0 0 0 0 0 0 0 0 0 0 0 0 0 0 0 0 0 0 0 0 0 0 0 0 0 0 0 0 0 0 0 0 0 0 LADDE
25  -I RESIDUE AA STRUCTURE BP1 BP2 ACC N-->O O-->H N-->O O-->H N TCO KAPPA A
```

生成粗粒化力场和拓扑

`martinize.exe`

<code>-f peptide.pdb</code>	输入构型文件
<code>-ss peptide.ss</code>	输入二级结构文件
<code>-x peptide(CG).pdb</code>	输出粗粒化构型文件
<code>-ff martini22</code>	指定使用的力场
<code>-o peptide.top</code>	输出拓扑文件
<code>-p backbone</code>	指定生成位置限制文件

101

修改得到的拓扑文件

- 根据指定的力场, 修改拓扑文件中的`#include`语句

The screenshot shows a Notepad2 window with the following content:

```
1 #include "martini.itp"
2
3
4
5 #include "Protein.itp"
6
7 [ system ]
8 ; name
9 Martini system from peptide.pdb
10
11 [ molecules ]
12 ; name ..... number
13 Protein ----- 1
```

The file includes two `#include` statements at the top. Below them is a `[system]` section with a `; name` entry set to `Martini`. At the bottom is a `[molecules]` section with a `; name number` entry for `Protein` with a value of `1`.

102

毒品

维基百科，自由的百科全书

毒品，是指某些会使人严重成瘾或是无成瘾性但会产生幻觉的物质。

目录

- 1 定义
 - 1.1 国际惯例
 - 1.2 中华民国
 - 1.3 中华人民共和国
- 2 常见滥用药品
- 3 主要产地
- 4 使用
- 5 戒毒
- 6 危害
- 7 管制
 - 7.1 对贩毒罪设置死刑的部分国家
 - 7.2 中华民国
 - 7.3 中华人民共和国
 - 7.4 其他国家
- 8 相关言论
 - 8.1 倡导者
 - 8.2 成瘾性
- 9 管制药品合法化争论(部分药物)
 - 9.1 品种合法化
 - 9.2 管制下的合法化
- 10 流行文化取材
 - 10.1 中华民国(台湾)
 - 10.2 香港
 - 10.3 中国大陆
 - 10.4 美国
- 11 相关条目
- 12 参考文献
- 13 外部链接



定义

国际惯例

西方并没有“毒品”一词，社会上习惯将毒品的使用称为药品滥用或药品娱乐性使用。其中药品的定义不包括像乙醚这样可导致人失去知觉的化学药品以及砒霜、敌敌畏、氰化物等可直接导致人死亡的剧毒物质，而是特指出于“非医疗目的”而反复连续使用、能够产生“依赖性”（即成瘾性）的精神药品或麻醉药品。

华语国家立法限制视为毒品的药物，其实有许多并没有生理的成瘾性，例如LSD；但是没有生理成瘾性并不代表没有心理成瘾性，而心理成瘾性不一定比生理成瘾性更易处理。禁止这些药物的另一大原因是其具有致幻效应而使行为变得无法预测。

西方医学、社会学等学术界也会把尼古丁（烟草制品的有效成分）和酒精的使用称为药物娱乐性使用（也就是说学术上，烟草酒精与海洛因、可卡因、安非他命的差别只是合法与非法的差别），因为烟酒同样有强烈成瘾性，并能给人体带来重大伤害。

中华民国

《毒品危害防制条例》本条例所称毒品，指具有成瘾性、滥用性及对社会危害性之麻醉药品与其制品及影响精神物质与其制品。毒品依其成瘾性、滥用性及对社会危害性分为四级，其品项如下：

- 第一级 海洛因、吗啡、鸦片、可卡因及其相类制品。
- 第二级 罂粟、古柯、大麻、配西汀、潘他唑新及其相类制品。
- 第三级 西可巴比妥、异戊巴比妥、纳洛芬、K他命及其相类制品。
- 第四级 速可巴比妥、阿普唑他及其相类制品。

前项毒品之分级及品项，由中华民国法务部会同卫生福利部组成审议委员会。医药及科学上需用之麻醉药品与其制品及影响精神物质与其制品之管理，另以法律定之。

中华人民共和国

根据《中华人民共和国刑法》定义：毒品是指鸦片、海洛因、甲基苯丙胺（冰毒）、吗啡、大麻、可卡因以及国家规定管制的其他能够使人形成瘾癖的麻醉药品和精神药品^[1]。

中华人民共和国《麻醉药品及精神药品品种目录》中列明了121种麻醉药品和130种精神药品。

常见滥用药品



烟草（植物，多数国家合法，但其危害不输管制药品）



酒精（部分国家非法，滥用会造成重大危害）



大麻（植物，部分国家合法）



原始鸦片



古柯（植物）



海洛因，又称白粉（美国政府图片）



可卡因（处方药）



药用罂粟（植物）



吗啡（处方药）



右旋安非他命（处方药，兴奋剂）



甲基苯丙胺又称甲基安非他命、冰毒



摇头丸又称快乐丸、E仔（非法来源）



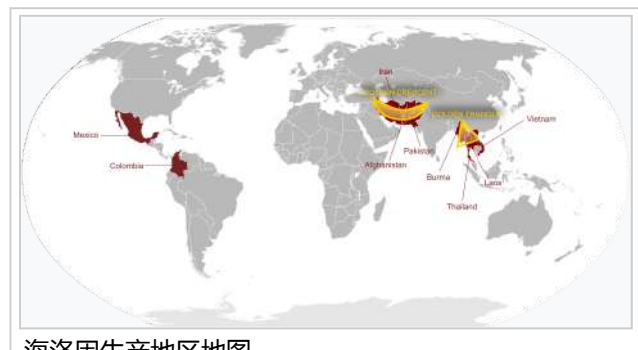
异戊巴比妥又称青发（处方药，迷幻剂）

samuel

- 含有鸦片成分的药物（例如红丸、甘草片、曲马多、可待因）
- 一粒眠（Erimine），又称五仔，主要成分硝甲西洋
- 魔菇（亦称迷幻蘑菇）^[2]
- 忽得（甲喹酮 / 安眠酮）
- 咳药水

主要产地

阿富汗、巴基斯坦和伊朗交界处的“金新月”，缅甸、老挝和泰国交界处的“金三角”，哥伦比亚、厄瓜多尔和秘鲁交界处的“银三角”，尼日利亚和加纳交界处的“黑三角”为世界四大毒品原植物种植地。“金新月”的海洛因主要贩卖到俄罗斯、欧洲和伊朗，“金三角”的海洛因主要贩卖到中国内地、香港、台湾、日本和澳洲，“银三角”的可卡因主要贩卖到美国、加拿大和欧洲，“黑三角”的可卡因主要贩卖到欧洲。朝鲜的毒品很多在中国东三省泛滥，据说每个集体农庄都被划出125英亩土地种植罂粟。数据表明朝鲜每年生产40吨鸦片，是世界第三大鸦片出口国和第六大海洛因出口国，年出口毒品收入5亿美元。^[3]就目前趋势及毒品类型，特别是化学合成类之毒品，仅需适当材料及步骤即可制成，例如安非他命。



海洛因生产地区地图

使用

究其使用方法主要分以下几种使用方式：

- 静脉注射（部分毒品属于管制性麻醉药品，需在医生处方下的医疗行为使用，例如癌末病患的止痛）
- 直接口服
- 吸食毒品挥发气体（含烟卷）
- 加入食物或饮料中

戒毒

长期使用毒品会造成对毒品的耐受性，也就是说身体需要使用更大的量，才能达到预期的效果。因此当不再使用该毒品后，身体会出现戒断症状（脱瘾反应）。例如：长期使用海洛因，停用24小时内，就会出现海洛因戒断症状，如：流眼泪、流鼻水、打哈欠、全身骨头酸痛像蚂蚁在咬、腹泻、呕吐、焦虑不安与失眠等症状。并非所有毒品都会导致戒断症状。

在成功戒除毒品之后，身体的戒断症状也会消失，而对毒品的耐受性会逐渐回复到未吸食前的剂量。此时，若依然照着戒除前的大剂量吸食，可能因吸食过量暴毙。^[4]

危害

毒品除了造成身体危害外，还有共用针具大幅增加艾滋病病患人数、吸食毒品的金钱消耗造成的犯罪率上升、吸毒者转为贩毒者增加毒瘾人数及吸食毒品后精神状态不佳增加的社会危险。贩售毒品还是阿富汗塔利班和盖达组织、意大利的黑手党、俄罗斯和墨西哥的黑帮、哥伦比亚的反政府武装最大的收入来源，对于相关国家和国际社会的和平与稳定造成了极大的困扰。

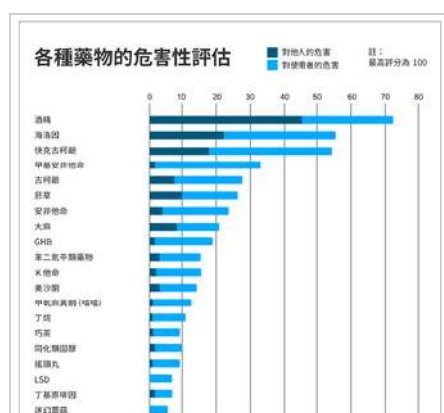
合法毒品对社会危害也很大，例如酒精及二手烟对社会的危害高于不少非法毒品。

在戒毒困难的情况下，许多国家的政府干脆提供免费针具给吸毒者，至少可以大幅降低艾滋病造成的巨额成本；荷兰在禁止摇头丸的情况下，同时允许公开贩售测试摇头丸成分的产品，在无法全面禁止摇头丸的情况下，让使用者自行淘汰品质差的摇头丸。有不少国家也会提供免费或低价美沙酮代替鸦片类毒品，瑞士甚至直接提供海洛因给成瘾者，减少吸毒者的经济负担及衍生的犯罪问题。也有不少国家提倡使用含有尼古丁的贴片或口香糖，可以减少二手烟对他人危害，也可以让烟瘾者解瘾时仅受到尼古丁的危害、而不会受到烟草内其他物质的伤害。

管制

对贩毒罪设置死刑的部分国家

- 中华人民共和国
- 越南
- 泰国
- 印尼
- 马来西亚
- 新加坡
- 伊朗
- 沙特阿拉伯
- 伊拉克
- 阿联酋
- 巴基斯坦
- 孟加拉国



酒精和烟草等合法药物造成的伤害未必小于非法药物，根据一项2010年请药物伤害专家进行的评比显示，酒精是最为危险的。图中最高可能的伤害度定为100，并以此定所有药物的相对伤害度；而浅蓝色的部分为某种药物对他人的伤害，深蓝色的部分为该药物对使用者自身造成的伤害。

中华民国

中华民国行政院卫生署管制药品管理局对毒品的分类，最新版本为2002年1月23日修正。（详见下表）

第一级毒品（民国105年3月25日版本）

（除特别规定外，皆包括其异构物Isomers、酯类Esters、醚类Ethers、及盐类Salts）

中华民国《毒品危害防制条例》第4条：制造、运输、贩卖第一级毒品者，处死刑或无期徒刑，处无期徒刑者，得并科新台币2000万元以下罚金。

- 乙酰托啡因 (Acetorphine)
- 可卡因 (Cocaine)
- 二氢去氧吗啡
(Desomorphine)
- 二氢爱托啡因
(Dihydroetorphine)
- 爱托啡因 (Etorphine)
- 海洛因 (Heroin)
- 酚派丙酮 (Ketobemidone)
- 鸦片 (Opium)
- 吗啡 (Morphine)

第二级毒品 (民国105年3月25日版本)

(除特别规定外，皆包括其异构物Isomers、酯类Esters、醚类Ethers及盐类Salts)

中华民国《毒品危害防制条例》第4条：制造、运输、贩卖第二级毒品者，处无期徒刑或7年以上有期徒刑，并科处新台币1000万元以下罚金。

- 乙酰阿法甲基吩坦尼 (Acetyl-alpha-methylfentanyl)
- 乙酰二氢可待因 (Acetyldihydrocodeine)
- 乙酰美沙多 (Acetylmethadol)
- α-甲基吩坦尼 (Alpha-methylfentanyl)
- α-美沙多 (Alpha-methadol)
- α-甲基硫吩坦尼 (Alpha-methylthiofentanyl)
- α-普鲁汀 (Alphaprodine)
- 阿华吩坦尼 (Alfentanyl)
- 丙烯普鲁汀 (Allylprodine)
- α-乙酰美沙多 (Alphacetyl-methadol)
- α-美普鲁汀 (Alphameprodine)
- 阿米庚酸 (Amineptine)
- 安非他命 (Amphetamine)
- 安尼勒立汀 (Anileridine)
- 苯才西汀 (Benzethidine)
- 芳基吗啡 (Benzylmorphine)
- 芳基哌嗪 (Benzylpiperazine, BZP)
- β-乙酰美沙多 (Betacetylmethadol)
- β-羟基吩坦尼 (Betahydroxyfentanyl)
- β-羟基甲基吩坦尼 (Betahydroxy-3methyl-fentanyl)
- β-美普鲁汀 (Betameprodine)
- β-美沙多 (Betamethadol)
- β-普鲁汀 (Betaprodine)
- 培集屈密特 (Bezitramide)
- 二甲氧基溴 (Brolamfetamine)
- 大麻 (Cannabis)
- 大麻脂 (Cannabis resin)
- 大麻浸膏 (Cannabis extracts)
- 大麻酊 (Cannabis tinctures)
- 卡吩坦尼 (Carfentanyl)
- 卡西酮 (Cathinone)
- 氯甲基安非他命 (Chloromethamphetamine、1-Chlorophenyl-N-methylpropan-2-amine、1-Chlorophenyl-2-methylaminopropane、CMA)
- 气硝胺咪 (Clonitazene)
- 古柯 (Coca)
- 可待因 (Codeine)
- 甲基溴可待因 (Codeine-methylbromide)
- N氧化可待因 (Codeine-N-oxide)
- 可多克净 (Codoxime)
- 罂粟草膏 (Concentrated Poppy straw)
- 赛普诺啡 (Cyprenorphine)

- 甲乙胺二塞吩丁烯 (Ethylmethyl-thiambutene)
- 乙基吗啡 (Ethylmorphine)
- 乙环利定 (Eticyclidine)
- 爱托尼他净 (Etonitazene)
- 爱托失立汀 (Etoxeridine)
- 乙基色胺 (Eryptamine)
- 吻坦尼 (Fentanyl)
- 芬乃他林 (Fenetylline)
- 氟甲基安非他命 (Fluoromethamphetamine、1-Fluorophenyl-N-methylpropan-2-amine、1-Fluorophenyl-2-methylaminopropane、FMA)
- 佛莱西汀 (Furethidine)
- 伽玛羟基丁酸 (Gamma Hydroxybutyric Acid、Gammahydroxybutyrate、GHB)
- 羟二氢吗啡 (Hydromorphonol)
- 二氢可待因酮 (Hydrocodone)
- 二氢吗啡酮 (Hydromorphone)
- 羟基配西汀 (Hydroxypethidine)
- 伊波盖因 (Ibogaine)
- 异美沙冬 (Isomethadone)
- 左旋甲基安非他命 (Levomethamphetamine)
- 左旋甲基吗汎 (Levomethorphan)
- 左旋安非他命 (Levamphetamine)
- 左旋吗拉密特 (Levomoramide)
- 左旋吗汎 (Levorphanol)
- 左旋吩咐西吗汎 (Levophenacylmorphan)
- 离胺右旋安非他命 (Lisdexamphetamine)
- 麦角二乙胺 (LSD、Lysergide, 摆脚丸)
- 二亚甲基双氧安非他命 (MDA, HIGH客)
- N-α-二甲基-3,4-(亚甲二氧基) 苯乙基胺 (MDMA,N-α-dimethyl-3,4-(methylenedioxo) phenethylamine) (快乐丸、摇头丸)
- 甲氯奎酮 (Mecoloqualone)
- 三甲氧苯乙胺 (Mescaline)
- 美他唑新 (Metazocine)
- 美沙冬 (Methadone)
- 美沙冬中间物 (Methadone-intermediate)
- 甲基安非他命 (Methamphetamine)
- N-乙基-3-比啶二苯基乙醇酸 (N-ethyl-3-piperidyl benzilate)
- N-羟基二亚甲基双氧安非他命 (N-hydroxy-MDA)
- N-甲基-3-比啶二苯基乙醇酸 (N-methyl-3-piperidylbenzilate)
- 烟碱酰二氢可待因 (Nicodicodine)
- 烟碱酰可待因 (Nicocodeine)
- 烟碱酰吗啡 (Nicomorphine)
- N-N-二甲基安非他命 (N-N-dimethyl-amphetamine)
- 去甲基乙酰美沙多 (Noracymethadol)
- 原可待因 (Norcodeine)
- 左旋原吗汎 (Norlevorphanol)
- 原美沙冬 (Normethadone)
- 原吗啡 (Normorphine)
- 原匹潘浓 (Norpipanone)
- 罂粟 (Opium Poppy)
- 东罂粟碱 (Oripavine)
- 羟氢可待因酮 (Oxycodone)
- 羟二氢吗啡酮 (Oxymorphone)
- 对二氟吩坦尼 (Para-fluorofentanyl)
- 六氢大麻酚 (Parahexyl)
- 对-甲氧基甲基安非他命 (Paramethoxymethamphetamine、PMMA)
- 苯环利定 (Phencyclidine, 天使尘)
- 潘他唑新 (Pentazocine, 速赐康)
- 三,四-亚甲基双氧苯基甲胺戊酮 (Pentylylone)
- 一-苯乙基-四-苯基-四-醋酸比啶酯 {PEPAP,1-phenethyl-4-phenyl-4-piperidinol acetate (ester) }
- 配西汀 (Pethidine)
- 配西汀中间物-A (Pethidine intermediate-A)
- 配西汀中间物-B (Pethidine intermediate-B)
- 配西汀中间物-C (Pethidine intermediate-C)
- 配有特 (Peyote)
- 芬那多松 (Phenadoxone)
- 狄安普鲁密特 (Phenampromide)
- 吩那唑新 (Phenazocine)
- 吩诺吗汎 (Phenomorphan)
- 吩诺配立汀 (Phenoperidine)
- 福可汀 (Pholcodine)
- 四密诺汀 (Piminodine)

- 右旋安非他命
(Dexamphetamine)
- 右旋吗拉密特
(Dextromoramide)
- 右旋普帕西芬
(Dextropropoxyphene)
- 狄安普鲁密特 (Diamprodime)
- 二乙胺二塞吗丁烯
(Diethylthiambutene)
- 二乙基色胺 (DET)
- 狄芬诺新 (Difenoxin)
- 二氢可待因 (Dihydrocodeine)
- 二氢吗啡 (Dihydromorphine)
- 狄门诺沙多 (Dimenoxadol)
- 狄美菲坦诺 (Dimepheptanol)
- 二甲胺二塞吗丁烯
(Dimethylthiambutene)
- 二甲基色胺 (DMT)
- 吗福林二苯丁酸乙酯
(Dioxaphetylbutyrate)
- 狄芬诺西莱 (Diphenoxylate)
- 狄匹潘浓 (Dipipanone)
- 二甲氨基安非他命 (DMA)
- 羟基四氢甲基二苯吡喃
(DMHP)
- 二甲氨基乙基安非他命
(DOET)
- 二甲氨基甲苯异丙胺 (DOM、
STP)
- 托蒂巴醇 (Drotebanol)
- 爱哥宁 (Ecgonine)
- 爱哥宁衍化物 (Ecgonine
Derivatives)

- 外消旋甲基安非他命
(Methamphetamine
Racemate)
- 甲奎酮 (Methaqualone , 白板)
- 甲基卡西酮 (Methcathinone)
- 甲氧基甲基卡西酮
(Methoxymethcathinone)
- 四-甲基阿米雷司 (4-
methylaminorex)
- 甲基去氧吗啡
(Methyldesorphine)
- 甲基二氢吗啡
(Methyldihydromorphine)
- 三-甲基吩坦尼 (3-
Methylfentanyl)
- 三,四-亚甲基双氧焦二异丁基酮
(3,4-亚甲基双氧焦洛戊酮)
(3,4-
methylenedioxypyrovalerone、
MDPV)
- 三-甲基硫吩坦尼 (3-Methylthio-
fentanyl)
- 甲基卡西酮 (Methcathinone)
- 美杜邦 (Metopon)
- 二-甲氨基-α甲基-4.5- (亚甲二氧
基) 苯乙基胺 (MMDA,2-
methoxy-α-methyl-4.5-
(methylenedioxy)
phenethylamine)
- 吗拉特中间物 (Moramide-
intermediate)
- 吗啡甲溴化物 (Morphine
methobromide)
- 甲基磺胺吗啡 (Morphine
methylsulfonate)
- 吗啡立汀 (Morpheridine)
- N-氧化吗啡及其衍化物
(Morphine-N-oxide and its
Derivatives)
- 一-甲基-四-苯基-四-丙酸氧比啶
(MPPP,1-methyl-4-phenyl-4-
piperidinol
propionate (ester))
- 密罗啡因 (Myrophine)
- 那密浓 (Nabilone)
- N-乙基安非他命 (N-ethyl-
amphetamine)
- N-乙基-二亚甲基双氧安非他命
(N-ethyl-MDA)
- 匹立屈密特 (Piritramide)
- 副甲氧基安非他命 (PMA)
- 罂粟草 (Poppy straw)
- 普鲁亥他净 (Proheptazine)
- 普鲁配立汀 (Properidine)
- 普鲁匹兰 (Propiram)
- 裸头草辛 (Psilocine)
- 西洛西宾 (Psilocybine)
- 外消旋甲基吗啡
(Racemethorphan)
- 外消旋吗拉密特
(Racemoramide)
- 外消旋吗啡 (Racemorphan)
- 瑞吩坦尼 (Remifentanil)
- 环丙胺比咯烷 (Rolicyclidine)
- 苏芬坦尼 (Sufentanil)
- 他喷他赛 (Tapentadol)
- 替诺环定 (Tenocyclidine、
TCP)
- 1- (1- (2-塞吩) 环己烷基) 比
咯啶 (TCPY,1- (1- (2-thienyl)
cyclohexyl) pyrrolidine)
- 四氢大麻酚
(Tetrahydrocannabinol)
- 蒂巴康 (Thebacon)
- 蒂巴因 (Thebaine)
- 硫芬坦尼 (Thiofentanyl)
- 痛辛定 (Tilidine)
- 三甲氨基安非他命 (TMA)
- 屈美配立汀 (Trimeperidine)

第三级毒品 (民国105年3月25日版本)

(除特别规定外，皆包括其异构物Isomers、酯类Esters、醚类Ethers及盐类Salts)

中华民国《毒品危害防制条例》第4条：制造、运输、贩卖第三级毒品者，处5年以上有期徒刑，并科处新台币700万元以下罚金。

- N- (1-氨基-3-甲基-1-羰基丁烷-2-基) -1- (环己基甲基) -1H- 呋唑-3-羧酰胺 (N-(1-amino-3-methyl-1-oxobutan-2-yl)-1-(cyclohexylmethyl)-1H-indazole-3-carboxamide、AB-CHMINACA)
- 异戊巴比妥 (Amobarbital , 青发)
- 溴甲基卡西酮 (Bromomethcathinone、BMC)
- 四-溴-二,五-二甲氧基苯基乙基胺 (4-Bromo-2,5-dimethoxyphenethylamine、2C-B)
- 2-(4-溴-2,5-二甲氧基苯基)-N-(2-甲氧基苯甲基)乙胺 (2-[4-bromo-2,5-dimethoxyphenyl]N-[(2-methoxyphenyl)methyl]ethanamine、25B-NBOMe)
- 伯替唑他 (Brotizolam)

《删除，民国105年3月25日公告：改列第四级管制药品》

- 丁基原啡因 (Buprenorphine)
- 布他比妥 (Butalbital)
- 去甲麻黄碱 (Cathine)
- 氯安非他命 (Chloroamphetamine、1-Chlorophenylpropan-2-amine、1-Chlorophenyl-2-aminopropane、CA)
- 氯甲基卡西酮 (Chloromethcathinone、CMC)
- 可待因 (Codeine , Codeine preparation with a content more than 1.0 gram and less than 5.0 grams of codeine per 100 milliliters (or 100 grams))

修正：含量每100毫升（或100公克）1.0公克以上，未满5.0公克

- 2-[(1R,3S) -3-羟基环己基]-5-(2-甲基辛基-2-基)苯酚 (CP47,497、2-[(1R,3S) -3-hydroxycyclohexyl]-5-(2-methyloctan-2-yl) phenol)
- 环巴比妥 (Cyclobarbital)
- 二氢可待因 (Dihydrocodeine , Dihydrocodeine preparation with a content more than 1.0 gram and less than 5.0 grams of dihydrocodeine per 100 milliliters (or 100 grams))

- 一,一-双甲基庚基-11-羟基-四氢大麻酚 (1,1-Dimethylheptyl-11-hydroxy-tetrahydrocannabinol)
- 二-(三-甲氧基苯基)-2-乙胺环己酮 (2-〈3-methoxyphenyl〉-2-〈ethylamino〉 cyclohexanone、Methoxetamine、MXE)
- 一-(五-氟戊基)-三-(1-萘甲酰)吲哚 (AM-2201、1-[(5-fluoropentyl)-1H-indol-3-yl]-〈naphthalen-1-yl〉methanone)
- 一-(五-氟戊基)-三-(1-四甲基环丙基甲酰)吲哚 (1-[(5-fluoropentyl)-1H-indol-3-yl]2,2,3,3-tetramethylcyclopropyl)methanone、XLR-11)
- 氟甲基卡西酮 (Fluoromethcathinone、1-Fluorophenyl-2-methylaminopropan-1-one、FMC)
- 氟硝西泮 (Flunitrazepam , FM2)
- 格鲁米特 (Glutethimide)
- 一-戊基-三-(1-萘甲酰)吲哚 (JWH-018、Naphthalen-1-yl-〈1-pentylinol-3-yl〉methanone)
- 一-丁基-三-(1-萘甲酰)吲哚 (JWH-073、Naphthalen-1-yl-〈1-butylinol-3-yl〉methanone)
- 二-(二-甲氧基苯基)-1-(1-戊基-吲哚-3-基)乙酮 (JWH-250、2-〈2-methoxyphenyl〉-1-〈1-pentylinol-3-yl〉ethanone)
- 氯胺酮 (Ketamine , K仔、K他命、愷他命)
- 三,四-亚甲基双氧甲基卡西酮 (3,4-methylenedioxymethcathinone、Methylone、bk-MDMA)
- 三,四-亚甲基双氧-N-乙基卡西酮 (3,4-methylenedioxy-N-ethylcathinone、Ethylone)
- 四-甲基甲基卡西酮 (Mephedrone、4-methylmethcathinone)
- 一-戊基-3-(4-甲基-1-萘甲酰)吲哚 (〈4-methyl-1-naphthyl〉-〈1-pentylinol-3-yl〉methanone)
- 四-甲基乙基卡西酮 (4-Methylethcathinone、4-MEC)
- 派醋甲酯 (Methylphenidate)

- 纳布芬 (Nalbuphine)
- 《删除，民国105年3月25日公告：减列为非管制药品》
- 纳洛芬 (Nalorphine)
- 去甲羟吗啡酮 (Noroxymorphone)
- 硝甲西洋 (硝甲氮平 , Nimetazepam)
- 《修正，民国105年3月25日公告：改列第四级管制药品》
- 对-甲氧基乙基安非他命 (Paramethoxyethylamphetamine、4-Methoxy-N-ethylamphetamine、PMEA)
- 戊巴比妥 (Pentobarbital)
- 芬纳西洋 (Phenazepam)
- 苯甲吗林 (Phenmetrazine)
- 西可巴比妥 (Secobarbital , 红中)
- 特拉吗窦 (Tramadol)

《删除，民国105年3月25日公告：改列第四级管制药品》

- 三唑仑 (Triazolam)
- 三氟甲苯哌嗪 (1-〈3-trifluoromethylphenyl〉piperazine、TFMPP)
- 洁比普洛 (Zipeprol)

修正：含量每100毫升（或100公克）1.0公克以上，未满5.0公克

第四级毒品（民国105年3月25日版本）

（包括毒品先驱原料，除特别规定外，皆包括其异构物Isomers、酯类Esters、醚类Ethers及盐类Salts）

中华民国《毒品危害防制条例》第四条：制造、运输、贩卖第四级毒品者，处1年以上7年以下有期徒刑，并科新台币300万元以下罚金。

- 5-甲氧基-N,N-二异丙基色胺 (5-MeO-DIPT , 5-methoxy-N,N-diisopropyltryptamine)
- 二丙烯基巴比妥 (Allobarbital)
- 阿普唑他 (Alprazolam)
- 二乙胺苯丙酮 (Amfepramone)
- 阿米雷斯 (Aminorex)
- 巴比妥 (Barbital)
- 甲苯异丙胺 (Benzphetamine)
- 溴西洋 (溴氮平 , Bromazepam)
- 伯替唑他 (Brotizolam)
- 丁巴比妥 (Butobarbital)
- 美妥芬诺 (Butorphanol)
- 卡吗西洋 (卡氮平 , Camazepam)
- 氯二氮平 (Chlordiazepoxide)
- 氯巴占 (甲酮氮平 , Clobazam)
- 氯苄雷司 (Cllobenzorex)
- 氯硝西洋 (可那氮平、氯硝氮平 , Clonazepam)
- 氯拉酸 (氯氮平酸盐 , Clorazepate)
- 氯西洋 (氯氮平 , Clotiazepam)
- 氯噁唑他 (氯唑仑 , Cloxazolam)
- 可待因 (Codeine) 内服液 (含糖浆剂) 含量每100毫升未满1.0公克之医师处方用药
- 地洛西洋 (地洛氮平 , Delorazepam)
- 右旋普帕西芬复方制剂 (Dextropropoxyphene Mixture Preparation)
- 安定 (二氮平 , Diazepam)
- 麻黄碱 (Ephedrine)
- 麦角新碱 (Ergometrine、Ergonovine)
- 麦角胺碱 (Ergotamine)

- 舒乐安定 (伊叠唑仑 , Estazolam)
- 乙氯维诺 (乙氯烯醇) (Ethchlorvynol)
- 炔己蚁胺 (环己炔胺 , Ethinamate)
- 氟氮平酸酯 (Ethyl loflazepate)
- 芬坎法明 (苯莰甲胺 , Fencamfamin)
- 芬普雷司 (氰乙基安非他命 , Fenproporex)
- 氟地西洋 (氟二氮平 , Fludiazepam)
- 氟安定 (氟路洛 , Flurazepam)
- 哈拉西洋 (三氟氮平 , Halazepam)
- 卤噁唑他 (卤唑仑 , Haloxazolam)
- 凯他唑他 (酮唑仑 , Ketazolam)
- 勒非他命 (二甲二苯乙胺 , Lefetamine、1-dimethylamino-1,2-diphenylethane、SPA)
- 氯普唑他 (氯唑仑 , Loprazolam)
- 劳拉西洋 (乐耐平 , Lorazepam)
- 氯甲西洋 (甲基乐耐平 , Lormetazepam)
- 麦角酸 (Lysergic acid)
- 吗 (咪唑 , Mazindol)
- 美达西洋 (美达氮平 , Medazepam)
- 美芬雷司 (Mefenorex)
- 甲丙氨酯 (美普巴迈 , Meprobamate)
- 美舒卡 (Mesocarb)
- 甲基苯巴比妥 (Methylphenobarbital、Mephobarbital)
- 甲乙啶酮 (甲乙啶酮 , Methyprylon)
- 咪达唑他 (咪氟唑仑 , Midazolam)
- 美服培酮 (Mifepristone)
- 莫待芬宁 (Modafinil)
- 硝甲西洋 (硝甲氮平) (Nimetazepam)
- 硝西洋 (耐妥眠 , Nitrazepam)
- 去甲西洋 (原氮平 , Nordiazepam)
- 鸦片 (Opium) 复方制剂含量每100毫升 (或100公克) 0.5公克以上
- 去甲羟安定 (欧沙氮平、去甲羟氮平 , Oxazepam)
- 噻唑他 (甲唑仑 , Oxazolam)
- 匹吗 (苯唑 , Pemoline)
- 苯双甲吗 (二苯甲吗 , Phendimetrazine)
- 苯巴比妥 (Phenobarbital)
- 甲基苯乙基胺 (二甲苯乙胺 , Phentermine)
- 二氢可待因内服液 (Physician prescribes Dihydrocodeine oral liqu-id [including syrup] , 含糖浆剂) 含量每100毫升未满1.0公克之医师处方用药
- 四那西洋 (丙炔氮平 , Pinazepam)
- 苯甲醇 (苯甲醇 , Pipradrol)
- 普拉西洋 (环丙氮平 , Prazepam)
- 丙泊酚 (Propofol , 牛奶针)
- 丙已君 (普西卓林、甲环乙胺 , Propylhexedrine)
- 焦二异丁基酮 (焦洛戊酮 , Pyrovalerone)
- 仲丁比妥 (Secbutabarbital、Butabarbital)
- 替马西洋 (羟二氮平、甲羟氮平 , Temazepam)
- 四氢西洋 (四氢二氮平 , Tetrazepam)
- 特拉吗窦 (Tramadol)
- 硫美妥 (Thiamylal , 5-allyl-5-(1-methylbutyl)-2-thiobarbiturate)
- 乙烯比妥 (乙烯丁巴比妥) (Vinylbital)
- 札来普隆 (Zaleplon)
- 佐匹克隆 (Zopiclone)
- 佐沛眠 (Zolpidem)

中华人民共和国

中华人民共和国《中华人民共和国禁毒法》第三条规定：禁毒是全社会的共同责任。国家机关、社会团体、企业事业单位以及其他组织和公民，应当依照本法和有关法律的规定，履行禁毒职责或者义务。

《中华人民共和国禁毒法》第四条规定：禁毒工作实行预防为主，综合治理，禁种、禁制、禁贩、禁吸并举的方针。禁毒工作实行政府统一领导，有关部门各负其责，社会广泛参与的工作机制。

有关毒品犯罪的刑事规范，系中华人民共和国刑法第三百四十七条至第三百五十七条，名为“走私、贩卖、运输、制造毒品罪”

中华人民共和国国家食品药品监督管理局（2008年机构改革并入卫生部）、中华人民共和国公安部、中华人民共和国卫生部联合颁布《中华人民共和国关于公布麻醉药品和精神药品品种目录（2007年版）的通知》，根据《麻醉药品和精神药品管理条例》第三条的规定，于2007年10月11日公布《麻醉药品品种目录（2007年版）》和《精神药品品种目录（2007年版）》，自2008年1月1日起施行。（详见下表显示）

麻醉药品品种目录（2007年版）

- 醋托啡 (Acetorphine)
- 乙酰阿法甲基芬太尼
(Acetylalphamethylfentanyl)
- 醋美沙朵 (Acetylmethadol)
- 阿芬太尼 (Alfentanil)
- 烯丙罗定 (Allylprodine)
- 阿醋美沙朵
(Alphacetylmethadol)
- 阿法美罗定 (Alphameprodine)
- 阿法美沙朵 (Alphamethadol)
- 阿法甲基芬太尼
(Alphamethylfentanyl)
- 阿法甲基硫代芬太尼
(Alphamethylthiofentanyl)
- 阿法罗定* (Alphaprodine)
- 阿尼利定 (Anileridine)
- 苯替啶 (Benzethidine)
- 苯吗啡 (Benzmorphine)
- 倍醋美沙朵
(Betacetylmethadol)
- 倍他羟基芬太尼
(Betahydroxyfentanyl)
- 倍他羟基-3-甲基芬太尼
(Betahydroxy-3-methylfentanyl)
- 倍他美罗定 (Betameprodine)
- 倍他美沙朵 (Betamethadol)
- 倍他罗定 (Betaprodine)
- 贝齐米特 (Bezitramide)
- 大麻与大麻树脂 (Cannabis and Cannabis resin)
- 氯尼他秦 (Clonitazene)
- 古柯叶 (Coca Leaf)
- 可卡因* (Cocaine)
- 可多克辛 (Codoxime)
- 罂粟秆浓缩物* (Concentrate of poppy straw)
- 地索吗啡 (Desomorphine)
- 右吗拉胺 (Dextromoramide)
- 地恩丙胺 (Diampromide)
- 二乙噻丁
(Diethylthiambutene)
- 地芬诺辛 (Difenoxin)
- 二氢埃托啡*
(Dihydroetorphine)
- 双氢吗啡 (Dihydromorphine)
- 地美沙朵 (Dimenoxadol)
- 地美庚醇 (Dimepheptanol)
- 二甲噻丁
(Dimethylthiambutene)
- 吗苯丁酯 (Dioxaphetyl butyrate)
- 地芬诺酯* (Diphenoxylate)
- 地匹哌酮 (Dipipanone)
- 羟蒂巴酚 (Drotebanol)

- 芽子碱 (Egonine)
- 乙甲噻丁
(Ethylmethylthiambutene)
- 依托尼秦 (Etonitazene)
- 埃托啡 (Etorphine)
- 依托利定 (Etoxeridine)
- 芬太尼* (Fentanyl)
- 呋替啶 (Furethidine)
- 海洛因 (Heroin)
- 氢可酮* (Hydrocodone)
- 氢吗啡醇 (Hydromorphonol)
- 氢吗啡酮 (Hydromorphone)
- 羟哌替啶 (Hydroxypethidine)
- 异美沙酮 (Isomethadone)
- 凯托米酮 (Ketobemidone)
- 左美沙芬 (Levomethorphan)
- 左吗拉胺 (Levomoramide)
- 左芬啡烷
(Levophenacylmorphan)
- 左啡诺 (Levorphanol)
- 美他佐辛 (Metazocine)
- 美沙酮* (Methadone)
- 美沙酮中间体 (Methadone intermediate)
- 甲地索啡 (Methyldesorphine)
- 甲二氢吗啡
(Methyldihydromorphine)
- 3-甲基芬太尼 (3-methylfentanyl)
- 3-甲基硫代芬太尼 (3-methylthiofentanyl)
- 美托酮 (Metopon)
- 吗拉胺中间体 (Moramide intermediate)
- 吗哌利定 (Morpheridine)
- 吗啡* (Morphine)
- 吗啡甲溴化物及其它五价氮吗啡衍生物 (Morphine Methobromide)
- 吗啡-N-氧化物 (Morphine-N-oxide)
- 1-甲基-4-苯基-4-哌啶丙酸酯 (MPPP)
- 麦罗啡 (Myrophine)
- 尼可吗啡 (Nicomorphine)
- 诺美沙朵 (Noracymethadol)
- 去甲左啡诺 (Norlevorphanol)
- 去甲美沙酮 (Normethadone)
- 去甲吗啡 (Normorphine)
- 诺匹哌酮 (Norpipanone)
- 阿片* (Opium)
- 羟考酮* (Oxycodone)
- 羟吗啡酮 (Oxymorphone)
- 对氟芬太尼
(Parafluorofentanyl)
- 1-苯乙基-4-苯基-4-哌啶乙酸酯 (PEPPAP)
- 哌替啶* (Pethidine)
- 哌替啶中间体A (Pethidine intermediate A)
- 哌替啶中间体B (Pethidine intermediate B)
- 哌替啶中间体C (Pethidine intermediate C)
- 苯吗庚酮 (Phenadoxone)
- 非那丙胺 (Phenampromide)
- 非那佐辛 (Phenazocine)
- 非诺啡烷 (Phenomorphan)
- 苯哌利定 (Phenoperidine)
- 匹米诺定 (Piminodine)
- 哌替米特 (Piritramide)
- 罂粟壳* (Poppy Shell)
- 普罗庚嗪 (Proheptazine)
- 丙哌利定 (Properidine)
- 消旋甲啡烷
(Racemethorphan)
- 消旋吗拉胺 (Racemoramide)
- 消旋啡烷 (Racemorphan)
- 瑞芬太尼* (Remifentanil)
- 舒芬太尼* (Sufentanil)
- 醋氢可酮 (Thebacon)
- 蒂巴因* (Thebaine)
- 硫代芬太尼 (Thiofentanyl)
- 替利定 (Tilidine)
- 三甲利定 (Trimeperidine)
- 醋氢可待因
(Acetyldihydrocodeine)
- 布桂嗪* (Bucinnazine)
- 可待因* (Codeine)
- 复方樟脑酊* (Compound Camphor Tincture)
- 右丙氧芬*
(Dextropropoxyphene)
- 双氢可待因*
(Dihydrocodeine)
- 乙基吗啡* (Ethylmorphine)
- 尼可待因 (Nicocodeine)
- 尼二氢可待因 (Nicodicodine)
- 去甲可待因 (Norcodeine)
- 福尔可定* (Pholcodine)
- 丙吡兰 (Propiram)
- 阿桔片* (Compound Platycodon Tablets)
- 吗啡阿托品注射液* (Morphine and Atropine Sulfate Injection)

注：1.上述品种包括其可能存在的盐和单方制剂 2.上述品种包括其可能存在的化学异构体及酯、醚 3.品种目录有*的麻醉药品为中华人民共和国生产及使用的品种

精神药品品种目录 (2007年版)

第一类

- 布苯丙胺
(Brolamfetamine (DOB))
- 卡西酮 (Cathinone)
- 二乙基色胺 (DET)
- 二甲氧基安非他明 (2,5-dimethoxyamphetamine, DMA)
- 羟基四氢甲基二苯吡喃
(DMHP)
- 二甲基色胺 (DMT)
- 二甲氧基乙基安非他明
(DOET)
- 乙环利定 (Eticyclidine)
- 乙色胺 (Eryptamine)
- 麦角二乙胺 (Lysergide)
- 二亚甲基双氧安非他明
(MDMA)
- 麦司卡林 (Mescaline)
- 甲卡西酮 (Methcathinone)
- 甲米雷司 (4-methylaminorex)
- 甲羟芬胺 (MMDA)
- 乙芬胺 (N-ethyl,MDA)
- 羟芬胺 (N-hydroxy, MDA)
- 六氢大麻酚 (Parahexyl)
- 副甲氧基安非他明
(Paramethoxyamphetamine, PMA)
- 赛洛新 (Psilocine)
- 赛洛西宾 (Psilocybine)
- 咯环利定 (Rolicyclidine)
- 二甲氧基甲苯异丙胺 (STP , DOM)
- 替苯丙胺 (Tenamfetamine, MDA)
- 替诺环定 (Tenocyclidine)
- 四氢大麻酚 (Tetrahydrocannabinol)
- 三甲氧基安非他明 (TMA)
- 4-甲基硫基安非他明 (4-methylthioamphetamine)
- 苯丙胺 (Amphetamine)
- 安非拉酮 (Amfepramone)
- 安咪奈丁 (Amineptine)
- 2,5-二甲氧基-4-溴苯乙胺 (4bromo-2,5-dimethoxyphenethylamine (2-CB))
- 丁丙诺啡* (Buprenorphine)
- 右苯丙胺 (Dexamphetamine)
- 二甲基安非他明
(Dimethylamphetamine)
- 芬乙茶碱 (Fenetylline)
- γ -羟丁酸 (γ -hydroxybutyrate, GHB)
- 氯胺酮 (K粉, Ketamine)
- 左苯丙胺
(Levamphetamine)
- 左甲苯丙胺
(Levomethamphetamine)
- 马吲哚* (Mazindol)
- 甲氯喹酮 (Mecloqualone)
- 去氧麻黄碱
(Metamfetamine)
- 去氧麻黄碱外消旋体
(Metamphetamine Racemate)
- 甲喹酮 (Methaqualone)
- 呓醋甲酯*
(Methylphenidate)
- 莫达非尼 (Modafinil)
- 苯环利定 (Phencyclidine)
- 芬美曲秦 (Phenmetrazine)
- 司可巴比妥*
(Secobarbital)
- δ -9-四氢大麻酚 (Delta-9-tetrahydrocannabinol)
- 三唑仑* (Triazolam)
- 齐培丙醇 (Zipeprol)

第二类

- 异戊巴比妥* (Amobarbital)
- 布他比妥 (Butalbital)
- 布托啡诺及其注射剂* (Butorphanol)
- 咖啡因* (Caffeine)
- 安钠咖* (Caffeine Sodium Benzoate,CNB)
- 去甲伪麻黄碱* (Cathine)
- 环己巴比妥 (Cyclobarbital)
- 地佐辛及其注射剂* (Dezocine)
- 右旋芬氟拉明 (Dexfenfluramine)
- 芬氟拉明* (Fenfluramine)
- 氟硝西洋 (Flunitrazepam)
- 格鲁米特* (Glutethimide)
- 呋芬雷司 (Furfennorex)
- 喷他佐辛* (Pentazocine)
- 戊巴比妥* (Pentobarbital)
- 丙己君 (Propylhexedrine)
- 阿洛巴比妥 (Allobarbital)
- 阿普唑仑* (Alprazolam)
- 阿米雷司 (Aminorex)
- 巴比妥* (Barbital)
- 苯非他明 (Benzphetamine)
- 溴西洋* Bromazepam
- 溴替唑仑 (Brotizolam)
- 丁巴比妥 (Butobarbital)
- 卡马西洋 (Camazepam)
- 氯氮卓* (Chlordiazepoxide)
- 氯巴占 (Clobazam)

- 氯硝西洋* (Clonazepam)
- 氯拉卓酸 (Clorazepate)
- 氯噻西洋 (Clotiazepam)
- 氯口恶唑仑 (Cloxazolam)
- 地洛西洋 (Delorazepam)
- 地西洋* (Diazepam)
- 艾司唑仑* (Estazolam)
- 乙氯维诺 (Ethchlorvynol)
- 炔己蚁胺 (Ethinamate)
- 氯氟卓乙酯* (Ethyl Loflazepate)
- 乙非他明 (Etilamfetamine)
- 芬坎法明 (Fencamfamin)
- 芬普雷司 (Fenproporex)
- 氟地西洋 (Fludiazepam)
- 氟西洋* (Flurazepam)
- 哈拉西洋 (Halazepam)
- 卤沙唑仑 (Haloxazolam)
- 凯他唑仑 (Ketazolam)
- 利非他明 (Lefetamine)
- 氯普唑仑 (Loprazolam)
- 劳拉西洋* (Lorazepam)
- 氯甲西洋 (Lormetazepam)
- 美达西洋 (Medazepam)
- 美芬雷司 (Mefenorex)
- 甲丙氨酯* (Meprobamate)
- 美索卡 (Mesocarb)
- 甲苯巴比妥 (Methylphenobarbital)
- 甲乙哌酮 (Methyprylon)
- 咪达唑仑* (Midazolam)
- 纳布啡及其注射剂* (Nalbuphine)
- 尼美西洋 (Nimetazepam)
- 硝西洋* (Nitrazepam)
- 去甲西洋 (Nordazepam)
- 奥沙西洋* (Oxazepam)
- 奥沙唑仑 (Oxazolam)
- 氨酚氢可酮片* (Paracetamol and Hydrocodone Bitartrate Tablets)
- 匹莫林* (Pemoline)
- 苯甲曲秦 (Phendimetrazine)
- 苯巴比妥* (Phenobarbital)
- 芬特明 (Phentermine)
- 匹那西洋 (Pinazepam)
- 呓苯甲醇 (Pipradrol)
- 普拉西洋 (Prazepam)
- 吡咯戊酮 (Pyrovalerone)
- 仲丁比妥 (Secbutabarbital)
- 替马西洋* (Temazepam)
- 四氢西洋 (Tetrazepam)
- 曲马多* (Tramadol)
- 乙烯比妥 (Vinylbital)
- 哒吡坦* (Zolpiden)
- 扎来普隆* (Zaleplone)
- 麦角胺咖啡因片 (Ergotamine and Caffeine Tablets)

注：1.上述品种包括其可能存在的盐和单方制剂（除非另有规定） 2.上述品种包括其可能存在的化学异构体及酯、醚（除非另有规定） 3.品种目录有*的精神药品为中华人民共和国生产及使用的品种

其他国家

[5]

相关言论

倡导者

- 佛洛依德将可卡因作为一医疗用药物，但他在缺乏证据下宣称可卡因无害，并造成好友深染毒瘾。
- 连横与其妻皆为日据台湾政府登记的阿民（即有吸食鸦片瘾的人民），连横并曾在台湾日日新报上撰写“《鸦片有益论》”，造成其在台湾汉文界无法立足而远奔中国大陆。

成瘾性

- 朱学恒分享其和社工洽谈的经验，毒品循环会迫使毒品使用人重复的偷、骗、抢金钱，并让身旁的家人及亲友对其失去信心，最后远离这些人。[6]

管制药品合法化争论(部分药物)

品种合法化

- 目前世界各地都有毒品合法化的争论，其中在全世界几乎是合法毒品的有烟草及酒精，而大麻在有些国家也是等同合法。
- 供应毒性较低的毒品予以成瘾者比较没有争议，最主要的例子是利用尼古丁贴片或口香糖来协助戒烟（相较于香烟的其他成分，尼古丁虽然成瘾性强，但对身体的伤害少一些）及利用美沙酮替代海洛因。
- 毒品的合法与否，其实跟近代当权者及主流社会是否使用有关，社会边缘人使用的都很容易被列为毒品，而主流社会及当权者会使用的烟酒就不会被列为毒品。要禁止鸦片的阻力就很小，因为当初喜好吸食鸦片的华裔在西方国家是边缘人，而亚洲的华人掌权者也都认为鸦片该禁绝。

管制下的合法化

- 争论的内容除了是否合法外（例如大麻），也有使用场合的争论（例如烟草）。
- 其中大麻引起最多争议，一直有大麻的伤害是否比烟酒轻微的争论。有些人认为大麻比烟草安全（但也有人指出吸大麻烟对身体的伤害比吸烟大^[7]），也有一些人表示大麻会伤害脑袋（但也有人指出酒精也会伤害脑袋），也有人以统计数据指出吸大麻者容易尝试更危险的毒品（但也有人认为大麻合法化可以有效减少这问题）。
- 许多研究结果显示，对于一些疾病的治疗，大麻的副作用比起许多合法药物只低不高（前提是不采用吸烟的方式吸食大麻）。
- 也有人指出，毒品所造成的问题中，有一部分必须归咎于将毒品视为非法的后果，如果毒品合法化并善加管理，则问题会少很多。（如颁布禁酒令反而会帮助黑帮、也会增加假酒，应该只针对酒驾及酗酒等有害行为禁止及辅导）持这种主张的包括诺贝尔经济学奖得主盖瑞·贝克。^[8]
- 烟草一直是一种高成瘾性、又会伤害旁人的毒品，可是因为大量的使用者而使得管制严格程度远低于其害处，香烟因此而成为全世界伤害性最强的毒品；好消息是近来美国主流社会、高学历者及当权者的抽烟率已经大降，烟草已经渐渐的成为边缘人才在用的毒品，因此对于烟草的限制已经越来越严格。不过相反的，吸大麻的人反而比抽烟的多。
- 荷兰可以合法拥有少量毒品。荷兰对消费和持有大麻的政策可追溯到1976年。当时，荷兰把毒品分为硬毒品和软毒品。硬毒品如海洛因、可卡因和安非他命，它们对公众健康构成难以承受的威胁；软毒品如大麻。这一政策的目的是向人们提供一个有管理的出口，减少人们接触街头软硬毒品贩的机会。起初，人们可以合法拥有30克以内的大麻。现在，荷兰有关毒品的法律中允许吸食者合法拥有5克毒品。^[9]

流行文化取材

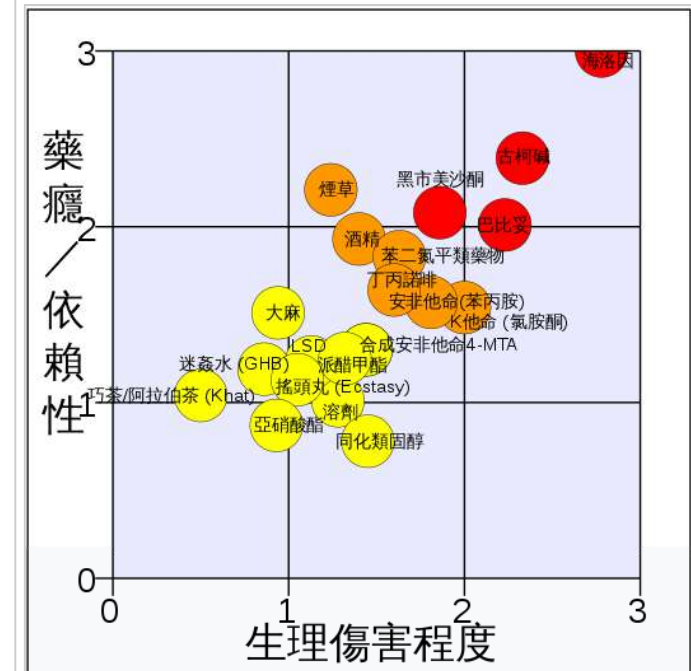
中华民国(台湾)

- 周杰伦 - 懦夫
- MC Hotdog - 毒

香港

于香港，有不少歌曲均和毒品有关，但大多对毒品作负面态度。

- 2007年电影《门徒》
- 2013年电影《扫毒》
- 2012年电视剧《雷霆扫毒》
- 陈秋霞 - 〈罂粟花〉



上图可以显示，合法毒品烟 (tabacco) 酒 (alcohol) 的伤害性及成瘾性其实不低。资料来自权威医学期刊：The Lancet。（纵轴是成瘾性、横轴是伤害性）

- RAIDAS - 〈危险游戏〉
- ZEN - 〈十字架〉
- 黄耀明 - 〈擢命舞〉
- 陈百强 - 〈摘星〉
- 软硬天师 - 〈十四号天空城〉
- 卫兰 - 〈999〉
- 农夫 - 〈不不不〉
- 农夫 - 〈天造之材〉

中国大陆

- 中国第一部禁毒题材电影：《白粉妹》（张良导演，刘薇、陈志坚主演，珠江电影制片厂1995年摄制）
- 1997年电视剧《红处方》
- 2013年电影《毒战》

美国

- Morphine (歌曲) - 迈克尔杰克逊
- 药命效应 - 电影
- 单身毒妈 - 电视剧
- 绝命毒师 - 电视剧
- Narcos 毒枭 - 电视剧

相关条目

- 精神转换药物 (psychedelic)
- 放心药
- 桃园县毒品危害防制中心
- 软性毒品

参考文献

1. 《中华人民共和国刑法》第三百五十七条
2. Reliable, non-judgmental information about psychoactive plants and chemicals and related issues (<http://www.erowid.org/splash.php>)
3. 朝鲜毒品攻陷东三省. 共识网. 2011-12-08. (原始内容存档于2016-03-04).
4. 台湾在2007年7月曾经发生2天之内9名减刑之毒犯因吸毒过量致命的事件，减刑第二天全台9毒贩吸毒暴毙-TVBS (http://www.gclub.com.tw/news/news_list.asp?no=aj100920070718180650)
5. 新毒品Spice肆虐英国 吸食者如行尸走肉-北京时间 (<http://item.btime.com/36bplq2u42h9le97v63hfff9nqo?from=mini>)
6. 真相总是伤人：毒品循环是如何运作的 - 东网即时 (http://tw.on.cc/tw/bkn/cnt/commentary/20160413/mobile/bkntw-20160413000522067-0413_04411_001.html)
7. <http://www.epochtimes.com/b5/6/3/27/n1267689.htm>
8. 1992年诺贝尔经济学奖得主盖瑞·贝克，提出使毒品合法化作为毒品问题的解决之道。贝克教授在他的文章《越来越多人能够接受毒品合法化的想法了》以及《应该让毒品的使用合法化吗》中，用美国当初以修改宪法的方式来结束禁酒政策的做法类比，认为应该沿用解除禁酒令的模式，让毒品的使用合法化。同时，再利用课税和重罚双管齐下的办法，将吸毒控制在可以接受的范围。《毒品合法化悖论--质疑毒品交易市场化理论》，<http://news.sohu.com/67/35/news145713567.shtml>
9. <http://news.sina.com.cn/w/2008-07-02/132115858158.shtml>

外部链接

- 中华人民共和国主席令第七十九号 (http://www.gov.cn/flfg/2007-12/29/content_847311.htm)
- 行政院卫生署管制药品管理局 (<http://cdmis.fda.gov.tw/>)
- 中华民国行政院 民国105年3月26日院台卫字第1040014011号公告.管制药品分级及品项 (<http://www.fda.gov.tw/tc/includes/GetFile.ashx?id=1100&chk=b105df22-6bda-473c-8da8-aeoe84d703b3&mid=46&name=fContent>)

- 戒毒资讯网（中华民国）(<http://refrain.moj.gov.tw/html/index.php>)
- 保安局禁毒处（香港）(<http://www.nd.gov.hk/>)
- 地图会说话-鸦片 (<http://blog.pixnet.net/Richter/post/18604152>)
- 常见的毒品介绍 (<http://drug.faceteen.org>)
- 上瘾五百年 (<http://www.books.com.tw/exep/prod/booksfile.php?item=0010199831>) (书)

取自“<https://zh.wikipedia.org/w/index.php?title=毒品&oldid=44589793>”

- 本页面最后修订于2017年6月1日 (星期四) 14:48。
- 本站的全部文字在知识共享 署名-相同方式共享 3.0协议之条款下提供，附加条款亦可能应用（请参阅使用条款）。Wikipedia®和维基百科标志是维基媒体基金会的注册商标；维基™是维基媒体基金会的商标。维基媒体基金会是在美国佛罗里达州登记的501(c)(3)免税、非营利、慈善机构。

多巴胺

维基百科, 自由的百科全书

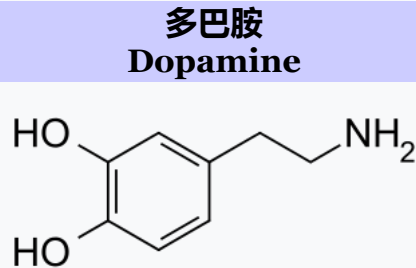
多巴胺 (英语 : **dopamine**, 摄取自3,4-dihydroxyphenethylamine) ; 化学式 : $C_6H_3(OH)_2-CH_2-CH_2-NH_2$) 是一种脑内分泌物, 属于神经递质, 可影响一个人的情绪。

它正式的化学名称为4-(2-乙胺基)苯-1,2-二酚, 简称“DA”。阿尔维德·卡尔森确定多巴胺为脑内信息传递者的作用, 这使他赢得了2000年诺贝尔医学奖。

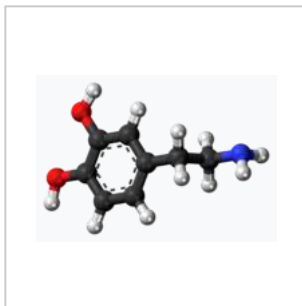
多巴胺是儿茶酚胺和苯乙胺家族中一种在脑和身体中扮演几个重要作用的有机化学物。其名称来自其化学结构: 它是一个胺由其前体一个分子L-DOPA除去羧基合成, 其发生在人脑细胞和肾上腺细胞中。在大脑中多巴胺作为神经递质, 通过神经元释放一种化学物将信号发送到其它神经细胞。大脑包括几个不同的多巴胺途径, 其中一个起著奖励-激励行为的主要作用。大多数类型的奖励增加多巴胺在脑中的浓度, 大部分成瘾药物增加多巴胺神经元活动。其他的脑多巴胺用来参与运动控制和控制各种激素的释放。

神经系统以外, 在身体的几个部分多巴胺作为局部化学信使的功能。在血管中它抑制去甲肾上腺素的释放, 并作为血管扩张剂(在正常浓度下); 在肾脏中它增加钠和尿的排泄; 在胰脏中它减少胰岛素生产; 在消化系统中它减少胃肠蠕动和保护肠粘膜; 并在免疫系统中它减少淋巴细胞的活性。血管除外, 多巴胺在这些外围系统局部合成, 在邻近该释放它的细胞旁发挥其作用。

几个重要的神经系统疾病与多巴胺系统的功能障碍有关, 而使用一些改变多巴胺作用的关键药物来治疗他们。帕金森氏病一种退行性状况引起身体震颤和运动障碍, 是通过中脑中称为黑质区的分泌神经元分泌多巴胺不足所引起。其代谢前体L-DOPA可以工业制造, 其纯销售形式为左旋多巴是最广泛使用的治疗方法。有证据表明精神分裂症涉及多巴胺活性水平的改变, 大多数经常使用的抗精神病药物具有降低多巴胺活动的主要效果。类似多巴胺拮抗剂药物, 也有一些是最有效抗恶心药物。不宁腿综合征与注意力不足过动症与多巴胺活性降低有关。高剂量多巴胺兴奋剂可以上瘾, 但也有一些使用较低剂量治疗过动症。多巴胺本身可制造成静脉注射的药物: 虽然不能从血液到达脑部, 其周边作用使其对心脏衰竭或休克的治疗是有用的, 尤其是对新生婴儿。



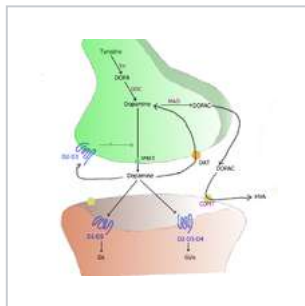
IUPAC名	4-(2-Aminoethyl)benzene-1,2-diol
同义词	2-(3,4-Dihydroxyphenyl)ethylamine; 3,4-Dihydroxyphenethylamine; 3-hydroxytyramine; Intropin; Revivan; Oxytyramine; Prolactin inhibiting factor; Prolactin inhibiting hormone
缩写	DA
源	substantia nigra; ventral tegmental area; many others
靶	system-wide
受体	D1; D2; D3; D4; D5
激动剂	cocaine; amphetamines; apomorphine; bromocryptine
拮抗剂	neuroleptics, metoclopramide
前体	L-DOPA
合成酶	DOPA decarboxylase
代谢酶	MAO; COMT
数据库链接	
CAS注册号	51-61-6 ✓ 62-31-7 (https://tools.wmflabs.org/magnustools/cas.php?language=en&cas=62-31-7&title=) (hydrochloride)
PubChem	CID: 681
DrugBank	DBoo988 ✓
ChemSpider	661 ✓
KEGG	Do7870 ✓



多巴胺



TAAR1



多巴胺在神经突触处

目录

- 1 简介
- 2 结构
- 3 生物化学
 - 3.1 分类
 - 3.2 释放与降解
- 4 主要多巴胺通道
- 5 多巴胺与思觉失调症
- 6 历史与发展
- 7 参见
- 8 参考文献
 - 8.1 引用
 - 8.2 来源
- 9 外部链接

简介

多巴胺是一种用来帮助细胞传送脉冲的化学物质，为神经传导物质的一种。这种传导物质主要负责大脑的情欲，感觉，将兴奋及开心的信息传递，也与上瘾有关。

爱情的感觉对应到生化层次，和脑里产生大量多巴胺起的作用有关。

吸烟和吸毒都可以增加多巴胺的分泌，使上瘾者感到开心及兴奋。多巴胺传递开心、兴奋情绪的这功能，医学上被用来治疗抑郁症。

多巴胺不足或失调则会令人失去控制肌肉的能力、或是导致注意力无法集中。失去控制肌肉能力，在严重时会导致手脚不自主地颤动、乃至罹患帕金森病。

当我们积极做某事时，脑中会非常活跃的分泌出大量多巴胺。它是一种使人类引起欲望的大脑神经递质，但**多巴胺分泌过量会过度消耗体力和热量，导致早死。**

极端情形如亨丁顿舞蹈症，是多巴胺分泌过多而导致的疾病，患者的四肢和躯干会如舞蹈般不由自主地抽动，造成日常行动不便，疾病发展到晚期，病人的生活将无法自理，失去行动能力，无法说话，容易噎到，甚至无法进食。

多巴胺最常被使用的形式为盐酸盐，为白色或类白色有光泽的结晶，无臭，味微苦。露置空气中及遇光后色渐变深。在水中易溶，在无水乙醇中微溶，在氯仿或乙醚中极微溶解。熔点243°C-249°C (分解)。

多巴胺在人体的功能可分为神经系统内与神经系统外两个部分。

多巴胺在脑的功能中，在运动控制、动机、唤醒、认知、奖励的功能上扮演重要角色，还与一些更基础的功能相关，例如哺乳、性欲、恶心。多巴胺类的神经元在人脑中的含量约有400,000个，其实是相对的少，并且只有在少数区域存在，但是却投射到很多脑区，并能引起有很强大的功用。这些神经元最早在1964年由Annica Dahlström和Kjell Fuxe标绘出来，并给予这些区域A开头的名字。在他们的模型中，A1-A7区包含正肾上腺素，A8-A14则包含多巴胺。以下是他们辨认出来包含多巴胺的区域：

- 黑质是中脑中一小块形成基底核的区域，其中多巴胺神经元多在黑质的致密部（A8）和其周遭（A9）被发现，和运动控制相关，若有失去大部分此区域的多巴胺神经元，会导致帕金森病。
- 腹侧被盖区（A10）则是另一块属于中脑的区域，是人脑中最多多巴胺神经元的地方，但实际上此区域仍然是非常的小。此区域的多巴胺神经元投射到伏核、前额叶皮质等其他区域，主要和奖励、动机的功能相关。
- 下视丘后叶也有一些多巴胺神经元（A11），投射到脊髓，但功能并不是很清楚。
- 弓形核（A12）和脑室旁核（A14）都在下视丘，这些多巴胺神经元投射到脑垂腺前叶，透过中央联合的循环组织，抑制催乳激素释放细胞分泌催乳激素。通常说到这里的调控时，多巴胺时常被称为催乳素抑制因子、抑制催乳激素贺尔蒙、催乳激素抑制素。
- 一样是在下视丘，不定区（A13）的多巴胺神经元则参与性腺激素释放激素的控制。
- 还有多巴胺神经元位在视网膜，被称为无轴突细胞，在日光的刺激下会活化，释放多巴胺致细胞外基质中，相对的，在夜晚就会沈寂下来。这些视网膜中的多巴胺能够抑制杆细胞而提升锥细胞的功能，最后产生对颜色敏感、并增加对比的效果，而其代价是在光线昏暗时便会降低其敏感度。

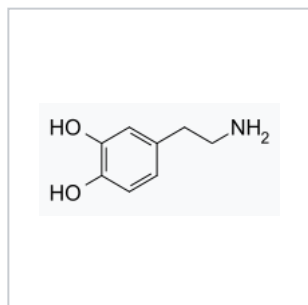
在神经系统外，在周边，多巴胺也在局限的区域透过外分泌或旁分泌产生功能：

- 首先是免疫系统，尤其是淋巴球，能够制造并分泌多巴胺，其功能主要是抑制淋巴球的活性，但此系统的功能为何还并不是很清楚。
- 肾的小管细胞能分泌多巴胺，且肾有许多细胞能表现多种多巴胺受器，多巴胺在此能增加肾的灌流、提高肾丝球的过滤，并增加钠离子的排泄。当肾部的多巴胺功能缺失时（可能肇因于高血压或基因的问题），会导致钠离子的排泄减少，造成高血压。
- 胰脏也可以分泌多巴胺（外分泌），其功能可能与保护肠道的黏膜和降低尝胃道蠕动相关，但还并不是很确定。
- 胰脏的胰岛也和多巴胺相关，有证据显示胰岛的 β 细胞制造胰岛素时，也会制造多巴胺受器，这些受器受到多巴胺作用的结果是降低胰岛素的释放，但这些多巴胺的来源还没有厘清的很清楚。

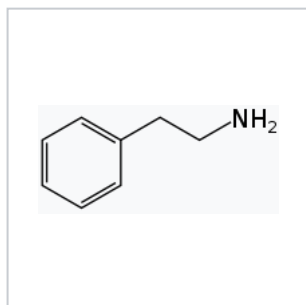
结构

多巴胺分子由儿茶酚结构(一个苯环与两个羟基侧基)经由乙基链连接一个胺基的。因此多巴胺可能是最简单的儿茶酚胺类家族，包括神经递质去甲肾上腺素和肾上腺素。存在一个苯环与胺连接，使得它取代的苯乙胺家族，其中包括大量的精神药物。

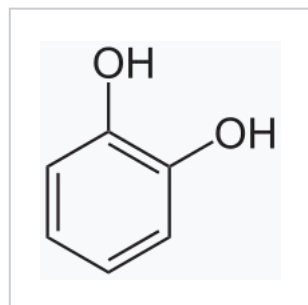
像大多数胺，多巴胺是一种有机碱。在酸性环境中，通常质子化。质子化形式是高度水溶性相对稳定的，但它是能够被氧化，如果暴露于氧或其它氧化剂。在碱性环境，多巴胺不会质子化。在这种游离碱形式，它是更少水溶性，也比较反应性高。因为质子化形式增加稳定性和水溶性的，多巴胺提供化学或药物使用的盐酸多巴胺—即创建了盐酸盐，当多巴胺与盐酸结合。在干燥形式时盐酸多巴胺是一种精细无色粉末。



多巴胺结构



苯乙胺结构



邻苯二酚结构

生物化学

多巴胺是脑内极其重要的神经递质，因为其作用特点又被称作**快乐物质**。多巴胺属于单胺类物质中的儿茶酚胺类，合成顺序依次为酪氨酸-左旋多巴-多巴胺-去甲肾上腺素最后通过单胺氧化酶和儿茶酚胺氧位甲基转移酶解失活。合成脑内的3/4的DA细胞体位于中脑前部或者中脑。黑质包含了灵长类脑DA神经元的主要部分，黑质又可分为致密部和网状部。黑质DA神经元的主要投射部位尾核壳核伏隔核。大脑皮层是另一个主要投射部位。

分类

目前共发现五种多巴胺受体，分为D1样 (D1 D5) D2样 (D2 D3 D4)。DA受体都隶属于G蛋白偶联受体的超级家族。

释放与降解

DA的释放是一种量子释放，胞裂外排 (exocytosis)。动作电位到达神经末梢时候，突触前膜通透性发生改变，Ca离子进入细胞，促进囊泡附着于前膜，继而形成小孔。由于嗜铬蛋白的收缩，将囊泡内容物排出。DA的降解分为两类，一种是酶解，另一种是再摄取。DA及单胺类在神经末梢中再摄取占总排出量的四分之三，突触间隙的DA可以被前膜，后膜，非神经组织摄取。先是通过细胞膜进入胞浆，这一阶段由NA-K-ATP供能。第二步是囊泡摄取，这一步由Mg-ATP供能。酶解部分由单胺氧化酶和儿茶酚胺氧位甲基转移酶解失活。

主要多巴胺通道

- 中脑皮层通路 (mesocortical system)
- 中脑边缘系统通道 (mesolimbic system)
- 黑质纹状体径路 (nigrostriatal system)
- 结节漏斗径路 (tuberoinfundibular system) [1]

奖赏机制，多巴胺的奖赏通路，各种成瘾物质均由位于中脑边缘皮质的通路发生作用：

1. 腹侧被盖核
2. 伏隔核
3. 前额叶皮层

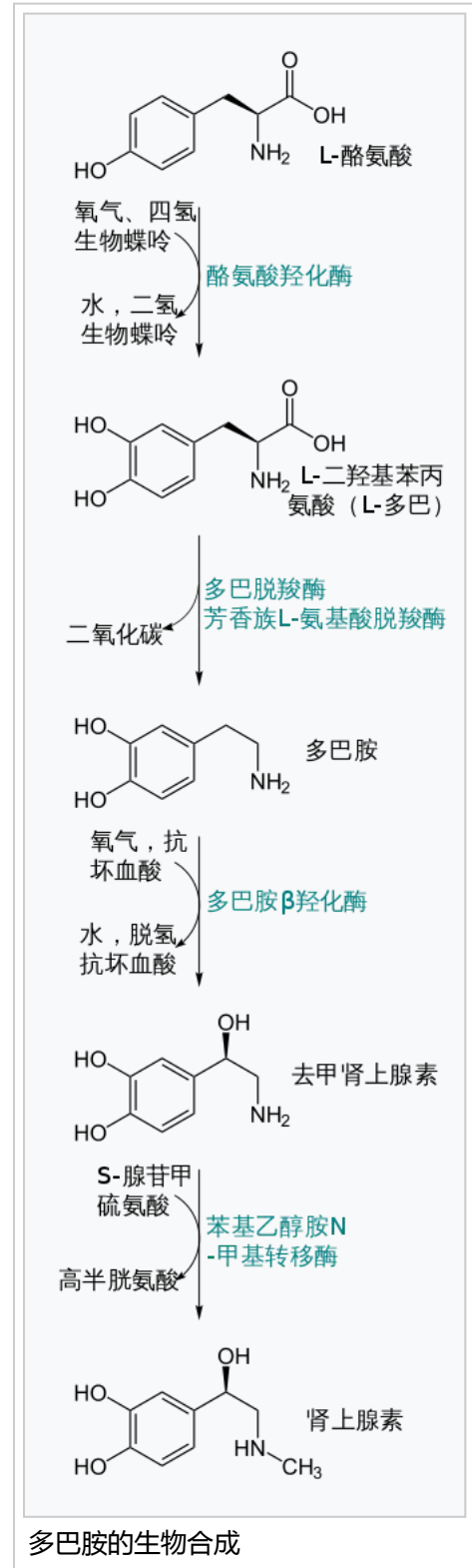
作用于此通路，促进多巴胺的释放使机体产生欣快感，停用后的戒断反应等等。D1D2受体均参与自我给药行为。

多巴胺与思觉失调症

引发精神医学的革命性进展的药物是氯丙嗪，它主要通过阻断边缘系统的D2受体发挥抗精神病作用。此后类似的药物不断被研发出来。

经典的精神分裂症的多巴胺假说：精神分裂症是由于多巴胺功能亢进造成的，一度在学术界占据垄断地位，直到目前为止所有的精神分裂症假说都不能与多巴胺无关。

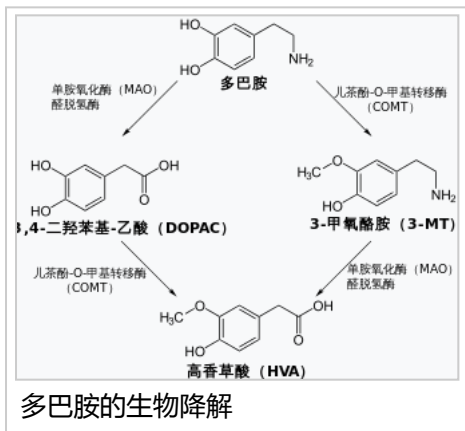
随着第二代抗精神病药物如氯氮平、利培酮的问世，其特点是对D2受体的低阻断效果，更多的是对5-HT，NE受体的阻断，调节谷氨酸多种受体发挥作用，对经典的多巴胺假说提出了质疑。



传统的抗精神病药物阻断中脑边缘系统D2受体发挥抗精神病作用，但是同时阻断了多巴胺在结节漏斗径路的D2受体，导致泌乳素分泌增多。传统的抗精神病药物亦阻断了黑质纹状体的D2受体，引发锥体外系反应如肌张力上升，类帕金森症状。临幊上多采用苯海索，金刚烷胺，溴隐亭对抗以上不良反应。

历史与发展

多巴胺最早是在1910年由乔治·巴格和詹姆斯·尤恩在英国伦敦惠康实验室合成。于1957年凯瑟琳·蒙塔古首先在人的大脑中鉴定出多巴胺。它被命名为多巴胺，因为它是一种单胺，其前体是3,4-二羟基苯(左旋多巴胺)。在1958年阿尔维德·卡尔森在瑞典国家心脏研究所化学药理学实验室中最早认识到多巴胺作为神经递质的功能。卡尔松被授予2000年诺贝尔生理学或医学奖，其表明多巴胺不仅是去甲肾上腺素和肾上腺素的前体，而且自身也是神经递质。



参见

- 上瘾
- 安非他命
- 抗精神病药物
- 邻苯二酚胺
- 儿茶酚氧位甲基转移酶素
- 可卡因
- 精神分裂症的多巴胺假说
- 神经传导物质
- 精神分裂

参考文献

引用

1. NEIL.R.CARLSON. 《PHYSIOLOGY OF BEHAVIOR》 9th EDITION. AMERICA:PEARSON,2006:119.

来源

书籍

- 江开达. 《神经精神药理学》 .

外部链接

- U.S. National Library of Medicine: Drug Information Portal - Dopamine (<http://druginfo.nlm.nih.gov/drugportal/dpdirect.jsp?name=Dopamine>)
- Dopamine: analyte monograph (<http://www.acb.org.uk/docs/NHLM/Dopamine.pdf>) - The Association for Clinical Biochemistry and Laboratory Medicine
- Biochemistry of Parkinson's Disease (<http://shorterlink.co.uk/12310>) (英文)

取自“<https://zh.wikipedia.org/w/index.php?title=多巴胺&oldid=44688355>”

-
- 本页面最后修订于2017年6月9日 (星期五) 07:32。
 - 本站的全部文字在知识共享署名-相同方式共享 3.0 协议之条款下提供，附加条款亦可能应用（请参阅使用条款）。Wikipedia®和维基百科标志是维基媒体基金会的注册商标；维基™是维基媒体基金会的商标。维基媒体基金会是在美国佛罗里达州登记的501(c)(3)免税、非营利、慈善机构。

“冰毒”有多毒？

• 方舟子 •

一个编剧因为吸一种俗称“冰毒”的毒品被抓。于是就有人出来替他说话，说“冰毒”是一种软性毒品，对人没有危害。更有人进而说，毒品的危害是被夸大的，其实吸毒就跟人跑步、看世界杯比赛一样，后者也会让人觉得爽，因此上瘾的。那么“冰毒”究竟是什么东西？它的毒害究竟有多大？

冰毒的化学名称叫甲基苯丙胺，有四种吸入方式：口服、鼻吸、抽吸和注射。不管用什么方式，冰毒都要进入血液中，随着血液循环到达大脑，才会让人产生快感。大脑里有许许多多神经细胞。每个神经细胞由两个部分组成：细胞体和突起。突起又分为两种，比较短的叫树突，是用来从其他神经细胞接收信号传递给细胞体的；比较长的叫轴突，是用来把信号传递给其他神经细胞的树突的。不同的神经细胞就是通过轴突和树突相互交流的，接触的地方叫突触。但是它们并不相互连接在一起，中间存在间隙。要把信号从一个神经细胞的轴突传到另一个神经细胞的树突，需要穿越突触间隙，这就要用到一类物质叫神经递质。当一个神经细胞要传递信号时，它的细胞体就指令其轴突释放神经递质到突触间隙中，神经递质再穿过间隙，到达另一个神经细胞的树突，和上面相应的受体结合，信号就传过去了。信号传过去之后，神经递质就从受体上脱离，被原先的神经细胞吸收，供下一次的神经信号传导使用。

神经递质有很多种，其中一种叫多巴胺，它的释放会让人产生快感。在我们的大脑中枢有一区域被称为奖励中心，一旦我们从事了某种有利于生存、繁衍的活动，奖励中心的神经细胞轴突就会释放多巴胺，多巴胺穿过突触间隙和树突上的多巴胺受体结合，把快乐的信息传递过去，让我们觉得很愉快，从而激励我们以后继续从事这些活动。在正常情况下，这些多巴胺会很快地从受体上脱离，神经细胞轴突上有多巴胺转运蛋白，把脱离的多巴胺吸收回去，快感也就消失了。

但是一旦冰毒到达奖励中心，情况就变得不正常了。冰毒在浓度比较低时，能抑制多巴胺转运蛋白，突触之间的多巴胺不能被重吸收，多巴胺会积蓄下来。而在冰毒浓度比较高时，多巴胺转运蛋白的转运方向干脆被逆转，本来是要把多巴胺吸收进轴突的，却变成了把轴突中的多巴胺大量地释放到突触间隙。这样突触之间的多巴胺浓度急剧上升，会让人产生强烈的快感，而且快感一直持续下去，直到冰毒被代谢掉。这个过程可以持续长达十几个小时。然而一旦快感消失，吸毒者就陷入了极度的沮丧之中，比吸毒之前更觉得郁闷，想要马上再来一剂冰毒重新找到快感，而对生活中其他原本令人愉快的事情都失去了兴趣。

然而最初的那种快感是难以找回来的。这是因为身体会很快地做出调整，例如减少多巴胺转运蛋白的数量，试图适应多巴胺释放过多的状况。这时就需要不断地加大冰毒的剂量才能有快感。最终，大剂量的冰毒也没法产生快感，但是又不能不用，否则身体就会出现痛苦。所以到后来，毒瘾患者吸毒主要是为了避免

毒瘾发作出现的痛苦，而不是产生快感。如果不吸，很多人在一天之内就会出现痛苦的戒断反应，吸毒时间越长出现戒断反应的时间越快。长期吸食冰毒会让吸毒者的精神状态出现严重的问题，例如陷入严重的抑郁，产生自己威力无比的妄想和受迫害妄想，出现幻觉、精神分裂。

但冰毒的危害还不限于此。多巴胺能与氧气反应产生自由基，自由基能对细胞造成损伤。冰毒刺激多巴胺的大量释放和在突触之间的大量累积，就会对神经细胞造成损伤、死亡。冰毒还会影响到其他神经递质例如5-羟色胺、去甲肾上腺素的释放，对与这些神经递质有关的神经细胞造成损伤、死亡。所以冰毒是一种广泛的神经毒素，会对大脑的结构和功能造成损伤。这些损伤有的是可逆的，在戒毒之后可以逐渐恢复，但是有的损伤在戒毒多年之后仍然存在，有可能是不可逆的永久损伤。冰毒造成的大脑损伤会影响到人的认知、记忆和运动能力，例如曾经吸过冰毒的人，即使在戒毒之后，患帕金森病的风险仍然比一般人高。冰毒还能对人体造成其他方面的伤害，例如冰毒会让血压急剧升高，长期使用会对大脑中的血管造成永久性损伤，加大了导致中风的风险。还有，不管用什么方式吸食，长期吸食冰毒的人牙齿都会受到永久性损伤、脱落，有一口特殊的烂牙。

冰毒通过绑架人体的奖励系统，短时间内让人产生快感，然而它对人的心理、生理的毒害却是长期的、巨大的，绝不是什么“软性毒品”。而且一旦吸食冰毒成瘾，就很难戒掉。目前没有有效的药物能够帮助戒掉冰毒，只能通过改变生活方式和接受行为疗法的长期治疗。戒毒的关键是要摆脱吸毒文化圈，与毒友绝交，避免再接触到毒品，想吸也得不到毒品。如果那些吸毒的娱乐明星还混娱乐圈，关十年也没用，放出来了照样吸。吸毒成瘾是一种没法治愈的慢性病，关键是用各种手段尽量延长复发的时间，能延长到死前都不复发，才算成功。一入毒门深似海，绝不要出于好奇去尝试吸毒。

2014. 7. 2.

(《新华每日电讯》2014. 7. 4)

(XYS20140711)

◇◇新语丝(www.xys.org) (xys8.dxiong.com) (xys.ebookdiy.com) (xys2.dropin.org) ◇◇

苯丙胺

维基百科, 自由的百科全书

安非他命 (英文名称 : **Amphetamine** ^[note 1]) 为一种中枢神经兴奋剂 , 用来治疗注意力不足过动症、嗜睡症、和肥胖症。“Amphetamine”一名撷取自 alpha-methylphenethylamine。

安非他命于公元 1887 年被发现 , 以两种对映异构体的形式存在 ^[note 2] , 分别是左旋安非他命和右旋安非他命。

准确来说 , 安非他命指的是特定的化学物质-外消旋纯胺类型态 ^{[24][25]} , 这个物质等同于安非他命的两个对映异构体 : 左旋安非他命和右旋安非他命的等比化合物之纯胺类型态。然而 , 实际上安非他命一词已被广泛的用来表示任何由安非他命对映异构体构成的物质或安非他命对映异构体本身。 ^{[21][26][25]}

安非他命是一种中枢神经兴奋剂 , 适度适量地使用能提升整体抑制控制能力 ^{[27][28]} 。在医疗用的剂量范围内 , 安非他命能带来情绪以及执行功能的变化 , 例如 : 欣快感的增强、性欲的改变、清醒度的提升、大脑执行功能的进化。安非他命所改变的生理反应包含 : 减少反应时间、降低疲劳、以及肌耐力的增强。然而 , 若摄取剂量远超过医疗用的剂量范围 , 将会导致大脑执行功能受损以及横纹肌溶解症。摄取过分超越医疗用剂量范围的安非他命可引发严重的药物成瘾。然而长期摄取医疗剂量范围的安非他命并不会产生上瘾的风险。

此外 , 服用远超医疗用剂量范围的安非他命会引起精神疾病 (例如 : 妄想 ^[参 1] 、偏执 ^[参 2]) 。然而长期摄取医疗剂量范围的安非他命并不会引起上述疾病。

那些为享乐而摄入的安非他命通常会远超过医疗用剂量范围 , 且伴随着非常严重甚至致命的副作用。 ^[sources 1]

历史上 , 安非他命也曾被用来治疗鼻塞 (nasal congestion) 和抑郁。

安非他命也被用来提升表现、促进大脑的认知功能及在助兴时 (非医疗用途情况下) 被作为增强性欲 ^[a] 、和欣快感促进剂。

安非他命在许多国家为合法的处方药 ^[参 3] 。然而 , 私自散布和囤积安非他命被视为非法行为 , 因为安非他命被用于非医疗用途的助兴可能性极高。 ^[sources 2]

首个药用安非他命的药品名称为 Benzedrine 。当今药用安非他命 ^[参 4] 以下列几种形式存在 : 外消旋安非他命 ^[参 5] 、 Adderall ^[note 3] 、 dextroamphetamine 、或对人体无药效的前驱药物体 ^[参 6] : lisdexamfetamine 。

安非他命借着自身作用于儿茶酚胺神经传导元素 : 正肾上腺素及多巴胺的特点来活化 trace amine receptor , 进而增加单胺类神经递质和神经递质 (excitatory neurotransmitter) 在脑内的活动。 ^[sources 3]

安非他命属于替代性苯乙胺类的物质。由安非他命衍伸出的物质被归纳在替代性苯乙胺 ^[参 7] 的分类中 ^[note 4] , 比如说 : 安非他酮 ^[参 8] 、 cathinone 、 MDMA 、和甲基苯丙胺 ^[参 9] 。安非他命也与人体内可自然生成的两个属于痕量胺的神经传导物质 -- 特别是苯乙胺 (phenethylamine) 和 N-Methylphenethylamine-- 有关。 Phenethylamine 是安非他命的原始化合物 , 而 N-methylphenethylamine 则是安非他命的位置异构体 (只有在甲基族中才会区分出此位置异构体) 。 ^[sources 4]

目录

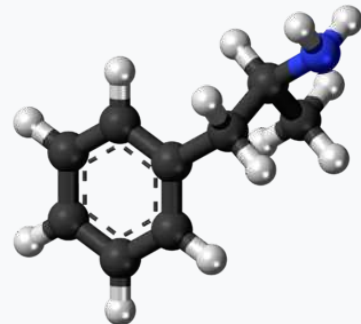
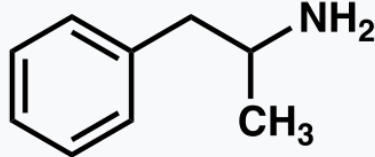
- 1 用途
 - 1.1 医疗
 - 1.2 提升表现
- 2 医疗上的禁忌
- 3 副作用
 - 3.1 生理
 - 3.2 心理
- 4 严重过量
 - 4.1 成瘾
 - 4.1.1 分子生物机转 (Biomolecular mechanisms)
 - 4.1.2 药物治疗 (Pharmacological treatments)
 - 4.1.3 行为治疗 (Behavioral treatments)
 - 4.2 依赖和戒断症状 Dependence and withdrawal
 - 4.2.1 DSM中，安非他命中毒及戒断症状之标准 (DSM criteria for intoxication and withdrawal)
 - 4.2.2 安非他命戒断症状的频率列表 (Table of symptoms of amphetamine withdrawal by frequency)
 - 4.3 中毒与致病 (Toxicity and psychosis)
 - 4.3.1 中毒
 - 4.3.2 致病
- 5 交互作用 (Interactions)
- 6 药学 (Pharmacology)
 - 6.1 药效动力学 (Pharmacodynamics)
 - 6.1.1 多巴胺
 - 6.1.2 去甲肾上腺素
 - 6.1.3 血清素
 - 6.1.4 其他的中枢神经递质、肽、和激素 Other neurotransmitters, peptides, and hormones
 - 6.2 药物代谢动力学
 - 6.3 相关的内部生成化合物/混和物 (endogenous compound)
- 7 历史、社会与文化
 - 7.1 合法状态与条件
 - 7.2 药品
- 8 备注A
- 9 备注B
- 10 备注C
- 11 注释
- 12 英文名称对照
- 13 引用
 - 13.1 来源
- 14 参见
- 15 外部链接

用途

医疗

安非他命是用来治疗注意力不足过动症 (ADHD) 、嗜睡症 (一种睡眠疾病) 、和肥胖症。有时候安非他命会以仿单标示外使用的方式处方来治疗顽固性忧郁症及顽固性强迫症^{[1][15] [43] [50]}。在动物试验中，已知非常高剂量的安非他命会造成某些动物的多巴胺系统和神经系统的受损。^{[51][52]}但是，在人体试验中，注意力不足过动症患者在接受安非他命的治疗后，则发现安非他命可促进大脑的发育及神经的成长。^{[53][54][55]}

安非他命 (Amphetamine) (INN)



系统 (IUPAC) 命名名称

(RS)-1-phenylpropan-2-amine

临床数据

读音

/æm'fetəmi:n/

Drugs.com

amphetamine (<https://www.drugs.com/amphetamine.html>)

医疗法规

US FDA: Amphetamine (<http://www.accessdata.fda.gov/scripts/cder/drugsatfda/index.cfm?function=Search.SearchAction&SearchTerm=Amphetamine&SearchType=BasicSearch>)

妊娠分级

US: C (不排除有风险的可能)

依赖性

生理依赖: 无
心理依赖: 中等

成瘾性

中等

给药途径

医用: 口服给药, 鼻腔给药, 静脉注射^[1]
非医疗用 (Recreational) : 口服给药, 鼻腔给药, Insufflation (medicine), 栓剂, 静脉注射

合法状态

合法状态

AU: 受管控 (S8)
CA: Schedule I
NZ: Class B
UK: Class B
US: Schedule II
UN: Psychotropic
Schedule II

药代动力学数据

生物利用度

口服 75–100%^[2]

蛋白结合度

15–40%^[3]

代谢

Amphetamine only:
CYP2D6,^[4] Dopamine β-hydroxylase,^{[5][6][7]} Flavin-containing monooxygenase^{[5][8][9]}

代谢产物

4-hydroxyamphetamine,

回顾许多核磁共振摄影 (MRI) 的研究后发现，长期以安非他命治疗注意力不足过动症患者能显著降低患者大脑结构及大脑执行功能上的异常。并且优化大脑中数个部位，例如：基底神经节的右尾状核。[53][54][55]

众多临床研究的系统性及统合性回顾已确立长期使用安非他命治疗注意力不足过动症的疗效及安全。[56][57][58][59]

持续长达两年的随机对照试验[参 10][b]结果显示：长期使用安非他命治疗注意力不足过动症，是有效且安全的。[56][59]

两个系统性/统合性回顾的结果显示长期且持续地使用中枢神经兴奋剂治疗注意力不足过动症能有效地减少注意力不足过动症的核心症状（核心症状即为：过动、冲动和分心/无法专心）、增进生活品质、提升学业成就、广泛地强化大脑的执行功能。[note 5] 这些执行功能分别与下列项目有关：学业、反社会行为、驾驶习惯、药物滥用、肥胖、职业、日常活动、自尊心、服务使用（例如：学习、职业、健康、财金、和法律等）、社交功能。[57][59]

一篇系统性 / 统合性回顾标志了一个重要发现：一个为期九个月的随机双盲试验中，持续以安非他命治疗的ADHD患者，其智力商数平均增加4.5单位^[注 1]，且在专注力、冲动、过动的改善皆呈现持续进步的态势。[56] 另一篇系统性 / 统合性回顾则指出：根据迄今为止为时最长的数个临床追踪研究[参 11]，可以得到一个结论：即便从儿童时期开始以中枢神经兴奋剂治疗直到老年，中枢神经兴奋剂都能持续有效地控制ADHD的症状并且减少物质滥用的风险。[59] 研究表明，ADHD与大脑的执行功能受损有关。而这些受损的执行功能分别与大脑中部分的神经传导系统有关[参 12]。[60]；又此部分受损的神经传导系统和中脑皮质激素-多巴胺[参 13]的传导及蓝斑核[参 14]和前额叶[参 15]中的正肾上腺素[参 16]的传导相关。[60]

中枢神经兴奋剂，例如：methylphenidate和安非他命对于治疗ADHD都是有效的，因为中枢神经兴奋剂刺激了上述神经系统中的神经传导物质活动。[29][60][61]

至少超过80%的ADHD患者在使用中枢神经兴奋剂治疗后，其ADHD的症状可以获得改善。[62]

使用中枢神经兴奋剂治疗的ADHD患者相较之下，普遍与同侪及家庭成员的关系较佳并且在学校拥有较好的表现。兴奋剂能使ADHD患者较不易分心、冲动、且拥有较长的专注力时间和范围。[63] [64]

根据考科蓝协作组织[参 17]所提供的文献回顾结果[note 6]指出：使用中枢神经兴奋剂治疗的ADHD患者即便其症状改善，相较于使用非中枢神经兴奋剂，仍因副作用而有较高的停药率。[66] [67]

回顾结果也发现，中枢神经兴奋剂并不会恶化抽动综合征的症状，例如：妥瑞氏症，除非服用dextroamphetamine[c]的剂量过高才有可能在部分妥瑞氏症合并注意力不足过动症患者身上观察到抽动综合征的症状恶化。[68]

中枢神经兴奋剂只要依照医师指示用药，都是相当安全的。[69][70][70][71] 中枢神经兴奋剂，例如：利他林与专思达，可能导致：心悸、头痛、胃痛、丧失食欲、失眠、因相对专注而变得冷淡（面无表情）等副作用，因此6岁以下的儿童不适宜服用。（副作用产生与否因人而异）[72]

随着时间推进与各方的努力，中枢神经兴奋剂的相关副作用已可借由包括但不限于剂量调整、服药时间、饭前饭后服用、服药频率等服药模式之改变以及改变药物组合等方式获得相当程度的减少。[73] [74] [75] [70] [76]

提升表现

认知方面 (Cognitive)

	4-hydroxynorephedrine, 4-hydroxyphenylacetone, 苯甲酸, 马尿酸, 苯丙醇胺, 苯基丙酮[4][10][11]
起效	IR dosing: 30–60 minutes ^[12] XR dosing: 1.5–2 hours ^[13] [14]
生物半衰期	D-amph: 9–11 hours ^{[4][15]} L-amph: 11–14 hours ^{[4][15]} PH值-dependent: 8–31 hours ^[16]
作用时间	IR dosing: 3–7 hours ^{[13][17]} XR dosing: 12 hours ^{[13][14]} [17]
排泄	Primarily 肾; PH值-dependent range: 1–75% ^[4]
识别信息	
CAS注册号	300-62-9 (http://www.commonchemistry.org/ChemicalDetail.aspx?ref=300-62-9) ✓
ATC代码	No6BA01
PubChem	CID 3007 (https://pubchem.ncbi.nlm.nih.gov/summary/summary.cgi?cid=3007)
IUPHAR/BPS	4804 (http://www.guidetopharmacology.org/GRAC/LigandDisplayForward?ligandId=4804)
DrugBank	DBo0182 (http://www.drugbank.ca/drugs/DBo0182) ✓
ChemSpider	13852819 (http://www.chemspider.com/Chemical-Structure.13852819.html) ✓
UNII	CK833KGX7E (http://fdasis.nlm.nih.gov/srs/srsdirect.jsp?regno=CK833KGX7E) ✓
KEGG	Do7445 (http://www.kegg.jp/entity/Do7445) ✓
ChEBI	CHEBI:2679 (https://www.ebi.ac.uk/chebi/searchId.do?chebiId=CHEBI:2679) ✓
ChEMBL	CHEMBL405 (https://www.ebi.ac.uk/chembl/compoundinspect/CHEMBL405) ✓
NIAID ChemDB	018564 (http://chemdb.niaid.nih.gov/CompoundDetails.aspx?AIDSNO=018564)
其他名称	α-methylphenethylamine
PDB配体ID	FRD (PDBe (http://www.ebi.ac.uk/pdbe-srv/PDBeXplore/ligand/?ligand=FRD), RCSB PDB (http://www.rcsb.org/pdb/search/smartsSubquery.do?smartSe

公元2015年中，一篇系统性回顾^[参 18]和一篇元分析/整合分析^[参 19]回顾了数篇优秀的临床试验^[参 20]报告后发现，低剂量（医疗用剂量）的安非他命能适度但不强烈地促进一个人的认知功能，包含工作记忆（working memory）、长期的情节记忆（episodic memory）、抑制控制以及在一些方面的注意力（attention）。

^[77] ^[78] 安非他命强化认知功能的效果已知是部分透过间接活化在大脑前额叶（prefrontal cortex）的dopamine receptor D₁ 和adrenoceptor α₂。^[29] ^[77] 一篇2014年的系统性回顾发现低剂量（医疗用剂量）的安非他命能促进和稳固记忆的形成以及记忆品质（memory consolidation），进而提升一个人的回忆（recall of information）的能力。^[79] 低剂量（医疗用剂量）的安非他命也可增加大脑皮层（质）区的效率，这能让一个人的工作记忆（working memory）获得进步。^[29] ^[80] 安非他命和其他用于治疗ADHD的中枢神经刺激剂能透过提升task saliency来增加一个人去做事情的动机、并强化一个人的警觉心（清醒度），因而能刺激一个人开始做“以目标为导向”的行为。^[29] ^[81] ^[82] 中枢神经兴奋剂（例如：安非他命）能提升一个人在困难且枯燥的任务中的表现。^[29] ^[82] ^[83] 超过医疗用剂量范围（包含其误差范围及容许最大上限）的安非他命剂量将不利于工作记忆（working memory）和其他的认知功能。^[29] ^[82]

生理 (physical)

虽然安非他命可以提升速度、耐力（延迟疲劳的发生）、肌耐力、身体素质和警觉心并减少心理反应时间。^[30] ^[34] ^[30] ^[84] ^[85] 然而，“非因医疗需求使用安非他命”在各种运动场合都是被严格禁止的。^[86] ^[87]

安非他命借由抑制多巴胺在中枢神经系统中的回收及外流来促进耐力和反应时间的提升。^[84] ^[85] ^[88] 安非他命和其他作用于多巴胺系统的药物一样，都能增加在固定施力（levels of perceived exertion）下的动力（能）输出。这是因为安非他命能夺取（override）体温的“安全开关”的控制权并将身体核心温度（core temperature limit）的上限提高以取得在体温安全上限提高前被身体保留的能量。^[85] ^[89] ^[90] 于医疗用剂量范围（包含其误差范围），安非他命的副作用不至于影响运动员的运动表现；^[30] ^[84] 然而，当摄取的剂量过多时，安非他命可能会引起严重的后果，例如：横纹肌溶解症和体温过高（hyperthermia）。^[31] ^[33] ^[84]

医疗上的禁忌

根据国际化学品安全规划署（IPCS, International Programme on Chemical Safety）和美国食品药品管理局（USFDA），^[note 7] 安非他命不建议处方给有药物滥用、心血管疾病、对于各种刺激严重反应过度、和严重焦虑历史的人。^[note 8] ^[92] ^[93] 安非他命也不被建议处方给正经历动脉血管硬化（血管硬化）、中度到重度高血压、青光眼（眼压过高）、或甲状腺机能亢进（身体在体内制造出过量的甲状腺 贺尔蒙/激素）的人。^[92] ^[93] ^[94] 曾对中枢神经刺激剂有药物过敏的人以及正在服用单胺氧化酶抑制剂（MAOI）或单胺氧化酶抑制剂类药物（MAOIs），可能不适合使用安非他命。即便曾有合并使用安非他命和单胺氧化酶抑制剂后仍一切平安的案例。^[92] ^[93] ^[95] ^[96]

IPCS和美国食品药品管理局也同意患有神经性厌食症（anorexia nervosa）、双极性情感疾患（bipolar disorder）、忧郁、高血压、狂躁（mania）、思觉失调症、Raynaud's phenomenon、心脏病发（seizures）、抽动综合征（tics）、妥瑞氏症（Tourette's disease）、和有甲状腺问题、肝肾问题的人在使用安非他命时应密切追踪上述疾病的变化。^[92] ^[93]

人体试验证明，医疗用剂量下的安非他命并不会导致胎儿或新生儿畸形(i.e., it is not a human teratogen)。然而超越医疗用剂量甚多的安非他命确实会增加胎儿或新生儿畸形的机会。^[93]

研究观察发现，安非他命会进入母亲的母乳中，因此建议母亲不要在使用安非他命药物的期间内授乳。^[92] ^[93]

由于安非他命可能影响食欲继而导致可反转的身高及体重的成长迟缓，^[note 9] 因此建议儿童或青少年在用药期间定期测量自己的身高及体重。^[92]

副作用

安非他命的副作用以及其发生率和严重度大致上与使用的剂量呈正相关。^[34] ^[31] ^[33] ^[34] 成分为安非他命的药品，诸如：Adderall、Dexedrine、和安非他命的等价物质（generic equivalents）目前皆已获得美国食品药品管理局（USFDA）许可用于长期性的治疗。^[44] ^[33]

摄取大幅超出医疗剂量的安非他命将大幅增加严重副作用出现的风险。^[34]

{{#ifeq:Side effects|Side effects|

archSubtype=ChemCompIdQuery&chemCompId=FRD&polymorphicType=Any))

化学信息

化学式 C₉H₁₃N

摩尔质量 135.20622 g/mol^[18]

SMILES

InChI

物理性质

密度 0.9±0.1 g/cm³

熔点 11.3 °C (52.3 °F)
(predicted)^[19]

沸点 203 °C (397 °F) at 760 毫米
汞柱^[20]

(verify)

生理

在治疗剂量下，生理副作用会因年龄或个人情况而有所不同^[33]。心血管方面的副作用包含：迷走-血管反射导致的高血压或是低血压、雷诺氏症（Raynaud's phenomenon）（因小动脉收缩而导致流往手脚的血流减少）、以及心搏过速（tachycardia）。^{[33][34][97]}

男性方面而言，副作用可能包含：勃起障碍、频繁勃起、或是勃起时间过长（prolonged erections）。^[33]

消化方面的副作用可能包含：腹痛、丧失胃口（appetite loss）、反胃（nausea）以及体重降低（weight loss）。^{[33][98]} 其他潜在的副作用包含：视觉模糊（blurred vision）、口干（dry mouth）、磨牙（excessive grinding of the teeth）、流鼻血（nosebleed）、多汗（profuse sweating）、药物性鼻炎（rhinitis medicamentosa，药物导致的鼻塞）、癫痫阈值/触发门槛降低（seizure threshold），以及抽搐（tics）。^[sources 5] 在一般的治疗剂量下鲜少发生危险副作用^[34]。

安非他命刺激延脑的呼吸中枢（medullary respiratory centers），使得呼吸变得较快速且较深。^[34] 正常人在治疗剂量下，此作用通常难以察觉；然而，此作用在呼吸已经受损的病人身上有可能变得明显。^[34]

安非他命会使膀胱括约肌收缩（bladder sphincter，控制排尿的肌肉之一）收缩（contraction），而导致解尿困难^[34]。此效果可以应用在夜尿（bed wetting）或是失去膀胱控制能力的病人身上。^[34]

安非他命在胃肠道的作用是难以预测的^[34]。安非他命可能会减少胃肠活动力（内容物通过肠胃道的速率）^[34]；然而，安非他命亦可能在胃肠道的平滑肌（smooth muscle）处于松弛状态时，增加其活动力。^[34]

安非他命有轻微的止痛作用（analgesic effect）且可以增强鸦片类物质的止痛作用。^[34]

美国食药署2011年委任的研究发现：不论是小孩或是成人，“安非他命（于医疗情境下使用）”和“其他用于治疗ADHD的中枢神经兴奋剂”均和重大的心血管疾病（猝死、心脏病发、中风）无关^[sources 6]；然而，当病患已有心血管方面的疾病时，禁用此药。^[sources 7]

心理

严重过量

安非他命过量使用会引起许多症状，然而在适当的医疗照护下，不至于死亡。^{[93][104]}

药物过量症状的严重度与剂量成正比；与身体对安非他命的药物耐受性成反比。^{[34][93]} 已知每天摄取达到5公克的安非他命（每天最大摄取量的五十倍）会导致身体对安非他命产生药物耐受性。^[93] 严重过量的安非他命摄取所致的症状列于下方；安非他命中毒一旦到达出现全身抽搐（convulsion）和昏厥（coma）则必须立刻急救以避免死亡。^{[31][34]} 在2013年，安非他命、甲基安非他命和其他列于ICD-10 第五章：精神和行为障碍§使用化学药物、物质或酒精引起的精神和行为障碍中的安非他命相关物质的过量使用在世界上共导致3788人死亡。（3,425–4,145 人死亡、 95% 信赖区间）。^{[note 10][105]}

被过度活化达到病态程度的mesolimbic pathway（一个连接腹侧被盖区（ventral tegmental area）和伏隔核（nucleus accumbens）的多巴胺通道），在安非他命的成瘾中扮演着主要的角色。^{[106] [107]}

当一个人经常服用严重过量的安非他命，将伴随安非他命成瘾的高度风险，因为持续过量的安非他命会逐渐增加伏隔核的ΔFosB（“成瘾”与否的分子开关和主控蛋白 原文：a "molecular switch" and "master control protein" for addiction.）的档次。^{[108][109][110]} 一旦伏隔核的ΔFosB破表（over-expressed），这个人的“成瘾性行为”^[注 2]（例如：出现试图取得安非他命的冲动行为）将开始随之增加。^{[108][111]} 虽然目前没有治疗安非他命成瘾的有效药物，但规律的且每次都有持续一定时间的有氧运动能降低安非他命的成瘾风险也是治疗安非他命成瘾的天然疗法。^{[112][113] [sources 8]} 运动能提升临床治疗的预后，且可能与认知行为治疗（目前已知最有效的安非他命成瘾的临床治疗法）相搭配为联合疗法（combination therapy）。^{[112][114][115]}

严重过量的安非他命剂量所致的症状 (依照体内生物系统分类) Overdose symptoms by system

生物系统	轻度、中度过量 ^{[31][34][93]}	重度过量 ^[sources 9]
心脏血管系统	<ul style="list-style-type: none"> ▪ 心律不整 ▪ 高血压 或 低血压 	<ul style="list-style-type: none"> ▪ 心源性休克 (Cardiogenic shock) (心脏无法输出足够的血液。原文 : heart not pumping enough blood) ▪ 脑部大出血 ▪ 循环系统衰竭 (Circulatory collapse) (部分或全部的循环系统失去功能。原文 : partial or complete failure of the circulatory system)
中枢神经系统	<ul style="list-style-type: none"> ▪ 意识混浊 ▪ 反射亢进 (异常快速的反射) ▪ 严重的躁动 ▪ 颤抖 (不自主的肌肉颤动) 	<ul style="list-style-type: none"> ▪ 急性安非他命引起的严重精神病 (例如 : 妄想^[注 3] and 偏执^[注 4]) ▪ 冲动的、突然的、重复的动作 (Compulsive and repetitive movement) ▪ 血清素综合征 (Serotonin syndrome) (excessive serotonergic nerve activity) ▪ Sympathomimetic toxidrome (excessive adrenergic nerve activity)
肌肉骨骼系统	<ul style="list-style-type: none"> ▪ 肌肉酸痛 (Muscle pain) 	<ul style="list-style-type: none"> ▪ 横纹肌溶解症 (快速的肌肉溶解 rapid muscle breakdown)
呼吸系统	<ul style="list-style-type: none"> ▪ 呼吸过速 	<ul style="list-style-type: none"> ▪ 肺水肿 (肺部积水) ▪ 肺高压 (肺动脉的高血压) ▪ Respiratory alkalosis (血液中二氧化碳浓度异常减少 reduced blood CO₂)
生殖泌尿系统 (Urogenital system)	<ul style="list-style-type: none"> ▪ 排尿疼痛 (Painful urination) ▪ 尿液滞留 (Urinary retention) (较不易排尿 inability to urinate) 	<ul style="list-style-type: none"> ▪ 无尿症 (No urine production) ▪ 肾脏衰竭
其他 (Other)	<ul style="list-style-type: none"> ▪ 体温升高 (elevated body temperature) ▪ 瞳孔放大 (Mydriasis/dilated pupils) 	<ul style="list-style-type: none"> ▪ 高或低血钾 (blood potassium) ▪ 重度高烧 (Hyperpyrexia, extremely elevated core body temperature) ▪ 代谢性酸中毒 (excessively acidic bodily fluids)

成瘾

长期服用远超医疗用剂量范围的安非他命会导致安非他命成瘾

“成瘾及生理、心理依赖”的相关术语词汇表^{[117][109][118][119]}

(Addiction)。然而长期摄取医疗剂量范围的安非他命并不会引起上述问题。^{[37][38][39]} 安非他命滥用 (例如 : 长期摄取严重过量的安非他命) 会导致大脑对于该剂量产生药物耐受性。渐渐地 , 滥用者必须服用更大量的安非他命以换取同样的效果。^{[127][128]}

分子生物机转 (Biomolecular mechanisms)

当前关于“长期安非他命滥用所致的成瘾”的模型 (model) 中 , 已知会改变一些脑部的结构 (特别是伏隔核)^{[129][130][131]}。造成脑部结构改变的最重要的转录因子 (transcription factor) 为 : ΔFosB 、 cAMP response element binding protein (CREB) 、和 nuclear factor kappa B (NF-κB)。^{[note 11] [130]} ΔFosB 在药物成瘾的发展过程中扮演着至关重要的角色 , 主要的原因在于其在伏隔核中 D1-type medium spiny neuron 的破表 (over-expression) , 为“成瘾”及“成瘾衍生的行为”及“神经元为了适应新常态所做的调适”的充分且必要条件。^{[note 12] [108][109][130]}

一旦 Δ FosB充分破表 (sufficiently overexpressed), 将诱发越来越严重的成瘾状态并伴随 Δ FosB值的持续创新高。 [108][109] Δ FosB已被证明与酒精成瘾、大麻成瘾、古柯碱成瘾、派醋甲酯成瘾、尼古丁成瘾、鸦片成瘾、phencyclidine成瘾、异丙酚、和安非他命的替代性物质成瘾、及其他成瘾有关。 [sources 10] Δ JunD为一个转录因子；而G9a为组织蛋白甲基转移酶的一种。 Δ JunD和G9a直接与伏隔核中的 Δ FosB值的升高成反比。 [109][130][135]

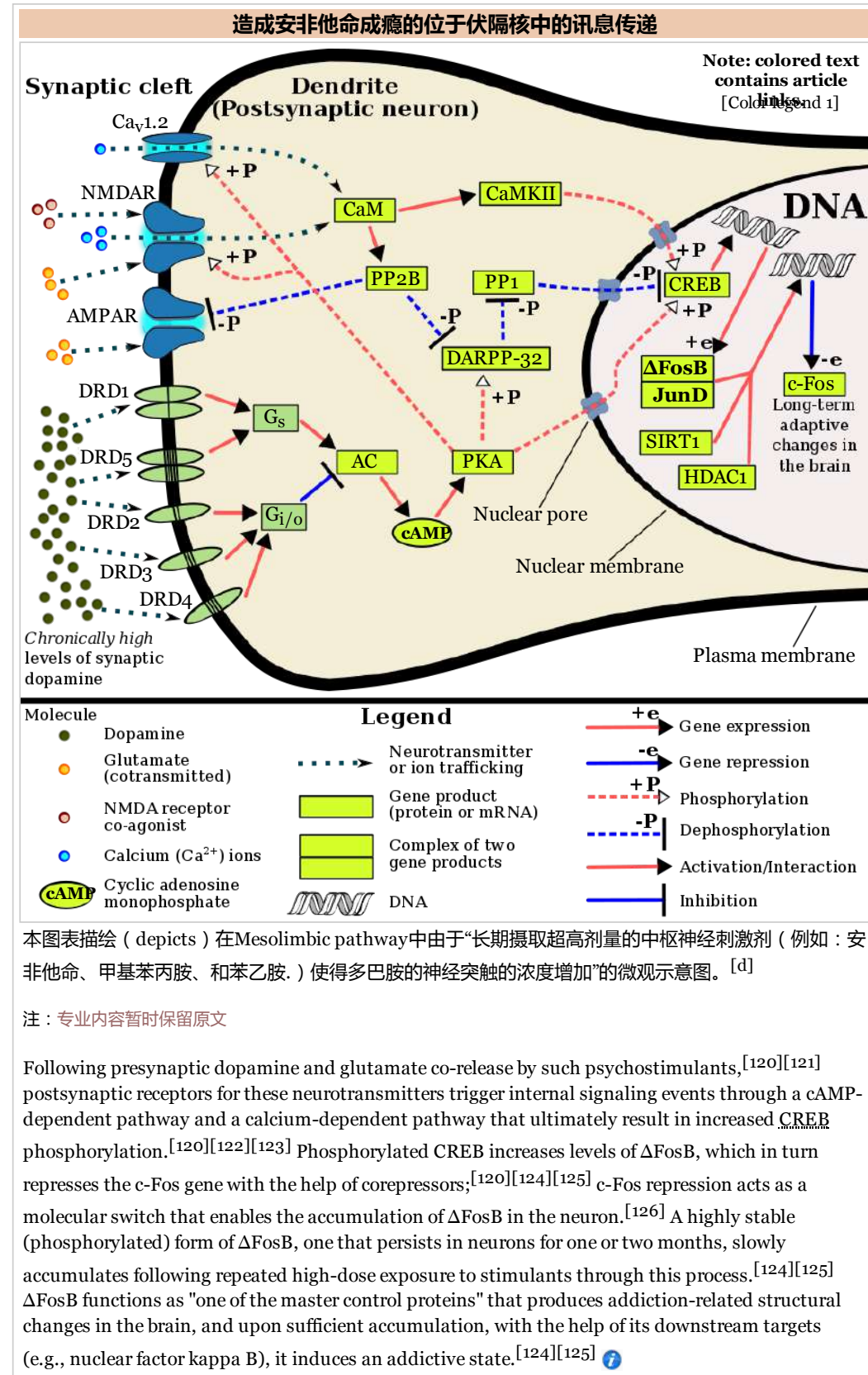
利用载体让伏隔核中的 Δ JunD充分破表, 可以使由长期药物滥用所致的渐进式神经元和行为改变完全停止。(比如说: Δ FosB所致的改变)。 [130] Δ FosB也在人们于天然酬赏 (natural reward) 中的行为反应调节上扮演重要的角色。天然酬赏 (natural rewards) 包含: 美味的食物 (palatable food)、性爱 (sex)、运动 (exercise)、..... [111][130][136] 因为天然酬赏以及成瘾性药物皆会激发 Δ FosB (这些酬赏让大脑刺激 Δ FosB的增加。原文:i.e., they cause the brain to produce more of it), 长期过度地从事上述行为将可能导致类似的成瘾之病理生理 (pathological)。 [111][130]

Δ FosB是导致“安非他命成瘾”、“安非他命引起的性成瘾”中最关键的致瘾因素。“安非他命引起的性成瘾”为“安非他命使用”加上“过度的性活动”所引发的“冲动之下的性行为”。 [注 5][111][137][138] 这类的性成瘾与多巴胺失调综合征相关, 有时此症会出现在正在服用作用于多巴胺的药物的人身上。 [注 6][111][136]

安非他命调节基因 (gene regulation) 的效果端视剂量与路径 (dose- and route-dependent) 而定。 [131] 绝大多数主题为“基因调节 (gene regulation)”和“成瘾 (addiction)”的研究都是透过动物试验以及利用静脉注射的方式对实验动物注射超高剂量的安非他命来进行。 [131] 少数几个透过人体试验 (依照体重来决定医疗用剂量) 来进行的研究表明, 口服医疗用剂量的安非他命并不会影响基因调节, 即便有, 也是极为轻微的。这表示安非他命用作医疗用途是十分安全的。 [131][131]

药物治疗 (Pharmacological treatments)

截至2014年5月并没有能够有效治疗安非他命成瘾的药理疗法 [139][140][141]。2015年到2016年间的论文回顾结果指出: 选择性TAAR1促进剂有非常大的可能在将来被用来治疗中枢神经兴奋剂的成瘾; [46][142] 然而, 截至2016年2月, 已知可作为选择性TAAR1促进剂的物质都属于试验性药物。 [46][142] 安非他命成瘾与伏隔核中的多巴胺接收器们以及位置相同 (co-localized) 的



NMDA 接受器们的活化高度相关；^[note 13] ^[107] 镁离子借由封锁一个接受器-钙离子通道，来阻断 NMDA 接受器们。^[107]^[143] 一篇论文回顾做成结论：根据动物试验，因成瘾而使用中枢神经刺激剂的人，可以发现过量的中枢神经兴奋剂显著降低脑细胞内部的镁离子活动。^[注 7]^[107] 利用镁元素补充剂，能降低安非他命使用者自我服用^[e]的机会。然而这不被认为是有效治疗安非他命成瘾的单一疗法（mono-therapy）。

行为治疗 (Behavioral treatments)

认知行为治疗是当前治疗中枢神经刺激剂成瘾的疗法。^[115] 除此之外，运动在生物神经元产生的效果的研究中表明维持每天从事有氧运动（例如：跑步等）的习惯，能避免药物成瘾缠身；本身也是一个对于治疗安非他命成瘾的有效附加疗法。^[sources 8] 运动能让所有疾病的预后都更加乐观，特别是对于中枢神经刺激剂成瘾。^[112]^[114]^[144] 值得一提的是，有氧运动能降低擅自服用中枢神经兴奋剂的欲望^[f]，降低再次擅自服用中枢神经兴奋剂的概率（reinstatement）(i.e., relapse)、降低“试图取得药物所做出的举动（drug-seeking behavior）”、降低多巴胺接收器 D₂在纹状体中的密度。^[111]^[144] 它在病生理学中的脚色是相对于“兴奋剂的使用”和“兴奋剂的效果”，它会引起纹状体中DRD2密度的减少。^[111] 一篇论文回顾提到，借由改变纹状体（striatum）中的ΔFosB、c-Fos immunoreactivity或部分的脑内回馈系统（reward system）来避免药物成瘾在一个人身上的发展。^[113]

Summary of addiction-related plasticity

神经可塑性和行为可塑性的形式 (Form of neuroplasticity or behavioral plasticity)	增强物的种类 Type of reinforcer						来源 Sources
	鸦片类 Opiates	中枢神经刺激剂 Psychostimulants	高脂肪或高糖食物 High fat or sugar food	性交 Sexual intercourse	运动与神经元关系 Movement and neuronal activity	环境丰富化 Environmental enrichment	
伏隔核中D1-type中的 Δ FosB表现 (Δ FosB expression in nucleus accumbens D1-type MSNs)	↑	↑	↑	↑	↑	↑	[111]
行为可塑性 Behavioral plasticity							
摄取量的增加 (Escalation of intake)	Yes	Yes	Yes				[111]
中枢神经刺激剂跨敏化作用 (Psychostimulant cross-sensitization)	Yes	不适用 Not applicable	Yes	Yes	削减 Attenuated	Attenuated	[111]
未经过处方而自行撕下摄取中枢神经刺激剂 (Psychostimulant self-administration)	↑	↑	↓		↓	↓	[111]
强化“在特定地点摄取兴奋剂的习惯” Psychostimulant conditioned place preference	↑	↑	↓	↑	↓	↑	[111]
强化“试图取得该致瘾药物的行为” (Reinforcement of drug-seeking behavior)	↑	↑			↓	↓	[111]
神经化学物质的可塑性 Neurochemical plasticity							
伏隔核中 CREB 磷酸化 (CREB phosphorylation in the nucleus accumbens)	↓	↓	↓		↓	↓	[111]
伏隔核中对于多巴胺的过敏反应 (Sensitized dopamine response in the nucleus accumbens)	No	Yes	No	Yes			[111]
经过变动的纹状体多巴胺接收器的讯号发送 (Altered striatal dopamine signaling)	↓DRD2, ↑DRD3	↑DRD1, ↓DRD2, ↑DRD3	↑DRD1, ↓DRD2, ↑DRD3		↑DRD2	↑DRD2	[111]
经过变动的纹状体鸦	No change	↑μ-opioid receptors	↑μ-opioid	↑μ-opioid	未改变	未改变	[111]

片样肽受体的讯号发送 (Altered striatal opioid signaling)	or ↑μ-opioid receptors	↑κ-opioid receptors	receptors	receptors	No change	No change	
发生于纹状体鸦片肽的改变 (Changes in striatal opioid peptides)	↑dynorphin No change: enkephalin	↑dynorphin	↓enkephalin		↑dynorphin	↑dynorphin	[111]
多巴胺通道的神经突触的可塑性 (Mesocorticolimbic synaptic plasticity)							
伏隔核中树突的数量 (Number of dendrites in the nucleus accumbens)	↓	↑		↑			[111]
伏隔核中Dendritic spine的密度 (Dendritic spine density in the nucleus accumbens)	↓	↑		↑			[111]

注解 : Not applicable (N/A) = 不适用 ; No change = 没有改变 ; DRD2 = 多巴胺受体D2 ; Attenuated = 削减 ; ↑ = 上升 ; ↓ = 下降 ; enkephalin = 脑啡肽 ; dynorphin = 强啡肽 ; opioid receptor = 鸦片接收器。

依赖和戒断症状 Dependence and withdrawal

根据另一篇由考科蓝协作组织所做的一篇论文回顾指出当一个长期严重摄取安非他命或甲基安非他命的药物成瘾者某天突然停止摄取安非他命或甲基安非他命 , 那么根据许多成瘾个案的报告显示 , 具有时效性 (time-limited) 的戒断症状将在他们上一次摄取安非他命后的 24 小时内出现。在成瘾患者停用安非他命后 , 安非他命的戒断症状的出现率接近九成。这九成都出现至少六个定义在“精神疾病诊断与统计手册”安非他命戒断症状”中的症状。年纪与剂量和戒断症状的严重度呈正相关。安非他命的戒断症状共有两个阶段且总共可能历时三周或更多。第一阶段 (撞墙期 marked "crush" phase) 约持续一周。 [145] [145] 安非他命的戒断症状可能包含 : 对于各种刺激极度敏感、躁动不安 (irritability) 、焦虑、对于安非他命有难以抑制的渴求、烦躁、疲倦、食欲放大、过动或行动迟缓、缺乏动机、嗜睡、和清醒梦 (lucid dreams) 。 [146] [145]

这些特征及症状必须非由其他疾病 (包含心理疾病) 引起 , 且无法归因于其他物质的滥用。满足上述条件 , 才符合“安非他命戒断症状”综合征的诊断标准。 [147] [145]

通过美国食品药品管理局严格审核的安非他命药品说明书上并未提到任何安非他命在医疗用剂量下突然停用会导致任何安非他命戒断症状的出现。 [94] [148] [149] [150]

DSM 中 , 安非他命中毒及戒断症状之标准 (DSM criteria for intoxication and withdrawal)

DSM-5 中关于兴奋剂中毒的标准如下 :

- A. 最近曾经服用过安非他命类的物质、可卡因或其他兴奋剂
- B. 在服用兴奋剂时 (或者服用后很快表现出) 临床表现出显著问题行为或心理变化 (如 : 欣快症或感情迟钝 ; 群性、社交性的改变 ; 过于警觉 ; 人际交往敏感 ; 焦虑、紧张或者恼怒 ; 刻板行为 ; 判断力受损) 。
- C. 在服用兴奋剂时或服用后即刻表现出以下任意两种 (或以上) 症状 :
 - 心动过速或心动过缓
 - 瞳孔扩散
 - 血压升高或降低
 - 出汗或发冷
 - 感到恶心或呕吐
 - 体重降低
 - 精神运动性焦躁或精神运动性迟滞
 - 肌肉无力、呼吸抑制、胸口疼痛或心律失常
 - 精神错乱、癫痫、运动困难、肌张力障碍或昏迷

包括其他物质中毒的情况在内，其他身体情况不可能出现该发病迹象、症状，并且也无法理解为其他的精神问题。

DSM-5中关于兴奋剂戒断症状的标准如下：

- A. 停止服用（或减少服用）长期的安非他命类物质、可卡因或其他兴奋剂。
- B. 在A的情况发生后的几小时至几天内，出现烦躁的情绪并伴有以下任意两种（或以上）的心理变化：

- 疲劳
- 生动而不愉快的梦
- 失眠或嗜睡
- 食欲增大
- 精神运动性焦躁或精神运动性迟滞

B中的症状或迹象导致了临床显著的压力，或者在社会、工作等重要方面功能出现受损。

安非他命戒断症状的频率列表 (Table of symptoms of amphetamine withdrawal by frequency)

停止服用硫酸安非他命后，个人报告的戒断症状的百分比

症状	频率
无症状	14%
易怒	78%
疼痛和痛苦	58%
感到沮丧	50%
社交能力受损	46%
发抖、出冷汗	36%
难以入睡	32%
虚脱	22%
恶心、呕吐	16%
头痛	14%
难以保持清醒	12%
食欲增大	12%
便秘	10%
食欲缩小	8%
腹泻	6%

[151]

个人尝试戒毒和接受医学指导戒毒的原因与百分比

原因	个人尝试戒毒	医学指导戒毒
对生活整体现状（犯罪、无聊、金钱）不满	42 (89%)	6 (37%)
对心理健康感到担忧（偏执、忧虑、依赖）	25 (53%)	3 (19%)
家庭原因（父母或配偶的压力，子女出生）	24 (51%)	5 (31%)
身体健康（动脉注射、血管萎陷、感染）	17 (36%)	4 (25%)
避免入狱	0	2 (12%)
其他原因	2 (4%)	0

[151]

用来协助戒毒的方法 (Methods used to assist detoxication)

	自我尝试戒毒 (Self detoxication)	被迫戒毒 (Enforced detoxication)
服用更多其他药物 (Increased consumption of other drugs)	-	-
大麻 (Cannabis)	22 (27%)	10 (59%)
Temazepam	21 (26%)	-
酒精 (Alcohol)	17 (21%)	2 (12%)
鸦片类物质 (Opiates)	12 (15%)	1 (6%)
Diazepam	4 (5%)	-
巴比妥类药物 (Barbiturates)	3 (4%)	1 (6%)
心理学技巧 (Psychosocial techniques)	-	-
转移注意力 (例如 : 工作、看电视) [Keeping occupied with other things (working, watching television)]	35 (21%)	1 (6%)
不再与药物成瘾的朋友来往 (Cutting off contact with drug-using friends)	31 (19%)	-
获得人们的支持 (家庭、社会中的支持团体) Gaining support from others (friends giving up, family, support groups)	11 (7%)	-
把药物及针头丢掉 (Throwing away drugs and needles)	5 (3%)	-

[151]

中毒与致病 (Toxicity and psychosis)**中毒**

在啮齿动物 (rodents) 和灵长类动物 (primates) 的药物试验发现到，够高的安非他命剂量会导致多巴胺神经中毒甚或致使多巴胺末梢神经受损退化并降低转运体和接收器的功能。 [152][153] 目前并无证据显示安非他命会直接荼毒人类的神经。 [注 8] [154][155] 然而，超高剂量 (large doses) 的安非他命摄取量可能会产生体温过高的现象并间接导致：多巴胺的神经性中毒 (dopaminergic neurotoxicity) 、过多的活性氧类 (reactive oxygen species) 生成、自然氧化 (autoxidation) 增加。 [sources 11] 从高剂量的安非他命摄取量引起的神经中毒的生物模式中发现，人体核心体温高于40 °C是“高剂量的安非他命摄取量”是否引起神经中毒的“必要条件”。 [153] 在动物试验中，若动物的脑温长期超过40 °C，容易因过多的活性氧类 (reactive oxygen species) 生成、受干扰的细胞蛋白功能和短暂的血脑屏障 (blood-brain barrier) 标准放宽而促使安非他命性的神经中毒发生。 [153]

致病

严重的安非他命过量可能造成“中枢神经刺激剂过量所引发的精神异常 (stimulant psychosis) ”，症状包含但不限于幻觉 (delusion) 和被害妄想、疑神疑鬼、妄想、偏执 (paranoia) 等。 [35] 一篇由考科蓝协作组织所做的论文回顾及统整发现在所有因摄取严重过量的“安非他命、 dextro-安非他命、及甲基安非他命”而导致精神异常的患者中，有5%-15%的患者即便经过治疗，仍无法完全康复。 [35][158]

根据同一篇由考科蓝协作组织所做的论文回顾及统整，至少一个实验 (trial) 显示抗精神病药物 (antipsychotic) 能有效解决因严重过量的安非他命所致的急性精神异常症状。 [35]

“摄取医疗剂量的安非他命所致的急性精神异常”是非常罕见的 (very rare)。
(非常罕见 very rare : < 1/1000 ; 罕见 rare : 1/101~1/1000) [36][92]

交互作用 (Interactions)

参见 : Amphetamine § Contraindications

目前已知许多种物质都会和安非他命发生药物相互作用，导致安非他命或参与作用的另一物质的药效或分解过程发生改变。^{[4][159]}用于分解安非他命的酶的抑制剂（如CYP2D6、FMO3）都会延长其半衰期，这意味着药效会更持久。^{[8][159]}安非他命也会和MAOIs产生交互作用，特别是MAOI类中的monoamine oxidase A抑制剂（monoamine oxidase A inhibitors）。<-- inhibitors, -->

因为MAOIs和安非他命两者都会增加儿茶酚胺（i.e., 正肾上腺素 和 多巴胺）在血浆中的浓度^[159]；因此MAOIs与安非他命合并使用是危险的^[159]。安非他命会调节几乎所有作用于中枢神经的药物的活动。特别需要注意的是，安非他命可能会降低镇静剂（sedative）和中枢神经抑制剂（depressant）的效果，并增加其他中枢神经刺激剂（stimulant）和抗抑郁药（anti-depressants）的效果。^[159]

安非他命也可能降低抗高血压药（anti-hypertensives）和抗精神病药（anti-psychotics）的药效，这是因为安非他命本身对于血压及多巴胺系统的作用。^[159]

锌的补充剂 可能会将低安非他命用于治疗注意力不足过动症时的最小有效剂量（minimum effective dose）。^{[note 15][163]}

整体来说，安非他命并不会与日常生活中常见的食物起任何重大的交互作用，但安非他命的吸收和排泄会分别受到肠胃内容物（gastrointestinal content）的pH值和尿液的酸碱值影响。^{[g][159]} 酸性物质会减少安非他命的吸收并增加尿液的排泄；碱性物质正好相反。^{[h][159]}

由于pH值在安非他命的吸收这件事上具有影响力，所以安非他命也会和 氢离子泵阻断剂（PPI, proton pump inhibitors）和 H₂受体阻抗剂（H₂ antihistamines）等中和胃酸的制酸剂产生交互作用。^[159]

药学 (Pharmacology)

一些未翻译的非现代汉语已进行隐藏，欢迎参与翻译。

药效动力学 (Pharmacodynamics)

Amphetamine exerts its behavioral effects by altering the use of monoamines as neuronal signals in the brain, primarily in catecholamine neurons in the reward and executive function pathways of the brain.^{[45][61]} The concentrations of the main neurotransmitters involved in reward circuitry and executive functioning, dopamine and norepinephrine, increase dramatically in a dose-dependent manner by amphetamine due to its effects on monoamine transporters.^{[45][61][164]} The reinforcing and motivational salience-promoting effects of amphetamine are mostly due to enhanced dopaminergic activity in the mesolimbic pathway.^[29] The euphoric and locomotor-stimulating effects of amphetamine are dependent upon the magnitude and speed by which it increases synaptic dopamine and norepinephrine concentrations in the striatum.^[1]

Amphetamine has been identified as a potent full agonist of trace amine-associated receptor 1 (TAAR1), a G_s-coupled and G_q-coupled G protein-coupled receptor (GPCR) discovered in 2001, which is important for regulation of brain monoamines.^{[45][165]} Activation of TAAR1 increases cAMP production via adenylyl cyclase activation and inhibits monoamine transporter function.^{[45][166]} Monoamine autoreceptors (e.g., D₂ short, presynaptic α₂, and presynaptic 5-HT_{1A}) have the opposite effect of TAAR1, and together these receptors provide a regulatory system for monoamines.^{[45][46]} Notably, amphetamine and trace amines bind to TAAR1, but not monoamine autoreceptors.^{[45][46]} Imaging studies indicate that monoamine reuptake inhibition by amphetamine and trace amines is site specific and depends upon the presence of TAAR1 co-localization in the associated monoamine neurons.^[45] 截至2010年 co-localization of TAAR1 and the dopamine transporter (DAT) has been visualized in rhesus monkeys, but co-localization of TAAR1 with the norepinephrine transporter (NET) and the serotonin transporter (SERT) has only been evidenced by messenger RNA (mRNA) expression.^[45]

In addition to the neuronal monoamine transporters, amphetamine also inhibits both vesicular monoamine transporters, VMAT1 and VMAT2, as well as SLC1A1, SLC22A3, and SLC22A5.^[sources 12] SLC1A1 is excitatory amino acid transporter 3 (EAAT3), a glutamate transporter located in neurons, SLC22A3 is an extraneuronal monoamine transporter that is present in astrocytes, and SLC22A5 is a high-affinity carnitine transporter.^[sources 12] Amphetamine is known to strongly induce cocaine- and amphetamine-regulated transcript (CART) gene expression,^{[173][174]} a neuropeptide involved in feeding behavior, stress, and reward, which induces observable increases in neuronal development and survival *in vitro*.^{[174][175][176]} The CART receptor has yet to be identified, but there is significant evidence that CART binds to a unique G_i/G_o-coupled GPCR.^{[176][177]} Amphetamine also inhibits monoamine oxidase at very high doses, resulting in less dopamine and phenethylamine metabolism and consequently higher concentrations of synaptic monoamines.^{[18][178]} In humans, the only post-synaptic receptor at which amphetamine is known to bind is the 5-HT_{1A} receptor, where it acts as an agonist with micromolar affinity.^{[179][180]}

The full profile of amphetamine's short-term drug effects in humans is mostly derived through increased cellular communication or neurotransmission of dopamine,^[45] serotonin,^[45] norepinephrine,^[45] epinephrine,^[164] histamine,^[164] CART peptides,^{[173][174]} endogenous opioids,^{[181][182][183]} adrenocorticotrophic hormone,^{[184][185]} corticosteroids,^{[184][185]}

and glutamate,[167][169] which it effects through interactions with CART, 5-HT_{1A}, EAAT₃, TAAR₁, VMAT₁, VMAT₂, and possibly other biological targets. [sources 13]

Dextroamphetamine is a more potent agonist of TAAR₁ than levoamphetamine.[186] Consequently, dextroamphetamine produces greater CNS stimulation than levoamphetamine, roughly three to four times more, but levoamphetamine has slightly stronger cardiovascular and peripheral effects.[34][186]

多巴胺

In certain brain regions, amphetamine increases the concentration of dopamine in the synaptic cleft.[45] Amphetamine can enter the presynaptic neuron either through DAT or by diffusing across the neuronal membrane directly.[45] As a consequence of DAT uptake, amphetamine produces competitive reuptake inhibition at the transporter.[45] Upon entering the presynaptic neuron, amphetamine activates TAAR₁ which, through protein kinase A (PKA) and protein kinase C (PKC) signaling, causes DAT phosphorylation.[45]

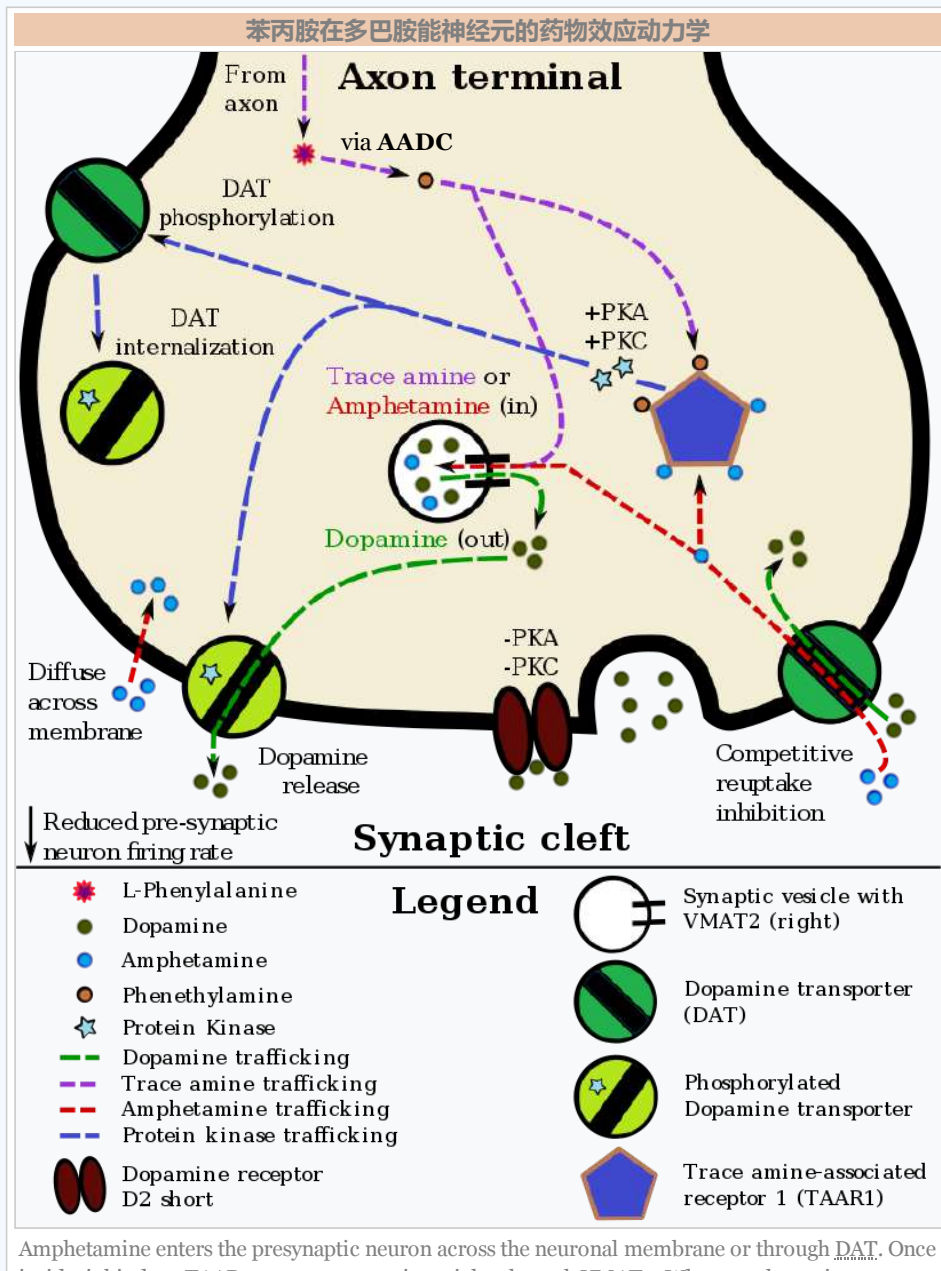
Phosphorylation by either protein kinase can result in DAT internalization (non-competitive reuptake inhibition), but PKC-mediated phosphorylation alone induces the reversal of dopamine transport through DAT (i.e., dopamine efflux).[45][187] Amphetamine is also known to increase intracellular calcium, an effect which is associated with DAT phosphorylation through an unidentified Ca²⁺/calmodulin-dependent protein kinase (CAMK)-dependent pathway, in turn producing dopamine

efflux.[165][167][188] Through direct activation of G protein-coupled inwardly-rectifying potassium channels, TAAR₁ reduces the firing rate of dopamine neurons, preventing a hyper-dopaminergic state.[189][190][191]

Amphetamine is also a substrate for the presynaptic vesicular monoamine transporter, VMAT₂.[164][192] Following amphetamine uptake at VMAT₂, amphetamine induces the collapse of the vesicular pH gradient, which results in the release of dopamine molecules from synaptic vesicles into the cytosol via dopamine efflux through VMAT₂.[164][192] Subsequently, the cytosolic dopamine molecules are released from the presynaptic neuron into the synaptic cleft via reverse transport at DAT.[45][164][192]

去甲肾上腺素

Similar to dopamine, amphetamine dose-dependently increases the level of synaptic norepinephrine, the direct precursor of epinephrine.[47][61] Based upon neuronal TAAR₁ mRNA expression, amphetamine is thought to affect norepinephrine analogously to dopamine.[45][164][187] In other words, amphetamine induces TAAR₁-mediated efflux and non-competitive



Amphetamine enters the presynaptic neuron across the neuronal membrane or through DAT. Once inside, it binds to TAAR₁ or enters synaptic vesicles through VMAT₂. When amphetamine enters the synaptic vesicles through VMAT₂, dopamine is released into the cytosol (yellow-orange area). When amphetamine binds to TAAR₁, it reduces postsynaptic neuron firing rate via potassium channels and triggers protein kinase A (PKA) and protein kinase C (PKC) signaling, resulting in DAT phosphorylation. PKA-phosphorylation causes DAT to withdraw into the presynaptic neuron (internalize) and cease transport. PKC-phosphorylated DAT may either operate in reverse or, like PKA-phosphorylated DAT, internalize and cease transport. Amphetamine is also known to increase intracellular calcium, an effect which is associated with DAT phosphorylation through a CAMKIIα-dependent pathway, in turn producing dopamine efflux.

reuptake inhibition at phosphorylated NET, competitive NET reuptake inhibition, and norepinephrine release from VMAT₂.^{[45][164]}

血清素

Amphetamine exerts analogous, yet less pronounced, effects on serotonin as on dopamine and norepinephrine.^{[45][61]} Amphetamine affects serotonin via VMAT₂ and, like norepinephrine, is thought to phosphorylate SERT via TAAR1.^{[45][164]} Like dopamine, amphetamine has low, micromolar affinity at the human 5-HT1A receptor.^{[179][180]}

其他的中枢神经递质、肽、和激素 Other neurotransmitters, peptides, and hormones

Acute amphetamine administration in humans increases endogenous opioid release in several brain structures in the reward system.^{[181][182][183]} Extracellular levels of glutamate, the primary excitatory neurotransmitter in the brain, have been shown to increase in the striatum following exposure to amphetamine.^[167] This increase in extracellular glutamate presumably occurs via the amphetamine-induced internalization of EAAT3, a glutamate reuptake transporter, in dopamine neurons.^{[167][169]} Amphetamine also induces the selective release of histamine from mast cells and efflux from histaminergic neurons through VMAT₂.^[164] Acute amphetamine administration can also increase adrenocorticotrophic hormone and corticosteroid levels in blood plasma by stimulating the hypothalamic–pituitary–adrenal axis.^{[43][184][185]}

药物代谢动力学

安非他命的口服生物体可利用率^[参 21]与肠胃的pH值连动；^[159]安非他命非常容易在肠道被吸收，dextroamphetamine的生体可利用率在多数的情况下高于75%。^[2]安非他命呈弱碱性，其pKa值介于9–10之间；^[4]因此，当pH值呈碱性时，多数的安非他命会以其易溶于脂类的纯胺类型态形式存在。在此情况下，身体会通过肠道上皮组织富含脂类的细胞膜^[参 22]来吸收安非他命。^[4]^[159]相反地，酸性的pH值表示安非他命主要以易溶于水的离子^[参 23]（盐）形式存在，因此较少能被吸收。^[4]大约15–40%循环于血管中的安非他命与血浆蛋白^[参 24]相连接。^[3]安非他命的对映异构物的半衰期会随着尿液的pH值而有所不同。^[4]当尿液的酸碱值落在正常范围内，dextroamphetamine和levoamphetamine的半衰期分别为9–11小时及11–14小时。^[4]酸性饮食会导致安非他命的对映异构物的半衰期降低至8–11小时；碱性饮食则会使安非他命的对映异构物的半衰期增加到16–31小时。^{[10][16]}

成分为安非他命或其衍生物的短效药品大约在口服后三小时在体内达到最高血浆浓度；而成分为安非他命或其衍生物的长效药品则在口服后大约七小时在体内达到最高血浆浓度。^[4]

安非他命主要透过肾脏来代谢，大约30–40%的药物以药物本身原始的型态从酸碱度正常的尿液中排出。^[4]当尿液是碱性时，安非他命倾向以其纯胺类型态存在，因此较少被排泄。^[4]

当尿液的pH值失常时，各种安非他命的分解物在尿液中重新结合的程度将从最低1%到最高75%。该程度的高低大多取决于尿液的酸碱值，尿液越酸，结合率越高；尿液愈碱，结合率越低。^[4]安非他命通常于口服后两天内自体内完全代谢完毕。^[10]安非他命确切的半衰期及药效作用期随着（小于两天的）重复服用导致的血浆内安非他命浓度（plasma concentration of amphetamine）的增加而延长。^[193]

对人体无药效的前驱药物体（prodrug）：lisdexamphetamine并不若安非他命一样容易受肠胃道环境的pH值影响；^[194]lisdexamphetamine在肠道被吸收进入血管的血液后很快就会透过水解（hydrolysis）的方式转化为dextroamphetamine。而参与这水解反应的酶（enzymes）与红血球有关。^[194]

Lisdexamphetamine的半衰期通常小于一个小时。^[194]

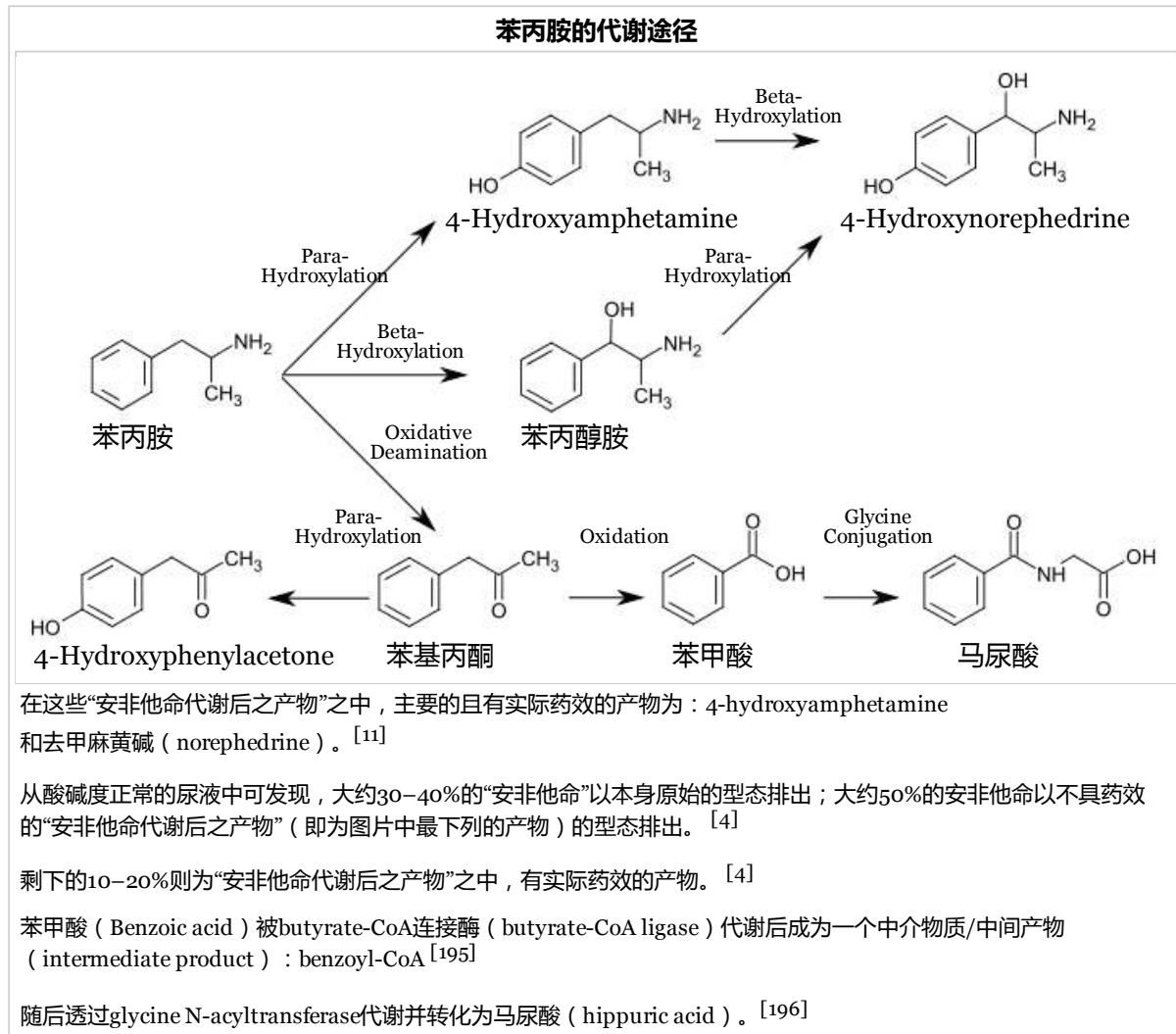
细胞色素 P450 2D6（Cytochrome P450 2D6、或CYP2D6）、多巴胺β羟化酶（Dopamine β-hydroxylase、或DBH）、flavin-containing monooxygenase 3、butyrate-CoA ligase、和 glycine N-acyltransferase为已知在人体中参与^[注 9]“安非他命”及“安非他命代谢后之产物”的代谢反应的酶（enzyme）。^[sources 14]

“安非他命代谢后之产物”包含：4-hydroxyamphetamine、4-hydroxynorephedrine、4-hydroxyphenylacetone、苯甲酸（benzoic acid）、马尿酸（hippuric acid）、苯丙醇胺（norephedrine）、苯基丙酮（phenylacetone）^[注 10]^{[4][10][11]}。

在这些“安非他命代谢后之产物”之中，有实际药效的产物（sympathomimetics）为：4-hydroxyamphetamine^[197]、4-hydroxynorephedrine^[198]、和 norephedrine^[199]。

安非他命的主要代谢途径包含：aromatic para-hydroxylation、aliphatic alpha-、beta-hydroxylation、N-oxidation、N-dealkylation、和 deamination。^{[4][10]}

下图为已知的“安非他命”代谢途径和“安非他命代谢后之产物”：[4][8][11]



相关的内部生成化合物/混和物 (endogenous compound)

历史、社会与文化

合法状态与条件

药品

备注A

- 别名有：1-phenylpropan-2-amine (IUPAC name), α -methylbenzeneethanamine, α -methylphenethylamine, amphetamine (International Nonproprietary Name [INN]), β -phenylisopropylamine, desoxynorephedrine, and speed.[18][21][22]
- 对映异构体指的是两个形状相同但方向相反的两个分子，他们又称为彼此的镜中影像。[23] Levoamphetamine 和 dextroamphetamine 分别被简称为 L-amph 或 levamfetamine (INN) 和 D-amph 或 dexamfetamine (INN) [18]
- "Adderall"是一个品牌名称。因为以下几个安非他命的异构物的英文名称太长了："dextroamphetamine sulfate, dextroamphetamine saccharate, amphetamine sulfate, and amphetamine aspartate"，因此本文单独以此名称来表示此安非他命的此种混合物。
原文对照："Adderall" is a brand name as opposed to a nonproprietary name; because the latter ("dextroamphetamine sulfate, dextroamphetamine saccharate, amphetamine sulfate, and amphetamine aspartate"^[44]) is excessively long, this article exclusively refers to this amphetamine mixture by the brand name.
- “安非他命”一词也意指一个化学分类，但与“替代性安非他命”这个化学分类不同的是，“安非他命”类在学术上并无标准的定义。[5][25]
有一个“安非他命”类的定义严格限定分类中仅有：安非他命的racemate and enantiomers 和 甲基安非他命methamphetamine的 racemate and enantiomers。[25] 大多数“安非他命”类的定义为那些在药理学上以及结构上与安非他命相关的化合物。[25]
为避免让amphetamine 和 amphetamines 把读者给弄糊涂了，本条目中仅会使用amphetamine、amphetamines来表示racemic amphetamine, levoamphetamine, and dextroamphetamine；‘替代性安非他命 (substituted amphetamines)’来表示安非他命的结构分类。
原文对照：Due to confusion that may arise from use of the plural form, this article will only use the terms "amphetamine" and

"amphetamines" to refer to racemic amphetamine, levoamphetamine, and dextroamphetamine and reserve the term "substituted amphetamines" for its structural class.

5. 研究证实, 长期以中枢神经兴奋剂治疗ADHD能在下列这些方面产生大幅的进步: 学业、驾驶、降低药物滥用、降低肥胖、自尊、和社交功能等。 [57]

在上述领域中, 最为突出的领域为: 学业(例如: GPA分数 grade point average、成果测验分数 achievement test scores、受教育的时间长度 length of education、和教育程度 education level)、自尊(例如: 自尊心测验分数 self-esteem questionnaire assessments、尝试自杀的次数、自杀率等)和社交功能(例如: peer nomination scores、社交技巧、家庭关系 quality of family、同侪关系 quality of peer、和浪漫关系/情侣关系 romantic relationships) [57]

长期以“药物治疗合并行为治疗”的模式来治疗ADHD, 能够比单独以药物治疗, 产生更全面且更长足的进步。 [57]

6. 考科蓝协作组织对于历年众多的“随机对照试验”的系统性回顾、数据统整分析后所得出的总结, 基本上都是非常有水准且深具参考价值的。 [65]
7. 美国食品药品管理局核准的药品使用指引及医疗上的禁忌(放在药盒中的仿单/说明书)并非为了限制医师的决策而是为了避免药商恣意宣称药物的作用。医师可以此为参考, 并依照每位病人的实际情况做出独立的判断。 [91]
8. 然而根据一篇回顾性论文, 安非他命可以处方给曾有药物滥用历史的人, 不过需要有对患者适度的药品控管, 例如: 每天由医护人员配给处方剂量。 [1]
9. 曾受此副作用的用药者, 身高及体重在在短暂停药后恢复至应有水准是可以被预期的。 [56][59][97] 根据追踪, 持续三年过程不停歇的安非他命治疗(没有合并任何积极减少安非他命副作用的疗法的情况下)平均会减少2公分的最终身高。 [97]
10. “95%信赖区间”指的是: 有95%的概率, 真实的死亡人数介于3,425和4,145之间。
11. 转录因子是一种可以增加或降低一个特定基因的基因表现的蛋白。

原文: Transcription factors are proteins that increase or decrease the expression of specific genes. [132]

12. 简单来说, 这里的“充分且必要(necessary and sufficient)”关系指的是“ΔFosB在伏隔核中的破表(over-expression)”与“成瘾衍生的行为”及“神经元为了适应新常态所做的调适”永远都是一起发生。

13. NMDA接受器们为与电压相关的ligand-gated ion channels。ligand-gated ion channels这个通道需要glutamate以及一个共同促进剂(co-agonist):(D-serine或大豆属glycine)的同时连接才能被开启。

原文: NMDA receptors are voltage-dependent ligand-gated ion channels that requires simultaneous binding of glutamate and a co-agonist (D-serine or glycine) to open the ion channel. [143]

14. 该篇回顾表示magnesium L-aspartate及氯化镁(magnesium chloride)能大幅改善成瘾行为。

原文: The review indicated that magnesium L-aspartate and magnesium chloride produce significant changes in addictive behavior; [107] other forms of magnesium were not mentioned.

15. The human dopamine transporter contains a high affinity extracellular zinc binding site which, upon zinc binding, inhibits dopamine reuptake and amplifies amphetamine-induced dopamine efflux *in vitro*. [160][161][162] The human serotonin transporter and norepinephrine transporter do not contain zinc binding sites. [162]

备注B

1. 智力测验结果与专注力有关, 详见注意力不足过动症#智力
2. 因成瘾所致的行为
3. 妄想的英文名称为: delusion
4. 偏执的英文名称为: paranoia
5. 原文: Consequently, ΔFosB is the most significant factor involved in both amphetamine addiction and amphetamine-induced sex addictions, which are compulsive sexual behaviors that result from excessive sexual activity and amphetamine use.
6. 原文: These sex addictions are associated with a 多巴胺失调综合征 which occurs in some patients taking 作用于多巴胺的药物.
7. 原文: One review suggested that, based upon animal testing, pathological (addiction-inducing) psychostimulant use significantly reduces the level of intracellular magnesium throughout the brain.
8. Original texts: There is no evidence that amphetamine is directly neurotoxic in humans.
9. 酶做为反应的催化剂catalyst, 并不实际参与反应。
10. 不是苯丙酮

备注C

1.

 离子通道

 G蛋白 & 偶联受体

 (Text color) 转录因子

注释

- a. 安非他命是一种春药
- b. 又称为“随机分配且包含控制组的临床试验”, 是临床试验的一种
- c. 中枢神经兴奋剂的一种

- d. 原文: This diagram depicts the signaling events in the Mesolimbic pathway that are induced by chronic high-dose exposure to psychostimulants that increase the concentration of synaptic dopamine, like 安非他命, 甲基苯丙胺, and 苯乙胺.
- e. (self-administration, i.e., doses given to oneself)

- f. 原文 : aerobic exercise decreases psychostimulant self-administration
- g. 原文 : In general, there is no significant interaction when consuming amphetamine with food, but the pH of gastrointestinal content and urine affects the absorption and excretion of amphetamine, respectively.

- h. 原文 : Acidic substances reduce the absorption of amphetamine and increase urinary excretion, and alkaline substances do the opposite.

英文名称对照

- 1. 英文名称为 : delusions
- 2. 英文名称为 : paranoia
- 3. 英文名称为 : Prescription drug
- 4. 英文名称为 : Pharmaceutical amphetamine
- 5. 英文名称为 : racemic amphetamine
- 6. 英文名称为 : Prodrug
- 7. 英文名称为 : substituted amphetamine
- 8. 英文名称为 : Bupropion
- 9. 英文名称为 : methamphetamine
- 10. 英文名称为 : Randomized controlled trials
- 11. 英文名称为 : follow-up studies
- 12. 英文名称为 : neurotransmitter systems
- 13. 英文名称为 : dopamine
- 14. 英文名称为 : locus coeruleus
- 15. 英文名称为 : prefrontal cortex
- 16. 英文名称为 : nor-epinephrine或nor-adrenaline
- 17. 英文名称为 : Cochrane Collaboration
- 18. 英文名称为 : systematic review
- 19. 英文名称为 : meta-analysis
- 20. 英文名称为 : 临床试验
- 21. 英文名称为 : bioavailability
- 22. 英文名称为 : cell membrane
- 23. 英文名称为 : cation
- 24. 英文名称为 : plasma protein

引用

1. [15][29][30][31][32][33][34][35][36][37][38][39]
2. [1][25] [29] [30] [31] [40] [41] [42] [32] [26] [24][43]
3. [1] [15] [29] [40] [43] [45] [46]
4. [47] [48] [49]
5. [33][34][97][98][99]
6. [100][101][102][103]
7. [92][93][100][102]
8. [111][112][113][114][144]
9. [22][31][34][104][116]
10. [108][111][130][133][134]
11. [51][153][156][157]
12. [164][167][168][169][170][171][172]
13. [45][164][168][169][173][179]
14. [4][5] [6] [7] [8] [9] [195] [196]

来源

1. 引用错误 : 没有为名为Amph_Uses的参考文献提供内容
2. Pharmacology. Dextroamphetamine. DrugBank. University of Alberta. 2013-02-08 [2013-11-05].
3. Pharmacology. Amphetamine. DrugBank. University of Alberta. 2013-02-08 [2013-11-05].
4. Adderall XR Prescribing Information (PDF). United States Food and Drug Administration. Shire US Inc: 12–13. December 2013 [2013-12-30].
5. Glennon RA. Phenylisopropylamine stimulants: amphetamine-related agents. (编) Lemke TL, Williams DA, Roche VF, Zito W. Foye's principles of medicinal chemistry 7th. Philadelphia, USA: Wolters Kluwer Health/Lippincott Williams & Wilkins. 2013: 646–648 [2015-09-11]. ISBN 9781609133450. "The phase 1 metabolism of amphetamine analogs is catalyzed by two systems: cytochrome P450 and flavin monooxygenase. ... Amphetamine can also undergo aromatic hydroxylation to *p*-hydroxyamphetamine. ... Subsequent oxidation at the benzylic position by DA β -hydroxylase affords *p*-hydroxynorephedrine. Alternatively, direct oxidation of amphetamine by DA β -hydroxylase can afford norephedrine."
6. Taylor KB. Dopamine-beta-hydroxylase. Stereochemical course of the reaction (PDF). J. Biol. Chem. January 1974, **249** (2): 454–458 [2014-11-06]. PMID 4809526. "Dopamine- β -hydroxylase catalyzed the removal of the pro-R hydrogen atom and the production of 1-norephedrine, (2S,1R)-2-amino-1-hydroxyl-1-phenylpropane, from d-amphetamine."
7. Horwitz D, Alexander RW, Lovenberg W, Keiser HR. Human serum dopamine- β -hydroxylase. Relationship to hypertension and sympathetic activity. Circ. Res. May 1973, **32** (5): 594–599. PMID 4713201. doi:10.1161/01.RES.32.5.594. "Subjects with exceptionally low levels of serum dopamine- β -hydroxylase activity showed normal cardiovascular function and normal β -hydroxylation of an administered synthetic substrate, hydroxyamphetamine."
8. Krueger SK, Williams DE. Mammalian flavin-containing monooxygenases: structure/function, genetic polymorphisms and role in drug metabolism. Pharmacol. Ther. June 2005, **106** (3): 357–387. PMC 1828602. PMID 15922018. doi:10.1016/j.pharmthera.2005.01.001. "Table 5: N-containing drugs and xenobiotics oxygenated by FMO (<https://www.ncbi.nlm.nih.gov/pmc/articles/PMC1828602/table/T5/>)"

9. Cashman JR, Xiong YN, Xu L, Janowsky A. N-oxygenation of amphetamine and methamphetamine by the human flavin-containing monooxygenase (form 3): role in bioactivation and detoxication. *J. Pharmacol. Exp. Ther.* March 1999, **288** (3): 1251–1260. PMID 10027866.
10. Pharmacology and Biochemistry. Amphetamine. Pubchem Compound. National Center for Biotechnology Information. [2013-10-12].
11. Santagati NA, Ferrara G, Marrazzo A, Ronsisvalle G. Simultaneous determination of amphetamine and one of its metabolites by HPLC with electrochemical detection. *J. Pharm. Biomed. Anal.* September 2002, **30** (2): 247–255. PMID 12191709. doi:10.1016/S0731-7085(02)00330-8.
12. Pharmacology. amphetamine/dextroamphetamine. Medscape. WebMD. [2016-01-21]. "Onset of action: 30–60 min"
13. Millichap JG. Chapter 9: Medications for ADHD. (编) Millichap JG. Attention Deficit Hyperactivity Disorder Handbook: A Physician's Guide to ADHD 2nd. New York, USA: Springer. 2010: 112. ISBN 9781441913968. "Table 9.2 Dextroamphetamine formulations of stimulant medication
Dexedrine [Peak:2–3 h] [Duration:5–6 h] ...
Adderall [Peak:2–3 h] [Duration:5–7 h]
Dexedrine spansules [Peak:7–8 h] [Duration:12 h] ...
25. Yoshida T. Chapter 1: Use and Misuse of Amphetamines: An International Overview. (编) Klee H. *Amphetamine Misuse: International Perspectives on Current Trends*. Amsterdam, Netherlands: Harwood Academic Publishers. 1997: 2 [2014-12-01]. ISBN 9789057020810.
"Amphetamine, in the singular form, properly applies to the racemate of 2-amino-1-phenylpropane. ... In its broadest context, however, the term [*amphetamines*] can even embrace a large number of structurally and pharmacologically related substances."
26. Amphetamine. Medical Subject Headings. United States National Library of Medicine. [2013-12-16].
27. Spencer RC, Devilbiss DM, Berridge CW. The Cognition-Enhancing Effects of Psychostimulants Involve Direct Action in the Prefrontal Cortex. *Biol. Psychiatry*. June 2015, **77** (11): 940–950. PMID 25499957. doi:10.1016/j.biopsych.2014.09.013. "The procognitive actions of psychostimulants are only associated with low doses. Surprisingly, despite nearly 80 years of clinical use, the neurobiology of the procognitive actions of psychostimulants has only recently been systematically investigated. Findings from this research unambiguously demonstrate that the cognition-enhancing effects of psychostimulants involve the preferential elevation of catecholamines in the PFC and the subsequent activation

参见

- 结合亲和性
- 体能锻炼

外部链接

- CID 3007 (<https://pubchem.ncbi.nlm.nih.gov/compound/3007>) from PubChem – Amphetamine
- CID 5826 (<https://pubchem.ncbi.nlm.nih.gov/compound/5826>) from PubChem – Dextroamphetamine
- CID 32893 (<https://pubchem.ncbi.nlm.nih.gov/compound/32893>) from PubChem – Levoamphetamine
- Comparative Toxicogenomics Database entry: Amphetamine (<http://ctdbase.org/query.go?type=ixn&chemqt>equals&chem=name%3AAamphetamine&actionDegreeTypes=increases&actionDegreeTypes=decreases&actionDegreeTypes=affected&actionTypes=ANY&geneqt>equals&gene=&pathwayqt>equals&pathway=&taxonqt>equals&taxon=TAXON%3A9606&goqt>equals&go=&sort=chemNmSort&perPage=500&action=Search>)
- Comparative Toxicogenomics Database entry: CARTPT (<http://ctdbase.org/detail.go?type=gene&acc=9607&qid=2119242>)
- YouTube上的Drug abuse and drug addictions (<https://www.youtube.com/watch?v=PLbKSbFnKYVYo7Rmg3OOd8OpHMCu1dDaUq#t=ohomos>)
- YouTube上的Mechanism of Drug Addiction in the Brain, Animation. (<https://www.youtube.com/watch?v=NxHNxmJv2bQ#t=ohomos>)
- YouTube上的Drug dependence (https://www.youtube.com/watch?v=PLbKSbFnKYVYo52TitB2-YHF2mGJp3_QJH#t=ohomos)

取自“<https://zh.wikipedia.org/w/index.php?title=苯丙胺&oldid=44948730>”

-
- 本页面最后修订于2017年6月27日 (星期二) 09:43。
 - 本站的全部文字在知识共享 署名-相同方式共享 3.0协议之条款下提供，附加条款亦可能应用（请参阅使用条款）。 Wikipedia®和维基百科标志是维基媒体基金会的注册商标；维基™是维基媒体基金会的商标。
维基媒体基金会是在美国佛罗里达州登记的501(c)(3)免税、非营利、慈善机构。

甲基苯丙胺

维基百科, 自由的百科全书

甲基苯丙胺或甲基安非他命 (英语：**methamphetamine**)，其盐酸盐或硫酸盐又称**冰毒**，微带苦味，呈白色或无色，为结晶体或粉末状，易溶于水，是一种人工合成的兴奋剂。属苯乙胺类，可还原伪麻黄碱而得。甲基苯丙胺可使机体产生强烈快感，并具成瘾性。此物质呈对映异构现象，分别为左、右旋甲基苯丙胺。

目录

- 1 历史
- 2 医用
- 3 病理原理
- 4 中毒反应
- 5 合成过程
- 6 理化性质
- 7 上瘾
- 8 作用
 - 8.1 副作用
 - 8.2 禁忌症
- 9 流行文化
- 10 参见
- 11 参考文献
 - 11.1 脚注
 - 11.2 书目
- 12 外部链接

历史

甲基苯丙胺与苯丙胺的化学结构非常相似。甲基苯丙胺是由日本化学家长井长义于1893年自麻黄碱成功合成。1919年由绪方章完成了结晶化。在近代，苯丙胺的用途及社会评价由轻视转变至具争议性到现在的嫌恶。

甲基苯丙胺在第二次世界大战分别由同盟国与轴心国以Pervitin^[10]之注册名称分发予前线，纳粹军广发甲基苯丙胺予士兵以作兴奋剂之用，特别是在苏德战争时的党卫队人员及德意志国防军。希特勒亦曾注射甲基苯丙胺。日本曾给士兵服用冰毒以提高战斗力。1941年武田制药与大日本制药（日本住友制药）曾出产市贩品，以及提供必须超长时间工作的军需工厂工人使用，故在日本本土、台湾、及日占区都遗留下许多成瘾患者。

1950年代，美国政府颁布法令将甲基苯丙胺规定为处方药，根据1951年出版的Arthur Grollman所著的《病理与药理学》一书，它可用于治疗嗜睡、后脑炎、帕金森综合征、酒精中毒，以及肥胖症。

1960年代，制造甲基苯丙胺的地下工厂开始普遍；1962年，冰毒首次作为一种违法毒品，被旧金山的摩托车黑帮制造出来，并在美国太平洋沿岸四处分发。这个黑帮很快便有了大批仿效者：制作冰毒所需要的原料非常普通，并且容易得到，比如外用酒精、碱液、麻黄碱和伪麻黄碱；最后一种当时作为非处方药供应。于是，作坊式实验室曾经生产了大量的违法甲基苯丙胺；墨西哥黑帮把大量廉价品带进了墨西哥。可以放进导管中抽吸的结晶甲基苯丙胺块在1980年代的夏威夷出现，并很快蔓延到美国大陆地区，成为最受欢迎的毒品种类。及至1980年，非医疗使用激增。其中，加州的圣地牙哥市更被称为北美的冰毒圣地（英国《经济学人》，1989年12月2日号）。

美国到1983年才制定法律管制持有甲基苯丙胺的前驱体和制造设备。1986年，美国制定了一份联邦管制药物取缔法，名为 Federal Controlled Substance Analogue Enforcement Act，以打击“设计毒品”(designer drugs)泛滥。尽管如此，吸食甲基苯丙胺仍在美国郊区(尤其是中西部和南部)上升，直至今日。而各州都在加紧立法打击。

2005年8月8日号《新闻周刊》(Newsweek)发表关于甲基苯丙胺及其滥用的专题文章[1] (<http://www.msnbc.msn.com/id/8770112/site/newsweek/>)，内容批判布什政府的相关政策，指其投放在教育和预防的资源不足。而布什政府的回应是，大麻是“引子毒品”(gateway drug)，意思是预防滥用大麻就可以预防滥用诸如冰毒等“硬性”毒品。

医用

d-甲基安非他命，药品商标Desoxyn®，医疗上用于治疗注意力不足过动症(ADHD)、嗜睡症以及极端的肥胖症等。它的右旋异构体(R+异构体)可以用于治疗注意力不足过动症，但不带甲基的安非他命更常用。它的右旋异构体药品商标为“Desoxyn”，可以用于治疗嗜睡症及肥胖。当安非他命和甲基安非他命致使患者太多副作用时，Desoxyn作为次选药物。在精神方面的作用上，右旋的R(+)构型是左旋的S(-)构型的5倍^[11]。

病理原理

甲基苯丙胺的耐受性随长期使用而增加。初次吸食者，30毫克即引起中毒。长期滥用者，为了达到初期使用时的欣快效应，会将剂量增至2000毫克，引起急性中毒，可造成惊厥、昏迷甚至死亡。

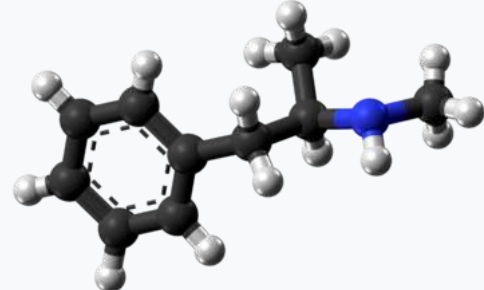
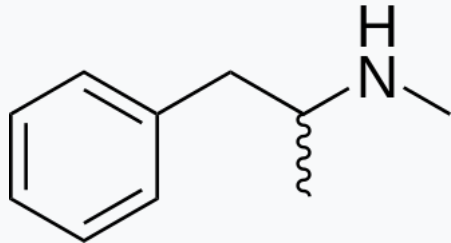
中毒反应

- 过量使用可导致急性中毒。严重者出现精神混乱、性欲亢进、焦虑、烦躁、幻觉状态、死亡。
- 长期滥用可造成慢性中毒、体重下降、消瘦、溃疡、脓肿、指甲脆化、夜间磨牙、龋齿、死亡。
- 高剂量或反复使用可产生中毒性精神病，表现有被害妄想、幻视，也可能出现听幻觉和触幻觉。亦称苯丙胺精神病。

合成过程

甲基苯丙胺与甲卡西酮(methcathinone)、苯丙胺、以及其他兴奋剂的结构相似，可以用化学还原方法从麻黄碱或伪麻黄碱制得。大多数制备的原料属于日用品或可以从商店直接买到。因此合成甲基苯丙胺显得简单易行。在网络上可以找到许多转化合成方法，通常不大可信。最有经验的行家或求教于化学课，或从那些生产安非他命的人员那儿学来。几乎每一种方法都要用到高度危险的化学品和流程。大多数的生产方法涉及到将麻黄碱/伪麻黄碱分子中羟基的氢化。在美国最通常的方式用到红磷和碘，形成氢碘酸。另一个日渐普遍的方法是使用Birch

甲基苯丙胺



系统(IUPAC)命名名称

N-methyl-1-phenylpropan-2-amine

临床数据

商品名	Desoxyn
Drugs.com	Monograph (https://www.drugs.com/monograph/methamphetamine-hydrochloride.html)
医疗法规	US FDA: Desoxyn (https://www.accessdata.fda.gov/scripts/cder/drugatfda/index.cfm?fuseaction=Search.SearchAction&SearchTerm=Desoxyn&SearchType=BasicSearch)
妊娠分级	US: C (不排除有风险的可能)
依赖性	生理: 无 心理: 高
成瘾性	非常高
给药途径	Medical: oral Recreational: oral, intravenous, insufflation, inhalation, suppository

合法状态

合法状态	AU: 受管控(S8) CA: Schedule I UK: Class A US: Schedule II UN: Schedule II 处方药 (Rx-only)
------	---

药代动力学数据

生物利用度	Oral: Varies widely ^[1] Rectal: 99% IV: 100%
-------	---

还原法^[12]，用一次性锂电池中的金属锂替代金属钠（金属钠较难获得）。Birch还原法是极其危险的，因为碱金属和无水液氨都有极高的反应性。而且当加入反应物时，液氨的温度使其极易爆沸。另一种方法是苯基丙酮与甲胺的还原胺化反应（Borch还原）^[13]，所用的都是美国缉毒局的I级化学品。其他较不常见的方法使用其他的氢化法，比如用氢气和催化剂。

理化性质

甲基苯丙胺为人工合成，结构与苯丙胺和MDMA（摇头丸）近似，比起其他毒品，结构较简单，分子量较小。

上瘾

- 甲基苯丙胺是一种高度心理上瘾的毒品，对于上瘾的人来说，在精神上和社会交际上放弃使用很难。对于大多数上瘾的人来说，再次复发是很常见的。为了不再沉溺其中，许多被挽回的上瘾者参加了十二步项目，比如CMA（一个帮助戒掉甲基苯丙胺的组织）。

作用

- 短期内增强精神力，动力和大脑活力
- 大剂量服用会增加愉悦幸福感
- 体重减轻（可能产生不利作用，根据具体情况而定）
- 增强性刺激
- 醒酒
- 增强性功能，男性持久力
- 驱除睡意

副作用

使用甲基苯丙胺的其他一般副作用包括：

- 心脏血管：高血压
- 内分泌：体温升高
- 眼睛：瞳孔放大
- 肠胃体统：痢疾，恶心，呕吐
- 神经：思想偏执和精神分裂
- 神经：兴奋之后紧接着心理抑郁
- 皮肤：皮疹，蚁走感（感觉蚂蚁在身体里钻爬）
- 生殖：勃起功能障碍
- 牙齿：牙龈破损
- 感染：葡萄球菌感染
- 其他：厌食症，失眠症，狂躁不安，体重减轻

长时间使用的严重副作用：

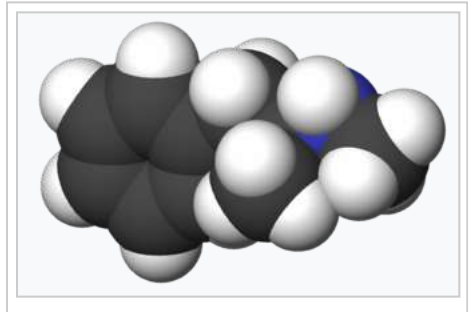
- 安非他命精神病
- 临床的抑郁症
- 肾脏损坏
- 肝功能损伤

蛋白结合度	Varies widely ^[1]
代谢	CYP2D6, ^[2] DBH ^[3] 、FMO3, ^[4] XM-ligase, ^[5] and ACGNAT ^[6]
生物半衰期	9–12 hours ^[7]
排泄	肾
识别信息	
CAS注册号	537-46-2 (http://www.commonchemistry.org/ChemicalDetail.aspx?ref=537-46-2) ✓
ATC代码	No6BA03
PubChem	CID 1206 (https://pubchem.ncbi.nlm.nih.gov/summary/summary.cgi?cid=1206)
IUPHAR/BPS	4803 (http://www.guidetopharmacology.org/GRAC/LigandDisplayForward?ligandId=4803)
DrugBank	DB01577 (http://www.drugbank.ca/drugs/DB01577) ✓
ChemSpider	1169 (http://www.chemspider.com/Chemical-Structure.1169.html) ✓
UNII	44RAL3456C (http://fdasis.nlm.nih.gov/srs/srsdirect.jsp?regno=44RAL3456C) ✓
KEGG	D08187 (http://www.kegg.jp/entry/D08187) ✓
ChEBI	CHEBI:6809 (https://www.ebi.ac.uk/chebi/searchId.do?chebiId=CHEBI:6809) ✓
ChEMBL	CHEMBL1201201 (https://www.ebi.ac.uk/chembldb/index.php/compound/inspect/CHEMBL1201201) ✓
其他名称	N-methylamphetamine, desoxyephedrine
化学信息	
化学式	C ₁₀ H ₁₅ N
摩尔质量	149.2337 g/mol
SMILES	
InChI	
物理性质	
熔点	3 °C (37 °F) [8]
沸点	212 °C (414 °F) [9] at 760 MM HG
(verify)	

禁忌症

有以下症状的人不能使用甲基苯丙胺：

- 青光眼
- 高血压
- 心脏血管疾病
- 使用不可逆转的单胺氧化酶抑制剂之后的14天内不能使用甲基苯丙胺。如果身体健康，结合使用可逆转的单胺氧化酶抑制剂是安全的，例如吗氯贝胺。



流行文化

美剧《绝命毒师》中主角制的毒品，故事中制作纯度可达到99.2%。

参见

- | | | | |
|--------------------------------|-----------|---------------------|-------|
| ▪ 毒品 | ▪ 右旋甲基苯丙胺 | ▪ 苯乙胺 | ▪ 摆头丸 |
| ▪ 苯丙胺 | ▪ 非法毒品交易 | ▪ 伪麻黄素 | |
| ▪ 甲基苯丙胺
(desoxyephedrine) | ▪ 麻黄碱 | (pseudoephedrine) | |
| | ▪ 甲卡西酮 | ▪ 药物管制 | |

参考文献

脚注

1. Toxicity. Methamphetamine. PubChem Compound. National Center for Biotechnology Information. [31 December 2013].
2. Adderall XR Prescribing Information (PDF). United States Food and Drug Administration: 12–13. December 2013 [30 December 2013].
3. Lemke TL, Williams DA, Roche VF, Zito W. Foye's Principles of Medicinal Chemistry 7th ed. Philadelphia: Wolters Kluwer Health/Lippincott Williams & Wilkins. 2013: 648. ISBN 1609133455. "Alternatively, direct oxidation of amphetamine by DA β -hydroxylase can afford norephedrine."
4. Krueger SK, Williams DE. Mammalian flavin-containing monooxygenases: structure/function, genetic polymorphisms and role in drug metabolism. Pharmacol. Ther. June 2005, **106** (3): 357–387. PMC 1828602. PMID 15922018. doi:10.1016/j.pharmthera.2005.01.001.
5. 引用错误：没有为名为Benzoic1的参考文献提供内容
6. 引用错误：没有为名为Benzoic2的参考文献提供内容
7. 引用错误：没有为名为Schep的参考文献提供内容
8. Properties: Predicted – EP|Suite. Methamphetamine. Chemspider. [3 January 2013].
9. Chemical and Physical Properties. Methamphetamine. PubChem Compound. National Center for Biotechnology Information. [31 December 2013].
10. SID 271075 PubChem Substance Page on Methamphetamine (<http://pubchem.ncbi.nlm.nih.gov/summary/summary.cgi?sid=271075>)
11. 张建新, 张大明, 等. 从甲基苯丙胺的对映体特征推断前体化学品. 卫生研究, 2009, 04. <http://www.cnki.com.cn/Article/CJFDTOTAL-WSYJ200904015.htm>
12. Illinois Attorney General. Illinoisattorneygeneral.gov. [2011-01-09]. 已忽略文本“Basic Understanding Of Meth”(帮助)
13. A Synthesis of Amphetamine. J. Chem. Educ. 51, 671 (1974). Erowid.org. [2011-01-09].

书目

- *Methamphetamine Use: Clinical and Forensic Aspects*, by Errol Yudko, Harold V. Hall, and Sandra B. McPherson. CRC Press, Boca Raton, Fl, 2003.
- *YAA BAA. Production, Traffic and Consumption of Methamphetamine in Mainland Southeast Asia*, by Pierre-Arnaud CHOUVY & Joël MEISSONNIER Singapore University Press, 232 p., 2004. (<http://www.pa-chouvy.org/yaabaa-methamphetamine-production-traffic-consumption.htm>)
- Fighting Methamphetamine in the Heartland: How Can the Federal Government Assist State and Local Efforts? (<http://www.usdoj.gov/dea/pubs/cngrtest/cto20604.htm>) Statement of Armand McClinton Assistant Special

Agent in Charge Indianapolis District Office Drug Enforcement Administration Before the House Committee on Government Reform Subcommittee on Criminal Justice, Drug Policy and Human Resources, February 6, 2004

- *Phenethylamines I Have Known And Loved: A Chemical Love Story*, Alexander Shulgin and Ann Shulgin , (ISBN 978-0-9630096-0-9) . a.k.a. PiHKAL. synthesis. online (<http://fj.sina.com.cn/xm/news/sz/2012-05-26/091038464.html>)

外部链接

- Second National Conference on Methamphetamine ~ Science & Response: 2007 (<http://www.methconference.org>) This year's conference will once again be driven by collaboration and diversity - it will introduce the latest in methamphetamine research and innovative programming to the widest audience possible.
- A Key to Methamphetamine-Related Literature (http://www.nyhealth.gov/diseases/aids/harm_reduction/crystalmeth/docs/meth_literature_index.pdf) This is a comprehensive thematic index of methamphetamine-related journal articles with links from citations to the corresponding PubMed abstracts.
- Life or Meth - Content Geared Towards The Gay Community (<http://www.lifeormeth.com/>)
- Newsweek - "America's Most Dangerous Drug" (<http://www.msnbc.msn.com/id/8770112/site/newsweek/>), see also Slate - "Meth Madness At Newsweek" (<http://slate.msn.com/id/2123838/>)
- Erowid Methamphetamine Vault (<http://fj.sina.com.cn/xm/news/sz/2012-05-26/091038464.html>)
- Frontline: The Meth Epidemic (Accessed 2/15/06) (<http://www.pbs.org/wgbh/pages/frontline/meth/>)
- Geopium: Geopolitics of Illicit Drugs in Asia (<http://www.geopium.org>)
- Special Report on Meth in California's Central Valley (<http://www.valleymeth.com>)
- "New Yorker" story on the impact of widespread methamphetamine abuse (http://www.newyorker.com/printables/fact/050523fa_fact)
- BBC story on high levels of use of methamphetamine amongst the male gay community (<http://news.bbc.co.uk/1/hi/uk/4604047.stm>)
- Drug Enforcement Administration (<http://www.usdoj.gov/dea/>):
 - Brief on amphetamines (http://www.dea.gov/concern/meth_factsheet.html)
- Asia & Pacific Amphetamine - Type Simulant Information Centre (<http://www.apaic.org>) - a very extensive information source managed by the United Nations Office on Drugs and Crime.
- Rotten Library: Methamphetamine (<http://www.rotten.com/library/crime/drugs/methamphetamine/>)
- Meth In Missouri (<http://methinmissouri.livejournal.com/>) A research blog on meth culture (especially in Missouri) that seeks your input- stories, comments, questions
- Montana Meth Project (<http://www.notevenonce.com/>)
- Is Meth A Plague, A Wildfire, Or the Next Katrina? ~ Reason.com (<http://www.reason.com/sullum/o90205.shtml>)
- Crystal Breaks (<http://www.crystalbreaks.org>) A Chicago-area campaign addressing meth use in the gay community.
- Crystal Meth Anonymous (<http://www.crystalmeth.org>) A 12-Step-based Meth Recovery group.
- Meth Strike Force (<http://2stopmeth.org/main.php?pg=gallery>) GALLERY and more

取自“<https://zh.wikipedia.org/w/index.php?title=甲基苯丙胺&oldid=44904428>”

-
- 本页面最后修订于2017年6月24日 (星期六) 08:09。
 - 本站的全部文字在知识共享署名-相同方式共享 3.0 协议之条款下提供，附加条款亦可能应用（请参阅使用条款）。 Wikipedia®和维基百科标志是维基媒体基金会的注册商标；维基™是维基媒体基金会的商标。维基媒体基金会是在美国佛罗里达州登记的501(c)(3)免税、非营利、慈善机构。

可卡因

维基百科，自由的百科全书

可卡因 (INN : **Cocaine**) , 又译为**古柯碱**。为一强烈的兴奋剂，常拿来做为娱乐性药物^[8]。可卡因常以粉末方式由鼻腔吸入或是静脉注射的方式使用。可能造成的心灵影响有思觉失调、欣快感，或者精神激动。生理上的症状可能包括心跳过速、出汗与瞳孔放大^[9]。高剂量的可卡因会造成高血压或中暑^[10]。使用后数秒到分钟即出现效果，并持续5到90分钟^[9]。可卡因偶尔也会用于医疗用途，例如局部麻醉与减少鼻部手术的出血^[11]。

可卡因具有成瘾性，原因是由于其作用于脑中的奖赏路径。短时间使用后，会出现依赖性的高风险^[8]。使用可卡因也会增加中风、心肌梗死、肺部问题、败血症与猝死的风险^{[8][12]}。一般街头犯罪上贩卖的可卡因，常见的会混入局部麻醉药、玉米淀粉、奎宁或者糖类等会增加额外毒性的物质^[13]。持续反复使用可卡因，会减少感觉快乐的能力与身体疲累^[8]。

可卡因是5-羟色胺、去甲肾上腺素，和多巴胺的再摄取抑制剂，会使脑部这三种神经递质的浓度上升^[8]。可卡因可以轻易地通过血脑屏障，而且可能会造成血脑屏障的破坏^{[14][15]}。可卡因是由古柯的叶子制成，此一植物的主要产地在南美^[9]。2013年合法生产的可卡因数量有419公斤^[16]。估计美国每年非法可卡因的市场在一千亿到五千亿美元之间，可卡因可再经过进一步的加工，制成霹雳可卡因^[8]。

每年用药人数约在1400万至2100万人之间，其中北美洲的用量最大，其次为欧洲和南美洲^[8]。其中 1-3% 的发达国家人口在他的一生中至少使用过可卡因一次^[17]。2013年，可卡因直接导致约4300人死亡，比起1990年的2400人上升了许多^[18]。秘鲁人从远古时代就有嚼食古柯叶的习俗^[13]。1860年，可卡因首次由古柯叶内纯化出来^[8]。1961年起，国际麻醉品单一公约要求各国将所有非医学用途的可卡因使用入罪规范^[18]。

目录

- 1 历史
- 2 上瘾成因及危险
 - 2.1 毒性比较
- 3 参考文献
- 4 外部链接

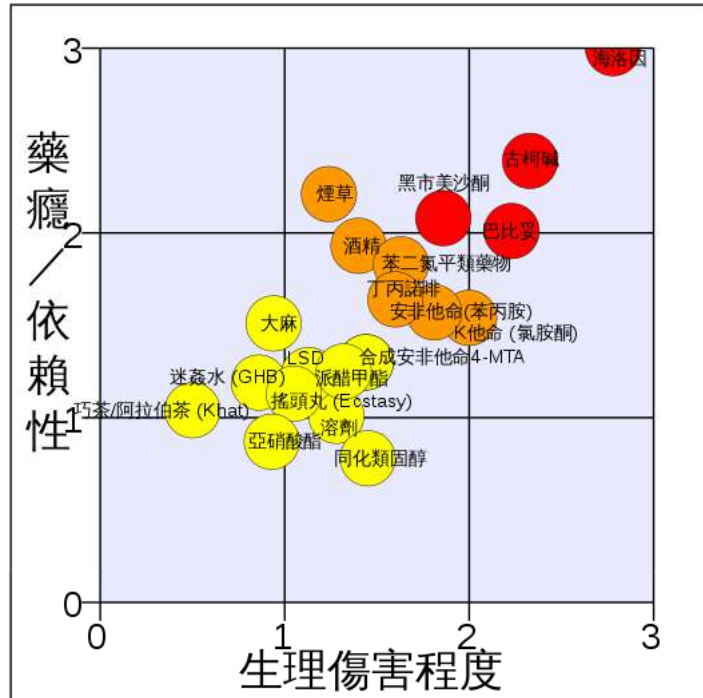
历史

- 最早是亚美利哥·韦斯普奇 (Amerigo Vespucci) 于公元1499年写下他对于嚼古柯叶者的印象，这是欧洲人最早的相关记载。在他眼中，这种人两颊塞满奇怪的草药，反刍般地咀嚼不停，实在是他所见过最丑陋最野蛮的人^[19]。
- 1855年，德国化学家斐德烈 (G.Friedrich) 首度从古柯叶中提取出麻药成分，并命名为“Erythroxylon”。四年后，斐德烈的同事纽曼 (A.Newman) 又精制出更高纯度的物质，替名为“可卡因” (Cocaine) 。首部以古柯树为研究的药用书籍则在1859年出版。
- 1860年，已有医生由古柯叶中提炼出可卡因，并作为医学用之麻醉药品。
- 1880年代初期，以6%可卡因成分之药酒问世，称为马林安尼。
- 1884年，著名的心理学家佛洛伊德推荐使用可卡因来作为酒精与吗啡上瘾之替代药品。
- 1886年问世之可口可乐，尚含有微量可卡因，不过可口可乐后于1906年排除此配方。
- 2009年时，红牛能量饮料 (Red Bull Energy Drink) 曾被台湾及香港验出有微量可卡因成分，但不会影响人体。

上瘾成因及危险

毒性比较

资料来自权威医学期刊：《柳叶刀》关于常见管制药品其伤害性及成瘾性比较，包括烟草、酒。

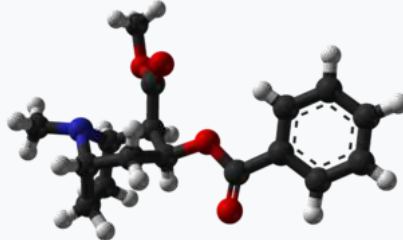
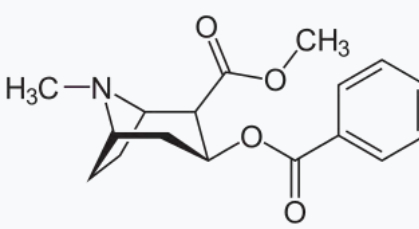


可卡因成瘾最大原因是吸食者需寻求更多的可卡因来逃离这种吸食后之沮丧感。另外，因可卡因造成死亡的例子并不多见。不过，可卡因仍会对吸食者造成身体上的严重戕害，例如：阻碍脑部神经传递质多巴胺、并影响正肾上腺素、血清素正常摄取，加速大脑老化^[20]。除此，可卡因还会严重影响神经系统、血管的收缩、瞳孔的扩大及导致心跳不正常。

因为可卡因成瘾性强，并对吸食者产生健康伤害，1914年，美国即宣布可卡因为禁药，该禁令延续至今。与美国相同，至今绝大部分国家都将可卡因视为毒品，至今可卡因仍为西方世界主要毒品之一。

参考文献

- Freye, Enno. Pharmacology and abuse of cocaine, amphetamines, ecstasy and related designer drugs a comprehensive review on their mode of action, treatment of abuse and intoxication Online-Ausg. Dordrecht: Springer. 2009: 63. ISBN 9789048124480.
- Hamid Ghodse. Ghodse's Drugs and Addictive Behaviour: A Guide to Treatment 4. Cambridge University Press. 2010: 91. ISBN 9781139485678.
- Introduction to Pharmacology Third Edition. Abingdon: CRC Press. 2007: 222–223. ISBN 9781420047424.
- Fattinger K, Benowitz NL, Jones RT, Verotta D. Nasal mucosal versus gastrointestinal absorption of nasally administered cocaine. Eur. J. Clin. Pharmacol. 2000, **56** (4): 305–10. PMID 10954344. doi:10.1007/s002280000147.
- Barnett G, Hawks R, Resnick R. Cocaine pharmacokinetics in humans. J Ethnopharmacol. 1981, **3** (2–3): 353–66. PMID 7242115. doi:10.1016/0378-8741(81)90063-5.



系统 (IUPAC) 命名名称

methyl (1*R*,2*R*,3*S*,5*S*)-3- (benzoyloxy)-8-methyl-8-azabicyclo[3.2.1] octane-2-carboxylate

临床数据

Drugs.com Micromedex详细消费者药物信息 (<https://www.drugs.com/con/cocaine.html>)

妊娠分级 US: C (不排除有风险的可能)

依赖性 Physical: Yes^{[1][2]}
Psychological: High^[2]

成瘾性 High^[3]

给药途径 外用、口服、insufflation、静脉注射

合法状态

合法状态 AU: 受管控 (S8)
CA: Schedule I
NZ: Class A
UK: Class A
US: Schedule II
UN: Narcotic Schedules I and III
处方药 (Rx-only)

药代动力学数据

生物利用度 口服: 33%^[4]
Insufflated: 60^[5]–80%^[6]
Nasal spray: 25^[7]–43%^[4]

代谢 肝脏 (CYP3A4)

生物半衰期 1 小时

排泄 肾脏 (苯甲酰芽子碱和芽子碱甲酯)

识别信息

CAS注册号 50-36-2 (<http://www.commonchemistry.org/ChemicalDetail.aspx?ref=50-36-2>) ✓

6. Jeffcoat AR, Perez-Reyes M, Hill JM, Sadler BM, Cook CE. Cocaine disposition in humans after intravenous injection, nasal insufflation (snorting), or smoking. *Drug Metab. Dispos.* 1989, **17** (2): 153–9. PMID 2565204.
7. Wilkinson P, Van Dyke C, Jatlow P, Barash P, Byck R. Intranasal and oral cocaine kinetics. *Clin. Pharmacol. Ther.* 1980, **27** (3): 386–94. PMID 7357795. doi:10.1038/clpt.1980.52.
8. Pomara, C; Cassano, T; D'Errico, S; Bello, S; Romano, AD; Riezzo, I; Serviddio, G. Data available on the extent of cocaine use and dependence: biochemistry, pharmacologic effects and global burden of disease of cocaine abusers.. *Current medicinal chemistry.* 2012, **19** (33): 5647–57. PMID 22856655.
9. Zimmerman, JL. Cocaine intoxication.. *Critical care clinics.* October 2012, **28** (4): 517–26. PMID 22998988.
10. Connors, NJ; Hoffman, RS. Experimental treatments for cocaine toxicity: a difficult transition to the bedside.. *The Journal of pharmacology and experimental therapeutics.* November 2013, **347** (2): 251–7. PMID 23978563.
11. Harper, SJ; Jones, NS. Cocaine: what role does it have in current ENT practice? A review of the current literature.. *The Journal of laryngology and otology.* October 2006, **120** (10): 808–11. PMID 16848922.
12. Sordo, L; Indave, BI; Barrio, G; Degenhardt, L; de la Fuente, L; Bravo, MJ. Cocaine use and risk of stroke: a systematic review.. *Drug and alcohol dependence.* 1 September 2014, **142**: 1–13. PMID 25066468.
13. Goldstein, RA; DesLauriers, C; Burda, AM. Cocaine: history, social implications, and toxicity--a review.. *Disease-a-month : DM.* January 2009, **55** (1): 6–38. PMID 19081448.
14. Sharma, HS; Muresanu, D; Sharma, A; Patnaik, R. Cocaine-induced breakdown of the blood–brain barrier and neurotoxicity. *International Review of Neurobiology.* 2009, **88**: 297–334. ISBN 978-0-12-374504-0. PMID 19897082. doi:10.1016/S0074-7742(09)88011-2.
15. Karch, Steven B. Karch's pathology of drug abuse 4. Boca Raton: CRC Press. 2009: 70. ISBN 9780849378812.
16. Narcotic Drugs 2014 (pdf). INTERNATIONAL NARCOTICS CONTROL BOARD. 2015: 21. ISBN 9789210481571.
17. GBD 2013 Mortality and Causes of Death, Collaborators. Global, regional, and national age-sex specific all-cause and cause-specific mortality for 240 causes of death, 1990–2013: a systematic analysis for the Global Burden of Disease Study 2013.. *Lancet.* 17 December 2014. PMID 25530442. doi:10.1016/S0140-6736(14)61682-2.
18. Room, R; Reuter, P. How well do international drug conventions protect public health?. *Lancet.* 7 January 2012, **379** (9810): 84–91. PMID 22225673.
19. 书名：上瘾五百年，David T. Courtwright著，薛绚译，立绪出版
20. 可卡因可能会加速大脑老化. [2012-04-29].

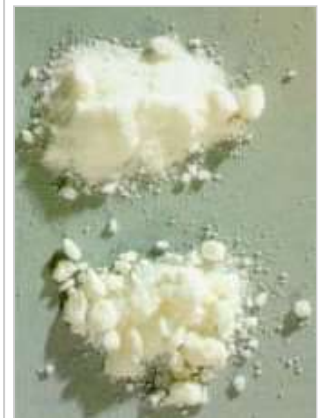
外部链接

- 可卡因的历史 (http://www.dls.ym.edu.tw/neuroscience/coca_c.html)
- 可卡因对人体的危害 (<http://drug.faceteen.org/Cocaine.html>)

取自“<https://zh.wikipedia.org/w/index.php?title=可卡因&oldid=44415830>”

ATC代码	No1BCo1 R02AD03, S01HA01, S02DA02
PubChem	CID 5760 (https://pubchem.ncbi.nlm.nih.gov/summary/summary.cgi?cid=5760)
IUPHAR/BPS	2286 (http://www.guidetopharmacology.org/GRAC/LigandDisplayForward?ligandId=2286)
DrugBank	DBoo907 (http://www.drugbank.ca/drugs/DBoo907) ✓
ChemSpider	10194104 (http://www.chemspider.com/Chemical-Structure.10194104.html) ✓
UNII	I5Y540LHVR (http://fdasis.nlm.nih.gov/srs/srsdirect.jsp?regno=I5Y540LHVR) ✓
KEGG	D00110 (http://www.kegg.jp/entry/D00110) ✓
ChEBI	CHEBI:27958 (https://www.ebi.ac.uk/chebi/searchId.do?chebiId=CHEBI:27958) ✓
ChEMBL	CHEMBL120901 (https://www.ebi.ac.uk/chembl/index.php/compound/inspect/CHEMBL120901) ✗
其他名称	benzoylmethylecgonine
PDB配体ID	COC (PDBe (http://www.ebi.ac.uk/pdbe-srv/PDBeXplore/ligand/?ligand=COC), RCSB PDB (http://www.rcsb.org/pdb/search/smartsSubquery.do?smartSearchSubtype=ChemCompIdQuery&chemCompId=COC&polymType=Any))
化学信息	
化学式	$C_{17}H_{21}NO_4$
摩尔质量	303.353 g/mol
SMILES	
InChI	
物理性质	
熔点	98 °C (208 °F)
沸点	187 °C (369 °F)
水溶液	HCl: 1800–2500 mg/mL (20 °C)
✗✓ (what is this?) (verify)	

- 本页面最后修订于2017年5月19日 (星期五) 11:11。
 - 本站的文字在知识共享署名-相同方式共享 3.0 协议之条款下提供，附加条款亦可能应用（请参阅使用条款）。
- Wikipedia®和维基百科标志是维基媒体基金会的注册商标；维基™是维基媒体基金会的商标。
维基媒体基金会是在美国佛罗里达州登记的501(c)(3)免税、非营利、慈善机构。



从古柯树叶提炼之纯古柯碱

作者: Raymond Stevens 来源: 《科学》 发布时间: 2010-11-30 11:13:31

选择字号: 小 中 大

科学家解析多巴胺神经递质受体

近日由斯克里普斯研究所的科学家领导的一个研究小组揭示了一个多巴胺神经递质受体的结构，研究论文发表在11月19号的《科学》(Science)杂志上。虽然多巴胺传递对于正常大脑功能是必不可少的，然而一直以来科学家们对于参与这一关键的神经元相互作用的分子生物学组成仍知之甚少。

这项研究工作是由威尔康乃尔医学院(Weill Cornell Medical College)、Receptos公司、国立药物滥用研究所和哥伦比亚大学内科与外科医生学院的研究人员协作完成。在新研究中，科学家们揭示了多巴胺D3受体(D3R)的结构。

“揭示D3R结构将有助于我们了解多巴胺受体亚家族的独特特性，尤其是发现D2与D3的特异性，”论文的资深作者、斯克里普斯研究所教授Raymond C. Stevens说：“这是一项史无前例的、重要的多巴胺相关性研究。”

“通过先进的样品制备技术结合晶体学技术，我们确定了人类多巴胺D3受体的结构。D3R结构的揭示将推动寻找靶向这一受体的新药。”Jean Chin博士说。Jean Chin在国立卫生研究院(NIH)工作，主要负责监管Stevens的研究资金，该研究资金主要来自美国国立研究院共同基金和蛋白结构计划的资金援助。

G蛋白偶联受体家族

在D3R之前，斯克里普斯研究所的科研人员已经揭示了三个G蛋白偶联受体(GPCRs)的结构。近期他们又得到了国立卫生研究院蛋白结构计划超过1600万美元的资金资助。

人类大约有1000个G蛋白偶联受体，这些受体的主要功能是将细胞外信号传递至细胞内，从而启动细胞反应改变细胞活性。目前在市场上销售的药物一半以上都是针对这些受体的，然而由于这些药物无法与受体紧密结合，有时候会引起一些副作用或是使得它们的效力低于预期。

“我们的长远目标是更好地了解G蛋白偶联受体结构与功能的关系，并获得新的生物学见解，”Stevens说：“最终我们将获得大量G蛋白偶联受体序列家族的结构及生化数据，并从中获得高质量的样本，从而对其他相近的家族成员进行可靠的模拟和预测性研究。”

Stevens和同事们花费了超过17年的时间才解开第一个G蛋白偶联受体——β2肾上腺素能受体的结构，这一研究成果在2007年公布于众。由于他的研究队伍拥有对这些受体结构和功能研究的强大平台，近年来他们多次发表了关于几个关键的G蛋白偶联受体的研究成果。2008年他们发现了与疼痛、心脏功能和呼吸相关的A2A腺苷受体的结构。2010年10月他们又公布了对免疫调节相关的CXCR4受体的研究数据。

“通过解析G蛋白偶联受体的结构和功能，研究人员精确地了解这些受体与它们的配体——神经递质、激素、气味甚至是光等相结合的机制，以及这些偶联激活或抑制关键的信号途径的机制，”Stevens说：“新结构的发现将大大推动我们对G蛋白偶联受体生物学的了解，提高药物发现的成功率。”

三年努力的成果

D3R结构的解开是由多个领域的科研人员历时三年时间共同协作研究获得的成果。

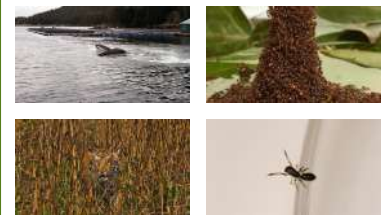
“D3R或许是我们解析的所有受体中结构最不稳定的。我们相信存在一些我们目前尚不清楚的脂质或其他的小分子对于这个受体产生了影响。现在我们还在继续开展研究希望找到D3R在试管中不稳定的原因，”Stevens说。

相关新闻

相关论文

- 1 科学家发现导致多发性硬化症相关受体
- 2 美研究称多巴胺基因变异影响青少年学习成绩
- 3 台湾研究人员发现“尼古丁受体”证实吸烟致乳癌
- 4 德国研究发现降压药B受体阻滞剂可降低乳腺癌扩散风险
- 5 “多巴胺D2受体”研究为治疗“第一晚效应”提供新思路
- 6 研究显示：多巴胺可提高人对快乐预期
- 7 《PLoS生物学》：研究揭示奖励促进认知的具体机制
- 8 日研究称精神分裂症或与多巴胺过剩有关

图片新闻



>>更多

一周新闻排行

一周新闻评论排行

- 1 中欧联合实验室20年 中法荷打造高精尖合作
- 2 以失败的名义，和航天一起走向更强
- 3 一博士生一年内发表《细胞》《自然》两篇论文
- 4 教育部公示“万人计划”教学名师初评人选
- 5 2017年度“香江学者计划”资助人选公布
- 6 庄小威访问母校中国科大会场“站”无虚席
- 7 大亚湾新发现：也许我们算错了核反应
- 8 第十五届上海市科技精英正式候选人公示
- 9 2017“千人计划”青年项目申报工作补充通知
- 10 清华大学党委换届 陈旭当选党委书记

>>更多

编辑部推荐博文

- 《科学网三条红线》修订，望周知
- 孔乙己之学术版
- 20世纪60年代的教学改革决定了现在的格局
- 贯穿一生的护牙指
- “高考状元”的升级版
- 探访应县木塔

>>更多

论坛推荐

- 有限元分析(四) —有限元方法(O.C.Zienkiewicz)曾攀译
- Manual of Engineering Drawing(工程绘图手册)
- 金属材料标准手册(上)(下)
- 2013年新著——摩擦学：基础与进展(英文版)
- 经典英文原著《电机及驱动》

研究证实eticlopride（一种用于多巴胺受体研究的实验化合物）可与D3R及D2R结合。由于D3R与D2R结构非常相似，仅存在一些非常微小的差异，通过解析D3R的结构研究人员构建出了D2R的结构模型。

“许多治疗精神分裂症的药物都可同时与D2R和D3R结合，但由于存在各种副作用使这些药物的功效受到了限制。了解受体的结构将有助于获得选择性的多巴胺受体药物，” Stevens说。

现在研究人员已经获得了有代表性的多巴胺受体结构，他们计划在接下来的工作中进一步研究其他受体亚家族例如阿片类受体或5-羟色胺受体。（来源：生物通）

更多阅读

[《科学》发表论文摘要（英文）](#)

特别声明：本文转载仅仅是出于传播信息的需要，并不意味着代表本网站观点或证实其内容的真实性；如其他媒体、网站或个人从本网站转载使用，须保留本网站注明的“来源”，并自负版权等法律责任；作者如果不希望被转载或者联系转载稿费事宜，请与我们接洽。

[打印](#) | [发E-mail给：](#) 

以下评论只代表网友个人观点，不代表科学网观点。

查看所有评论

读后感言：

验证码： 点击输入验证码

[发表评论](#)

[关于我们](#) | [网站声明](#) | [服务条款](#) | [联系方式](#) | [中国科学报社](#) | 京ICP备07017567号-12 京公网安备110402500057号

Copyright @ 2007-2017 中国科学报社 All Rights Reserved

地址：北京市海淀区中关村南一条乙三号

电话：010-62580783

· 重型机械空气动力学

[更多>>](#)

作者：黄辛 李晨阳 来源：科学网 www.sciencecn.com 发布时间：2017/7/6 11:20:33

选择字号：小 中 大

人源大麻素受体“阴阳双面”均获解析

上海科大GPCR团队再发重要成果

7月6日，上海科技大学iHuman研究所的科研团队在《自然》杂志上发表重要成果，成功解析了人源大麻素受体CB1与激动剂——四氢大麻酚（THC）类似物复合物的三维精细结构，揭示了大麻素受体在激动剂调控下的结构特征和激活机制。

G蛋白偶联受体（GPCR）是人体内最大的细胞膜表面受体家族，在细胞信号转导过程中发挥核心作用。作为药物研发领域的“宠儿”，目前有近40%的上市药物以GPCR为作用靶点。

GPCR有两类配体：起激活作用的配体（激动剂）使受体活化，而起抑制作用的配体（拮抗剂）则抑制受体活性的发挥。针对不同的GPCR，激动剂或拮抗剂配体具有不同的药物开发价值。

大麻素受体CB1是人体中枢神经系统表达量最高的GPCR之一，对人的精神和情绪调节至关重要。大麻素受体CB1的激动剂在疼痛、炎症、多发性硬化症及神经退行性疾病等的治疗中有非常大的潜力，但激动剂小分子，例如大麻里的主要精神类成分THC，是如何与CB1相互作用以及受体的活化机制等却尚不清楚。

iHuman研究团队与美国东北大学的Makriyannis实验室合作，成功解析了CB1与两种新型激动剂小分子的三维精细结构。研究结果为今后针对GPCR的药物设计提供了新的思路。

去年10月，iHuman研究所团队率先在《细胞》杂志上发表了人源大麻素受体CB1与一种拮抗剂小分子复合物的高分辨率三维结构。因此，此项研究不仅是继去年之后取得的又一重大突破，也等于从激动剂和拮抗剂两个方面，看清了这个受体的“阴阳双面”。

论文共同通讯作者之一——iHuman研究所副所长、教授刘志杰说：“这些成果不仅对内源性大麻素系统功能机制研究极其重要，对一系列疾病，如炎症、疼痛和多发性硬化症等的药物研发也有重要的指导意义。同时，对于大麻滥用及合法化等问题，该研究也有非常重要的社会价值。”



[打印](#) | [发E-mail给：](#) [go](#)

以下评论只代表网友个人观点，不代表科学网观点。

目前已**0**条评论

[查看所有评论](#)

读后感言 (您好:Jerkwin)

[发表评论](#)



- | 相关新闻 | 相关论文 |
|---|---|
| 1 复旦揭示甘露糖受体调节过敏性炎症反应新机制 | 1 复旦揭示甘露糖受体调节过敏性炎症反应新机制 |
| 2 西南大学等首次发现微孢子虫极管侵染相关受体蛋白 | 2 西南大学等首次发现微孢子虫极管侵染相关受体蛋白 |
| 3 上海药物所发现B型G蛋白偶联受体激活新机制 | 3 上海药物所发现B型G蛋白偶联受体激活新机制 |
| 4 《细胞》发表新成果：破解大麻素受体谜团 | 4 《细胞》发表新成果：破解大麻素受体谜团 |
| 5 浙江大学医学院揭示代谢与免疫新机制 | 5 浙江大学医学院揭示代谢与免疫新机制 |
| 6 上海科大解析出人源大麻素受体三维精细结构 | 6 上海科大解析出人源大麻素受体三维精细结构 |
| 7 一种独脚金内酯受体被发现 | 7 一种独脚金内酯受体被发现 |
| 8 邵峰院士：细胞内细菌与受体斗争的观察者 | 8 邵峰院士：细胞内细菌与受体斗争的观察者 |

图片新闻



>>更多

一周新闻排行

一周新闻评论排行

- | | |
|--|--|
| 1 中欧联合实验室20年 中法荷打造高精尖合作 | 1 中欧联合实验室20年 中法荷打造高精尖合作 |
| 2 以失败的名义，和航天一起走向更强 | 2 以失败的名义，和航天一起走向更强 |
| 3 一博士生一年内发表《细胞》《自然》两篇论文 | 3 一博士生一年内发表《细胞》《自然》两篇论文 |
| 4 教育部公示“万人计划”教学名师初评人选 | 4 教育部公示“万人计划”教学名师初评人选 |
| 5 2017年度“香江学者计划”资助人选公布 | 5 2017年度“香江学者计划”资助人选公布 |
| 6 庄小威访问母校中国科大 会场“站”无虚席 | 6 庄小威访问母校中国科大 会场“站”无虚席 |
| 7 大亚湾新发现：也许我们算错了核反应 | 7 大亚湾新发现：也许我们算错了核反应 |
| 8 第十五届上海市科技精英正式候选人公示 | 8 第十五届上海市科技精英正式候选人公示 |
| 9 2017“千人计划”青年项目申报工作补充通知 | 9 2017“千人计划”青年项目申报工作补充通知 |
| 10 清华大学党委换届 陈旭当选党委书记 | 10 清华大学党委换届 陈旭当选党委书记 |

[更多>>](#)

编辑部推荐博文

- 《科学网三条红线》修订，望周知
- 孔乙己之学术版
- 20世纪60年代的教学改革决定了现在的格局
- 贯穿一生的护牙指
- “高考状元”的升级版

Neurotransmitter and psychostimulant recognition by the dopamine transporter

Kevin H. Wang^{1†*}, Aravind Penmatsa^{1†*} & Eric Gouaux^{1,2}

Na⁺/Cl⁻-coupled biogenic amine transporters are the primary targets of therapeutic and abused drugs, ranging from antidepressants to the psychostimulants cocaine and amphetamines, and to their cognate substrates. Here we determine X-ray crystal structures of the *Drosophila melanogaster* dopamine transporter (dDAT) bound to its substrate dopamine, a substrate analogue 3,4-dichlorophenethylamine, the psychostimulants D-amphetamine and methamphetamine, or to cocaine and cocaine analogues. All ligands bind to the central binding site, located approximately halfway across the membrane bilayer, in close proximity to bound sodium and chloride ions. The central binding site recognizes three chemically distinct classes of ligands via conformational changes that accommodate varying sizes and shapes, thus illustrating molecular principles that distinguish substrates from inhibitors in biogenic amine transporters.

Signals by the biogenic amine neurotransmitters—dopamine (DA)¹, serotonin² and noradrenaline³—at chemical synapses are terminated by the cognate neurotransmitter sodium symporters (NSSs)^{4–7}. Biogenic amines play profound roles in the development and function of the nervous system, as well as in animal behaviour and activity; thus NSSs are central to normal neurophysiology and are the targets of a spectrum of therapeutic and illicit agents, from antidepressants and antianxiety medications to cocaine and amphetamines⁸. Experimental and computational studies have shown that the DA, serotonin (SERT) and noradrenaline (NET) transporters harbour a conserved structural fold^{9,10}, first seen in the structure of LeuT¹¹. Owing to variations in amino acid sequences¹², however, the biogenic amine transporters possess distinct yet overlapping pharmacological ‘fingerprints’¹³.

The dopamine transporter (DAT)¹⁴ removes DA from synaptic and perisynaptic spaces, thus extinguishing its action at G-protein coupled DA receptors. To drive the vectorial ‘uphill’ movement of extracellular DA into presynaptic cells, DAT couples substrate transport to pre-existing sodium and chloride transmembrane gradients. Congruent with the multifaceted roles of DA in the nervous system, perturbation of dopaminergic signalling by disruption of native DAT function has profound consequences^{15–17}. On the one hand, the amphetamines, potent and widely abused psychostimulants, are DAT substrates that enhance synaptic levels of DA both by competing with DA transport by DAT and by inducing the release of DA from synaptic vesicles into the cytoplasm, from where DA is then effluxed through DAT into the synaptic space^{18–24}. On the other hand, the *Erythroxylum coca* leaf-derived alkaloid, cocaine, as well as synthetic cocaine derivatives are competitive inhibitors of DAT and enhance extracellular DA concentrations by locking the transporter in a transport inactive conformation^{14,25–27}. Widely prescribed antidepressants specifically inhibit serotonin and noradrenaline uptake and typically have weaker affinities towards DAT^{28,29}.

Mutagenesis, chemical modification, binding and transport studies have implicated the central or S1 binding site in DAT, akin to the leucine and tryptophan site in LeuT, as the binding site occupied by DA, amphetamines, cocaine and antidepressants^{25,26,30}. Moreover, the X-ray structure of a transport-inactive *Drosophila melanogaster* DAT

(dDAT) in complex with nortriptyline shows the antidepressant bound at the central site^{9,31}. Nevertheless, none of these studies have visualized the binding of DA, amphetamine or cocaine to an active DAT, nor have they illuminated distinctions in ligand pose and transporter conformation between substrates and inhibitors. Here we present X-ray structures of dDAT with substrates DA, methamphetamine or D-amphetamine, with the DA analogue 3,4-dichlorophenethylamine (DCP), and with cocaine or cocaine analogues.

Resurrection of transport activity

The previously reported structure of the dDAT-nortriptyline complex exploited a transport-inactive variant with five thermostabilizing mutations (dDAT_{cryst})⁹. We recovered transport function yet retained favourable crystallization properties by reverting three thermostabilizing mutations (V275A, V311A and G538L) to their wild-type identities and by shifting the deletion of extracellular loop 2 (EL2; Extended Data Fig. 1). This minimal functional construct, dDAT_{mfc}, has a melting temperature of 48 °C³², exhibits DA transport with a K_M of $8.2 \pm 2.3 \mu\text{M}$ and V_{max} of $2.4 \pm 0.2 \text{ pmol min}^{-1}$ per 10^6 cells, compared to wild-type dDAT (dDAT_{wt}) with a K_M of $2.1 \pm 0.7 \mu\text{M}$ and V_{max} of $4.5 \pm 0.4 \text{ pmol min}^{-1}$ per 10^6 cells (s.e.m., Fig. 1a). The dDAT_{mfc} construct binds nisoxetine with a K_d of 36 nM compared to a K_i of 5.6 nM for wild-type dDAT³¹ (Extended Data Fig. 2).

The central binding site in DAT, NET and SERT can be divided to subsites A, B and C^{29,33}. Subsites A and C are well conserved in dDAT versus human DAT (hDAT), whereas subsite B, a pocket sculpted by TMs (transmembrane helices) 3 and 8, differs from hDAT in that residues lining this pocket in dDAT are Asp121 and Ser426 (Extended Data Fig. 3). We introduced mutations D121G (TM3) and S426M (TM8) into the dDAT_{cryst} and dDAT_{mfc} constructs to mimic hDAT subsite B³³. These mutations enhanced the affinities for nisoxetine, β-CFT (2β-carbomethoxy-3β-(4-fluorophenyl)tropine) and DCP (Extended Data Figs 2, 4). Although constructs harbouring subsite B substitutions improved crystallization propensity, transport activity was extinguished (Extended Data Fig. 3c). Nevertheless, structures bearing these mutations were solved in complexes with cocaine, β-CFT, RTI-55(2β-carbomethoxy-3β-(4-iodophenyl)tropine)

¹Vollum Institute, Oregon Health & Science University, 3181 SW Sam Jackson Park Road, Portland, Oregon 97239, USA. ²Howard Hughes Medical Institute, Oregon Health & Science University, 3181 SW Sam Jackson Park Road, Portland, Oregon 97239, USA. [†]Present addresses: Amgen, Division of Molecular Structure and Characterization, Cambridge, Massachusetts 02142, USA (K.H.W.) and Molecular Biophysics Unit, Indian Institute of Science, Bangalore 560012, India (A.P.).

*These authors contributed equally to this work.

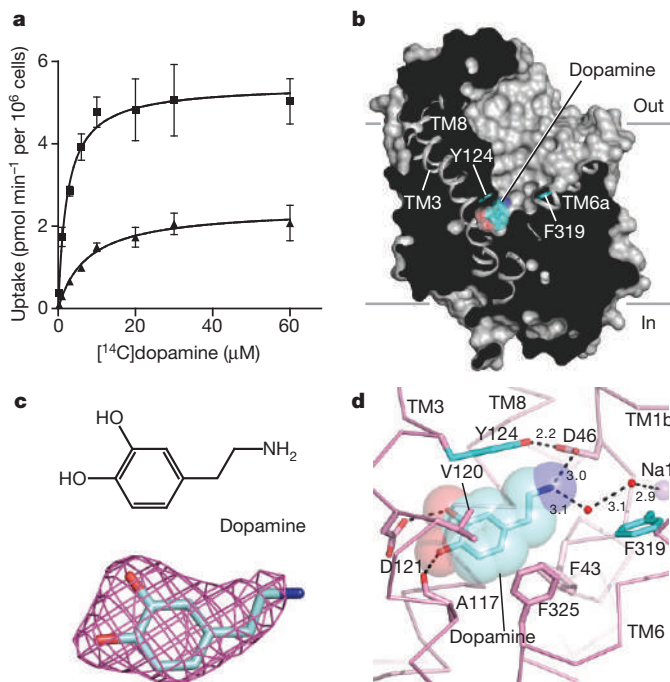


Figure 1 | Dopamine occupies central binding site. **a**, Michaelis–Menten plots of specific DA uptake by dDAT_{WT} (squares) and dDAT_{mfc} (triangles). Graph depicts one representative trial of two independent experiments. Error bars represent s.d. values for technical replicates measured in triplicate. **b**, Surface representation of the dDAT_{mfc}–DA complex viewed parallel to the membrane, with DA displayed as cyan spheres. Residues Y124 and F319 are shown as cyan sticks on the left and right sides of DA, respectively. **c**, Chemical structure and $F_o - F_c$ density for DA (3.0 σ). **d**, Close-up view of DA in the binding pocket with hydrogen bonds shown as dashed lines. Sodium ions and water are shown as purple and red spheres, respectively.

or DCP (Supplementary Table 1). In the cocaine, RTI-55 and DCP complexes, superposition of structures with subsite B mutations onto structures of dDAT_{mfc} complexes did not reveal prominent structural changes in the binding pocket or deviations in the positions of bound ligand (Extended Data Table 1).

Dopamine bound to central binding site

The structure of dDAT_{mfc} bound to DA displays an outward-open conformation (Fig. 1b) where DA is situated in the central binding site, surrounded by TMs 1, 3, 6 and 8. The amine group points towards subsite A and interacts with the carboxylate of Asp46 at a distance of 3 Å. The catechol group occupies a subsite B cavity sculpted by Ala117, Val120, Asp121, Tyr124, Ser422 and Phe325 (Fig. 1c, d), residues predicted to interact with DA using homology models of DAT based on the substrate-bound occluded state of LeuT, analysis of uptake kinetics, and cysteine labelling studies^{10,25,26,34}. Despite a lack of steric interference from DA, Phe319, which is equivalent to Phe253 in LeuT (in which it occludes solvent access to the LeuT binding pocket), remains splayed away from DA, in an orientation seen in the nortriptyline-bound structure^{9,11}.

The location and interactions of DA with dDAT recall predictions made through homology models of hDAT, although discrepancies between the cocrystal structure and the homology models are also evident. Site-directed mutagenesis and molecular dynamics simulations pointed to the crucial role of Asp46 (Asp79 in hDAT) in the recognition of DA^{10,25,34,35}, a residue conserved amongst biogenic amine neurotransmitters. GAT (γ -amino butyric acid transporter), GlyT (glycine transporter), and LeuT contain glycine at the equivalent position owing to the presence of a compensatory carboxylate group in the substrates¹¹. One notable difference between the dDAT_{mfc}-DA structure and previous hDAT models, however, is a rotation in the χ_1

torsion angle of $\sim 130^\circ$ in the side chain of Asp46 to maintain a 3 Å distance to the amine group of DA. This rotation severs the indirect coordination between Asp46 and the sodium ion at site 1 as observed in the nortriptyline-dDAT_{cryst} complex⁹. Unlike previous simulation studies where DA binds in a dehydrated pocket³⁴, we observed non-protein electron density 3.1 Å from the amine group of DA, into which a water molecule was modelled. This water molecule forms a hydrogen bond with the water molecule that coordinates the sodium ion at site 1, resulting in a molecular network that links DA to the ion-binding sites. In the case of LeuT, substrate interaction with sodium site 1 is direct, with the carboxylate of leucine coordinating the sodium ion¹¹.

The catechol ring of DA interacts with TMs 3 and 8 by hydrogen bonds with the carboxylate group of Asp121 (Fig. 1d). Modelling studies predicted that DA occupies multiple poses within the binding pocket with the *meta*-hydroxyl either interacting with residues in TM8 equivalent to Ser421 or to Ser422 (dDAT numbering)³⁴. By contrast, in the structure of dDAT_{mfc}-DA, the *para*-hydroxyl group interacts with both the carbonyl oxygen of Ala117 and the carboxylate of Asp121 at distances of 2.8 and 3.1 Å, respectively, whereas the *meta*-hydroxyl group interacts with the side chain of Asp121 at a distance of 2.7 Å and faces Ser422 in TM8 at a distance of 3.8 Å.

The residues poised to interact with the catechol ring vary across DAT orthologues with invertebrate DAT orthologues retaining alanine and aspartate at positions equivalent to residues 117 and 121, respectively, whereas in most mammalian DATs residue Asp121 is replaced by glycine and Ala117 by serine⁹, the latter of which could act as a surrogate hydrogen bond partner for the catechol group. With hNET, the equivalent residues at 117 and 121 are Ala and Gly, raising the possibility of the catechol group of noradrenaline interacting with the hydroxyl of Ser420 in hNET (TM8; equivalent to Ser422 of dDAT and Ala423 in hDAT). We propose that these compensatory variations within subsite B dictate catecholamine recognition common to both DAT and NET. To explain why NET binds noradrenaline and DA with nearly equal apparent affinity yet DAT prefers DA³¹, we must invoke longer-range, indirect interactions, perhaps involving subsite B and the non-helical TM6a–6b ‘linker’ because the ‘Phe-box’ surrounding the β -carbon position is conserved between NET and DAT.

Recognition of D-amphetamine and methamphetamine

To understand how amphetamines are transported by DAT despite lacking the hydroxyl groups of the catecholamines, we characterized the interactions between amphetamines and dDAT by binding assays and crystallographic studies. (+)-methamphetamine displaces [³H]nisoxetine binding to dDAT_{mfc} with a K_i value of 31 µM, whereas D-amphetamine, which lacks the *N*-methyl group present in methamphetamine, has a K_i of 86 µM (Fig. 2a). D-amphetamine is 10 to 100-fold weaker in its ability to inhibit DA transport in the dDAT compared to its mammalian counterparts³¹. The weaker affinities of dDAT for amphetamines compared to mammalian DATs may be due in part to differences in residues of subsite B. Indeed, the presence of Asp121 and Ser426 in invertebrate DATs creates a polar environment that does not complement the non polar benzyl groups of amphetamines (Fig. 1d). In mammalian DATs both methamphetamine ($K_i = 0.5$ µM) and D-amphetamine ($K_i = 0.6$ µM) are nearly as effective as cocaine (0.2 µM) at inhibition of DA uptake³⁶. Although the maximal rate of transport (V_{max}) for D-amphetamine in hDAT is fivefold lower than for DA, the K_M values range from 0.8 to 2 µM²², consistent with the notion that mammalian subsite B is more complementary towards the binding of amphetamines than subsite B in invertebrate DATs.

The structures of (+)-methamphetamine-dDAT_{mfc} and D-amphetamine-dDAT_{mfc} displayed outward open conformations with electron densities for the drugs found in the central binding site (Extended Data Fig. 5; Fig. 2b). The amine groups of methamphetamine

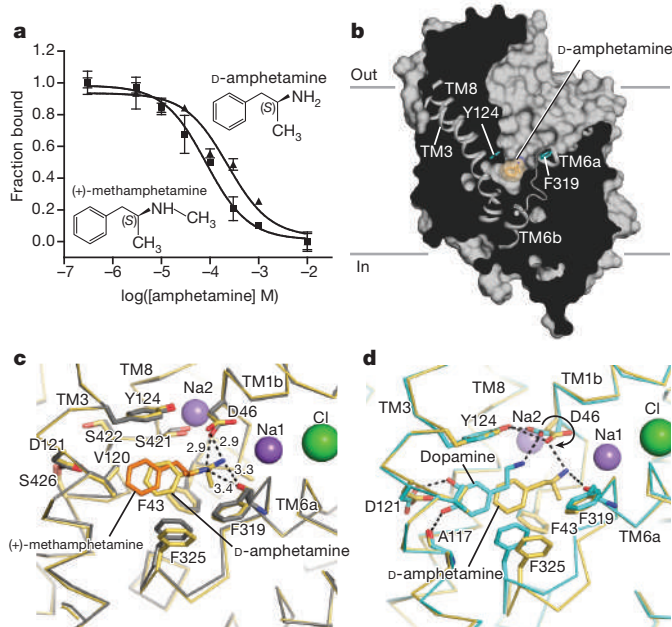


Figure 2 | Amphetamines bind to central site. **a**, Displacement of bound [³H]nisoxetine by methamphetamine ($K_i = 31 \mu\text{M}$; squares) and D-amphetamine ($K_i = 86 \mu\text{M}$; triangles). Graph depicts one representative trial of two independent experiments. Error bars represent s.e.m. values for technical replicates measured in triplicate. **b**, Surface representation of D-amphetamine-dDAT_{mfc} complex viewed parallel to the membrane with ligands shown as a light orange sphere. Residues Y124 and F319 are shown as cyan sticks on the left and right sides of DA, respectively. **c, d**, Superposition of binding pockets of the D-amphetamine-dDAT_{mfc} structure in pale orange with binding pockets of methamphetamine-dDAT_{mfc} (**c**, drug in orange, backbone in grey) and DA-dDAT_{mfc} in teal (**d**). Hydrogen bond interactions are represented as dashed lines. Asp46 undergoes a $\gamma 1$ torsion angle shift from -168° in DA-bound state to $+62^\circ$ in the D-amphetamine-dDAT_{mfc}.

and D-amphetamine lie closer to Asp46 at subsite A with hydrogen bonding distances of 2.9 Å, and the main chain carbonyl of Phe319 is positioned nearby at 3.3 Å (Fig. 2c). The amine group of D-amphetamine interacts with Asp46, which does not undergo the rotameric shift as seen in the DA-bound structure because D-amphetamine is situated in the centre of the pocket and not displaced by 2.8 Å towards TMs 3 and 8 as seen with DA (Fig. 2d). By contrast with earlier findings²⁵, we do not observe a disruption of the hydrogen bond between Asp46 and Tyr124 despite Asp46 clearly forming a hydrogen bond with the primary amine of D-amphetamine. Phe325 retains edge-to-face aromatic interactions with the phenyl group of amphetamines by way of a contraction of the TM6a–6b linker in comparison to the DA-bound state. Amphetamines adopt poses in the central binding that allow for interactions between their amino and aromatic groups and transporter subsites, thus explaining how the sterically smaller amphetamines compete with DA and act as substrates despite the absence of catechol-like hydroxyl groups.

Dopamine analogue stabilizes partially occluded state

DA is prone to oxidation and thus we sought a stable analogue for crystallographic and biochemical studies. Multiple high-affinity biogenic amine transporter inhibitors harbour halogen groups on the aromatic rings predicted to occupy subsite B^{33,37} and thus we screened halogenated phenethylamine derivatives for binding to dDAT (Extended Data Fig. 4d). We discovered that 3,4-dichlorophenethylamine (DCP) possessed the greatest affinity and, because it is approximately isosteric to DA, was selected for further study (Fig. 3a).

One DCP molecule is lodged in the central binding pocket, with the amine group forming a hydrogen bond with Asp46, and the

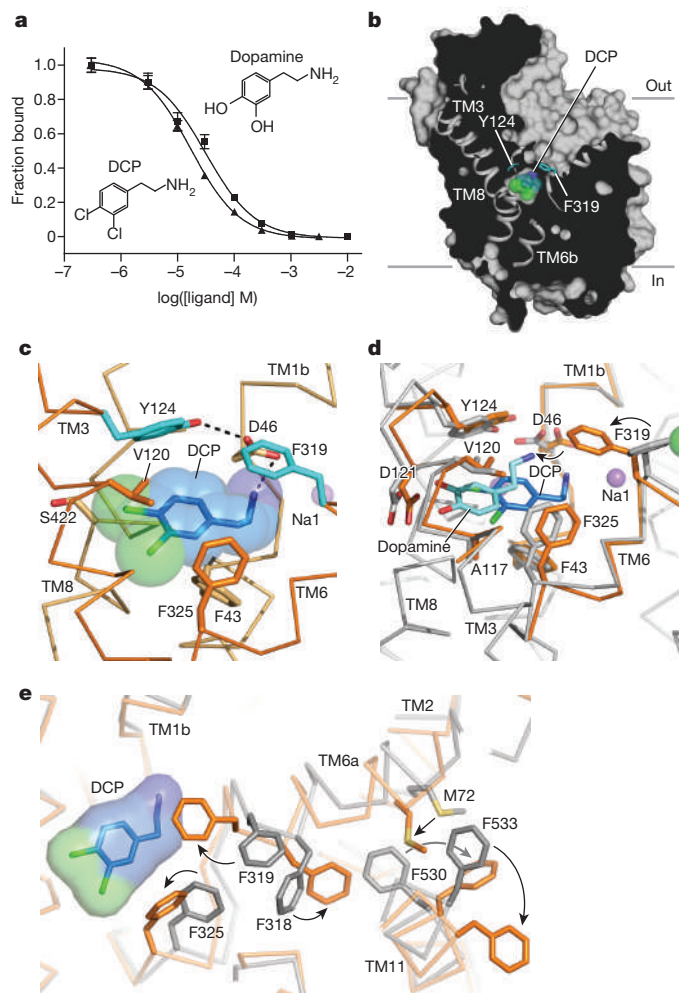


Figure 3 | DCP induces partial occlusion of central site. **a**, DCP and DA inhibit binding of [³H]nisoxetine to dDAT_{mfc} with K_i constants of 4.5 and 8.3 μM , respectively. Graph depicts one representative trial of two independent experiments, and data points indicate average values of technical replicates measured in triplicate for DA (squares) and DCP (triangles). Error bars represent s.d. values for individual data points measured in triplicate. **b**, Surface representation of the DCP-dDAT_{mfc} complex viewed parallel to the membrane with DCP shown as blue spheres and chloride in green. Residues Y124 and F319 are shown as cyan sticks on the left and right sides of DCP, respectively. **c**, Close-up view of DCP in the binding pocket showing the hydrogen bond between the primary amine of DCP and D46 with a distance of 3.2 Å. Sodium ions are shown as purple spheres. **d**, Superposition of DA- and DCP-bound dDAT_{mfc} structures reveals a 3.1 Å displacement in ligand position. The DA-dDAT_{mfc} and DCP-dDAT_{mfc} structures are coloured grey and orange, respectively. **e**, Conformational changes of phenylalanine side chain positions in the partially occluded state of DCP-dDAT_{mfc} compared to the outward open state of nortriptyline-dDAT_{cryst} coloured orange and grey, respectively.

dichlorophenyl ring bordered by Val120 and Phe325 in subsites B and C, respectively (Fig. 3b–d, Extended Data Fig. 6). The position of DCP in the pocket is closer to that of D-amphetamine in dDAT and of substrate leucine in LeuT¹¹, whereas the position of DA is shifted towards TMs 3 and 8, probably owing to hydrogen bonding between the catechol hydroxyl groups and Asp121. As a result, the position of Asp46 in the DCP-bound structure is superimposable with the positions seen in the amphetamine-bound structures. Interestingly, the side chain of Phe319 rotates to occlude the binding pocket, a conformational change not seen in any of the inhibitor- or DA-bound structures (Fig. 3c, d). This rotamer of Phe319 prevents solvent access to the pocket, leaving an aperture only ~ 1 Å wide on the extracellular side of DCP. The equivalent residue in LeuT, Phe253, adopts the same

orientation in the occluded substrate-bound form, supporting the notion that the rearrangements seen in the DCP-dDAT_{mfc} structure are on the pathway to a LeuT-like occluded state of dDAT¹¹. Unlike the DA-bound state, there is no evidence of a water molecule associated with DCP in the structures, suggesting that formation of an occluded state is associated with dehydration of the binding pocket (Fig. 3c, d), similar to LeuT.

The partially occluded binding pocket of the DCP-dDAT_{mfc} structure primarily results from rotations of TM1b and 6a ‘into’ the binding pocket, towards scaffold helices 3 and 8 and around axes centred near the non helical regions of TMs 1b and 6a (Extended Data Fig. 6a, c). In LeuT, studies of the transporter in solution and in the crystal show that TMs 1b and 6a, along with EL4, undergo conformational changes to close the extracellular gate^{11,38,39}. Comparisons with the outward-open nortriptyline-bound state of dDAT⁹ and the occluded state of LeuT indicate that, although the DCP ligand is nearly inaccessible to the extracellular solution, the inward rotations of TMs 1b (5.6°) and 6a ($\sim 7^\circ$) are less pronounced in dDAT than in LeuT¹¹ (Extended Data Fig. 6f, g). Nevertheless, these helical rotations position the side chain of Phe319 over the extracellular face of the binding pocket, and are associated with a series of phenylalanine side chain reorientations (Fig. 3e). TM11 undergoes an outward movement of 6° to accommodate these side chain shifts, and an inward movement of 5° is observed in TM2 (Extended Data Fig. 6b, d). Interestingly, TMs 2, 7 and 11 at the inner leaflet of the plasma membrane form a second cholesterol binding site (site 2) where a density for cholestrylo hemisuccinate (CHS) was observed in all the reported structures. Indeed, CHS enhances dDAT inhibitor affinity and we speculate that, in native membranes, cholesterol binds to sites 1 and 2, perhaps stabilizing DAT in an outward-open state (Extended Data Fig. 7)^{39–41}.

The occluded state is a Michaelis–Menten-like transport intermediate for LeuT and related transporters such as BetP, Mhp1 and MhsT^{42–44} when bound to substrate. Disparities in conformations observed between LeuT and dDAT in the presence of substrate, however, may reflect bona fide differences that are dependent on the relative stabilities of distinct substrate-bound states. Nevertheless, we cannot exclude crystal lattice effects, Fab binding, lipid, or solutes present in the crystallization solutions that may favour the outward-open conformation observed for the dDAT–substrate complexes reported here.

Cocaine binds in the central site

The structure of the dDAT_{mfc}–cocaine complex exhibits an outward-open conformation (Fig. 4a) with cocaine bound to the central pocket at a site overlapping the nortriptyline site⁴⁵, adjacent to the Na1 and Na2 sodium ions and the chloride ion. The tertiary amino group of cocaine forms a salt bridge with Asp46 (TM1b) (Fig. 4b). We observe that the TM6a–6b linker contracts, allowing Phe325 to form edge-to-face aromatic interactions with the benzyl ring of cocaine (Fig. 4c).

The negative electrostatic potential of subsite B in dDAT compared to mammalian DATs probably underlies the reduced affinity of dDAT for cocaine. Altering this charged pocket to mimic mammalian DATs with the mutations D121G and S426M yielded a dDAT construct with enhanced binding affinities for cocaine and β-CFT, but not for RTI-55 (Fig. 4d, Extended Data Fig. 4a, b). We speculate that the carboxylate group of Asp121 does not form favourable interactions with the 4-fluorophenyl and 4-iodophenyl groups of β-CFT and RTI-55, respectively, perhaps accounting for some of the discrepancies in relative binding affinities between hDAT and dDAT.

Ligand docking studies using a homology model of DAT, in combination with biochemical binding assays and ligand-dependent disulphide trapping experiments, have probed the orientation of cocaine in the central binding site^{25,26,30}. These studies predicted that the fluorophenyl moiety of β-CFT forms a hydrogen bond with the side chain equivalent to Asn125 in dDAT. Furthermore, the methyl ester of cocaine was thought to displace the side chain of Tyr124 to

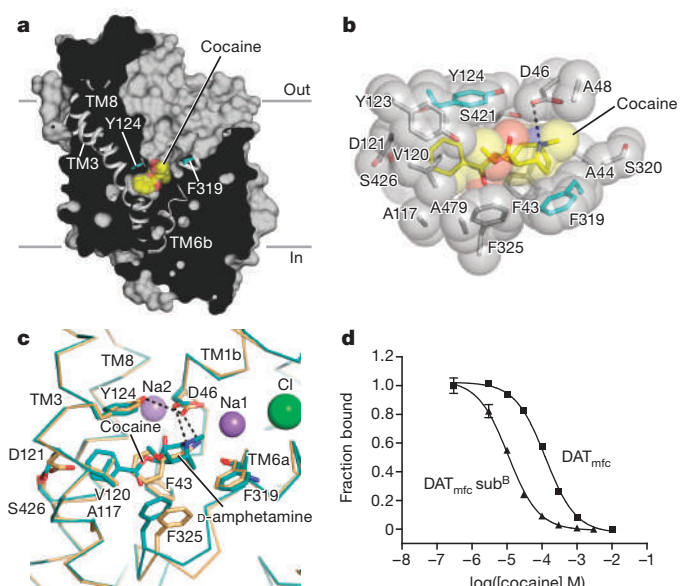


Figure 4 | Multivalent binding of cocaine. **a**, Surface representation of the structure of cocaine–dDAT_{mfc} viewed parallel to the membrane, with cocaine displayed as yellow spheres. Residues Y124 and F319 are shown as cyan sticks on the left and right sides of cocaine, respectively. **b**, Close-up view of cocaine in the binding pocket with residues interfacing with cocaine shown as spheres. The tertiary amine of cocaine is 3.4 Å from the carboxylate of D46. **c**, Superposition of the binding pocket of the D-amphetamine–dDAT_{mfc} structure in pale orange with the binding pocket of the cocaine–dDAT_{mfc} structure in teal. **d**, Displacement of [³H]nisoxetine by cocaine for dDAT_{mfc} (squares) and dDAT_{mfc} sub^B (triangles) constructs with inhibition constant (K_i) values of $33 \pm 3 \mu\text{M}$ and $3 \pm 0.3 \mu\text{M}$, respectively. Graph depicts one representative trial of two independent experiments, and data points indicate average values of technical replicates measured in triplicate.

abrogate the hydrogen bond between Tyr124 and Asp46 as a mechanism of inhibiting transporter function. The dDAT_{mfc}–cocaine structure contradicts the finding that cocaine disrupts the Asp46–Tyr124 interaction and does not place the side chain of Asn125 in a location where it could interact with the fluorophenyl group of β-CFT.

To validate the cocaine-bound structure and conclusively identify residues that interact with tropane-based ligands, structures of dDAT were solved in the presence of the cocaine analogues β-CFT and RTI-55. Anomalous scattering by the iodide of RTI-55 corroborated the location and placement of the aromatic moiety of cocaine proximal to TMs 3 and 8 (Extended Data Fig. 8a). The $F_o - F_c$ ‘omit’ electron density maps for cocaine, β-CFT, and RTI-55 are consistent with the methyl ester group protruding into the base of the extracellular vestibule without disrupting the Asp46–Tyr124 interaction (Extended Data Figs 5, 8b). The position of β-CFT places the fluoro group 6 Å from the amide nitrogen of Asn125, indicating that Asn125 does not directly participate in binding of β-CFT. Superpositions of the cocaine–dDAT_{mfc}, β-CFT–dDAT_{cryst}, and RTI-55–dDAT_{mfc} structures exhibited overall mean root-mean-square deviation (r.m.s.d.) values below 0.7 Å, and residues that make close contacts with the ligands overlap nearly entirely, indicating that the halide-substituted phenyl groups of β-CFT and RTI-55 do not markedly affect the architecture of the binding pocket (Extended Data Table 1).

Residues in the binding pocket that interact with cocaine are shared by β-CFT and RTI-55, with slight deviations in subsite B owing to the presence of halide substituents on these latter two inhibitors. At the distal end of the ligand, the halophenyl rings of β-CFT and RTI-55 or the benzoate of cocaine form van der Waals interactions primarily with Ala117, Val120, Tyr124, Phe325 and Ser422, all of which

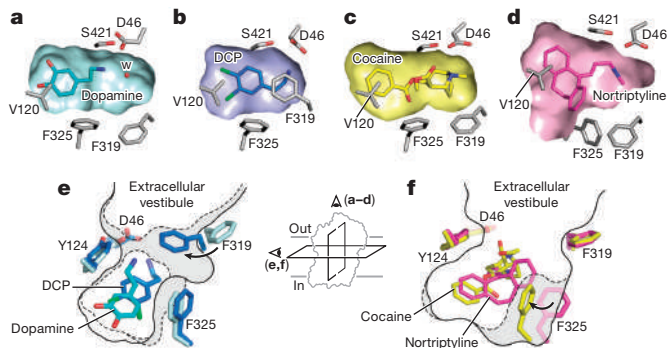


Figure 5 | Plasticity confers versatile recognition. **a–d**, Transverse sections of the binding pocket of dDAT_{mfc} are shown as surface representations in the DA-**(a)**, DCP-**(b)**, cocaine-**(c)** and nortriptyline-bound **(d)** structures. A water molecule (W) is observed in the vicinity of DA in **a**. **e,f**, Schematic representing plasticity within the substrate and drug binding pockets in occluded state of DCP-dDAT_{mfc} (broken lines) with DA-dDAT_{mfc} (solid line) **(e)** and cocaine-dDAT_{mfc} (broken lines) with nortriptyline-dDAT_{cryst} **(f**, grey, PDB ID 4M48) (solid line). Inset represents schematic to show field of view for **a–d** and **e,f**.

were previously predicted to interact with these tropane-based inhibitors^{25,46,47} (Fig. 4b). A comparison with the antidepressant nortriptyline-dDAT_{cryst} structure⁹ reveals that the smaller benzoate group of cocaine is accommodated with a shift of the TM6a–6b linker and a rotation of Phe325 into the binding pocket, which was not previously predicted. The tropane rings of cocaine, β-CFT and RTI-55 are bordered by Phe43, Ala44, Asp46, Ala48, Phe319 and Ser421. The side chain of Phe319 maintains a similar orientation as seen in the dDAT–nortriptyline structure owing to the bulky tropane ring and the methyl ester group present in all three tropane inhibitors. Overall, the docking and photolabelling studies predicted the location and orientation of cocaine and its analogues to overlap with the DA-binding site of DAT^{25,26,30}. Our structures validate these findings yet indicate distinctions that have implications for the mechanism of inhibition by tropane ligands. Taken together, structures of dDAT in complex with tropane ligands suggest that inhibition is achieved by combining a free amine with bulky tropane and aromatic moieties to limit conformational movements of the transporter.

Plasticity of the substrate binding pocket

The inhibitor- and substrate-bound structures of dDAT indicate that the binding pocket of dDAT accommodates ligands of varying sizes largely by adjusting the orientation of the discontinuous region of TM6 and the side chains of Phe319 and Phe325 (Fig. 5; Extended Data Table 2a). Ligand recognition by dDAT is bipartite and requires an amine group that interacts with the carbonyl oxygens of Phe43 and Phe319 or the carboxylate of Asp46 in subsite A, in combination with an aromatic group that is stabilized by van der Waals interactions with residues lining a hydrophobic cleft formed by TMs 3, 6, and 8 of subsite B. The substrates DA, D-amphetamine, and methamphetamine each contain one phenyl ring linked to an ethylamine chain, requiring Phe325 to rotate inward to contract the size of the pocket and maintain edge-to-face aromatic interactions with these ligands (Extended Data Fig. 8c, Fig. 5a, e). In the DCP-dDAT_{mfc} structure, Phe319 also rotates inward to cover the ligand, and similar to LeuT, this reorientation of Phe319 is required for the formation of the occluded state (Extended Data Fig. 8d, Fig. 5b, e). In order for Phe319 to cover DCP in the pocket, rotation of Phe319 is accompanied by the inward tilting of TM6a to bring the hinge region of TM6 towards the ligand (Extended Data Fig. 6). Accommodation of the single phenyl rings in tropane inhibitors requires Phe325 to assume a position similar to that seen in the DA-bound structure to provide edge-to-face aromatic interactions (Fig. 5c, f). To enlarge the binding pocket for multiple aromatic rings, the side chains of Phe319 and

Phe325 are splayed outward as seen in the antidepressant-bound structures (Fig. 5d, f).

These structures provide a molecular explanation for the distinction between substrates and inhibitors of biogenic amine transporters. Substrates such as DA and amphetamines contain amine and aromatic functional groups at opposing ends of the molecule that interact with both the extracellular gate of TMs 1b and 6a and the scaffold TMs 3 and 8. In contrast, inhibitors exploit the flexibility of the binding pocket to bind to the outward open transporter with high affinity, acting like wedges to lock the transporter in an outward-open conformation. Tropane ligands achieve inhibition by inserting benzyl or halo-phenyl groups into the cavity of subsite B, with the tropane ring oriented to sterically hinder the movement of the extracellular gate. Antidepressants, like nortriptyline, differ from tropane inhibitors by coupling bulky aromatic moieties with an amine group to block conformational flexibility in the transporter.

Conclusions

Structures of dDAT in complex with both substrates and inhibitors emphasize the role of subsites in the pocket of dDAT in defining ligand specificity, a concept that can be expanded to understand variation in pharmacological profiles between biogenic amine transporters³³. The DA-bound structure suggests that interactions between the catechol ring and subsite B, together with hydrogen bonding between the amine group of DA and Asp46, drive closure of the extracellular gates TMs 1b and 6a to form the occluded state. D-amphetamine and methamphetamine are bound in a manner distinct from DA in the pocket, and the absence of hydroxyl groups in amphetamines indicates that hydrophobic interactions must be sufficient for amphetamines to interact with subsite B residues and bridge the scaffold TMs 3 and 8 with the extracellular gating helices. The conformations of the DA, amphetamine and DCP-bound complexes probably represent snapshots following substrate and ion binding but before full closure of the extracellular gate, rather than the occluded conformation seen in LeuT bound to its substrates^{11,48,49}. Questions extending from the substrate-bound structures involve the conformational changes required for DAT to transition to other states of the transport cycle and the roles of subsites A and B in neurotransmitter transport by mammalian DATs. Furthermore, the inhibitor-bound structures of dDAT provide a scaffold for addressing the mechanistic distinction between addictive and non-reinforcing analogues of cocaine^{25,45,50}.

Online Content Methods, along with any additional Extended Data display items, are available in the online version of the paper; references unique to these sections appear only in the online paper.

Received 6 November 2014; accepted 23 March 2015.

Published online 11 May 2015.

- Carlsson, A., Lindqvist, M. & Magnusson, T. 3,4-Dihydroxyphenylalanine and 5-hydroxytryptophan as reserpine antagonists. *Nature* **180**, 1200 (1957).
- Twarog, B. M. & Page, I. H. Serotonin content of some mammalian tissues and urine and a method for its determination. *Am. J. Physiol.* **175**, 157–161 (1953).
- von Euler, U. Sympathin in adrenergic nerve fibres. *J. Physiol. (Lond.)* **105**, 26 (1946).
- Hertting, G. & Axelrod, J. Fate of tritiated noradrenaline at the sympathetic nerve-endings. *Nature* **192**, 172–173 (1961).
- Iversen, L. L. Role of transmitter uptake mechanisms in synaptic neurotransmission. *Br. J. Pharmacol.* **41**, 571–591 (1971).
- Iversen, L. L. & Kravitz, E. A. Sodium dependence of transmitter uptake at adrenergic nerve terminals. *Mol. Pharmacol.* **2**, 360–362 (1966).
- Kristensen, A. S. et al. SLC6 neurotransmitter transporters: structure, function, and regulation. *Pharmacol. Rev.* **63**, 585–640 (2011).
- Pramod, A. B., Foster, J., Carvelli, L. & Henry, L. K. SLC6 transporters: structure, function, regulation, disease association and therapeutics. *Mol. Aspects Med.* **34**, 197–219 (2013).
- Penmatsa, A., Wang, K. H. & Gouaux, E. X-ray structure of dopamine transporter elucidates antidepressant mechanism. *Nature* **503**, 85–90 (2013).
- Koldosø, H., Christiansen, A. B., Sinding, S. & Schiøtt, B. Comparative modeling of the human monoamine transporters: similarities in substrate binding. *ACS Chem Neurosci* **4**, 295–309 (2013).

11. Yamashita, A., Singh, S. K., Kawate, T., Jin, Y. & Gouaux, E. Crystal structure of a bacterial homologue of Na^+/Cl^- -dependent neurotransmitter transporters. *Nature* **437**, 215–223 (2005).
12. Beuming, T., Shi, L., Javitch, J. A. & Weinstein, H. A comprehensive structure-based alignment of prokaryotic and eukaryotic neurotransmitter/ Na^+ symporters (NSS) aids in the use of the LeuT structure to probe NSS structure and function. *Mol. Pharmacol.* **70**, 1630–1642 (2006).
13. Gu, H., Wall, S. C. & Rudnick, G. Stable expression of biogenic amine transporters reveals differences in inhibitor sensitivity, kinetics, and ion dependence. *J. Biol. Chem.* **269**, 7124–7130 (1994).
14. Kilty, J. E., Lorang, D. & Amara, S. G. Cloning and expression of a cocaine-sensitive rat dopamine transporter. *Science* **254**, 578–579 (1991).
15. Kurian, M. A. et al. Homozygous loss-of-function mutations in the gene encoding the dopamine transporter are associated with infantile parkinsonism-dystonia. *J. Clin. Invest.* **119**, 1595–1603 (2009).
16. Giros, B., Jaber, M., Jones, S. R., Wightman, R. M. & Caron, M. G. Hyperlocomotion and indifference to cocaine and amphetamine in mice lacking the dopamine transporter. *Nature* **379**, 606–612 (1996).
17. Mergy, M. A. et al. The rare DAT coding variant Val559 perturbs DA neuron function, changes behavior, and alters *in vivo* responses to psychostimulants. *Proc. Natl Acad. Sci. USA* **111**, E4779–E4788 (2014).
18. Zaczek, R., Culp, S., Goldberg, H., McCann, D. J. & De Souza, E. B. Interactions of [^3H]amphetamine with rat brain synaptosomes. I. Saturable sequestration. *J. Pharmacol. Exp. Ther.* **257**, 820–829 (1991).
19. Bönnisch, H. The transport of (+)-amphetamine by the neuronal noradrenaline carrier. *Naunyn Schmiedebergs Arch. Pharmacol.* **327**, 267–272 (1984).
20. Eshleman, A. J., Henningsen, R. A., Neve, K. A. & Janowsky, A. Release of dopamine via the human transporter. *Mol. Pharmacol.* **45**, 312–316 (1994).
21. Goodwin, J. S. et al. Amphetamine and methamphetamine differentially affect dopamine transporters *in vitro* and *in vivo*. *J. Biol. Chem.* **284**, 2978–2989 (2009).
22. Sitte, H. H. et al. Carrier-mediated release, transport rates, and charge transfer induced by amphetamine, tyramine, and dopamine in mammalian cells transfected with the human dopamine transporter. *J. Neurochem.* **71**, 1289–1297 (1998).
23. Sonders, M. S., Zhu, S. J., Zahniser, N. R., Kavanaugh, M. P. & Amara, S. G. Multiple ionic conductances of the human dopamine transporter: the actions of dopamine and psychostimulants. *J. Neurosci.* **17**, 960–974 (1997).
24. Wall, S. C., Gu, H. & Rudnick, G. Biogenic amine flux mediated by cloned transporters stably expressed in cultured cell lines: amphetamine specificity for inhibition and efflux. *Mol. Pharmacol.* **47**, 544–550 (1995).
25. Beuming, T. et al. The binding sites for cocaine and dopamine in the dopamine transporter overlap. *Nature Neurosci.* **11**, 780–789 (2008).
26. Bisgaard, H. et al. The binding sites for benzatropines and dopamine in the dopamine transporter overlap. *Neuropharmacology* **60**, 182–190 (2011).
27. Sørensen, G. et al. Neuropeptide Y Y5 receptor antagonism attenuates cocaine-induced effects in mice. *Psychopharmacology (Berl.)* **222**, 565–577 (2012).
28. Richelson, E. & Pfennig, M. Blockade by antidepressants and related compounds of biogenic amine uptake into rat brain synaptosomes: most antidepressants selectively block norepinephrine uptake. *Eur. J. Pharmacol.* **104**, 277–286 (1984).
29. Sørensen, L. et al. Interaction of antidepressants with the serotonin and norepinephrine transporters: mutational studies of the S1 substrate binding pocket. *J. Biol. Chem.* **287**, 43694–43707 (2012).
30. Dahal, R. A. et al. Computational and biochemical docking of the irreversible cocaine analog RTI 82 directly demonstrates ligand positioning in the dopamine transporter central substrate binding site. *J. Biol. Chem.* **289**, 29712–29727 (2014).
31. Pörzgen, P., Park, S. K., Hirsh, J., Sonders, M. S. & Amara, S. G. The antidepressant-sensitive dopamine transporter in *Drosophila melanogaster*: a primordial carrier for catecholamines. *Mol. Pharmacol.* **59**, 83–95 (2001).
32. Abdul-Hussein, S., Andrell, J. & Tate, C. G. Thermostabilisation of the serotonin transporter in a cocaine-bound conformation. *J. Mol. Biol.* **425**, 2198–2207 (2013).
33. Wang, H. et al. Structural basis for action by diverse antidepressants on biogenic amine transporters. *Nature* **503**, 141–145 (2013).
34. Huang, X. & Zhan, C. G. How dopamine transporter interacts with dopamine: insights from molecular modeling and simulation. *Biophys. J.* **93**, 3627–3639 (2007).
35. Kitayama, S. et al. Dopamine transporter site-directed mutations differentially alter substrate transport and cocaine binding. *Proc. Natl Acad. Sci. USA* **89**, 7782–7785 (1992).
36. Han, D. D. & Gu, H. H. Comparison of the monoamine transporters from human and mouse in their sensitivities to psychostimulant drugs. *BMC Pharmacol.* **6**, 6 (2006).
37. Newman, A. H., Zou, M. F., Ferrer, J. V. & Javitch, J. A. [^3H]MFZ 2–12: a novel radioligand for the dopamine transporter. *Bioorg. Med. Chem. Lett.* **11**, 1659–1661 (2001).
38. Kazmier, K. et al. Conformational dynamics of ligand-dependent alternating access in LeuT. *Nature Struct. Mol. Biol.* **21**, 472–479 (2014).
39. Krishnamurthy, H. & Gouaux, E. X-ray structures of LeuT in substrate-free outward-open and apo inward-open states. *Nature* **481**, 469–474 (2012).
40. Hong, W. C. & Amara, S. G. Membrane cholesterol modulates the outward facing conformation of the dopamine transporter and alters cocaine binding. *J. Biol. Chem.* **285**, 32616–32626 (2010).
41. Zhao, Y. et al. Substrate-modulated gating dynamics in a Na^+ -coupled neurotransmitter transporter homologue. *Nature* **474**, 109–113 (2011).
42. Malinauskaitė, L. et al. A mechanism for intracellular release of Na^+ by neurotransmitter/sodium symporters. *Nature Struct. Mol. Biol.* **21**, 1006–1012 (2014).
43. Perez, C., Koshy, C., Yildiz, O. & Ziegler, C. Alternating-access mechanism in conformationally asymmetric trimers of the betaine transporter BetP. *Nature* **490**, 126–130 (2012).
44. Weyand, S. et al. Structure and molecular mechanism of a nucleobase-cation-sympot-1 family transporter. *Science* **322**, 709–713 (2008).
45. Loland, C. J. et al. Relationship between conformational changes in the dopamine transporter and cocaine-like subjective effects of uptake inhibitors. *Mol. Pharmacol.* **73**, 813–823 (2008).
46. Lee, S. H. et al. Importance of valine at position 152 for the substrate transport and 2β -carbomethoxy- 3β -(4-fluorophenyl)tropane binding of dopamine transporter. *Mol. Pharmacol.* **57**, 883–889 (2000).
47. Chen, J. G., Sachpatzidis, A. & Rudnick, G. The third transmembrane domain of the serotonin transporter contains residues associated with substrate and cocaine binding. *J. Biol. Chem.* **272**, 28321–28327 (1997).
48. Singh, S. K., Piscitelli, C. L., Yamashita, A. & Gouaux, E. A competitive inhibitor traps LeuT in an open-to-out conformation. *Science* **322**, 1655–1661 (2008).
49. Claxton, D. P. et al. Ion/substrate-dependent conformational dynamics of a bacterial homolog of neurotransmitter:sodium symporters. *Nature Struct. Mol. Biol.* **17**, 822–829 (2010).
50. Schmitt, K. C., Rothman, R. B. & Reith, M. E. Nonclassical pharmacology of the dopamine transporter: atypical inhibitors, allosteric modulators, and partial substrates. *J. Pharmacol. Exp. Ther.* **346**, 2–10 (2013).

Supplementary Information is available in the online version of the paper.

Acknowledgements We thank J. Coleman, C.-H. Lee, S. Mansoor and other Gouaux laboratory members for helpful discussions, L. Vaskalis for assistance with figures and H. Owen for help with manuscript preparation. We acknowledge the staff of the Berkeley Center for Structural Biology at the Advanced Light Source and the Northeastern Collaborative Access Team at the Advanced Photon Source for assistance with data collection. This work was supported by an NIMH Ruth Kirschstein postdoctoral fellowship and Brain and Behavior Research Foundation Young Investigator research award (K.H.W.), a postdoctoral fellowship from the American Heart Association (A.P.) and by the NIH (E.G.) and the Methamphetamine Abuse Research Center of OHSU (P50DA018165 to E.G.). E.G. is an investigator with the Howard Hughes Medical Institute.

Author Contributions A.P., K.H.W. and E.G. designed the project. A.P. and K.H.W. performed protein purification, crystallography and biochemical assays. A.P., K.H.W. and E.G. wrote the manuscript.

Author Information The coordinates for the structure have been deposited in the Protein Data Bank under the accession codes 4XP1, 4XP9, 4XP6, 4XPA, 4XP4, 4XP5, 4XPB, 4XPF, 4XPG, 4XPH, 4XPT (see Supplementary Table 1 for details). Reprints and permissions information is available at www.nature.com/reprints. The authors declare no competing financial interests. Readers are welcome to comment on the online version of the paper. Correspondence and requests for materials should be addressed to E.G. (gouauxe@ohsu.edu).

METHODS

Constructs. dDAT constructs employed in this study include:

subsite B mutations (sub^B). Denotes the addition of mutations D121G (TM helix 3) and S426M (TM helix 8) in the binding pocket.

dDAT_{wt}. Full-length dDAT without thermostabilizing mutations, fused to a C-terminal GFP tag.

dDAT_{del}. Contains an N-terminal deletion from 1–20 (Δ 1–20) and a deletion in extracellular loop 2 (EL2) from 164–191, with thermostabilizing mutations V74A and L415A.

ts² dDAT_{cryst}. Contains thermostabilizing mutations (V74A, L415A), Δ 1–20, a deletion in EL2 from Δ 164–206, and a thrombin site (LVPRGS) replacing residues 602–607 (Supplementary Table 1). Structure reported of this construct with sub^B mutations in complex with cocaine and RTI-55.

ts⁵ dDAT_{cryst}. Identical to *ts² dDAT_{cryst}* except that it contains three additional thermostabilizing mutations (V275A, V311A, G538L) (Supplementary Table 1). Equivalent construct containing sub^B mutations reported for β -CFT.

dDAT_{mfc}. Contains thermostabilizing mutations (V74A, L415A), Δ 1–20, a modified deletion in EL2, that is, Δ 162–202, and a thrombin site replacing residues 602–607 (Supplementary Table 1). Structures in complex with cocaine, RTI-55, d-amphetamine, (+)-methamphetamine, DA and 3,4-dichlorophenethylamine (DCP) are reported. Structure of dDAT_{mfc} containing sub^B mutations reported in complex with DCP.

dDAT_{mfc} 201. Identical to dDAT_{mfc} except the deletion in EL2 is from Δ 162–201. (Supplementary Table 1). Structure of dDAT_{mfc} 201 containing sub^B mutations reported in complex with DCP.

Expression and purification. The dDAT constructs were expressed as C-terminal green fluorescent protein (GFP)–His₆ fusions using baculovirus-mediated transduction of mammalian HEK-293S GnT^I[−] cells^{51,52}. Membranes harvested from cells post-infection were homogenized with 1× TBS (20 mM Tris pH 8.0, 100 mM NaCl) and solubilized with a final concentration of 20 mM *n*-dodecyl β -D-maltoside (DDM) and 4 mM cholesteryl hemisuccinate (CHS) in 1× TBS. Detergent-solubilized material was incubated with cobalt-charged metal affinity resin and eluted with 1× TBS containing 1 mM DDM and 0.2 mM CHS along with 80 mM imidazole (pH 8.0). The GFP–His₆ tag was removed using thrombin digestion followed by concentrating the metal ion affinity purified protein. The thrombin-digested protein was subjected to size exclusion chromatography through a Superdex 200 10/300 column pre-equilibrated with buffer containing 20 mM Tris pH 8.0, 300 mM NaCl, 4 mM decyl β -D-maltoside, 0.2 mM CHS and 0.001% (w/v) 1-palmitoyl-2-oleoyl-sn-glycero-3-phosphoethanolamine (POPE). Peak fractions greater than 0.5 mg ml^{−1} were collected and pooled together. Ascorbic acid (25 mM) was added to the protein solution used to crystallize the DA–dDAT_{mfc} complex, to serve as antioxidant. All procedures were carried out at 4 °C.

Fab complexation and crystallization. Antibody fragment (Fab) 9D5 was used to complex with the protein at a molar ratio of 1.2 (Fab):1 (protein). The Fab–DAT complex solution was incubated with 1–2 mg solid drug for 30 min on ice followed by concentration in a 100 kDa cutoff concentrator to 3.5–5 mg ml^{−1}. The concentrated protein was spun down to remove excess drug and insoluble aggregates and plates were set up by hanging drop vapour diffusion. Crystals of Fab–DAT complex grew primarily in conditions containing PEG 400 or PEG 350 monomethyl ether or PEG 600 as the precipitant (Extended Data Table 2b). The pH range of crystallization was 8.0–9.0 for dDAT_{cryst}-based constructs and in the range of 6.5–8.0 with dDAT_{mfc}-based constructs (Extended Data Table 2b). Crystals of dDAT_{mfc} were primarily obtained by streak seeding with a cat whisker dipped in crystals formed with sub^B containing constructs, 2–5 days after drops were set up. All crystals were grown at 4 °C.

Data collection and structure refinement. Crystals were directly flash-cooled in liquid nitrogen when the PEG 400 concentration in the mother liquor exceeded 36%. For crystals grown in wells containing less than 36% PEG 400, crystals were transferred into cryoprotection solution identical to the reservoir solution but with 40% PEG 400. In conditions with 30–34% PEG 600 as the primary precipitant, 10% of ethylene glycol was added to provide additional cryoprotection. Data were collected either at ALS (5.0.2; 8.2.1) or APS (24-IDC and IDE). Anomalous data for iodine containing RTI-55 complexed with dDAT was collected at 1.6 Å as described in the crystallographic data table. Data were processed using either HKL2000^{52,53} or XDS⁵⁴. Molecular replacement was carried out for all data sets using coordinates 4M48 with Fab 9D5 and dDAT_{cryst} used as independent search models, using PHASER in the PHENIX software suite^{55,56}. Iterative cycles of refinement and manual model building were carried out using PHENIX and COOT⁵⁷, respectively, until the models converged to acceptable levels of R-factors and stereochemistry.

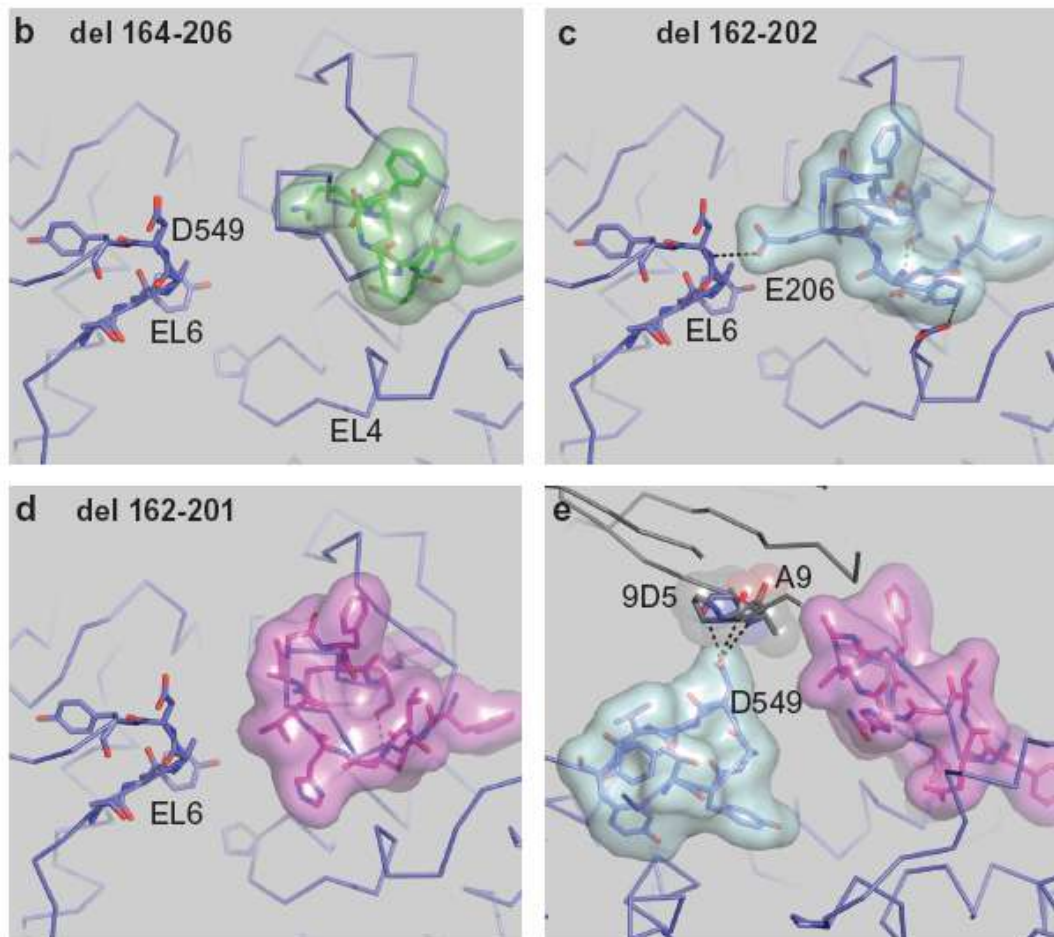
Radiolabel binding and uptake assays. All binding assays were carried out by scintillation proximity assay (SPA) method⁵⁸. Reactions contained 5–20 nM protein, 0.5 mg ml^{−1} Cu-YSi beads, SEC buffer, and [³H]nisoxetine] from 0.1 to 300 nM for saturation binding assays. Competition binding assays were done with 30 nM [³H]nisoxetine and increasing concentrations of unlabelled competitor. K_i values were estimated from IC₅₀ values using the Cheng–Prusoff equation. Fits were plotted using Graphpad Prism v4.0.

For uptake assays HEK 293S cells were infected with baculovirus expressing dDAT_{mfc} or dDAT_{wt}, and sodium butyrate was added to 10 mM 8–12 h post-infection. At 24 h, infected cells were adhered to Cytostar-T plates for 2 h, after which the culture media were replaced with uptake buffer (20 mM HEPES pH 7.4, 120 mM NaCl, 5 mM KCl, 2.5 mM CaCl₂, 1.2 mM MgSO₄, 10 mM D-glucose, 1 mM tropolone, 1 mM L-ascorbic acid^{59,60}). Uptake assays were carried out using [¹⁴C]DA over a range of 0.3–60 µM in 100 µl total volume. Samples were read every five minutes for a time course over twenty-five minutes. The linear initial rate of uptake was plotted in the presence and absence of 10 µM nortriptyline to calculate the specific uptake rate. Data were fitted to a standard Michaelis–Menten equation to obtain K_M and V_{max} values. The significance of specific uptake was assessed at each concentration of DA using a two-tailed Welch's t-test with 2 degrees of freedom.

51. Reeves, P. J., Callewaert, N., Contreras, R. & Khorana, H. G. Structure and function in rhodopsin: high-level expression of rhodopsin with restricted and homogeneous N-glycosylation by a tetracycline-inducible N-acetylglucosaminyltransferase I-negative HEK293S stable mammalian cell line. *Proc. Natl. Acad. Sci. USA* **99**, 13419–13424 (2002).
52. Goehring, A. *et al.* Screening and large-scale expression of membrane proteins in mammalian cells for structural studies. *Nature Protocols* **9**, 2574–2585 (2014).
53. Otwinowski, Z. & Minor, W. Processing of X-ray diffraction data collected in oscillation mode. *Methods Enzymol.* **276**, 307–326 (1997).
54. Kabsch, W. *XDS. Acta Crystallogr. D* **66**, 125–132 (2010).
55. McCoy, A. J. *et al.* Phaser crystallographic software. *J. Appl. Crystallogr.* **40**, 658–674 (2007).
56. Afonine, P. V. *et al.* Towards automated crystallographic structure refinement with phenix.refine. *Acta Crystallogr. D* **68**, 352–367 (2012).
57. Emsley, P. & Cowtan, K. Coot: model-building tools for molecular graphics. *Acta Crystallogr. D* **60**, 2126–2132 (2004).
58. Quick, M. & Javitch, J. A. Monitoring the function of membrane transport proteins in detergent-solubilized form. *Proc. Natl. Acad. Sci. USA* **104**, 3603–3608 (2007).
59. Eshleman, A. J. *et al.* Metabolism of catecholamines by catechol-O-methyltransferase in cells expressing recombinant catecholamine transporters. *J. Neurochem.* **69**, 1459–1466 (1997).
60. Dehnes, Y. *et al.* Conformational changes in dopamine transporter intracellular regions upon cocaine binding and dopamine translocation. *Neurochem. Int.* **73**, 4–15 (2014).

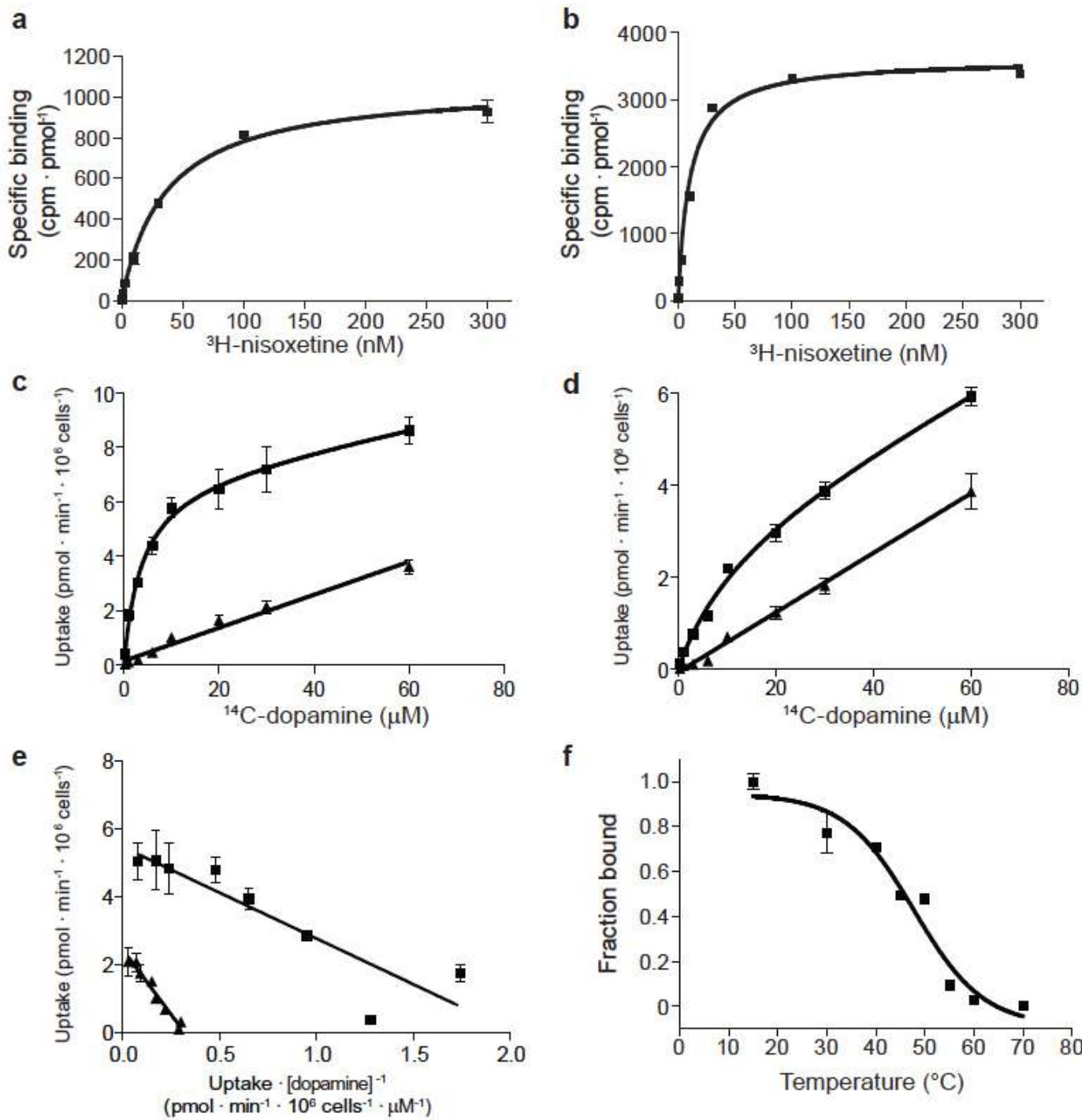
a

Extracellular Loop (EL) 2 deletions			
wtdDAT	WNTPNCRPFESQNASRVPVIGNYSDLYAMGNQSLLYNETYMNGSSLDTSAVGHVEGFQSA		
del164-206 (DAT _{cryst})	WNTPNCRPFESQ-----163-----207-----GFQSA		
del162-202 (DAT _{mfc})	WNTPNCRPFE-----161-----203-----GHVEGFQSA		
del162-201	WNTPNCRPFE-----161-----202-----VGHVEGFQSA		


Extended Data Figure 1 | Design of the minimal functional construct.

a. Thermostabilizing (ts) mutations V275A, V311A, G538L were removed. Modification of the EL2 deletion from 164–206 to 162–202, which recovered transport activity. The del 162–201 construct has robust dopamine uptake activity. **b.** Structural organization of EL2 regions. Organization of dDAT_{cryst} with a deletion of region 164–206 depicted as green surface. **c.** EL2 structure in

dDAT_{mfc} with the deletion 162–202 depicted as cyan surface showing contacts between EL2 and EL6. **d.** EL2 organization in the construct with a deletion from 162–201 depicted as magenta surface. **e.** Fab 9D5 interferes with the interaction between EL2 and EL6 in the crystal lattice, with loops depicted as magenta and cyan surfaces, respectively. Fab disrupts the EL organization in all structures. The del 162–201 sub^B structure is shown.

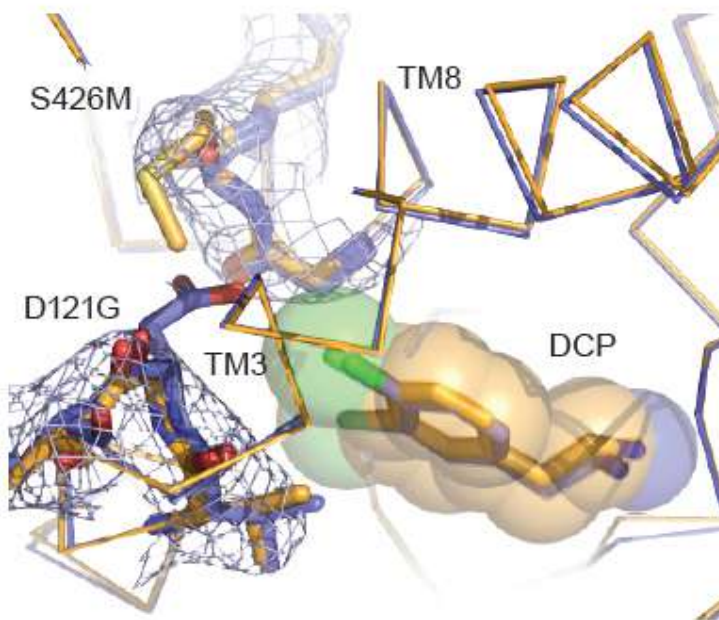
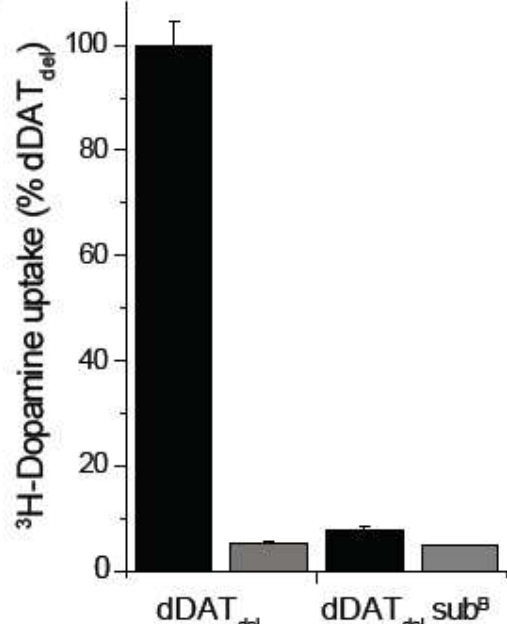


Extended Data Figure 2 | Measurement of dissociation constants using purified dDAT_{mfc} protein, and dopamine uptake in whole cells.
a, dDAT_{mfc} binds [³H]nisoxetine with a K_d of 36 ± 3 nM (s.e.m.). **b**, dDAT_{mfc} with sub^B mutations binds [³H]nisoxetine with a K_d of 10 ± 1 nM (s.e.m.). **c, d**, Michaelis-Menten plots of [¹⁴C]dopamine uptake by HEK293S cells expressing dDAT_{wt} or dDAT_{mfc}, respectively, which yielded K_M of 2.1 ± 0.7 μM and V_{max} of 4.5 ± 0.4 pmol min⁻¹ per 10^6 cells for dDAT_{wt} and a K_M of 8.2 ± 2.3 μM and V_{max} of 2.4 ± 0.2 pmol min⁻¹ per 10^6 cells for dDAT_{mfc} (s.e.m.). One representative plot of total and background counts (in the presence of 10 μM nortriptyline) is shown of two experimental trials as squares and triangles, respectively. Data points and error bars show the average and standard deviation, respectively, of technical replicates ($n = 3$). Welch's

t-test indicates that the specific uptake signal at each concentration of dopamine is significant with a two-tailed *P* value < 0.02 . **e**, Eadie-Hofstee plot of specific dopamine uptake shown in Fig. 1a and panels **c** and **d** of this figure. Data for dDAT_{wt} and dDAT_{mfc} are shown as squares and triangles, respectively, and error bars denote s.d. of technical replicates ($n = 3$). **f**, The thermal melting curve of dDAT_{mfc} solubilized from HEK293S membranes in the presence of 100 nM [³H]nisoxetine exhibits a melting temperature of 48 ± 2 °C (s.e.m.). The fraction bound describes the signal remaining after incubation at the specified temperature for 10 min, normalized to the signal at 4 °C. Data points show the mean values for one experimental trial, and error bars show the s.d. of technical replicates ($n = 3$).

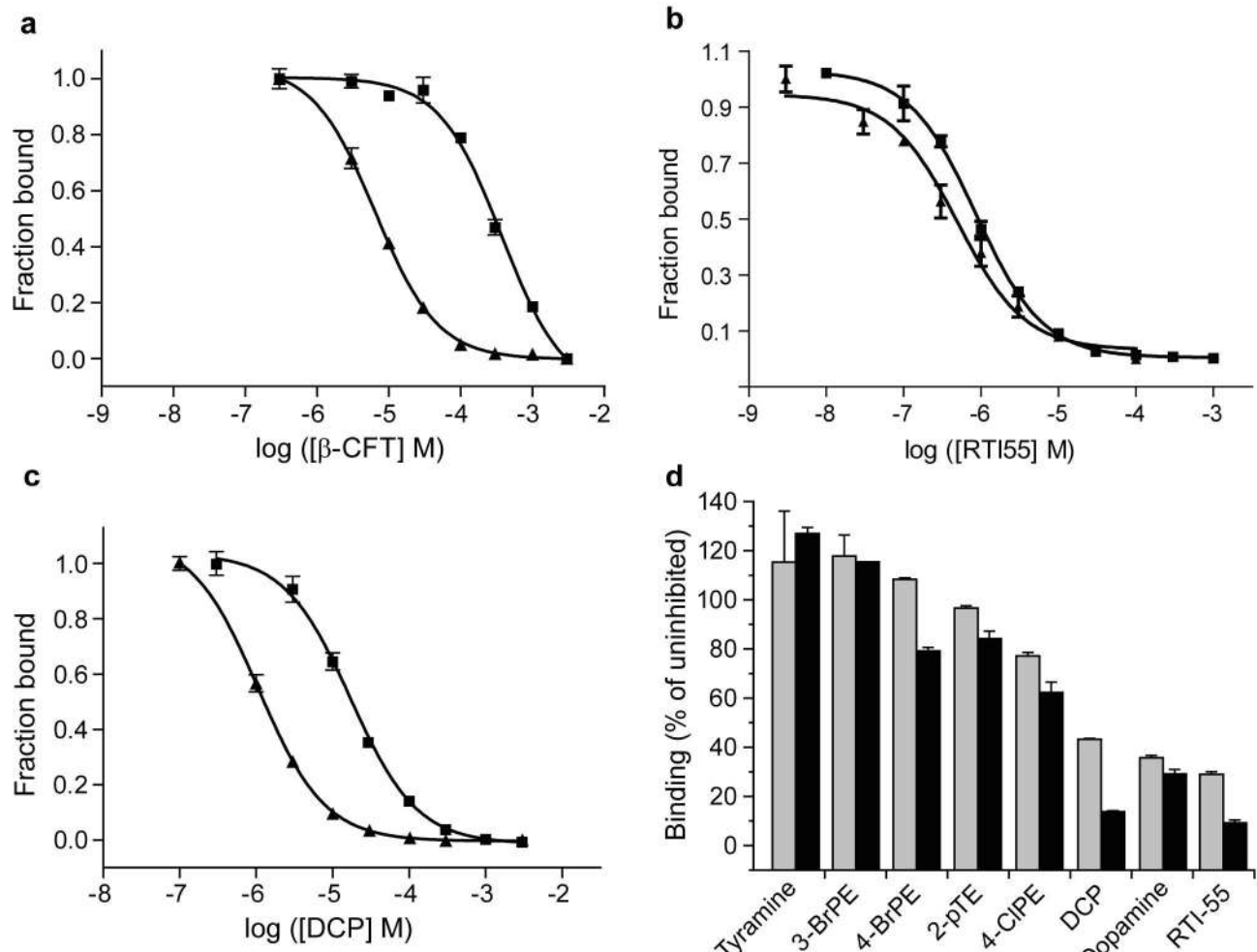
a**Locations of Subsite B mutations**

	D121G (TM3)	S426M (TM8)
dDAT	116-IAFYVDFYYNV-126	421-SSFGGSEAIITALSD-435
hDAT	148-ISLYVGFFYNV-158	422-SAMGGMESVITGLID-436
hNET	144-IALYVGFYYNV-154	419-SSMGGMEAVITGLAD-433
hSERT	168-IAFYIASYYNT-178	438-STFAGLEGVITAVLD-452

b**c****Extended Data Figure 3 | Mutagenesis and effects of DAT subsite B.**

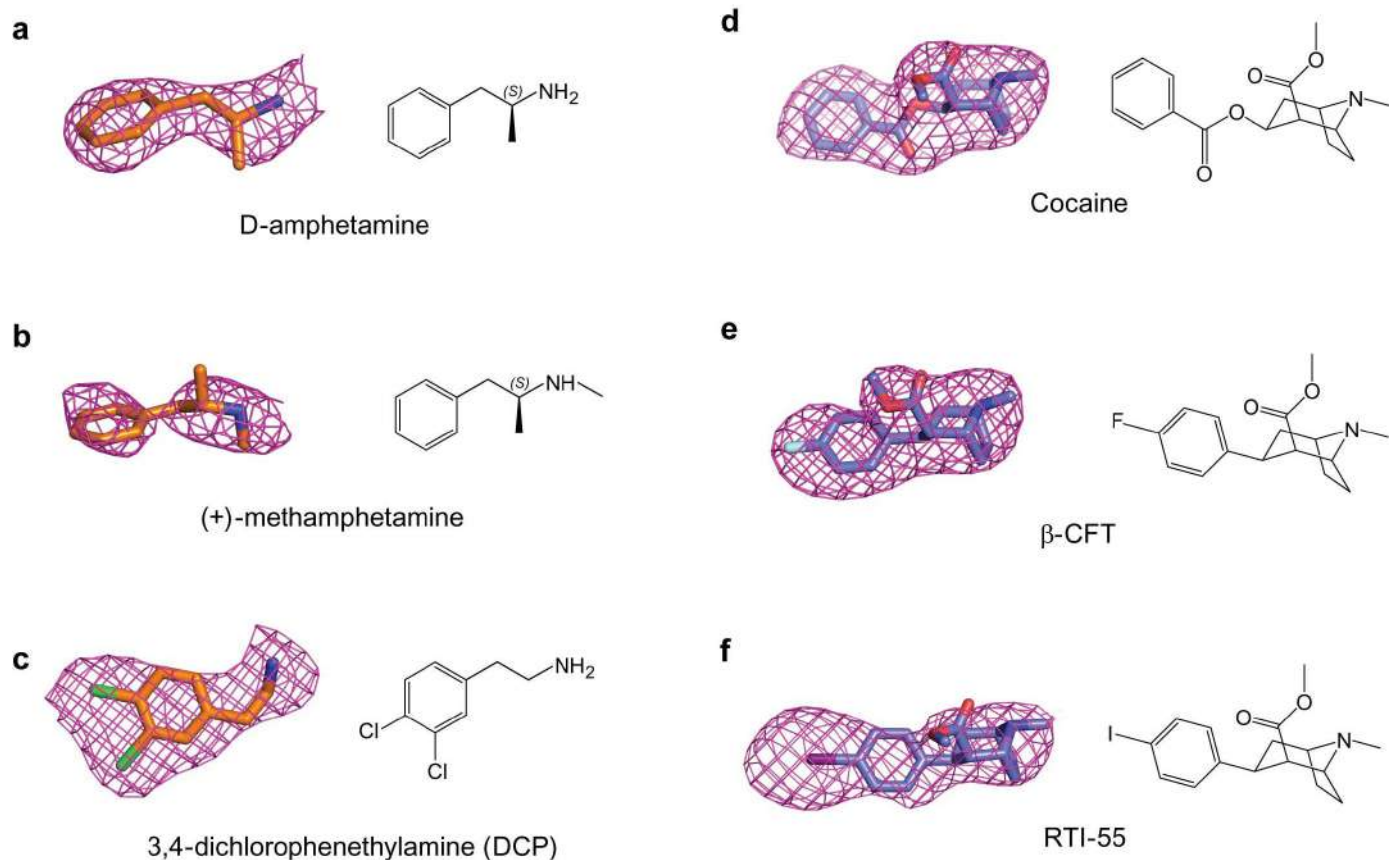
a, Sequence alignment of subsite B regions for dDAT and human NSS orthologues. **b**, $2F_o - F_c$ density contoured at 0.9σ around the vicinity of the D121G (TM3) and S426M mutations (TM8). **c**, Abrogation of dopamine

transport activity by dDAT_{wt} bearing both subsite B mutations in infected HEK293S cells. Data show the average uptake and error bars show the data range of technical duplicates for a single trial. Reactions were performed without and with 100 μ M desipramine in black and grey bars, respectively.

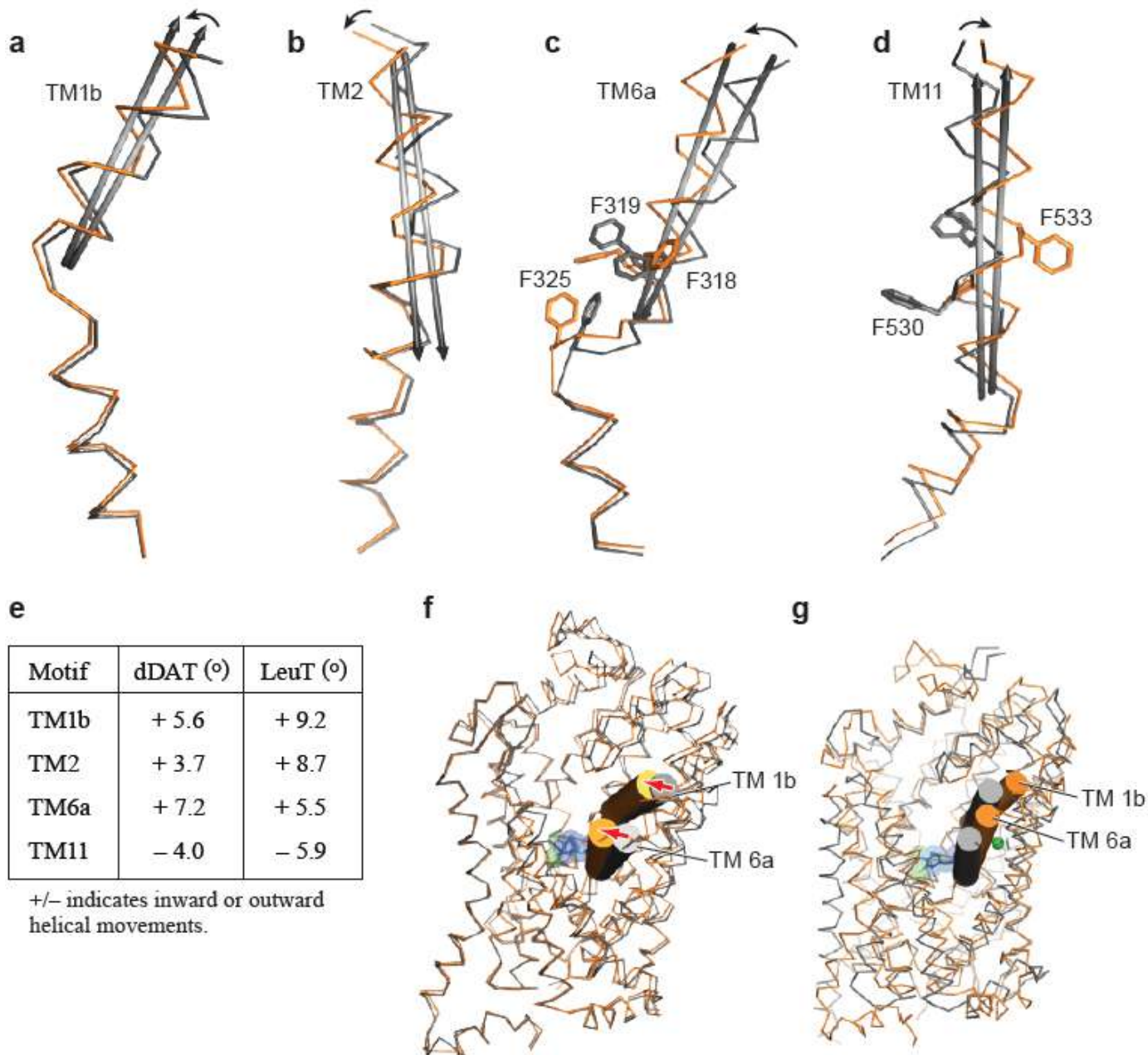


Extended Data Figure 4 | Measurement of inhibition constants using purified dDAT protein. **a–c**, Inhibition of [^3H]nisoxetine binding to dDAT_{mfc} (squares) and dDAT_{mfc} sub^B (triangles). K_i inhibition constants for dDAT_{mfc} and dDAT_{mfc} sub^B are, respectively, $98 \pm 4 \mu\text{M}$, and $1.4 \pm 0.1 \mu\text{M}$, (**a**, β -CFT), $371 \pm 25 \text{nM}$ and $271 \pm 59 \text{nM}$ (**b**, RTI-55), and $4.5 \pm 0.3 \mu\text{M}$, and $267 \pm 20 \text{nM}$ (**c**, DCP). All errors are s.e.m. One representative trial of two is shown for all experiments in panels **a–c**, and data points and error bars denote

the average values for fraction bound and standard deviation, respectively, for technical replicates ($n = 3$). **d**, Inhibition of [^3H]nisoxetine (50 nM) binding to dDAT_{del} by 1 and 10 μM unlabelled compound (grey and black bars, respectively). Error bars show the data range of technical replicates ($n = 2$). Abbreviations: 3-BrPE, 3-bromophenethylamine; 4-BrPE, 4-bromophenethylamine; 2-pTE, 2-(pTolyl)ethylamine, 4-ClPE, 4-chlorophenethylamine; DCP, 3,4-dichlorophenethylamine.

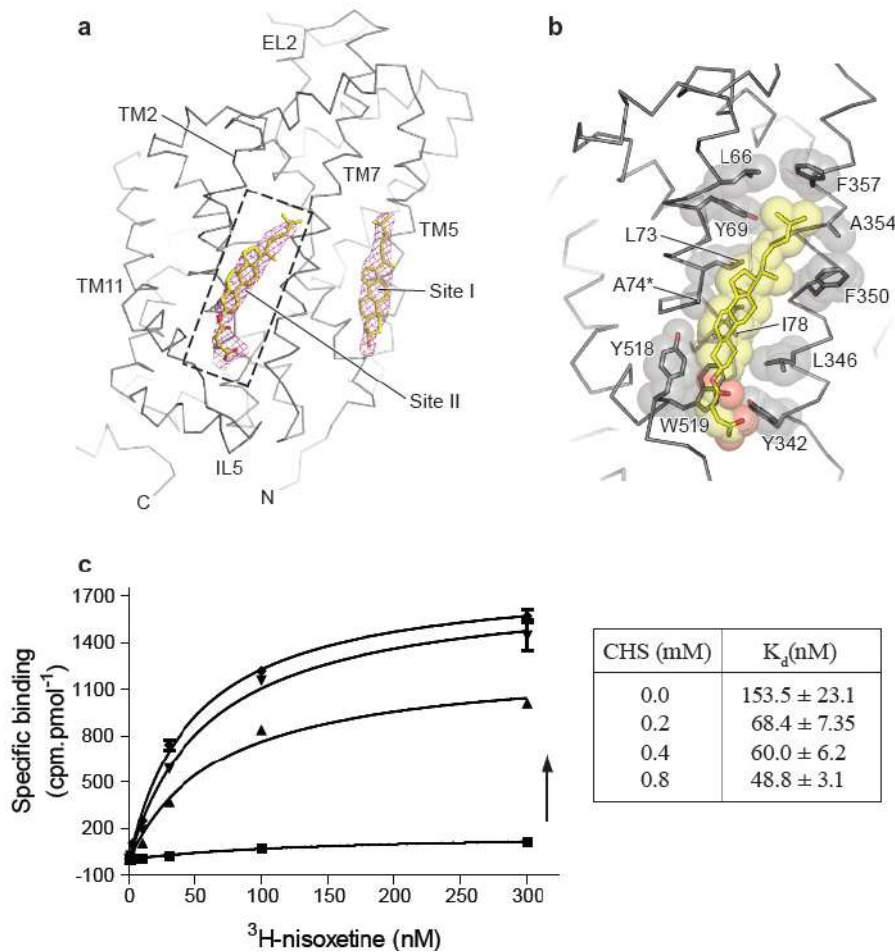


Extended Data Figure 5 | $F_o - F_c$ densities for ligands complexed with dDAT. **a**, D-amphetamine (2.4σ); **b**, (+)-methamphetamine (1.8σ); **c**, DCP (2.2σ); **d**, cocaine (2.2σ); **e**, β -CFT (2.2σ); **f**, RTI-55 (2.6σ).



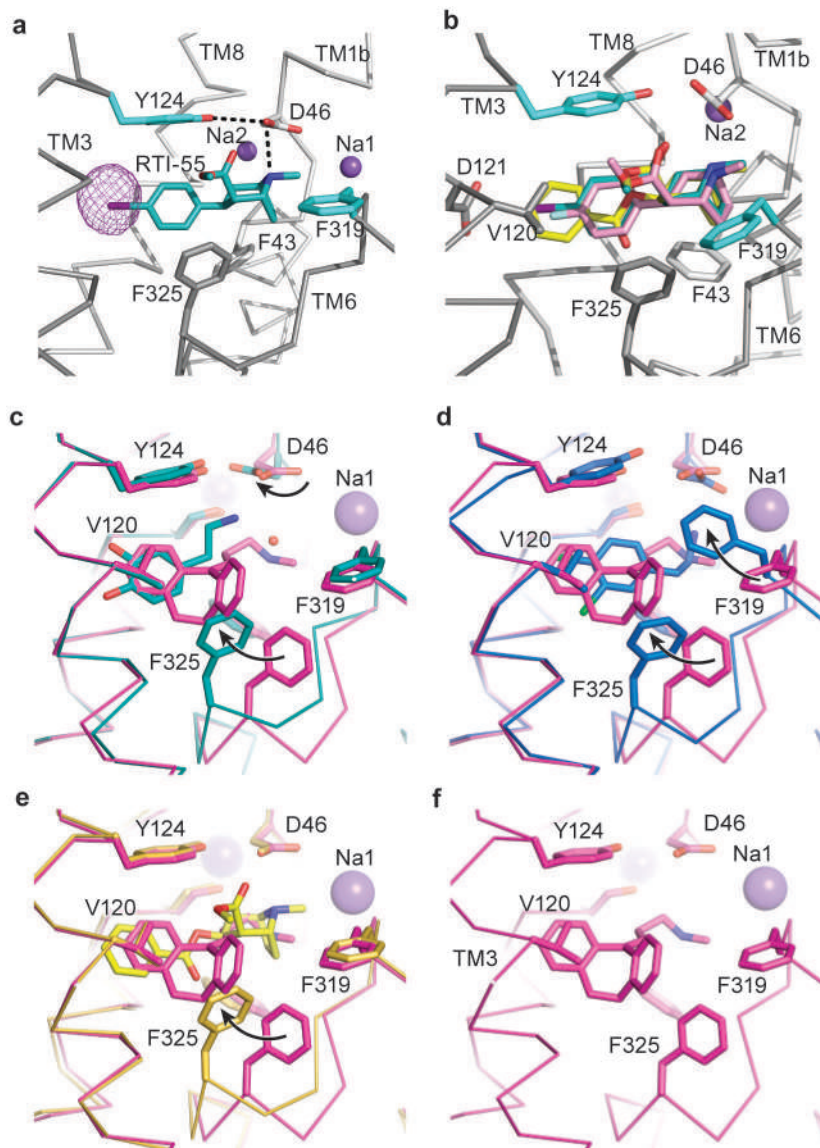
Extended Data Figure 6 | Helical movements in dDAT_{mfc} upon binding to substrate analogue DCP (orange) and inhibitor nortriptyline (grey).
a–d, Helices undergoing maximal shifts are **a**, TM1b; **b**, TM2; **c**, TM6a; **d**, TM11. Arrows in black represent direction of shift. **e**, Table comparing angular shifts between nortriptyline-dDAT_{cryst} (PDB ID 4M48) and DCP-dDAT_{mfc} structures in column one, and between the outward-open Trp-LeuT (PDB ID 3F3A) and outward-occluded Leu-LeuT (PDB ID 2A65) structures in

column two. **f**, Superposition of the outward open state of nortriptyline-dDAT_{cryst} (PDB ID 4M48) and DCP-dDAT_{mfc} structures in grey and orange ribbon, respectively. Extracellular gating TMs 1b and 6a are shown as cylinders. Arrows in red indicate inward movement of TMs 1b and 6a. **g**, Superposition of the occluded state of LeuT (PDB ID 2A65) and DCP-dDAT_{mfc} structures in grey and orange ribbon, respectively.



Extended Data Figure 7 | Cholesterol binding sites in DAT. **a**, Cholesterol binding sites seen on the dDAT surface corresponding to the inner leaflet of the plasma membrane, with a second novel cholesterol site into which a cholestrylo hemisuccinate (CHS) could be modelled. $F_o - F_c$ densities for cholesterol contoured at 2.0σ . **b**, Close-up view of cholesterol site II at the junction of TM2, TM7 and TM11 interacting with multiple hydrophobic residues. Asterisk

denotes thermostabilizing mutant V74A. **c**, Effect of CHS concentration on [³H]nisoxetine binding to DAT_{mfc} construct. Graph depicts one representative trial of two independent experiments, and total and background counts were measured using technical replicates ($n = 3$) for each binding curve at each CHS concentration. Arrow represents increasing concentration of CHS. Error bars represent s.d.



Extended Data Figure 8 | Analogs of cocaine and binding site comparisons. **a**, The position of RTI-55 in the binding pocket with anomalous difference density for iodide displayed as purple mesh and contoured at 4σ . **b**, Superposition of cocaine, β -CFT, and RTI-55 using the RTI-55-dDAT_{mfc} structure. Ligands are shown as sticks and coloured yellow (cocaine), pink (β -CFT), and teal (RTI-55). Sodium ions are shown as purple spheres.

c-f, Residues that line the binding pocket are superposed between the nortriptyline-dDAT_{cryst} (magenta, PDB ID 4M48) and those of **c**, DA-dDAT_{mfc} (cyan), **d**, DCP-dDAT_{mfc} (marine), **e**, cocaine-dDAT_{mfc} (yellow). **f**, Organization of S1 binding site in complex with nortriptyline (PDB ID 4M48). Black arrows describe the change in rotamers and positions of D46, F319, and F325 compared to the nortriptyline-bound structure.

Extended Data Table 1 | Superposition statistics of dDAT structures

	ntt ts ⁵ dDAT _{cryst}	cocaine dDAT _{mfc}	β -CFT ts ⁵ dDAT _{cryst} sub ^B	RTI-55 dDAT _{mfc} sub ^B	RTI-55 dDAT _{mfc}	DCP dDAT _{mfc} sub ^B	DCP dDAT _{mfc}	DA dDAT _{mfc}	meth dDAT _{mfc}	amph dDAT _{mfc}
ntt ts ⁵ dDAT _{cryst}	—	0.46	0.37	0.52	0.70	0.74	0.76	0.53	0.53	0.48
cocaine dDAT _{mfc}	—	—	0.27	0.46	0.67	0.74	0.79	0.52	0.54	0.37
β -CFT ts ⁵ dDAT _{cryst} sub ^B	—	—	—	0.43	0.64	0.70	0.73	0.50	0.50	0.52
RTI-55 ts ² dDAT _{cryst} sub ^B	—	—	—	—	0.73	0.75	0.82	0.55	0.59	0.60
RTI-55 dDAT _{mfc}	—	—	—	—	—	0.83	0.64	0.97	0.53	0.58
DCP dDAT _{mfc} sub ^B	—	—	—	—	—	—	0.41	0.75	0.57	0.61
DCP dDAT _{mfc}	—	—	—	—	—	—	—	0.64	0.64	0.63
DA dDAT _{mfc}	—	—	—	—	—	—	—	—	0.64	0.41
meth dDAT _{mfc}	—	—	—	—	—	—	—	—	—	0.35
amph dDAT _{mfc}	—	—	—	—	—	—	—	—	—	—

Extended Data Table 2 | a, Ligand surface and interface areas*; b, crystallization conditions for ligand–DAT complexes

a	Ligand	Total surface area (Å ²)	Buried Surface area (Å ²)	% Buried
	Nortriptyline (4M48)	475.9	448.4	94.2
	Cocaine	484.7	447	92.2
	RTI-55	466.2	416.7	89.4
	β-CFT	439.2	403.1	91.8
	dopamine	311.9	279.1	89.5
	DCP	337.3	321.5	95.3
	methamphetamine	325.7	301	92.4
	D-amphetamine	308.3	284.5	92.3

b	Ligand	Construct	Condition
1	Cocaine	dDAT _{mfc}	PEG 400 37%, Na MES pH 6.8 (0.1M)
2	RTI-55	dDAT _{mfc}	PEG 400 41%, Tris pH 8.0 (0.1M)
3	Methamphetamine	dDAT _{mfc}	PEG 400 38%, Tris pH 8.0 (0.1M)
4	D-amphetamine	dDAT _{mfc}	PEG 600 36%, MOPS pH 7.0 (0.1M)
5	DA (dopamine)	dDAT _{mfc}	PEG 600 31%, Tris pH 8.0 (0.1M)
6	DCP	dDAT _{mfc}	PEG 400 38%, Tris pH 8.0 (0.1M)
7	Cocaine	dDAT _{cryst} ts ² sub ^B	PEG 400 38%, Tris-Bicine pH 8.5 (0.1M)
8	RTI-55	dDAT _{cryst} ts ² sub ^B	PEG 400 39%, Bicine pH 8.8 (0.1M)
9	β-CFT	dDAT _{cryst} sub ^B	PEG 400 38%, Bicine pH 8.8 (0.1M)
10	DCP	dDAT _{mfc} sub ^B	PEG 400 33%, Na MES pH 6.5 (0.1M)
11	DCP	dDAT _{mfc} 201 sub ^B	PEG400 34%, Na MES pH 6.5 (0.1M)

*Surface areas calculated by PDBePISA. (<http://www.ebi.ac.uk/pdbe/pisa>)

References and Notes

1. M. A. Brzezinski *et al.*, *Geophys. Res. Lett.* **29**, 1564 (2002).
2. K. Matsumoto, J. L. Sarmiento, M. A. Brzezinski, *Global Biogeochem. Cycles* **16**, 1031 (2002).
3. S. Takeda, *Nature* **393**, 774 (1998).
4. J. L. Sarmiento, N. Gruber, M. A. Brzezinski, J. P. Dunne, *Nature* **427**, 56 (2004).
5. J. L. Sarmiento *et al.*, *Global Biogeochem. Cycles* **21**, GB1590 (2007).
6. Y. Rosenthal, E. A. Boyle, L. Labeyrie, *Paleoceanography* **12**, 787 (1997).
7. U. S. Ninnemann, C. D. Charles, *Earth Planet. Sci. Lett.* **201**, 383 (2002).
8. D. A. Hodell, K. A. Venz, C. D. Charles, U. S. Ninnemann, *Geochem. Geophys. Geosyst.* **4**, 1004 (2003).
9. E. A. Boyle, *Annu. Rev. Earth Planet. Sci.* **20**, 245 (1992).
10. L. C. Skinner, S. Fallon, C. Waelbroeck, E. Michel, S. Barker, *Science* **328**, 1147 (2010).
11. A. D. Moy, W. R. Howard, M. K. Gagan, *J. Quat. Sci.* **21**, 763 (2006).
12. I. N. McCave, L. Carter, I. R. Hall, *Quat. Sci. Rev.* **27**, 1886 (2008).
13. U. S. Ninnemann, C. D. Charles, *Paleoceanography* **12**, 560 (1997).
14. A. M. Piotrowski, S. L. Goldstein, S. R. Hemming, R. G. Fairbanks, *Earth Planet. Sci. Lett.* **225**, 205 (2004).
15. K. R. Hendry, R. B. Georg, R. E. M. Rickaby, L. F. Robinson, A. N. Halliday, *Earth Planet. Sci. Lett.* **292**, 290 (2010).
16. C. L. de la Rocha, M. A. Brzezinski, M. J. DeNiro, *Geochim. Cosmochim. Acta* **61**, 5051 (1997).
17. M. Wille *et al.*, *Earth Planet. Sci. Lett.* **292**, 281 (2010).
18. See the supporting online material available on *Science Online*.
19. D. W. Lea, *Paleoceanography* **10**, 733 (1995).
20. R. F. Anderson *et al.*, *Science* **323**, 1443 (2009).
21. S. Barker *et al.*, *Nature* **457**, 1097 (2009).
22. Z. Chase, R. F. Anderson, M. Q. Fleisher, P. W. Kubik, *Deep Sea Res. Part II Top. Stud. Oceanogr.* **50**, 799 (2003).
23. R. B. Georg, A. J. West, A. R. Basu, A. N. Halliday, *Earth Planet. Sci. Lett.* **283**, 67 (2009).
24. P. N. Froelich *et al.*, *Paleoceanography* **7**, 739 (1992).
25. M. J. Ellwood, M. Kelly, W. A. Maher, P. De Deckker, *Earth Planet. Sci. Lett.* **243**, 749 (2006).
26. C. L. de la Rocha, M. A. Brzezinski, M. J. DeNiro, A. Shemesh, *Nature* **395**, 680 (1998).
27. L. E. Pichevin *et al.*, *Nature* **459**, 1114 (2009).
28. D. M. Sigman, M. P. Hain, G. H. Haug, *Nature* **466**, 47 (2010).

29. D. A. Hodell *et al.*, in *Proceedings of the Ocean Drilling Program, Scientific Results Volume*, R. Gersonde, D. A. Hodell, P. Blum, Eds. (Ocean Drilling Program, College Station, TX, 2002), vol. 177.
30. R. A. Mortlock *et al.*, *Nature* **351**, 220 (1991).
31. We acknowledge the Antarctic Research Facility at Florida State University for E33-22 core samples and the Ocean Drilling Program for ODP177 site 1089 core samples. This research was supported with funds from the Australian Research Council (grants DP0770820 and DP0771519). This manuscript benefited from the thoughtful comments of two anonymous reviewers.

Supporting Online Material

www.sciencemag.org/cgi/content/full/science.1194614/DC1
 Materials and Methods
 SOM Text
 Figs. S1 to S7
 Tables S1 to S4
 References

2 July 2010; accepted 28 September 2010
 Published online 21 October 2010;
10.1126/science.1194614

Structure of the Human Dopamine D3 Receptor in Complex with a D2/D3 Selective Antagonist

Ellen Y. T. Chien,¹ Wei Liu,¹ Qiang Zhao,¹ Vsevolod Katritch,² Gye Won Han,¹ Michael A. Hanson,³ Lei Shi,⁴ Amy Hauck Newman,⁵ Jonathan A. Javitch,⁶ Vadim Cherezov,¹ Raymond C. Stevens^{1*}

Dopamine modulates movement, cognition, and emotion through activation of dopamine G protein–coupled receptors in the brain. The crystal structure of the human dopamine D3 receptor (D3R) in complex with the small molecule D2R/D3R-specific antagonist eticlopride reveals important features of the ligand binding pocket and extracellular loops. On the intracellular side of the receptor, a locked conformation of the ionic lock and two distinctly different conformations of intracellular loop 2 are observed. Docking of R-22, a D3R-selective antagonist, reveals an extracellular extension of the eticlopride binding site that comprises a second binding pocket for the aryl amide of R-22, which differs between the highly homologous D2R and D3R. This difference provides direction to the design of D3R-selective agents for treating drug abuse and other neuropsychiatric indications.

Dopamine is an essential neurotransmitter in the central nervous system and exerts its effects through activation of five distinct dopamine receptor subtypes that belong to the G protein–coupled receptor (GPCR)

superfamily. The receptors have been classified into two subfamilies, D1-like and D2-like, on the basis of their sequence and pharmacological similarities (1). The D1-like receptors (D1R and D5R) couple to stimulatory G-protein α subunits ($G_{s/o}$), activating adenyl cyclase, whereas D2-like receptors (D2R, D3R, and D4R) couple to inhibitory G-protein α subunits ($G_{i/o}$), inhibiting adenyl cyclase. The high degree of sequence identity (2, 3) within the transmembrane (TM) helices between D2R and D3R (78%), and more importantly, the near-identity of the residues inferred to form the binding site in these receptors (4), have created a formidable challenge to developing D3R-selective compounds with drug-like physicochemical properties (3, 5). Antipsychotic drugs that block both D2R and D3R are used clinically to treat schizophrenia, but these agents can produce multiple side effects that can limit their tolerability. It has been hypothesized that selective targeting of the individual D2-like re-

ceptor subtypes might produce fewer side effects (6). Through extensive medicinal chemistry efforts, D3R-preferential antagonists and partial agonists (e.g., SB 277011A, NGB 2904, BP 897; see fig. S1) have been developed and shown to attenuate drug-seeking behaviors in animal models of relapse, without associated motor effects, supporting D3R blockade as a plausible target for therapeutic discovery (7–11) particularly for substance abuse (12). However, even the best D3R-preferential compounds are still highly lipophilic and display poor bioavailability or predicted toxicity that has precluded clinical trials. To better understand dopamine receptors and the molecular basis for pharmacological specificity within the dopamine receptors, we have determined the crystal structure of the human D3R in complex with eticlopride, a potent D2R/D3R antagonist (13, 14).

To crystallize the D3R, we modified it by introducing a point mutation in the transmembrane domain [Leu119^{3,41}Trp (15)] to enhance thermal stability (16), and replacing most of the third cytoplasmic loop (ICL3) (Arg222 to Arg318) with T4-lysozyme (D3R-T4L) (17). Further stabilization of the receptor was achieved by purifying with the antagonist eticlopride, which conferred the highest thermostability compared with five other ligands (18) (table S2). The engineered receptor retained near-native ligand binding properties (table S3) and crystallized from a lipidic mesophase in an orthorhombic space group. Diffraction data were anisotropic, extending to 2.9 Å in the c^* direction and 3.6 Å in the a^* direction. Overall, the structure was determined at 3.15 Å and included all data up to 2.9 Å where an improvement in map quality was observed (see fig. S8 and table S1). The structure was determined with two receptors arranged in an antiparallel orientation in the asymmetric unit of the crystal (fig. S2). Both copies of the receptor are very similar [root mean square deviation of 0.6 Å for the seven-TM bundle] and will be treated identically in the discussion

*Department of Molecular Biology, The Scripps Research Institute, 10550 North Torrey Pines Road, La Jolla, CA 92037, USA. ²Skaggs School of Pharmacy and Pharmaceutical Sciences, and San Diego Supercomputer Center, University of California, San Diego, La Jolla, CA 92093, USA. ³Receptos, 10835 Road to the Cure, Suite 205, San Diego, CA 92121, USA. ⁴Department of Physiology and Biophysics and HRH Prince Alwaleed Bin Talal Bin Abdulaziz Alsaud Institute for Computational Biomedicine, Weill Cornell Medical College, Cornell University, 1300 York Avenue, New York, NY 10021, USA. ⁵Medicinal Chemistry Section, National Institute on Drug Abuse—Intramural Research Program, Baltimore, MD 21224, USA. ⁶Center for Molecular Recognition and Departments of Psychiatry and Pharmacology, Columbia University College of Physicians and Surgeons, 630 West 168th, New York, NY 10032, USA.

To whom correspondence should be addressed. E-mail: stevens@scripps.edu

except where noted otherwise. The N-terminal 31 residues are not included in the deposited structure as they do not have interpretable density. The main fold of the D3R consists of the canonical seven-TM bundle of α helices (Fig. 1A), which resembles previously solved GPCR structures (19–22). Subtleties in the orientations of these helices, as well as differences in the intracellular and extracellular portions of the receptor, confer the pharmacological and biochemical properties unique to the D3R.

The extracellular region in general is characterized by high sequence diversity among the GPCR family, which translates into high structural diversity in terms of the presence of varied secondary-structure elements and the presentation of individual amino acids in the binding pocket (23, 24). In the D2R and D3R, for instance, the second extracellular loop (ECL2) is much shorter than in the β -adrenergic receptors (β ARs) and lacks the helical secondary structure. The portion of ECL2 in D3R (residues 182 to 185) that contributes to the ligand binding pocket is quite similar to that in the β ARs in both spatial positioning relative to bound ligand, and in the presentation of side chains in the ligand binding pocket. In the D3R, a disulfide bond is formed between Cys355 and Cys358 in ECL3 in addition to the canonical disulfide bond bridging ECL2 (Cys181) and helix III (Cys103^{3,25}) (25). Comparison of the D3R structure to the β 2AR structure reveals small shifts in the helical bundle; for example, the extracellular tips of helices VI and VII are tilted by $\sim 3 \text{ \AA}$ and $\sim 2 \text{ \AA}$, respectively (Fig. 1B), whereas the extracellular tips of helices III and V are about 3.5 \AA closer to each other in the D3R as compared with the β 2AR structure. The latter shift can be explained by the fact that a segment of ECL2 connecting the tips of helices V and III through a C181-Cys103^{3,25} disulfide bond in D3R and other D2-like receptors is one amino acid shorter than in β 2AR and D1-like dopamine receptors (see fig. S4, B and D).

A common feature thought to be important in many class A GPCRs is the ionic lock—a salt bridge between the charged Arg^{3,50} in the conserved “D[E]RY” motif and Asp/Glu^{6,30} at the cytoplasmic side of helices III and VI. This interaction is observed in all of the inactive rhodopsin crystal structures (Fig. 2A) (26, 27) and has been implicated through mutagenesis as a major factor in stabilizing the receptors in the inactive conformation (28, 29). Despite the presence of residues capable of forming this interaction, the ionic lock has not been found in any of the other GPCR crystal structures published to date (19–22) (Fig. 2, C to E). The absence of this interaction is puzzling given its presumed importance and has been thought to be partly attributable to the inclusion of the T4L fusion protein within ICL3, which may induce a non-native helical conformation within this region. However, the presence of an intact ionic lock in both molecules in the D3R structure estab-

lishes the possibility of forming this interaction in the presence of T4L (Fig. 2B). The propensity for formation of the ionic lock, therefore, may indicate different distributions of conformational states in different receptors that may have direct implications for basal signaling ac-

tivities. Differences between the two molecules observed in the crystallographic asymmetric unit may highlight particular areas of conformational flexibility in receptor structure. In chain A, ICL2 forms a 2.5 turn α helix that runs parallel to the membrane (Fig. 1A). The observation of this α

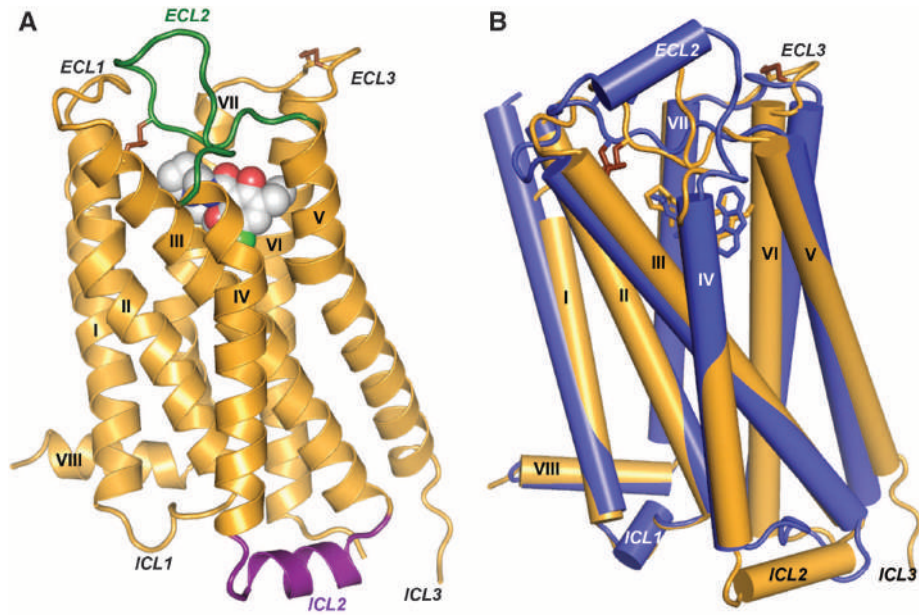
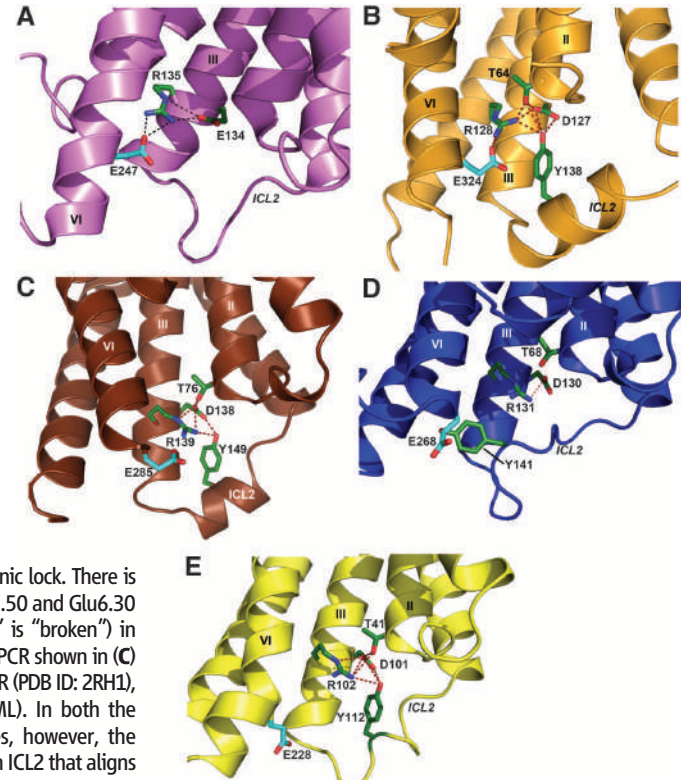


Fig. 1. Overall D3R structure with eticlopride and comparison with β 2AR structure. (A) A model of the D3R with the bound ligand eticlopride in space-filling representation; ECL2 is shown in green, ICL2 in purple, and disulfide bonds in brown (conformation of chain A shown). (B) Comparison of the TM domains of D3R (brown) and β 2AR (blue; PDB ID: 2RH1).

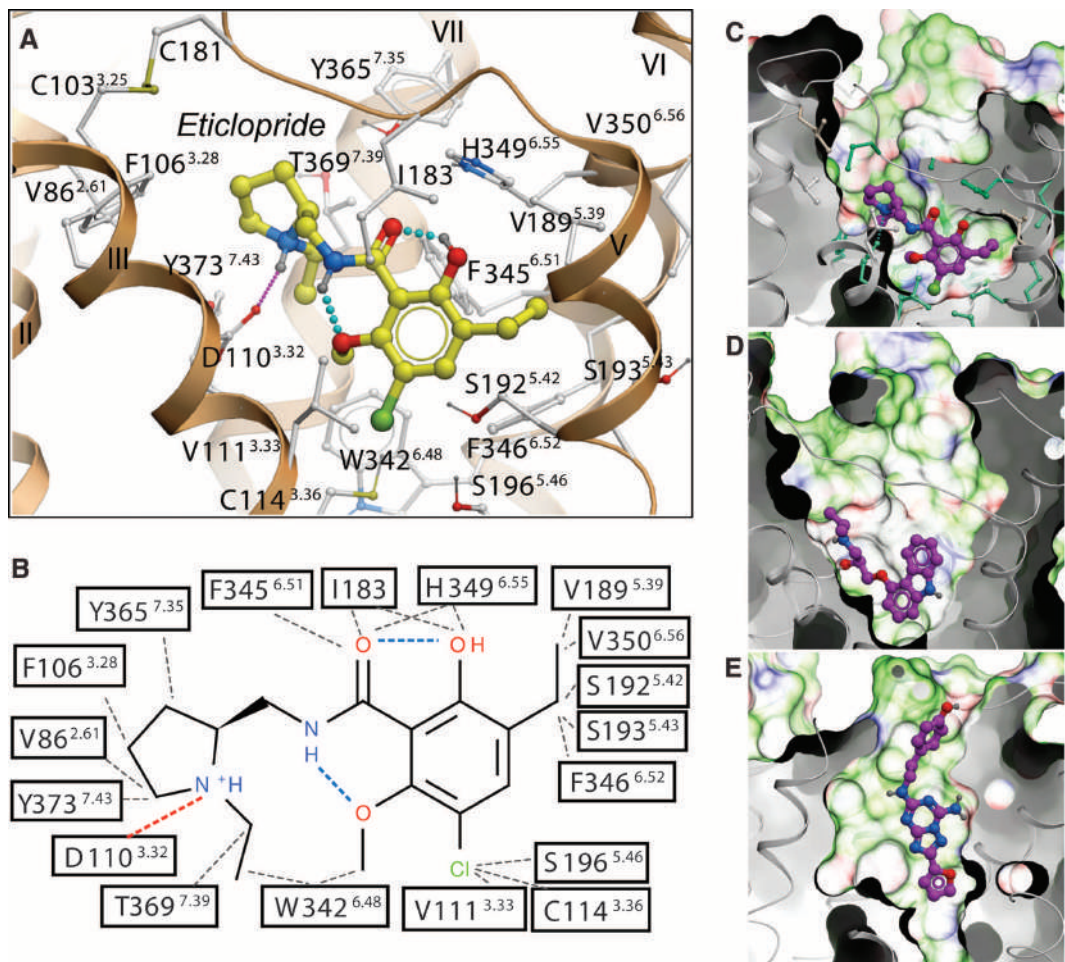
Fig. 2. Conformation of ICL2 and ionic lock motif in D3R and other GPCR structures. As also seen in (A) the inactive Rhodopsin structure (PDB ID: 1U19), the conserved ionic lock motif D[E]RY is in a “locked” conformation in (B) the D3R structure, i.e., with a salt bridge formed between Arg128^{3,50} and Glu324^{6,30}. In addition, the side chain of Tyr138 in the ICL2 α helix of the D3R is inserted into the seven-TM bundle forming hydrogen bonds with Thr64^{2,39}, Arg128^{3,50}, and Asp127^{3,49} (distances of 3.0, 3.2, and 3.2 \AA , respectively), potentially stabilizing the ionic lock. There is no salt bridge between Arg3,50 and Glu6,30 (and hence the “ionic lock” is “broken”) in other crystal structures of GPCR shown in (C) β 1AR (PDB ID: 2VT4), (D) β 2AR (PDB ID: 2RH1), and (E) α 2AR (PDB ID: 3EML). In both the β 1AR and α 2AR structures, however, the corresponding Tyr residue in ICL2 that aligns to Tyr138 in D3R forms two hydrogen bonds with the Asp^{3,49} and Arg^{3,50} side chains even in the absence of the closed ionic lock conformation. Salt bridges and hydrogen bond interactions are shown as dashed lines.



helix in only one copy of the receptor may be due to the conformational dynamics of ICL2 and the associated regions (30), as in chain B, ICL2 is unstructured and the intracellular ends of helices IV and V are shifted ~2.9 Å closer to each other relative to their positions in chain A (fig. S3C). The two different conformational states of ICL2 observed in the D3R structure suggest that this helix is transient, raising the possibility that interactions between ICL2 and the receptor ionic lock may modulate the signaling properties of the D3R and perhaps contribute to the tolerance property in D3R signaling that persists after agonist is removed (31).

Strong electron density was observed for eticlopride in the binding cavity (fig. S3, A and B), which is similar to the β_2 AR pocket (Fig. 3, C and D), as expected for receptors that bind closely related catecholamine ligands (32). The similarity includes a number of conserved side chains in the core binding site deep in the seven-TM bundle (10 of 18 eticlopride contact residues are conserved in the β_2 AR) and open access to this site through a crevice from the extracellular side. Compared with the β_2 AR, however, a part of the D3R access crevice is blocked by the inward shift of helices V and VI, and access to the ligand binding pocket is controlled by side chains of helices I, II, III, VII, and ECL2.

Fig. 3. Structural diversity of ligand binding sites in GPCR structures. (A) Close-up of the eticlopride binding site showing the protein-ligand interaction. (B) Chemical structure of eticlopride and interactions with the D3R residues; hydrophobic contacts are shown in gray dashed lines, hydrogen bonds in blue, and salt bridges in red. The ligand binding sites in (C) D3R, (D) β_2 AR (PDB ID: 2RH1), and (E) A_{2A}AR (PDB ID: 3EML) crystal structures are shown in exactly the same orientation. A semitransparent skin shows the molecular surface of the receptor, colored by the residue properties (green, hydrophobic; red, acidic; and blue, basic). Corresponding ligands (C) eticlopride, (D) carazolol, and (E) ZM241385 are shown with carbon atoms colored magenta. For the D3R pocket, residues conserved between D3R and β_2 AR are colored turquoise, and nonconserved residues are in gray.



Eticlopride occupies the part of the binding pocket defined by side chains from helices II, III, V, VI, and VII (Figs. 1 and 3A and table S4) that largely overlaps with the carazolol binding site in the β_2 AR (Fig. 1B). The tertiary amine in the ethyl-pyrrolidine ring of eticlopride is likely charged at physiological pH and forms a salt bridge (2.8 Å) to the carboxylate of Asp110^{3.32}, which is highly conserved in all aminergic receptors (Fig. 3, A and B). This salt bridge is structurally and pharmacologically critical for high-affinity ligand binding to the aminergic subfamily of GPCRs (4, 33). Another key component of the eticlopride pharmacophore is a substituted aromatic ring connected to the pyrrolidine by an amide bond that fits tightly within a hydrophobic cavity formed by Phe345^{6.51} and Phe346^{6.52} in helix VI; Val189^{5.39}, Ser192^{5.42}, and Ser193^{5.43} in helix V; and Val111^{3.33} in helix III, as well as Ile183 in ECL2. Polar substituents (e.g., OH, OCH₃) in the phenyl ring form intramolecular hydrogen bonds with both the N and O of the amide, thereby maintaining the compound in an almost planar conformation (Fig. 3, A and B), consistent with the small-molecule crystal structure determination (13).

Of the 18 eticlopride contact residues in the D3R structure, 17 are identical in the D2R (Val350^{6.56} is an isoleucine in D2R), whereas 5 differ in the D4R (see fig. S4). Qualitatively, this agrees with the finding that eticlopride, and some of its analogs, share similar affinities for the D2R and D3R with lower binding affinities for D4R. Mutation of four divergent residues in D2R to the aligned D4R residues led to a three-order-of-magnitude enhancement of binding to a D4R-selective antagonist (34). Most of the differences in ligand binding specificity between D4R and D2R/D3R can therefore be explained by the differences in physicochemical properties of the contact side chains, as the mutated D2 residues included three of the five nonconserved, eticlopride-contact residues—Val91^{2.61}Phe, Phe110^{3.28}Leu, and Tyr408^{7.35}Val.

The structural determinants of pharmacological specificity in the D3R and D2R are more subtle considering that the residues lining the binding pocket are essentially identical. In accordance with high conservation of the eticlopride binding site between D3R and D2R, the available structure-activity relationship (SAR) data suggest that, to achieve targeted selectivity (>100-fold), the ligand must extend toward the extracellular opening of the binding pocket [reviewed in (12)]. The D3R-selective pharmacophore consists of an extended aryl amide connected to an amine-containing scaffold by a relatively flexible four-carbon linker (fig. S1) (35). Previous

efforts to rationalize the structural basis of D3R selectivity have naturally focused on regions that are not conserved, with primary attention being given to ECL2, which has previously been implicated in ligand binding to the D2R (4, 36). Indeed, in chimeric studies, ECL2 has been found to play a role in both enantioselectivity and D3R selectivity of a number of compounds in which the butylamide linker is functionalized (37). In addition, roles for both ECL2 and ECL1 have been demonstrated for the D3R-selective tetrahydroisoquinoline, SB 269,652 (fig. S1) (38).

To explore the structural basis of selectivity, we created a homology model of D2R based on the D3R structure (18). Eticlopride could be reproducibly docked to the D3R structure and D2R model in orientations highly similar to that in the crystal structure. However, alignment of residues of the D3R and D2R indicates substantial differences in their extracellular electro-

static surfaces that could affect binding of other longer and bulkier ligands (figs. S5 and S6). Docking studies with the D3R-selective antagonist R-22 (37) revealed that the core amine-containing substituent (2,3-diCl-phenylpiperazine) binds in essentially the same binding pocket as eticlopride, whereas the indole-2-carboxamide terminus is oriented toward the extracellular part of the binding pocket consisting of ECL2/ECL1 and the junction of helices I, II, and VII, defining a second extracellular binding pocket (orange ellipse in Fig. 4A) that includes conserved Tyr373^{7,43} and Glu95^{2,65} (Fig. 4B). However, the residue at 1.39, which is spatially positioned between Tyr373^{7,43} and Glu95^{2,65}, is divergent (Tyr36^{1,39} in D3R and Leu41^{1,39} in D2R) (Fig. 4, C and D). Moreover, Tyr36^{1,39} is located in a stretch of five nonconserved residues at the extracellular end of helix I. Indeed, 44% of the extracellular half of helix I from 1.35 to 1.50 is not conserved between D2R and D3R (fig. S6), which should

lead to functionally relevant changes in packing in D2R at the junction of helices I, II, and VII (Fig. 4, C and D, and fig. S7), consistent with previous structure-function investigations (39–41). The lack of conservation of Thr368^{7,38} (Phe in D2R), which forms a hydrogen bond with the backbone of the conserved Tyr365^{7,35} in the D3R, may also contribute to a shift in the relative position of helices I and VII (Fig. 4, C and D) (42).

Such differences in packing and backbone configuration between the D2R and D3R, even when relatively subtle, are expected to lead to changes in selectivity even without changes in ligand contact side chains in the binding pocket. Indeed, molecular dynamics simulations of the D2R in an explicit lipid bilayer (18) suggest a reorganization of ECL3 and helices I, II, and VII that alters the configuration of the second binding pocket (Fig. 4D and fig. S7). Accordingly, the distance between the conserved residues Glu95^{2,65} (in the second binding pocket) and Tyr373^{7,43} (between the orthosteric binding site and the second binding pocket) is ~1 Å greater in the D3R than in the D2R because of distinct 2.65–1.39–7.43 interactions (Fig. 4, C and D, and fig. S7), representing subtle but critical differences in the relative disposition between the orthosteric binding site and the second binding pocket in the D2R and D3R (Fig. 4B).

The crystal structure of the human D3R provides an opportunity to identify subtle structural differences, at the molecular level, between closely related GPCRs that can be exploited for novel drug design. In particular, the structural observation of an extracellular binding pocket, which may interact with bitopic or allosteric ligands, highlights the importance of the extracellular loops that were once thought to only provide superficial definition to ligand binding. Highly D2R and D3R subtype-selective molecules will provide the tools necessary to parse behavioral actions associated with individual subtypes and identify mechanisms underlying side effects, resulting in improved medications for the treatment of neuropsychiatric disorders, including drug abuse.

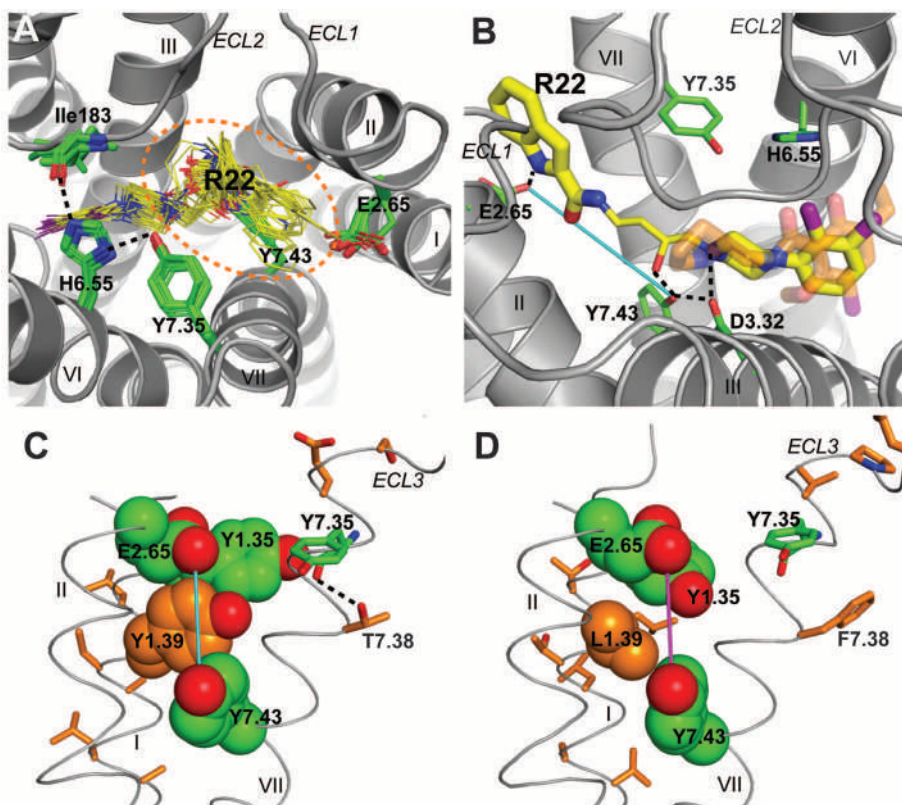


Fig. 4. The second binding pocket defined by R-22 is differentially modulated by nonconserved residues in D3R and D2R. **(A)** In addition to the core binding pocket, which essentially overlaps with that of eticlopride, the potential docking conformations of the core-constrained (see supporting online material) D3R-selective compound R-22 position the extended aryl amide within a second binding pocket comprising the junction of ECL1 and ECL2 and the interface of helices II, VII and I [dotted orange ellipse in (A)]. **(B)** In the docking pose with the most extended conformation of R-22 (yellow), the ligand makes contact with several key conserved residues, including Asp110^{3,32}, Tyr373^{7,43}, and Glu90^{2,65}. The linker region of R-22 connecting the aryl amide and phenylpiperazine moieties (see fig. S1) is in a thinner representation. The 2,3-diCl-phenylpiperazine occupies essentially the same space as bound eticlopride (orange). **(C and D)** Close-up view of the interface of helices II, VII, and I of the D3R (C) and D2R (D) showing the results of molecular dynamics simulations indicating that the nonconserved regions of helix I and position 7.38 (orange) may orient key conserved contact residues differently and alter the shape of the second binding pocket, as reflected by the simulated distances between Glu90^{2,65} and Tyr373^{7,43} in D3R (cyan) and D2R (magenta) (see fig. S7).

References and Notes

- O. Civelli, in *Psychopharmacology: The Fourth Generation of Progress*, F. Bloom, D. Kupfer, Eds. (Raven, NY, 1995), pp. 155–161.
- B. Levant, *Pharmacol. Rev.* **49**, 231 (1997).
- P. Sokoloff, B. Giros, M. P. Martres, M. L. Bouthenet, J. C. Schwartz, *Nature* **347**, 146 (1990).
- L. Shi, J. A. Javitch, *Annu. Rev. Pharmacol. Toxicol.* **42**, 437 (2002).
- P. Sokoloff *et al.*, *Eur. J. Pharmacol.* **225**, 331 (1992).
- A. Holmes, J. E. Lachowicz, D. R. Sibley, *Neuropharmacology* **47**, 1117 (2004).
- J. G. Gilbert *et al.*, *Synapse* **57**, 17 (2005).
- M. Pilla *et al.*, *Nature* **400**, 371 (1999).
- K. Spiller *et al.*, *Psychopharmacology (Berl.)* **196**, 533 (2008).
- S. R. Vorel *et al.*, *J. Neurosci.* **22**, 9595 (2002).
- Z. X. Xi *et al.*, *Neuropsychopharmacology* **31**, 1393 (2006).

12. C. A. Heidbreder, A. H. Newman, *Ann. N. Y. Acad. Sci.* **1187**, 4 (2010).
13. T. DePaulis, H. Hall, S. Ogren, *Eur. J. Med. Chem. Chim. Ther.* **20**, 273 (1985).
14. N. Griffon, C. Pilon, F. Sautel, J. C. Schwartz, P. Sokoloff, *J. Neural Transm.* **103**, 1163 (1996).
15. In Ballesteros-Weinstein numbering, a single most conserved residue among the class A GPCRs is designated $x.50$, where x is the transmembrane helix number. All other residues on that helix are numbered relative to this conserved position.
16. C. B. Roth, M. A. Hanson, R. C. Stevens, *J. Mol. Biol.* **376**, 1305 (2008).
17. D. M. Rosenbaum *et al.*, *Science* **318**, 1266 (2007).
18. Materials and methods are available as supporting material on *Science* online.
19. V. Cherezov *et al.*, *Science* **318**, 1258 (2007).
20. M. A. Hanson *et al.*, *Structure* **16**, 897 (2008).
21. V. P. Jaakola *et al.*, *Science* **322**, 1211 (2008).
22. T. Warne *et al.*, *Nature* **454**, 486 (2008).
23. J. M. Baldwin, *EMBO J.* **12**, 1693 (1993).
24. T. H. Ji, M. Grossmann, I. Ji, *J. Biol. Chem.* **273**, 17299 (1998).
25. A similar intraloop disulfide bond is present in the $\alpha_2\text{AR}$ structure and likewise is thought to constrain the position of ECL3 and orient His359 at the top of the ligand binding site.
26. T. Okada *et al.*, *J. Mol. Biol.* **342**, 571 (2004).
27. K. Palczewski *et al.*, *Science* **289**, 739 (2000).
28. J. A. Ballesteros *et al.*, *J. Biol. Chem.* **276**, 29171 (2001).
29. R. Vogel *et al.*, *J. Mol. Biol.* **380**, 648 (2008).
30. R. O. Dror *et al.*, *Proc. Natl. Acad. Sci. U.S.A.* **106**, 4689 (2009).
31. E. V. Kuzhikandathil, L. Westrich, S. Bakhos, J. Pasuit, *Mol. Cell. Neurosci.* **26**, 144 (2004).
32. R. Duman, E. J. Nestler, in *Psychopharmacology: The Fourth Generation of Progress*, F. Bloom, D. Kupfer, Eds. (Raven, NY, 1995), pp. 303–320.
33. C. D. Strader *et al.*, *J. Biol. Chem.* **266**, 5 (1991).
34. M. M. Simpson *et al.*, *Mol. Pharmacol.* **56**, 1116 (1999).
35. F. Boeckler, P. Gmeiner, *Pharmacol. Ther.* **112**, 281 (2006).
36. L. Shi, J. A. Javitch, *Proc. Natl. Acad. Sci. U.S.A.* **101**, 440 (2004).
37. A. H. Newman *et al.*, *J. Med. Chem.* **52**, 2559 (2009).
38. E. Silvano *et al.*, *Mol. Pharmacol.* **78**, 925 (2010).
39. W. Guo *et al.*, *EMBO J.* **27**, 2293 (2008).
40. L. Shi, M. M. Simpson, J. A. Ballesteros, J. A. Javitch, *Biochemistry (Mos.)* **40**, 12339 (2001).
41. G. L. Alberts, J. F. Pregenzer, W. B. Im, *Mol. Pharmacol.* **54**, 379 (1998).
42. J. A. Ballesteros, X. Deupi, M. Olivella, E. E. Haaksma, L. Pardo, *Biophys. J.* **79**, 2574 (2000).
43. This work was supported in part by Protein Structure Initiative (PSI) grant U54 GM074961 and PSI:Biology grant U54 GM094618 for structure production, NIH Roadmap grant P50 GM073197 for technology development, NIH grant R21 RR025336 (V.C.), and Pfizer. Additional support was provided by the National Institute on Drug Abuse Intramural Research Program (A.H.N.), grants DA022413 and MH54137 (J.A.J.), and grant DA023694 (L.S.). The content is solely the responsibility of the authors and does not necessarily represent the official views of the National Institute of General Medical Science or the NIH. We thank J. Velasquez for help with molecular biology, T. Trinh and K. Allin for help with baculovirus expression, D. Gray for assistance with eticlopride synthesis, M. Griffor for large-scale production of the receptor, X. Qiu for suggestions, and A. Walker for assistance with manuscript preparation. We acknowledge Y. Zheng, The Ohio State University and M. Caffrey, Trinity College (Dublin, Ireland), for the generous loan of the in meso robot (built with support from NIH grant GM075915), the National Science Foundation (grant IIS0308078), and Science Foundation Ireland (grant 02-IN1-B266); and J. Smith, R. Fischetti, and N. Sanishvili at the GM/CA-CAT beamline at the Advanced Photon Source, for assistance in development and use of the minibeam and beamtime. The GM/CA-CAT beamline (23-ID) is supported by the National Cancer Institute (grant Y1-CO-1020) and the National Institute of General Medical Sciences (grant Y1-GM-1104). Atomic coordinates and structure factors have been deposited in the Protein Data Bank with identification code 3PBL. A.H.N. is an inventor on a patent application from the National Institutes of Health that covers the use of R-22 and analogs as D3 receptor selective agents. R.C.S. is on the Board of Directors of Receptos, which does structure-directed drug discovery on GPCRs.

Supporting Online Materialwww.sciencemag.org/cgi/content/full/330/6007/1091/DC1**Materials and Methods**

Figs. S1 to S8

Tables S1 to S4

References

6 September 2010; accepted 21 October 2010
10.1126/science.1197410

Mcl-1 Is Essential for Germinal Center Formation and B Cell Memory

Ingela Vikstrom,¹ Sebastian Carotta,¹ Katja Lüthje,¹ Victor Peperzak,¹ Philipp J. Jost,¹ Stefan Glaser,¹ Meinrad Busslinger,² Philippe Bouillet,^{1,3} Andreas Strasser,^{1,3} Stephen L. Nutt,^{1,3} David M. Tarlinton^{1,3*}

Lymphocyte survival during immune responses is controlled by the relative expression of pro- and anti-apoptotic molecules, regulating the magnitude, quality, and duration of the response. We investigated the consequences of deleting genes encoding the anti-apoptotic molecules Mcl1 and Bcl2l1 (Bcl-x_L) from B cells using an inducible system synchronized with expression of activation-induced cytidine deaminase (*Aicda*) after immunization. This revealed Mcl1 and not Bcl2l1 to be indispensable for the formation and persistence of germinal centers (GCs). Limiting Mcl1 expression reduced the magnitude of the GC response with an equivalent, but not greater, effect on memory B cell formation and no effect on persistence. Our results identify Mcl1 as the main anti-apoptotic regulator of activated B cell survival and suggest distinct mechanisms controlling survival of GC and memory B cells.

Vertebrate immune responses are characterized by the clonal expansion of antigen-specific lymphocytes, by their differentiation into effector cells, and by the production of small, persistent populations of memory cells. An added feature of B cell immunity is the increasing affinity of the antibody response with time, with B cells expressing high-affinity antigen receptors (BCRs) preferentially recruited into the effector and memory compartments (1). The processes

underpinning changes in affinity of immunoglobulin receptors occur within germinal centers (GCs), which are transient structures that arise after T cell-dependent immunization (2–4). Thus, the factors governing the survival of GC B cells will determine the qualitative and quantitative attributes of the effector cells—which in this case are plasma cells—and memory B cells. Survival of GC B cells is mediated by both the intrinsic and extrinsic apoptotic cell death pathways (5), with roles proposed for Fas ligand (CD95L)/Fas (CD95) (6, 7), Bcl2l1 (Bcl-x_L) (8), Bcl2 (9, 10), and Bim (11). These studies, however, do not identify the prosurvival molecules that are physiologically relevant within the GC.

To address the components of the intrinsic apoptotic pathway regulating GC B cell behavior,

we first measured the expression of relevant proteins, comparing GC and follicular B cells (Fig. 1) (12). Besides Bcl2l1 and Bim expression being up-regulated and Bcl2 down-regulated as previously reported (6, 13, 14), Mcl1 protein was increased in GC B cells (Fig. 1).

Increases in Bcl2l1 and Mcl1 expression in GC B cells prompted us to examine the contribution of these prosurvival proteins to the production of memory B cells, plasma cells, and affinity maturation. We therefore conditionally deleted loxP-flanked alleles of *Bcl2l1* or *Mcl1* in B cells after antigen activation using a transgene-encoded Cre recombinase expressed concurrently with the activation-induced cytidine deaminase (*Aicda*) locus (15). The loxP-flanked alleles should therefore be deleted in B cells, initiating somatic hypermutation (SHM) or class-switch recombination (CSR), which are processes requiring activation-induced cytidine deaminase (AID) (16).

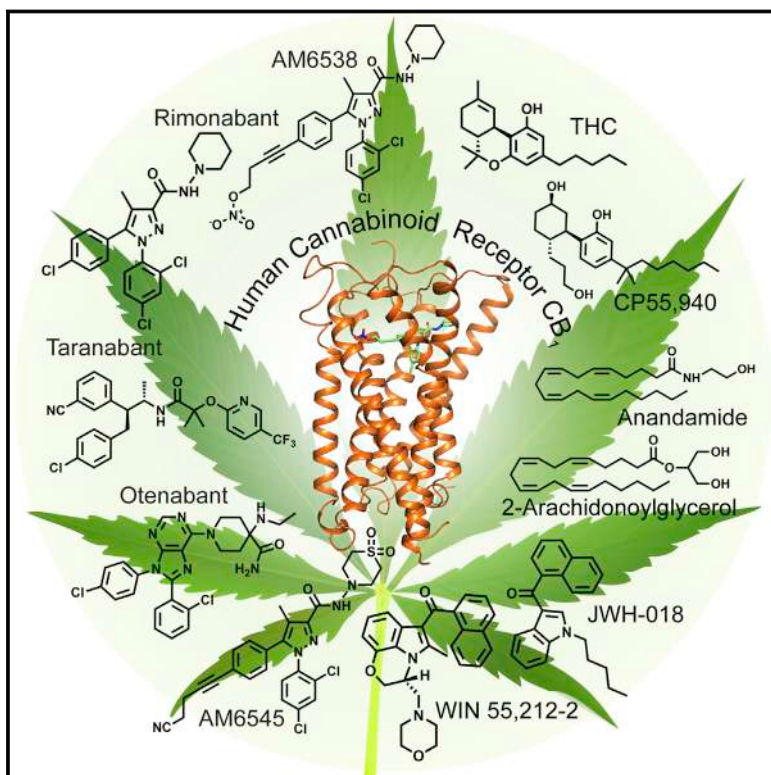
Bcl2l1^{fl/fl}/*Aicda*-Cre mice, with one *Bcl2l1* allele deleted (17) and one flanked by LoxP (fl) sites (18), were immunized with a T cell-dependent antigen composed of the 4-hydroxy-3-nitrophenyl (NP) hapten conjugated to keyhole limpet hemocyanin (NP-KLH). Cellular responses were analyzed 21 days later in *Bcl2l1*^{fl/fl}/*Aicda*-Cre and control mice, when GC and memory B cells coexist (6, 19). No significant difference in the frequency or number of antigen-specific (NP-IgG1⁺) B cells was observed in the spleens of *Bcl2l1*^{fl/fl}/*Aicda*-Cre mice as compared with controls, both in total and after subdivision into GC (CD38⁺) and memory (CD38⁻) compartments (Fig. 2, A and B). Similarly, no differences were seen 7 and 14 days after immunization, excluding the possibility of an early deficit being masked by compensation as

*To whom correspondence should be addressed. E-mail: tarlinto@wehi.edu.au

¹Walter and Eliza Hall Institute of Medical Research, 1G Royal Parade, Parkville, Victoria 3052, Australia. ²Research Institute of Molecular Pathology, Vienna Biocenter, Dr. Bohr-Gasse 7, A-1030 Vienna, Austria. ³Department of Medical Biology, University of Melbourne, Parkville, Victoria 3050, Australia.

Crystal Structure of the Human Cannabinoid Receptor CB₁

Graphical Abstract



Authors

Tian Hua, Kiran Vemuri, Mengchen Pu, ..., Alexandros Makriyannis, Raymond C. Stevens, Zhi-Jie Liu

Correspondence

Ibohn@scripps.edu (L.M.B.), a.makriyannis@northeastern.edu (A.M.), stevens@shanghaitech.edu.cn (R.C.S.), liuzhj@shanghaitech.edu.cn (Z.-J.L.)

In Brief

A look at ligand engagement with the human CB₁ receptor opens up avenues for design of new modulators with favorable physiological profiles.

Highlights

- AM6538 is presented as a stabilizing, tight binding antagonist of CB₁
- Crystal structure of human CB₁ in complex with AM6538 is determined
- Molecular docking predicts CB₁ binding modes of THC and synthetic cannabinoids
- Resolution of the binding pocket provides path for rational CB₁ drug design

Data Resources

5TGZ

Crystal Structure of the Human Cannabinoid Receptor CB₁

Tian Hua,^{1,2} Kiran Vemuri,³ Mengchen Pu,² Lu Qu,^{1,2} Gye Won Han,⁴ Yiran Wu,¹ Suwen Zhao,¹ Wenqing Shui,¹ Shanshan Li,¹ Anisha Korde,³ Robert B. Laprairie,⁵ Edward L. Stahl,⁵ Jo-Hao Ho,⁵ Nikolai Zvonok,³ Han Zhou,³ Irina Kufareva,⁶ Beili Wu,⁷ Qiang Zhao,⁷ Michael A. Hanson,⁸ Laura M. Bohn,^{5,*} Alexandros Makriyannis,^{3,*} Raymond C. Stevens,^{1,4,9,*} and Zhi-Jie Liu^{1,2,*}

¹iHuman Institute, ShanghaiTech University, Shanghai 201210, China

²National Laboratory of Biomacromolecules, Institute of Biophysics, Chinese Academy of Sciences, Beijing 100101, China

³Center for Drug Discovery, Department of Pharmaceutical Sciences and Department of Chemistry and Chemical Biology, Northeastern University, Boston, MA 02115, USA

⁴Departments of Biological Sciences and Chemistry, Bridge Institute, University of Southern California, Los Angeles, CA 90089, USA

⁵Departments of Molecular Therapeutics and Neuroscience, The Scripps Research Institute, Jupiter, FL 33458, USA

⁶University of California, San Diego, La Jolla, CA 92093, USA

⁷CAS Key Laboratory of Receptor Research, Shanghai Institute of Materia Medica, Chinese Academy of Sciences, Shanghai 201203, China

⁸GPCR Consortium, San Marcos, CA 92078, USA

⁹Lead Contact

*Correspondence: lbohn@scripps.edu (L.M.B.), a.makriyannis@northeastern.edu (A.M.), stevens@shanghaitech.edu.cn (R.C.S.), liuzhj@shanghaitech.edu.cn (Z.-J.L.)

<http://dx.doi.org/10.1016/j.cell.2016.10.004>

SUMMARY

Cannabinoid receptor 1 (CB₁) is the principal target of Δ⁹-tetrahydrocannabinol (THC), a psychoactive chemical from *Cannabis sativa* with a wide range of therapeutic applications and a long history of recreational use. CB₁ is activated by endocannabinoids and is a promising therapeutic target for pain management, inflammation, obesity, and substance abuse disorders. Here, we present the 2.8 Å crystal structure of human CB₁ in complex with AM6538, a stabilizing antagonist, synthesized and characterized for this structural study. The structure of the CB₁-AM6538 complex reveals key features of the receptor and critical interactions for antagonist binding. In combination with functional studies and molecular modeling, the structure provides insight into the binding mode of naturally occurring CB₁ ligands, such as THC, and synthetic cannabinoids. This enhances our understanding of the molecular basis for the physiological functions of CB₁ and provides new opportunities for the design of next-generation CB₁-targeting pharmaceuticals.

INTRODUCTION

Marijuana from *Cannabis sativa L.* has been used for both therapeutic and recreational purposes for many centuries (Lemberger, 1980; Li, 1973). In the 1940s, chemistry based on compounds isolated from the plant (Wollner et al., 1942) produced novel biologically active molecules (Adams et al., 1948; Ghosh et al., 1940); however, it was not until the 1960s that the active constituent of marijuana, Δ⁹-tetrahydrocannabinol (THC), a

terpenoid molecule, was isolated and characterized (Gaoni and Mechoulam, 1964). This provided an early molecular foundation for medicinal chemists to develop related structural analogs and new synthetic ligands (Makriyannis and Rapaka, 1990; Razdan, 1986). Initially, due to their lipophilic nature, it was assumed that cannabinoids exerted their effects by perturbing the physical properties of biological membranes (Makriyannis, 2014; Mavromoustakos et al., 1995). This assumption was challenged with the discovery, cloning, and expression of the first cannabinoid-specific membrane receptor, then designated as the cannabinoid receptor (CB) (Devane et al., 1988; Matsuda et al., 1990). With the subsequent identification of a second receptor, the designation evolved to CB₁ and CB₂ (Munro et al., 1993). The discovery of the endogenous agonists to the receptors, the endocannabinoids, anandamide (Devane et al., 1992), and 2-arachidonoyl glycerol (2-AG) (Mechoulam et al., 1995) soon followed.

Cannabinoid receptors belong to the class A G protein-coupled receptor (GPCR) family, signal through inhibitory G_{αi/o} heterotrimeric G proteins (Howlett, 1985), and interact with β-arrestins (Jin et al., 1999). CB₁ is the most highly expressed GPCR in the human brain and is expressed throughout the body, with the highest levels found in the central nervous system (Herkenham et al., 1990).

Cannabis has been used for centuries in many cultures to treat a wide range of medical conditions. More recently, therapeutic considerations have moved beyond the plant extract to explore and produce more pharmacologically refined compounds. CB₁-selective small-molecule agonists have shown therapeutic promise in a wide range of disorders, including pain and inflammation (Cravatt and Lichtman, 2004), multiple sclerosis (Pertwee, 2002; Pryce and Baker, 2015), and neurodegenerative disorders (Fernández-Ruiz et al., 2015). The first CB₁-selective antagonist/inverse agonist, rimonabant (SR141716, Acomplia [Sanofi-Aventis]) (Rinaldi-Carmona

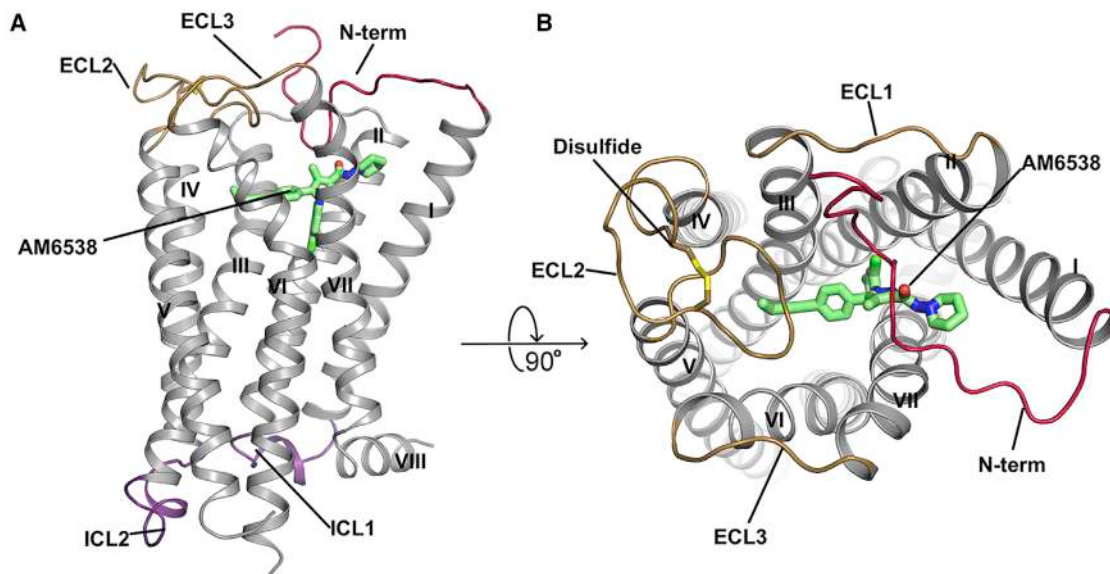


Figure 1. Overall Structure of CB₁-AM6538 Complex

(A) Side view of the CB₁-AM6538 complex. The receptor is shown in gray cartoon representation. The ligand AM6538, shown with green sticks, demarcates the binding pocket, which is partially occluded by the N-terminal loop (red). The nitrate group is not modeled in the experimental crystal structure, as the electron density was not observed. The extracellular loops (ECLs) are shown in brown and the intracellular loops (ICLs) are shown in purple.

(B) Top view of the extracellular side. The disulfide bond in ECL2 is shown as yellow sticks.

See also Figures S2 and S3.

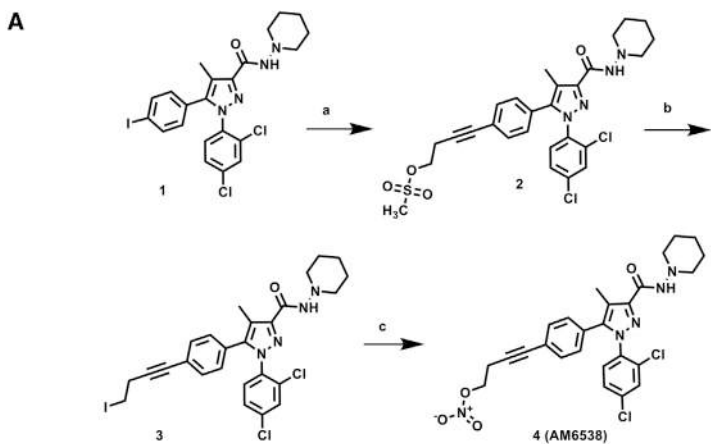
et al., 1994), received approval from the European Medical Agency as an adjunct to diet and exercise for treating obesity (Janero and Makriyannis, 2009). Antagonists of CB₁ have been explored as potential therapeutics for obesity-related metabolic disorders (Mazier et al., 2015), mental illness (Black et al., 2011; Rubino et al., 2015), liver fibrosis (Mallat et al., 2013), and nicotine addiction (Schindler et al., 2016). However, rimonabant and other ligands in its class were not approved in the United States due to concerns about adverse events, such as increased anxiety, depression, and suicidal ideation.

Numerous studies have investigated how ligands binding CB₁ can mediate downstream signaling. While the variety of compounds exhibiting different pharmacological profiles have provided clues regarding CB₁ activation, the molecular details defining the binding modes of both endogenous and exogenous ligands are still largely unknown (Guo et al., 1994; Makriyannis, 2014; Picone et al., 2005). In order to address this deficit in understanding, we have determined the crystal structure of CB₁ in complex with a tight binding antagonist AM6538. In conjunction with molecular docking, the structure was used to elucidate the binding modes of a diverse set of antagonists/inverse agonists and agonists of CB₁. The structural details of the cannabinoid receptor reported herein improve our understanding of how ligands engage to modulate the cannabinoid system and provide a useful model to facilitate the design of next-generation pharmaceuticals to avoid unwanted side effects. The findings provide insight into mechanisms of slow dissociation of antagonists, which may potentially translate into long acting pharmacological effects.

RESULTS

Synthesis of CB₁ Stabilizing Antagonist AM6538 for Structural Studies

One of the key factors facilitating the structure determination of CB₁ (Figure 1) is utilization of the antagonist AM6538, the synthesis of which resulted from the strategic modification of rimonabant to enhance its ability to stabilize the ligand-receptor complex and promote CB₁ crystal formation. In contrast with rimonabant, the 5-phenyl ring substituent was modified so as to introduce motifs (ex. alkyne unit) that could favor increased affinity for the CB₁ receptor (Tam et al., 2010). The rimonabant analog, AM251, (1, Figure 2A) (Lan et al., 1999), a compound that has been used extensively as a pharmacological standard CB₁-selective antagonist, was used as the precursor in the AM6538 synthetic process. Synthesis of AM6538 involves the functionalization of the iodo substituent at the para position of the 5-phenyl ring in AM251 with an acetylenic chain system consisting of four carbons and substituted at the omega carbon. To this end, we initially focused on targeting cysteine residues within CB₁ by introducing suitable electrophilic groups (Janero et al., 2015; Li et al., 2005; Mercier et al., 2010; Picone et al., 2005; Szymanski et al., 2011) at the fourth carbon of the alkyne unit, capable of forming a covalent bond with the cysteine thiol group. For AM6538, we introduced at this position a nitrate group (ONO₂) whose role was to serve as a polar group, which may be displaced by a suitable nucleophile (e.g., thiol) (Pattison and Brown, 1956; Yeates et al., 1985) at or near the binding domain or alternatively bind as an intact group so as to obtain a non-covalent, near-irreversible attachment by interacting with hydrogen bonding amino acid residues, as well as



Scheme 1. Synthesis of AM6538

a) but-3-yn-1-yl methanesulfonate, DMF, Pd(PPh₃)₄, CuI, Hunig's base, RT, 45%
 b) NaI, TBAI, acetone, reflux, 62%
 c) AgNO₃, MeCN, heat, 65%

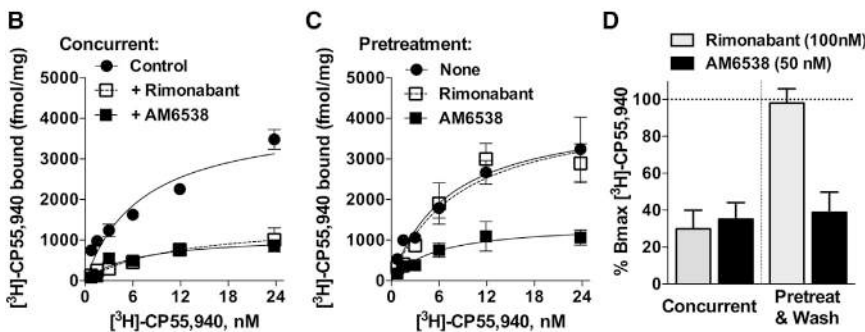


Figure 2. Synthesis and Characterization of AM6538

(A) Synthetic procedures for compound AM6538.
 (B) Saturation [³H]-CP55,940 binding assays in the absence (control) or presence of rimonabant (100 nM) or AM6538 (50 nM) demonstrates that both antagonists cause displacement of specific binding of the radioligand when present concurrently in the 1 hr binding assay.

(C) Following pretreatment of membranes (37°C, 6 hr) with buffer only (none), rimonabant (100 nM), or AM6538 (50 nM); membranes were washed with buffer 3x prior to [³H]-CP55,940 binding as described for (B).

(D) Percentage of remaining binding (B_{max}) detected following the conditions described in (B) (concurrent) and (C) (pretreat and wash). Both antagonists decrease the binding of [³H]-CP55,940 to ~30% when incubated concurrently during the 1 hr binding assay. Under pretreatment and washout conditions, rimonabant does not affect subsequent radioligand binding, while AM6538 continues to compete despite washing of the membranes.

See also Figure S1 and Table S1.

residues capable of $\pi-\pi$ interactions. In the present study, affinity mass spectrometry analysis suggests that AM6538 reacts with CB₁ as an intact molecule with no evidence of covalent modification of relevant cysteine residues.

AM6538 was a strong candidate for crystallographic studies of the receptor based on its high affinity and wash-resistant binding to CB₁ as determined by radioligand competition assays against the tritiated agonist, [³H]-CP55,940 ($K_i = 3.4 \pm 1.0$ nM) (Figures 2B–2D). This is in contrast to rimonabant, which can be readily washed out of membranes, permitting subsequent radioligand binding (Figures 2B–2D). Importantly, the crystallized CB₁ construct (described below) has comparable affinity for AM6538 as the wild-type receptor ($K_i = 5.1 \pm 0.9$ nM).

In functional assays, AM6538 is a competitive antagonist of the effects of CP55,940 and THC on CB₁-mediated inhibition of adenylyl cyclase activity and β -arrestin2 recruitment in overexpression systems (Figures S1A and S1B and Table S1). Competitive antagonism was confirmed by the [³⁵S]-GTP γ S binding assays performed in mouse cerebellum (Figure S1C). For comparison purposes, competitive antagonism was demonstrated for rimonabant in the same systems (Figure S1 and Table S1).

Structure Determination of CB₁-AM6538 Complex

To facilitate crystallization, it was necessary to modify the wild-type (WT) CB₁ sequence. Construct optimization proce-

dures (Lv et al., 2016) identified Flavodoxin (Chun et al., 2012) as a stabilizing fusion partner when inserted within the receptor's third intracellular loop (ICL3) at Val306 and Pro332. Additionally, the WT receptor was truncated on both the N and C termini by 98 and 58 residues, respectively. Finally, in order to improve the expression and thermostability of the receptor, four computationally predicted mutations (Thr210^{3,46}Ala [D'Antona et al., 2006], Glu273^{5,37}Lys, Thr283^{5,47}Val, and Arg340^{6,32}Glu) were introduced to the CB₁ sequence (Figures S2A–S2C) (superscripts denote amino acid position as described by Ballesteros and Weinstein [1995]). The modified CB₁ construct was inserted into a pTT5 vector for expression in HEK293F cells to generate protein (Figure S2D) that formed crystals in lipidic cubic phase supplemented with cholesterol (Figure S3E); the crystals diffracted to 2.8 Å (Table 1).

Based on affinity mass spectrometry analysis, intact AM6538 is associated with the CB₁ protein (Figure S3F). Electron density with three branches was observed near the orthosteric binding site and modeled as core AM6538 atoms with the terminal nitrate group omitted (Figures 3D and S3). A molecular dynamics (MD) simulation was performed on the CB₁-AM6538 complex with the nitrate group intact and modeled through docking analysis, and the results revealed that the root mean square fluctuation (RMSF) values for the nitrate group and the hinge carbon atom are higher, suggesting that the nitrate group is more mobile than other atoms in AM6538 (Figure S4B). As a modeled ligand with other possibilities to fit the electron density, further studies on ligand binding are under investigation.

Table 1. Crystallographic Data Collection and Refinement Statistics

Data Collection and Refinement Statistics	
Ligand	AM6538
Number of crystals	29
Data Collection	
Space group	C2
Cell dimensions	
a,b,c (Å)	116.56, 52.63, 143.63
β (°)	111.14
Number of reflections measured	160,794
Number of unique reflections	19,837
Resolution (Å)	47.30 - 2.80 (2.90-2.80)
R _{merge} ^a	0.126 (0.520)
Mean I/σ(I)	10.1 (2.1)
Completeness (%)	97.4 (94.1)
Redundancy	8.1 (4.6)
CC _{1/2}	0.999 (0.44)
Refinement	
Resolution (Å)	47.05 - 2.80
Number of reflections (test set)	19,827 (985)
R _{work} /R _{free}	0.207/0.238
Number of Atoms	
CB ₁	2,312
Flavodoxin	1,103
AM6538 ^b	33
Lipid and other	102
Average B Factor (Å ²)	
Wilson	73.6
Overall	87.4
CB ₁	110.6
Flavodoxin	66.6
AM6538	119.5
Lipid and other	79.7
rmsds	
Bond lengths (Å)	0.004
Bond angles (°)	0.638
Ramachandran Plot Statistics (%) ^c	
Favored regions	97.7
Allowed regions	2.3
Disallowed regions	0

^aData for high-resolution shells are shown in parenthesis.

^bNitrate group is excluded due to the absence of electron density.

^cAs defined in MolProbity.

Structural Features of CB₁ in Complex with AM6538

The overall CB₁ structural fold shares a similar architecture with previously solved class A GPCR structures, containing seven transmembrane (7TM) α-helices (I to VII) connected by three extracellular loops (ECL1–3), three intracellular loops (ICL1–3), and an amphipathic helix VIII (Figures 1A and S3A). The non-truncated

part of the N terminus of CB₁, residues 99–112, forms a V-shaped loop, which inserts into the ligand-binding pocket and functions as a plug, restricting access to the pocket from the extracellular side (Figures 1A and 1B). While the influence of crystal packing interactions on the conformation of the N terminus (Figure S3B) cannot be ruled out, it is interesting to note that the N terminus has been consistently observed in an ordered form in the structures of the related lipid receptors LPA₁ (lysophosphatidic acid receptor 1) (Chrencik et al., 2015) and S1P₁ (sphingosine 1-phosphate receptor 1) (Hanson et al., 2012) and that the function of CB₁ is very sensitive to the presence of the ordered portion of the N terminus (Andersson et al., 2003; Fay and Farrens, 2013). ECL2 in CB₁ consists of 21 residues folding into an intricate structure that projects four residues (268–271) into the binding pocket. Previous work has shown that the four residues are important for mediating interactions with certain classes of ligands (Ahn et al., 2009; Bertalovitz et al., 2010) and that the two cysteines (Cys257 and Cys264) in ECL2 are critical to the function of CB₁ (Fay et al., 2005). In the structure, the conformation of ECL2 is constrained by the presence of an intraloop disulfide bond (Cys257-Cys264) (Figure 1B) previously found in the structures of the closely related LPA₁ and S1P₁ receptors. The highly conserved disulfide bond between ECL2 and helix III (Cys^{3.25}) in most class A GPCRs is lacking in all three lipid receptor structures.

AM6538 Interactions in CB₁ Ligand-Binding Pocket

The position of the ligand-binding pocket of CB₁ is different from the previously described orthosteric binding sites of other class A GPCRs. AM6538 lies quite low in the binding pocket of CB₁, immediately above the conserved Trp356^{6.48} (Figures 3A and 3B). The ligand adopts an extended conformation with the ligand strain close to its local minimum as determined by quantum mechanical calculations (Figure S3D).

AM6538 forms mainly hydrophobic interactions with ECL2 and the N terminus, as well as with all CB₁ helices except helix IV (Figures 3A and 3B). As described above, the ligand has a pyrazole ring core with three functional groups. For clarity, we have termed the 2,4-dichlorophenyl ring “arm 1,” the 4-aliphatic chain substituted phenyl ring “arm 2,” and the piperidin-1-ylcarbamoyl “arm 3” (Figure 3C). The pyrazole ring core (including the 4-methyl group) is situated between helices II and VII, forming hydrophobic interactions with the side chains of Phe170^{2.57}, Phe379^{7.35}, and Ser383^{7.39} (Figure 3C) and is capped by the N-terminal loop interactions (Met103^{N-term}). Arm 1 is located in a narrow side pocket (Figure 3B) formed by helices II, III, VI, and VII and forms edge-face π-π interactions with the side chain of Phe170^{2.57} and with the backbone amide bond between Gly166^{2.53} and Ser167^{2.54}. This substituted ring moiety forms hydrophobic interactions with Val196^{3.32}, Trp356^{6.48}, Cys386^{7.42}, Leu387^{7.43}, and Met103^{N-term} (Figure 3C). The 2,4-dichlorophenyl ring in arm 1 fits well into the shape of the narrow side pocket (Figure S3C), which explains why 2,4-dichloro or 2-chloro substitutions result in optimal binding (Lange and Kruse, 2005).

Arm 2 of the ligand extends toward a long, narrow channel (Figure 3B) formed by helices III, V, VI, and ECL2. The phenyl group in arm 2 establishes π-π interactions with Phe102^{N-term}, Phe268^{ECL2}, and Trp356^{6.48}; hydrophobic interactions with

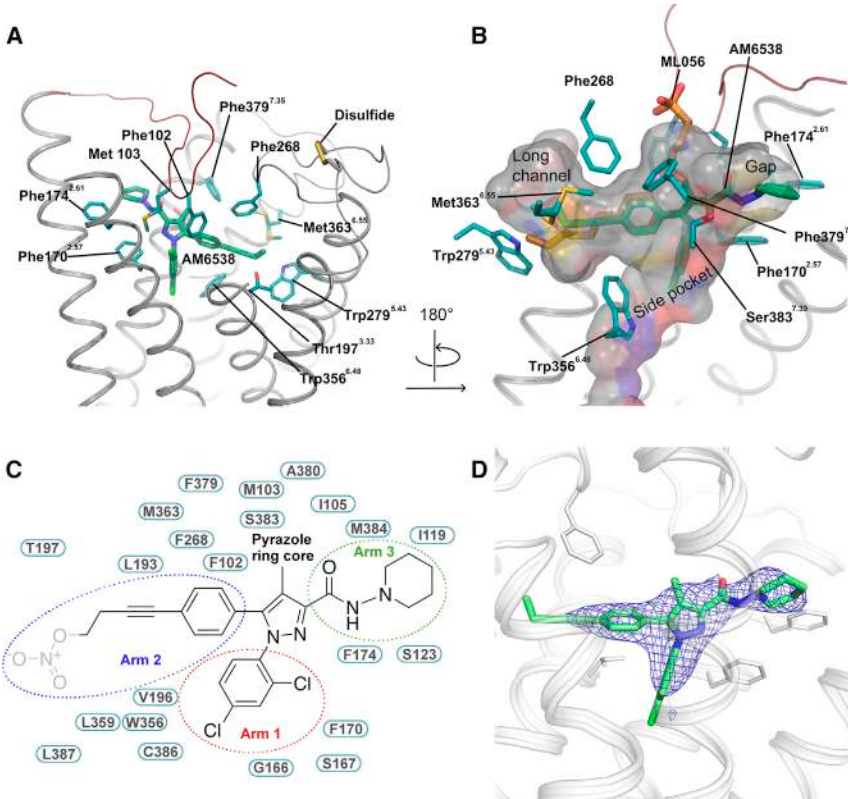


Figure 3. Analysis of the Ligand Binding Pocket of CB₁

(A) Key residues in CB₁ for AM6538 binding. AM6538 (green carbons) and CB₁ residues (teal carbons) involved in ligand binding are shown in stick representation. The receptor is shown in gray cartoon representation.

(B) The shape of the ligand binding pocket. AM6538 (green carbons) and ML056 (brown carbons) are shown in stick representation.

(C) Schematic representation of interactions between CB₁ and AM6538. The 2,4-dichlorophenyl ring in the red circle is termed as arm 1; the 4-aliphatic chain substituted phenyl ring in the blue circle is termed as arm 2; the piperidin-1-ylcarbamoyl in the green circle is termed as arm 3. The nitrate group, which was not observed in the electron density, is shown in gray.

(D) Electron density maps calculated from the refined structure of the CB₁-AM6538 complex. |Fo|-|Fc| omit map (blue mesh) of the ligand AM6538 is shown (contoured at 3 σ).

See also Figure S3.

Leu193^{3.29}, Val196^{3.32}, and Leu359^{6.51} are observed. A triple bond within the long aliphatic chain in arm 2 forms π-π interactions with Phe268^{ECL2} and Trp356^{6.48} and forms hydrophobic interactions with several residues, including Leu193^{3.29}, Val196^{3.32}, Thr197^{3.33}, Leu359^{6.51}, and Met363^{6.55} (Figure 3C). Interestingly, the binding mode of the long hydrophobic chain is similar to that of ML056 with the S1P₁ receptor (Figure 3B), implying that this could be a conserved binding pocket for long aliphatic chains in lipid-binding receptors. In regards to the nitrate group that has not been observed in the crystallographic structure, our docking experiments define a domain in which the nitrate group is interacting with residues Thr197^{3.33}, Tyr275^{5.39}, and Trp279^{5.43} through hydrogen bonding and π-π interactions (Figure S4A).

Finally, arm 3 extends toward a gap constituted by helices I, II, VII capped by the N-terminal loop (Figure 3B). It forms interactions with hydrophobic residues, Met103^{N-term}, Ile105^{N-term}, Ile119^{1.35}, Ser123^{1.39}, Phe170^{2.57}, Phe174^{2.61}, Ala380^{7.36}, Ser383^{7.39}, and Met384^{7.40} (Figure 3C). Unlike the π-π interactions formed by the other two arms, the interactions between arm 3 and the receptor are non-specific.

Among the interactions between AM6538 and CB₁, Phe170^{2.57} plays an important role by interacting with the pyrazole ring core, as well as rings in arm 1 and arm 3. Moreover, Phe170^{2.57} is pushed by the ligand to move toward helix I, resulting in a tilt of the last two turns (residues 170–177) of helix II toward helix I, compared to S1P₁ and LPA₁, the two closest homologs (Figures 4A and 4B). This tilted helix II, in turn, pushes

helix I by about 7 Å, mainly due to interactions with the two bulky residues Phe170^{2.57} and Phe174^{2.61}.

The role of Lys192^{3.28} in CB₁ has been intensively researched. It was reported that Lys192Ala/Lys192Gln/Lys192Glu mutants decreased the affinities of

several agonists such as CP55,940, HU-210, and anandamide (Chin et al., 1998; Hurst et al., 2002; Pan et al., 1998; Song and Bonner, 1996). Previously, it was suggested that Lys192^{3.28} has direct interactions with CB₁ ligands. However, in our CB₁ structure, Lys192^{3.28} does not interact directly with AM6538. Instead, it forms a salt bridge/hydrogen bond network that stabilizes the conformation of ECL1, the N terminus, and the extracellular parts of helices II and III. The side chain of Lys192^{3.28} points away from the binding pocket and forms salt bridges with Asp176^{2.63} and Asp184^{ECL1}, while Asp184^{ECL1} further stabilizes the N terminus by forming a hydrogen bond with the backbone of Phe102^{N-term} (Figure 4C).

Structural Comparison of the CB₁, LPA₁, and S1P₁ Receptors

CB₁, LPA₁, and S1P₁ receptors all bind lipid-derived endogenous ligands (anandamide/sn-2-arachidonoylglycerol, sphingosine-1-phosphate, lysophosphatidic acid) (Shimizu, 2009). Early sequence analysis revealed that CB₁ has a moderate sequence identity with LPA₁ (13% overall, 28% in TM regions) and S1P₁ (14% overall, 27% in TM regions) (Bramblett et al., 1995; Isberg et al., 2016) (Figure S5). Crystal structures of LPA₁ (Chrencik et al., 2015) and S1P₁ (Hanson et al., 2012) have been recently determined. The main structural difference between the three lipid receptors occurs in the extracellular portion, with the most striking being the unique conformation of the N-terminal loop of CB₁ (Figures 4A and 4B). For all three receptors, the N terminus has a role in ligand recognition. Comparing the ligand binding

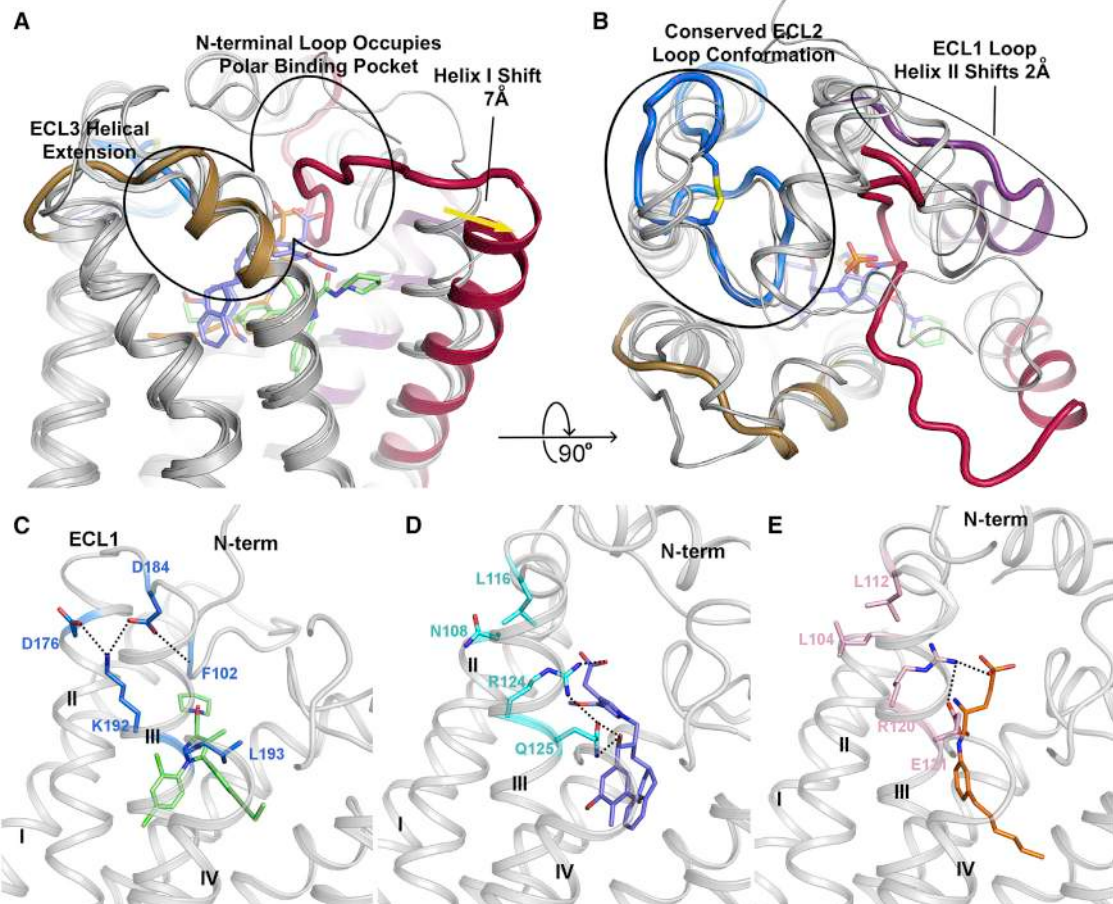


Figure 4. Comparison of CB₁, LPA₁, and S1P₁ Structural Features

(A) Side view of CB₁ with structurally divergent regions of LPA₁ (PDB: 4Z34) and S1P₁ (PDB: 3V2Y) overlaid. LPA₁ and S1P₁ receptors are shown in gray cartoons. The CB₁ N-terminal loop (red) occupies the polar binding pocket, helix I (red helix) is shifted out 7 Å compared with the other two receptors. ECL3 of CB₁ shows a three helical turn extension of helix VII (brown helix).

(B) 90° rotation of (A) for a top view of CB₁ with structurally divergent regions of LPA₁ (4Z34) and S1P₁ (3V2Y) overlaid. CB₁ shows a conserved conformation of ECL2 (blue) with the other two receptors, helix II is shifted out 2 Å (purple helix).

(C–E) The interaction network of position 3.28 of CB₁ (K192), LPA₁ (R124), and S1P₁ (R120). Polar interactions are represented by black dashed lines. (C) CB₁ is shown in gray cartoon, AM6538 is shown in green sticks and the key residues are shown in blue sticks; (D) LPA₁ is shown in gray cartoon, ONO-9780307 is shown in purple-blue sticks and the key residues are shown in cyan sticks; (E) S1P₁ is shown in gray cartoon, ML056 is shown in orange sticks and the key residues are shown in pink sticks.

See also Figure S5.

positions of the three receptors, AM6538 lies more horizontally than the ligands in LPA₁ and S1P₁, with arm 1 inserted deeper into the side pocket (Figure 4A). Consistently, the N-terminal loop in CB₁ is positioned deeper into the binding pocket compared to the N-terminal helices of LPA₁ and S1P₁, which are both positioned as a cap on their respective ligand binding pockets. As a consequence, helix I of CB₁ is pushed outward ~7 Å relative to LPA₁ and S1P₁ by arm 2, opening a wider gap between helices I and VII than what was observed in LPA₁ and S1P₁ (Figure 4A). Moreover, helix II and ECL1 change their conformation in CB₁, with helix II shifting 2 Å further from the binding pocket compared with LPA₁ and S1P₁, and ECL1 changing from a short helical region in LPA₁ and S1P₁ to a loop in CB₁ (Figure 4B). These conformational changes effectively enlarge the binding pocket of

CB₁, allowing access to the re-entrant N-terminal loop, and contribute to the extensive surface area and multiple subpockets associated with CB₁. Finally, the ECL3 region of CB₁ differs from that of its related receptors by a three helical turn extension of helix VII, which increases the rigidity and presumably decreases the flexibility of this loop region in CB₁ (Figure 4A).

The arrangement of Lys192^{3,28} in CB₁ is unique when compared with its equivalent residue Arg^{3,28} in LPA₁ and S1P₁. In LPA₁ and S1P₁, Arg^{3,28} points into the binding pocket forming a strong interaction with the phosphate head group of the ligands (Figures 4D and 4E); it is stabilized by the negatively charged or polar residue 3.29 (Gln125 in LPA₁ and Glu121 in S1P₁). However, in CB₁ the environment near Leu193^{3,29} and the ligand is hydrophobic, thus, it is energetically favorable for the positively

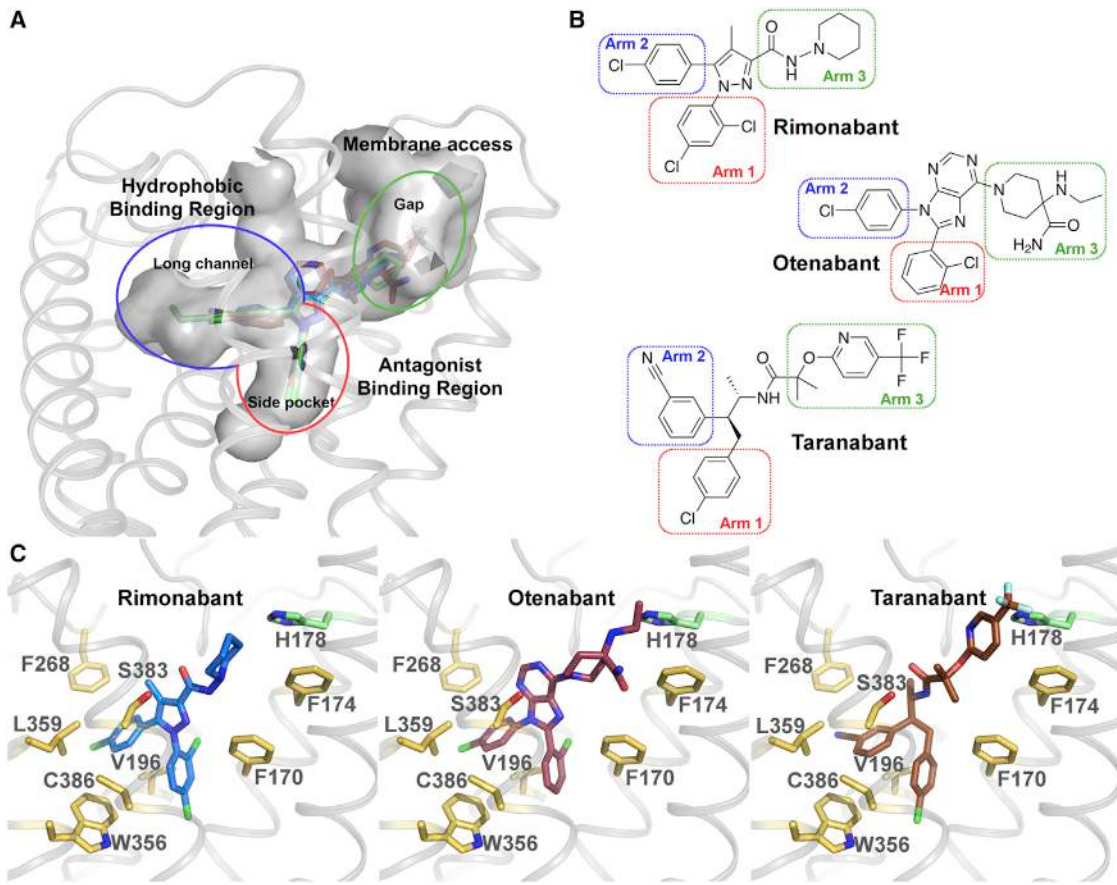


Figure 5. Docking of Different Antagonists in the CB₁ Crystal Structure

(A) CB₁ binding pocket with rimonabant (blue sticks), otenabant (raspberry sticks), and taranabant (brown sticks) are shown in gray surface representation. (B) Chemical structures of rimonabant, otenabant, and taranabant. The red/blue/green rectangles highlight previously described “arms” of the molecule termed arm 1/arm 2/arm 3 (see Figure 3C). (C) Predicted binding modes of rimonabant (blue sticks), otenabant (raspberry sticks), and taranabant (brown sticks) with CB₁. The interacting residues are shown in yellow sticks, and H178 is shown in green sticks.

See also Figure S4 and Table S2.

charged Lys192^{3,28} to point away from the binding pocket (Figure 4C). In fact, Lys192^{3,28} functions as a stabilization anchor by forming a salt bridge/hydrogen bond network instead of directly interacting with the ligand as Arg^{3,28} in LPA₁ and S1P₁. Another major difference of the endogenous ligands of CB₁, (anandamide, 2-AG), LPA₁ (LPA) and S1P₁ (S1P) is the head group. The heads of LPA₁ and S1P₁ ligands are negatively charged phosphate groups, while the heads of CB₁ ligands are neutral. In fact, phosphorylation of the head group of CB₁ ligands anandamide and 2-AG would transform them into ligands of LPA₁ (Chrencik et al., 2015).

Binding Modes of Representative Antagonists to CB₁

We performed docking of AM6538 and three CB₁ antagonists: rimonabant, otenabant, and taranabant (Figure 5, Table S2), which represent diverse scaffolds of CB₁ antagonists used in clinical trials. For each compound, the top one ranked pose was used for analysis. The docking pose of AM6538 reproduces the crystallographic pose (Figure S4A), with a root mean

square deviation (RMSD) of 0.55 Å. For the three antagonists, their first-ranked docking poses resemble that of AM6538 in the crystal structure, with three arms that fit into the three branches of the binding pocket, as described in the AM6538 binding mode (Figure 5A). As denoted for AM6538, the arms in the side pocket, long channel, and gap are termed arm 1, arm 2, and arm 3 (Figure 5B). The scaffolds of arm 1 and arm 2 of the three antagonists are very similar to each other, and so are the docking poses. The biggest difference is from arm 3, yet they are all quite bulky, which we speculate is the signature for CB₁ antagonists. Taranabant has the highest affinity with CB₁ among the three ligands (Table S2). It does not have a rigid aromatic ring at the core, allowing its arm 2 and arm 3 to have more freedom to form stronger interactions with surrounding residues (Figure 5C). Mutagenesis of Phe170^{2,57}Ala or Phe174^{2,61}Ala results in dramatically reduced functional affinity for rimonabant and AM6538, while neither mutation alters the potency of the agonist, CP55,940. More conservative mutations to tryptophan (Phe170^{2,57}Trp or Phe174^{2,61}Trp) at either site have no

appreciable effect on antagonist binding, further supporting the importance of the hydrophobic interactions at this site (Figures S4G and S4H). In addition, we performed 50 ns MD simulations to visually assess the predicted ligand-receptor interactions, starting from the docking poses. The RMSD values of AM6538, rimonabant, and otenabant are about 1.4 Å. For taranabant, the value is larger (about 3 Å), in accordance with its lack of the core aromatic ring (Figures S4C–S4F). The predicted interactions of the ligands are conserved during the short MD simulations. The central structure of AM6538 in MD simulation is closest to the docking pose.

Docking Poses of Representative Agonists of CB₁

Although the crystal structure we present is in the inactive state, we are able to investigate how representative agonists likely bind to the orthosteric pocket of CB₁ by integrating molecular docking, mutagenesis, and SAR data (Ahn et al., 2009; Aung et al., 2000; Bertalovitz et al., 2010). Six CB₁ agonists (Table S2)—the classical cannabinoids, THC and CP55,940; the endogenous agonists, anandamide and 2-AG; and indole derivatives, JWH-018 and WIN 55,212-2—were selected for docking studies. These agonists mainly interact with ECL2, N-terminal loop, helices III, VI, and VII, and they do not interact with helices I and II. Their predicted binding modes are shown in Figure 6. For THC and CP55,940, the rings reside between the N-terminal loop and ECL2, forming π-π interactions with Phe268^{ECL2} (Figures 6A and 6B), and the carbon chains extend into the long channel and interact with residues from helices III, VI, and VII. CP55,940 does not interact with helices I and II, which is supported by our mutagenesis studies: mutations on Phe170 and Phe174 (Phe170^{2.57}Ala/Trp or Phe174^{2.61}Ala/Trp) do not alter the potency of CP55,940 (Figure S4G). Anandamide and 2-AG were predicted to adopt a C-shaped conformation and occupy a similar space as THC (Figures 6C and 6D). Their hydrophilic heads are sandwiched between the N-terminal loop and ECL2, and their long aliphatic tails extend deeper into the long channel. JWH-018 and WIN 55,212-2, however, are predicted to bind deeper in the pocket than THC (Figures 6E and 6F). Both the indole rings and naphthalene rings form π-π interactions with Phe268^{ECL2}. The N-substituents reach the end of the long channel and interact with helix V. The binding mode of JWH-018 and WIN 55,212-2 is supported by mutations on helix V (McAllister et al., 2003; Song et al., 1999) and SAR study of N-alkyl chain length (Aung et al., 2000). Notably, all of the agonists interact with Phe268^{ECL2} and Phe379^{7.35} in our docking poses, which is consistent with mutagenesis studies on ECL2 (Ahn et al., 2009) and Phe379^{7.35} (Figure S4I). Any of the following individual mutations—Phe268^{ECL2}Trp, Pro269^{ECL2}Ala, His270^{ECL2}Ala, Ile271^{ECL2}Ala, or breaking of the disulfide bond Cys257-Cys264 on ECL2—dramatically decreased the binding of all three different types of agonists, yet had little impact on antagonist binding (Ahn et al., 2009). The prominent role of Phe379^{7.35} to facilitate CP55,940 functional affinity is supported by the loss of CP55,940 potency with the Phe379^{7.35} Trp mutation and an even greater loss of agonist activity with the Phe379^{7.35} Ala mutation (Figure S4I). While these mutations dramatically affected CP55,940 agonism, they had no impact on antagonist/inverse agonist (AM6538 or rimonabant) displacement of agonist (Figure S4J), further supporting the predicted binding pose of CP55,940 (Figure 6G).

DISCUSSION

The ligand used in this study, AM6538, was designed with the aim of stabilizing the ligand-CB₁ receptor complex and promoting CB₁ crystal formation. For this purpose, our approach focused on the use of the substituted diarylpyrazole chemotype based on the structure of rimonabant for obtaining highly utilized proprietary probes. Within this class of compounds, a slight modification of the chemotype led to AM251, a commonly used CB₁ inverse agonist/antagonist (Lan et al., 1999), and AM281, a CB₁ antagonist whose radiolabeling produced the first *in vivo* imaging agent for labeling CB₁ in nonhuman primates and humans (Berding et al., 2004; Gatley et al., 1998). AM6538 acts as a CB₁ stabilizing antagonist, and the ligand was effective in allowing structural determination of CB₁. AM6538 reacts as an intact molecule with no crystallographic evidence of covalent binding while at the same time not revealing the location of the terminal nitrate group in the X-ray structure. While radioligand binding studies demonstrate that AM6538 binds tightly to the receptor, the precise mode of action for stabilizing the receptor remains to be determined.

To date, there remains considerable controversy with regards to CB₁ ligands and their diverse medical applications. This is likely due in part to the wide availability and illicit nature of the most famous CB₁ pharmaceutical, marijuana. Marijuana has been widely used across many cultures to treat multiple conditions, with most of the results relayed via oral tradition, anecdote, political position, or with economic interest preventing an objective interpretation of therapeutic efficacy in any particular disease state (Whiting et al., 2015). The medicinal marijuana movement continues to gain support, and clinical trials with well-defined endpoints will continue to educate the medical and pharmaceutical communities regarding the relative benefits and drawbacks of targeting this physiological system. The crystal structure of CB₁ in complex with AM6538 reveals an expansive and complicated binding pocket network consisting of multiple sub-pockets and channels to various regions of the receptor. The three-arm ligand structure is common to CB₁ antagonists and inverse agonists and may be critical for stabilizing the inherent flexibility of the native receptor in a non-signaling conformation. Combining the 3D structure of CB₁ and molecular docking of the three representative antagonists, which act as inverse agonists, rimonabant, otenabant, and taranabant, the role of each arm is clearly illustrated. Arm 1 is crucial for high affinity binding, while arm 2 extends into the long channel. An aliphatic or aromatic ring on arm 3 pushes on helices I and II, causing them to bend outward, and potentially modulating the pharmacological signaling state of the receptor. Together with structure and modeling data, we speculate that a bulky ring on arm 3 is essential for CB₁ antagonism. This observation provides direction for designing more diverse compounds as we have learned that variable chemical groups are tolerated at the core of arm 3, a long carbon chain can be added at the *para*-position of the phenyl ring in arm 2. For example, introduction of a 4-cyanobut-1-ynyl at arm 2

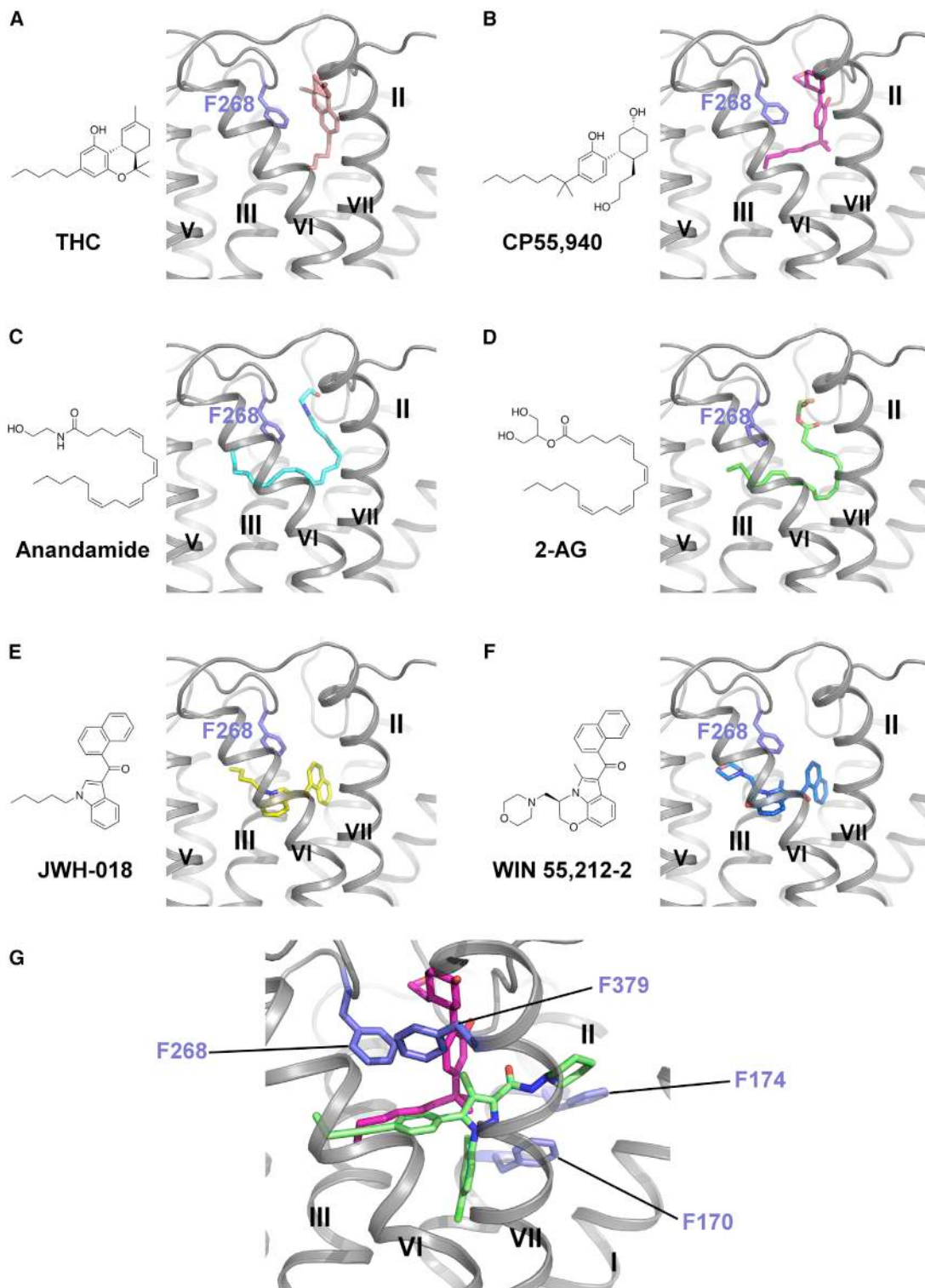


Figure 6. Docking Poses of Different Cannabinoid Receptor Agonists

(A–F) Chemical structures and predicted binding poses of THC (pink sticks) (A), CP55,940 (magenta sticks) (B), Anandamide (cyan sticks) (C), 2-AG (green sticks) (D), JWH-018 (yellow sticks) (E), and WIN 55,212-2 (blue sticks) (F).

(G) Zoom-in view of predicted CP55,940 binding pose. CP55,940 is shown in magenta sticks, AM6538 is shown in green sticks, and the key residues are shown in slate sticks.

See also Figure S4 and Table S2.

produces AM6545 (Table S2), a high-affinity CB₁ neutral antagonist (Tam et al., 2010).

Understanding the nuances of CB₁ binding and activation is important, as human use has noted differences between the phytocannabinoid agonist THC and the synthetic cannabinoid constituents of “Spice” or “K-2” such as JWH-018. In general, cannabinoid agonists are routinely abused substances; yet, while overdose of THC/marijuana has not been documented, there have been cases of severe and even deadly responses to the ingestion of such synthetic mixtures resulting in federal restrictions by many countries, including the US. It remains unclear as to why THC can have such a high safety margin, while the synthetic cannabinoid constituents can prove toxic with varying severities of serious side effects (Hermanns-Clausen et al., 2013). Going forward, the study of cannabinoids present in *Cannabis sativa* will provide clues to its high efficacy and safety margins and may continue to inspire a rich source of pharmacologically refined compounds and novel therapeutics; the utility of the crystal structure may provide inspiration for drug design toward refining efficacy and avoiding adverse events.

STAR METHODS

Detailed methods are provided in the online version of this paper and include the following:

- KEY RESOURCES TABLE
- CONTACT FOR REAGENT AND RESOURCE SHARING
- EXPERIMENTAL MODEL AND SUBJECT DETAILS
 - Mice
- METHOD DETAILS
 - Synthesis and Characterization of AM6538
 - Rational Design of Thermostabilizing Mutations of CB₁
 - Protein Engineering for Structure Determination
 - Protein Expression in Mammalian Expression System
 - Protein Purification
 - Lipidic Cubic Phase Crystallization of CB₁-AM6538 Complex
 - Data Collection and Structure Determination
 - Quantum Mechanical Optimization of AM6538
 - Docking Simulations of CB₁ Ligands
 - Molecular Dynamics Simulation of CB₁ in Complex with AM6538 and Representative Antagonists
 - Radioligand Binding Assay
 - WT and Mutant hCB₁-CHO Cell Line Generation for Functional Studies
 - Functional Analysis Studies
 - Protein Stability Assays
 - Affinity Mass Spectrometry Analysis of AM6538
- QUANTIFICATION AND STATISTICAL ANALYSIS
- DATA AND SOFTWARE AVAILABILITY
 - Data Resources

SUPPLEMENTAL INFORMATION

Supplemental Information includes five figures and two tables and can be found with this article online at <http://dx.doi.org/10.1016/j.cell.2016.10.004>.

AUTHOR CONTRIBUTIONS

Conceptualization, L.M.B., A.M., R.C.S., Z.-J.L.; Methodology, K.V., A.M. J.-H.H., R.B.L., E.L.S., B.W., Q.Z.; Validation, G.W.H.; Formal Analysis, T.H., M.P., L.Q., G.W.H., Y.W., S.Z., W.S., S.L., R.B.L., E.L.S., N.Z., B.W., Q.Z., M.A.H., L.M.B., A.M., Z.-J.L.; Investigation, T.H., K.V., L.Q., G.W.H., W.S., S.L., A.K., R.B.L., E.L.S., J.-H.H., N.Z., H.Z., I.K.; Writing – Original Draft, T.H.; Writing, Reviewing & Editing, T.H., K.V., Y.W., S.Z., W.S., I.K., M.A.H., L.M.B., A.M., R.C.S., Z.-J.L.; Visualization, T.H., M.P., M.A.H.; Supervision, L.M.B., A.M., R.C.S., Z.-J.L.

ACKNOWLEDGMENTS

This work was supported by the Ministry of Science and Technology of China grants 2014CB910400 and 2015CB910104 and The National Nature Science Foundation of China grant 31330019 to (Z.-J.L.); National Institutes of Health grants P01DA009158 (A.M. and L.M.B.), R37DA023142 (A.M.), and R01AI118985 (I.K.); and NSF grants. We thank the Shanghai Municipal Government, ShanghaiTech University, and GPCR Consortium for financial support. The synchrotron radiation experiments were performed at the BL41XU of Spring-8 with approval of the Japan Synchrotron Radiation Research Institute (JASRI) (proposal numbers 2015B1031 and 2016A2731), GM/CA@APS of Argonne National Lab, which is supported by the U.S. Department of Energy, Office of Science, Office of Basic Energy Sciences under contract number DE-AC02-06CH11357, and beamline BL17U1 (Shanghai Synchrotron Radiation Facility [SSRF]). We thank the Cloning, Cell Expression, and Protein Purification Core Facilities of iHuman Institute for their support. We thank A. Walker for assistance with the manuscript; we also thank F. Xu, V. Cherezov, V. Katritch, A. Ishchenko, H. Tao, J. Cheng, D. Liu, W. Zhong, and W. Liu for helpful discussions. The NIDA Drug supply program provided standards used in this study. A.M. is a founder of MAKScientific, LLC, a research company engaged in discovering medications for metabolic disorders with an interest in CB1. R.C.S. is a board member and shareholder with Birdrock Bio, an antibody therapeutic company with an interest in CB1.

Received: July 15, 2016

Revised: September 6, 2016

Accepted: October 3, 2016

Published: October 20, 2016

SUPPORTING CITATIONS

The following references appear in the Supplemental Information: Ben-Shabat et al., 1998; Felder et al., 1995; Fong et al., 2007; Griffith et al., 2009; Kuster et al., 1993; Showalter et al., 1996; Wiley et al., 1998.

REFERENCES

- Abagyan, R., and Totrov, M. (1994). Biased probability Monte Carlo conformational searches and electrostatic calculations for peptides and proteins. *J. Mol. Biol.* 235, 983–1002.
- Abraham, M.J., Murtola, T., Schulz, R., Páll, S., Smith, J.C., Hess, B., and Lindahl, E. (2015). GROMACS: High performance molecular simulations through multi-level parallelism from laptops to supercomputers. *SoftwareX* 1–2, 19–25.
- Adams, R., MacKenzie, S., Jr., and Loewe, S. (1948). Tetrahydrocannabinol homologs with double branched alkyl groups in the 3-position. *J. Am. Chem. Soc.* 70, 664–668.
- Adams, P.D., Afonine, P.V., Bunkóczki, G., Chen, V.B., Davis, I.W., Echols, N., Headd, J.J., Hung, L.W., Kapral, G.J., Grosse-Kunstleve, R.W., et al. (2010). PHENIX: a comprehensive Python-based system for macromolecular structure solution. *Acta Crystallogr. D Biol. Crystallogr.* 66, 213–221.
- Ahn, K.H., Bertalovitz, A.C., Mierke, D.F., and Kendall, D.A. (2009). Dual role of the second extracellular loop of the cannabinoid receptor 1: ligand binding and receptor localization. *Mol. Pharmacol.* 76, 833–842.

- Alexandrov, A.I., Mileni, M., Chien, E.Y., Hanson, M.A., and Stevens, R.C. (2008). Microscale fluorescent thermal stability assay for membrane proteins. *Structure* 16, 351–359.
- Andersson, H., D'Antona, A.M., Kendall, D.A., Von Heijne, G., and Chin, C.N. (2003). Membrane assembly of the cannabinoid receptor 1: impact of a long N-terminal tail. *Mol. Pharmacol.* 64, 570–577.
- Aung, M.M., Griffin, G., Huffman, J.W., Wu, M., Keel, C., Yang, B., Showalter, V.M., Abood, M.E., and Martin, B.R. (2000). Influence of the N-1 alkyl chain length of cannabimimetic indoles upon CB(1) and CB(2) receptor binding. *Drug Alcohol Depend.* 60, 133–140.
- Ballesteros, J.A., and Weinstein, H. (1995). Integrated methods for the construction of three-dimensional models and computational probing of structure-function relations in G protein-coupled receptors. In *Methods in Neurosciences*, C.S. Stuart, ed. (Academic Press), pp. 366–428.
- Ben-Shabat, S., Fride, E., Sheskin, T., Tamiri, T., Rhee, M.H., Vogel, Z., Bisogno, T., De Petrocellis, L., Di Marzo, V., and Mechoulam, R. (1998). An entourage effect: inactive endogenous fatty acid glycerol esters enhance 2-arachidonoyl-glycerol cannabinoid activity. *Eur. J. Pharmacol.* 353, 23–31.
- Berding, G., Müller-Vahl, K., Schneider, U., Gielow, P., Fitschen, J., Stuhrmann, M., Harke, H., Buchert, R., Donnerstag, F., Hofmann, M., et al. (2004). [123I]AM281 single-photon emission computed tomography imaging of central cannabinoid CB1 receptors before and after Delta9-tetrahydrocannabinol therapy and whole-body scanning for assessment of radiation dose in tourette patients. *Biol. Psychiatry* 55, 904–915.
- Bertalovitz, A.C., Ahn, K.H., and Kendall, D.A. (2010). Ligand Binding Sensitivity of the Extracellular Loop Two of the Cannabinoid Receptor 1. *Drug Dev. Res.* 71, 404–411.
- Black, M.D., Stevens, R.J., Rogacki, N., Featherstone, R.E., Senyah, Y., Giardino, O., Borowsky, B., Stummelin, J., Cohen, C., Pichat, P., et al. (2011). AVE1625, a cannabinoid CB1 receptor antagonist, as a co-treatment with antipsychotics for schizophrenia: improvement in cognitive function and reduction of antipsychotic-side effects in rodents. *Psychopharmacology (Berl.)* 215, 149–163.
- Bohn, L.M., Zhou, L., and Ho, J.H. (2015). Approaches to Assess Functional Selectivity in GPCRs: Evaluating G Protein Signaling in an Endogenous Environment. *Methods Mol. Biol.* 1335, 177–189.
- Bramblett, R.D., Panu, A.M., Ballesteros, J.A., and Reggio, P.H. (1995). Construction of a 3D model of the cannabinoid CB1 receptor: determination of helix ends and helix orientation. *Life Sci.* 56, 1971–1982.
- Caffrey, M., and Cherezov, V. (2009). Crystallizing membrane proteins using lipidic mesophases. *Nat. Protoc.* 4, 706–731.
- Cherezov, V., Hanson, M.A., Griffith, M.T., Hilgart, M.C., Sanishvili, R., Nagarajan, V., Stepanov, S., Fischetti, R.F., Kuhn, P., and Stevens, R.C. (2009). Rastering strategy for screening and centring of microcrystal samples of human membrane proteins with a sub-10 microm size X-ray synchrotron beam. *J. R. Soc. Interface* 6 (Suppl 5), S587–S597.
- Chin, C.N., Lucas-Lenard, J., Abadji, V., and Kendall, D.A. (1998). Ligand binding and modulation of cyclic AMP levels depend on the chemical nature of residue 192 of the human cannabinoid receptor 1. *J. Neurochem.* 70, 366–373.
- Chrencik, J.E., Roth, C.B., Terakado, M., Kurata, H., Omi, R., Kihara, Y., Warshawski, D., Nakade, S., Asmar-Rovira, G., Mileni, M., et al. (2015). Crystal Structure of Antagonist Bound Human Lysophosphatidic Acid Receptor 1. *Cell* 161, 1633–1643.
- Chun, E., Thompson, A.A., Liu, W., Roth, C.B., Griffith, M.T., Katritch, V., Kunken, J., Xu, F., Cherezov, V., Hanson, M.A., and Stevens, R.C. (2012). Fusion partner toolchest for the stabilization and crystallization of G protein-coupled receptors. *Structure* 20, 967–976.
- Collaborative Computational Project, Number 4 (1994). The CCP4 suite: programs for protein crystallography. *Acta Crystallogr. D Biol. Crystallogr.* 50, 760–763.
- Cravatt, B.F., and Lichtman, A.H. (2004). The endogenous cannabinoid system and its role in nociceptive behavior. *J. Neurobiol.* 61, 149–160.
- D'Antona, A.M., Ahn, K.H., and Kendall, D.A. (2006). Mutations of CB1 T210 produce active and inactive receptor forms: correlations with ligand affinity, receptor stability, and cellular localization. *Biochemistry* 45, 5606–5617.
- Devane, W.A., Dysarz, F.A., 3rd, Johnson, M.R., Melvin, L.S., and Howlett, A.C. (1988). Determination and characterization of a cannabinoid receptor in rat brain. *Mol. Pharmacol.* 34, 605–613.
- Devane, W.A., Hanus, L., Breuer, A., Pertwee, R.G., Stevenson, L.A., Griffin, G., Gibson, D., Mandelbaum, A., Etinger, A., and Mechoulam, R. (1992). Isolation and structure of a brain constituent that binds to the cannabinoid receptor. *Science* 258, 1946–1949.
- Emsley, P., Lohkamp, B., Scott, W.G., and Cowtan, K. (2010). Features and development of Coot. *Acta Crystallogr. D Biol. Crystallogr.* 66, 486–501.
- Fay, J.F., and Farrens, D.L. (2013). The membrane proximal region of the cannabinoid receptor CB1 N-terminus can allosterically modulate ligand affinity. *Biochemistry* 52, 8286–8294.
- Fay, J.F., Dunham, T.D., and Farrens, D.L. (2005). Cysteine residues in the human cannabinoid receptor: only C257 and C264 are required for a functional receptor, and steric bulk at C386 impairs antagonist SR141716A binding. *Biochemistry* 44, 8757–8769.
- Felder, E., and Schrott-Fischer, A. (1995). Quantitative evaluation of myelinated nerve fibres and hair cells in cochleae of humans with age-related high-tone hearing loss. *Hear. Res.* 91, 19–32.
- Felder, C.C., Joyce, K.E., Briley, E.M., Mansouri, J., Mackie, K., Blond, O., Lai, Y., Ma, A.L., and Mitchell, R.L. (1995). Comparison of the pharmacology and signal transduction of the human cannabinoid CB1 and CB2 receptors. *Mol. Pharmacol.* 48, 443–450.
- Feller, S.E., and MacKerell, A.D. (2000). An improved empirical potential energy function for molecular simulations of phospholipids. *J. Phys. Chem. B* 104, 7510–7515.
- Fernández-Ruiz, J., Romero, J., and Ramos, J.A. (2015). Endocannabinoids and Neurodegenerative Disorders: Parkinson's Disease, Huntington's Chorea, Alzheimer's Disease, and Others. *Handbook Exp. Pharmacol.* 231, 233–259.
- Fong, T.M., Guan, X.M., Marsh, D.J., Shen, C.P., Stribling, D.S., Rosko, K.M., Lao, J., Yu, H., Feng, Y., Xiao, J.C., et al. (2007). Antiobesity efficacy of a novel cannabinoid-1 receptor inverse agonist, N-[(1S,2S)-3-(4-chlorophenyl)-2-(3-cyanophenyl)-1-methylpropyl]-2-methyl-2-[[5-(trifluoromethyl)pyridin-2-yl]oxy]propanamide (MK-0364), in rodents. *J. Pharmacol. Exp. Ther.* 321, 1013–1022.
- Friesner, R.A., Banks, J.L., Murphy, R.B., Halgren, T.A., Klicic, J.J., Mainz, D.T., Repasky, M.P., Knoll, E.H., Shelley, M., Perry, J.K., et al. (2004). Glide: a new approach for rapid, accurate docking and scoring. 1. Method and assessment of docking accuracy. *J. Med. Chem.* 47, 1739–1749.
- Friesner, R.A., Murphy, R.B., Repasky, M.P., Frye, L.L., Greenwood, J.R., Halgren, T.A., Sanschagrin, P.C., and Mainz, D.T. (2006). Extra precision glide: docking and scoring incorporating a model of hydrophobic enclosure for protein-ligand complexes. *J. Med. Chem.* 49, 6177–6196.
- Gaoni, Y., and Mechoulam, R. (1964). Isolation, Structure, and Partial Synthesis of an Active Constituent of Hashish. *J. Am. Chem. Soc.* 86, 1646–1647.
- Gatley, S.J., Lan, R., Volkow, N.D., Pappas, N., King, P., Wong, C.T., Gifford, A.N., Pyatt, B., Dewey, S.L., and Makriyannis, A. (1998). Imaging the brain marijuana receptor: development of a radioligand that binds to cannabinoid CB1 receptors in vivo. *J. Neurochem.* 70, 417–423.
- Ghosh, R., Todd, A.R., and Wilkinson, S. (1940). 206. Cannabis indica. Part IV. The synthesis of some tetrahydrodibenzopyran derivatives. *J. Am. Chem. Soc.*, 1121–1125.
- Griffith, D.A., Hadcock, J.R., Black, S.C., Iredale, P.A., Carpino, P.A., DaSilva-Jardine, P., Day, R., DiBrino, J., Dow, R.L., Landis, M.S., et al. (2009). Discovery of 1-[9-(4-chlorophenyl)-8-(2-chlorophenyl)-9H-purin-6-yl]-4-ethylaminopiperidine-4-carboxylic acid amide hydrochloride (CP-945,598), a novel, potent, and selective cannabinoid type 1 receptor antagonist. *J. Med. Chem.* 52, 234–237.
- Guo, Y., Abadji, V., Morse, K.L., Fournier, D.J., Li, X., and Makriyannis, A. (1994). (-)-11-Hydroxy-7'-isothiocyanato-1',1'-dimethylheptyl-delta-8-THC: a

- novel, high-affinity irreversible probe for the cannabinoid receptor in the brain. *J. Med. Chem.* 37, 3867–3870.
- Halgren, T.A., Murphy, R.B., Friesner, R.A., Beard, H.S., Frye, L.L., Pollard, W.T., and Banks, J.L. (2004). Glide: a new approach for rapid, accurate docking and scoring. 2. Enrichment factors in database screening. *J. Med. Chem.* 47, 1750–1759.
- Hanson, M.A., Roth, C.B., Jo, E., Griffith, M.T., Scott, F.L., Reinhart, G., De-sale, H., Clemons, B., Cahalan, S.M., Schuerer, S.C., et al. (2012). Crystal structure of a lipid G protein-coupled receptor. *Science* 335, 851–855.
- Herkenham, M., Lynn, A.B., Little, M.D., Johnson, M.R., Melvin, L.S., de Costa, B.R., and Rice, K.C. (1990). Cannabinoid receptor localization in brain. *Proc. Natl. Acad. Sci. USA* 87, 1932–1936.
- Hermanns-Clausen, M., Kneisel, S., Szabo, B., and Auwärter, V. (2013). Acute toxicity due to the confirmed consumption of synthetic cannabinoids: clinical and laboratory findings. *Addiction* 108, 534–544.
- Howlett, A.C. (1985). Cannabinoid inhibition of adenylate cyclase. Biochemistry of the response in neuroblastoma cell membranes. *Mol. Pharmacol.* 27, 429–436.
- Hurst, D.P., Lynch, D.L., Barnett-Norris, J., Hyatt, S.M., Seltzman, H.H., Zhong, M., Song, Z.H., Nie, J., Lewis, D., and Reggio, P.H. (2002). N-(piperidin-1-yl)-5-(4-chlorophenyl)-1-(2,4-dichlorophenyl)-4-methyl-1H-pyrazole-3-carboxamide (SR141716A) interaction with LYS 3.28(192) is crucial for its inverse agonism at the cannabinoid CB1 receptor. *Mol. Pharmacol.* 62, 1274–1287.
- Isberg, V., Mordalski, S., Munk, C., Rataj, K., Harpsøe, K., Hauser, A.S., Vroeling, B., Bojarski, A.J., Vriend, G., and Gloriam, D.E. (2016). GPCRdb: an information system for G protein-coupled receptors. *Nucleic Acids Res.* 44 (D1), D356–D364.
- Janero, D.R., and Makriyannis, A. (2009). Cannabinoid receptor antagonists: pharmacological opportunities, clinical experience, and translational prognosis. *Expert Opin. Emerg. Drugs* 14, 43–65.
- Janero, D.R., Yaddanapudi, S., Zvonok, N., Subramanian, K.V., Shukla, V.G., Stahl, E., Zhou, L., Hurst, D., Wager-Miller, J., Bohn, L.M., et al. (2015). Molecular-interaction and signaling profiles of AM3677, a novel covalent agonist selective for the cannabinoid 1 receptor. *ACS Chem. Neurosci.* 6, 1400–1410.
- Jin, W., Brown, S., Roche, J.P., Hsieh, C., Celver, J.P., Kovoor, A., Chavkin, C., and Mackie, K. (1999). Distinct domains of the CB1 cannabinoid receptor mediate desensitization and internalization. *J. Neurosci.* 19, 3773–3780.
- Kabsch, W. (2010). Xds. *Acta Crystallogr. D Biol. Crystallogr.* 66, 125–132.
- Kandasamy, S.K., and Larson, R.G. (2006). Molecular dynamics simulations of model trans-membrane peptides in lipid bilayers: a systematic investigation of hydrophobic mismatch. *Biophys. J.* 90, 2326–2343.
- Katoh, K., and Standley, D.M. (2013). MAFFT multiple sequence alignment software version 7: improvements in performance and usability. *Mol. Biol. Evol.* 30, 772–780.
- Kuster, J.E., Stevenson, J.I., Ward, S.J., D'Ambra, T.E., and Haycock, D.A. (1993). Aminoalkylindole binding in rat cerebellum: selective displacement by natural and synthetic cannabinoids. *J. Pharmacol. Exp. Ther.* 264, 1352–1363.
- Lan, R., Liu, Q., Fan, P., Lin, S., Fernando, S.R., McCallion, D., Pertwee, R., and Makriyannis, A. (1999). Structure-activity relationships of pyrazole derivatives as cannabinoid receptor antagonists. *J. Med. Chem.* 42, 769–776.
- Lange, J.H., and Kruse, C.G. (2005). Keynote review: Medicinal chemistry strategies to CB1 cannabinoid receptor antagonists. *Drug Discov. Today* 10, 693–702.
- Lemberger, L. (1980). Potential therapeutic usefulness of marijuana. *Annu. Rev. Pharmacol. Toxicol.* 20, 151–172.
- Li, H.-L. (1973). An archaeological and historical account of cannabis in China. *Econ. Bot.* 28, 437–448.
- Li, C., Xu, W., Vadivel, S.K., Fan, P., and Makriyannis, A. (2005). High affinity electrophilic and photoactivatable covalent endocannabinoid probes for the CB1 receptor. *J. Med. Chem.* 48, 6423–6429.
- Lv, X., Liu, J., Shi, Q., Tan, Q., Wu, D., Skinner, J.J., Walker, A.L., Zhao, L., Gu, X., Chen, N., et al. (2016). In vitro expression and analysis of the 826 human G protein-coupled receptors. *Protein Cell* 7, 325–337.
- MacKerell, A.D., Bashford, D., Bellott, M., Dunbrack, R.L., Evanseck, J.D., Field, M.J., Fischer, S., Gao, J., Guo, H., Ha, S., et al. (1998). All-atom empirical potential for molecular modeling and dynamics studies of proteins. *J. Phys. Chem. B* 102, 3586–3616.
- Mackerell, A.D., Jr., Feig, M., and Brooks, C.L., 3rd. (2004). Extending the treatment of backbone energetics in protein force fields: limitations of gas-phase quantum mechanics in reproducing protein conformational distributions in molecular dynamics simulations. *J. Comput. Chem.* 25, 1400–1415.
- Makriyannis, A. (2014). 2012 Division of medicinal chemistry award address. Trekking the cannabinoid road: a personal perspective. *J. Med. Chem.* 57, 3891–3911.
- Makriyannis, A., and Rapaka, R.S. (1990). The molecular basis of cannabinoid activity. *Life Sci.* 47, 2173–2184.
- Makriyannis, A., and Vemuri, V.K. (April, 2016). Cannabinergic nitrate esters and related analogs. Patent Application US 2016/0096822 A1.
- Mallat, A., Teixeira-Clerc, F., and Lotersztajn, S. (2013). Cannabinoid signaling and liver therapeutics. *J. Hepatol.* 59, 891–896.
- Matsuda, L.A., Lolait, S.J., Brownstein, M.J., Young, A.C., and Bonner, T.I. (1990). Structure of a cannabinoid receptor and functional expression of the cloned cDNA. *Nature* 346, 561–564.
- Mavromoustakos, T., Yang, D.P., and Makriyannis, A. (1995). Small angle X-ray diffraction and differential scanning calorimetric studies on O-methyl-(--) δ -tetrahydrocannabinol and its 5' iodinated derivative in membrane bilayers. *Biochim. Biophys. Acta* 1237, 183–188.
- Mazier, W., Saucisse, N., Gatta-Cherifi, B., and Cota, D. (2015). The Endocannabinoid System: Pivotal Orchestrator of Obesity and Metabolic Disease. *Trends Endocrinol. Metab.* 26, 524–537.
- McAllister, S.D., Rizvi, G., Anavi-Goffer, S., Hurst, D.P., Barnett-Norris, J., Lynch, D.L., Reggio, P.H., and Abood, M.E. (2003). An aromatic microdomain at the cannabinoid CB(1) receptor constitutes an agonist/inverse agonist binding region. *J. Med. Chem.* 46, 5139–5152.
- McCoy, A.J., Grosse-Kunstleve, R.W., Adams, P.D., Winn, M.D., Storoni, L.C., and Read, R.J. (2007). Phaser crystallographic software. *J. Appl. Cryst.* 40, 658–674.
- Mechoulam, R., Ben-Shabat, S., Hanus, L., Ligumsky, M., Kaminski, N.E., Schatz, A.R., Gopher, A., Almog, S., Martin, B.R., Compton, D.R., et al. (1995). Identification of an endogenous 2-monoglyceride, present in canine gut, that binds to cannabinoid receptors. *Biochem. Pharmacol.* 50, 83–90.
- Mercier, R.W., Pei, Y., Pandarinathan, L., Janero, D.R., Zhang, J., and Makriyannis, A. (2010). hCB2 ligand-interaction landscape: cysteine residues critical to diarylpypyrazole antagonist binding motif and receptor modulation. *Chem. Biol.* 17, 1132–1142.
- Munro, S., Thomas, K.L., and Abu-Shaar, M. (1993). Molecular characterization of a peripheral receptor for cannabinoids. *Nature* 365, 61–65.
- Pan, X., Ikeda, S.R., and Lewis, D.L. (1998). SR 141716A acts as an inverse agonist to increase neuronal voltage-dependent Ca²⁺ currents by reversal of tonic CB1 cannabinoid receptor activity. *Mol. Pharmacol.* 54, 1064–1072.
- Pattison, F.L.M., and Brown, G.M. (1956). Organic Nitrates As Synthetic Intermediates: Preparations Of Nitrates And Some Representative Reactions. *Can. J. Chem.* 34, 879–884.
- Pertwee, R.G. (2002). Cannabinoids and multiple sclerosis. *Pharmacol. Ther.* 95, 165–174.
- Picone, R.P., Khanolkar, A.D., Xu, W., Ayotte, L.A., Thakur, G.A., Hurst, D.P., Abood, M.E., Reggio, P.H., Fournier, D.J., and Makriyannis, A. (2005). (--)-7'-Isothiocyanato-11-hydroxy-1',1'-dimethylheptyhexahydrocannabinol (AM841), a high-affinity electrophilic ligand, interacts covalently with a cysteine in helix six and activates the CB1 cannabinoid receptor. *Mol. Pharmacol.* 68, 1623–1635.
- Pryce, G., and Baker, D. (2015). Endocannabinoids in Multiple Sclerosis and Amyotrophic Lateral Sclerosis. *Handbook Exp. Pharmacol.* 231, 213–231.

- Razdan, R.K. (1986). Structure-activity relationships in cannabinoids. *Pharmacol. Rev.* **38**, 75–149.
- Rinaldi-Carmona, M., Barth, F., Héaulme, M., Shire, D., Calandra, B., Congy, C., Martinez, S., Maruani, J., Nélat, G., Caput, D., et al. (1994). SR141716A, a potent and selective antagonist of the brain cannabinoid receptor. *FEBS Lett.* **350**, 240–244.
- Robert, X., and Gouet, P. (2014). Deciphering key features in protein structures with the new ENDscript server. *Nucleic Acids Res.* **42**, W320–W324.
- Rubino, T., Zamberletti, E., and Parolaro, D. (2015). Endocannabinoids and Mental Disorders. *Handbook Exp. Pharmacol.* **231**, 261–283.
- Schindler, C.W., Redhi, G.H., Vemuri, K., Makriyannis, A., Le Foll, B., Bergman, J., Goldberg, S.R., and Justinova, Z. (2016). Blockade of Nicotine and Cannabinoid Reinforcement and Relapse by a Cannabinoid CB1-Receptor Neutral Antagonist AM4113 and Inverse Agonist Rimonabant in Squirrel Monkeys. *Neuropsychopharmacology* **41**, 2283–2293.
- Schrödinger (2015a). Glide, version 6.9 (Schrödinger, LLC).
- Schrödinger (2015b). Induced Fit Docking Protocol 2015-4, Glide version 6.4, Prime version 3.7 (Schrödinger, LLC).
- Sherman, W., Day, T., Jacobson, M.P., Friesner, R.A., and Farid, R. (2006). Novel procedure for modeling ligand/receptor induced fit effects. *J. Med. Chem.* **49**, 534–553.
- Shimizu, T. (2009). Lipid mediators in health and disease: enzymes and receptors as therapeutic targets for the regulation of immunity and inflammation. *Annu. Rev. Pharmacol. Toxicol.* **49**, 123–150.
- Showalter, V.M., Compton, D.R., Martin, B.R., and Abood, M.E. (1996). Evaluation of binding in a transfected cell line expressing a peripheral cannabinoid receptor (CB2): identification of cannabinoid receptor subtype selective ligands. *J. Pharmacol. Exp. Ther.* **278**, 989–999.
- Smart, O.S., Womack, T.O., Flensburg, C., Keller, P., Paciorek, W., Sharff, A., Vonrhein, C., and Brügge, G. (2012). Exploiting structure similarity in refinement: automated NCS and target-structure restraints in BUSTER. *Acta Crystallogr. D Biol. Crystallogr.* **68**, 368–380.
- Song, Z.H., and Bonner, T.I. (1996). A lysine residue of the cannabinoid receptor is critical for receptor recognition by several agonists but not WIN55212-2. *Mol. Pharmacol.* **49**, 891–896.
- Song, Z.H., Slowey, C.A., Hurst, D.P., and Reggio, P.H. (1999). The difference between the CB(1) and CB(2) cannabinoid receptors at position 5.46 is crucial for the selectivity of WIN55212-2 for CB(2). *Mol. Pharmacol.* **56**, 834–840.
- Szymanski, D.W., Papanastasiou, M., Melchior, K., Zvonok, N., Mercier, R.W., Janero, D.R., Thakur, G.A., Cha, S., Wu, B., Karger, B., and Makriyannis, A. (2011). Mass spectrometry-based proteomics of human cannabinoid receptor 2: covalent cysteine 6.47(257)-ligand interaction affording megagonist receptor activation. *J. Proteome Res.* **10**, 4789–4798.
- Tam, J., Vemuri, V.K., Liu, J., Bátka, S., Mukhopadhyay, B., Godlewski, G., Osei-Hyiaman, D., Ohnuma, S., Ambudkar, S.V., Pickel, J., et al. (2010). Peripheral CB1 cannabinoid receptor blockade improves cardiometabolic risk in mouse models of obesity. *J. Clin. Invest.* **120**, 2953–2966.
- Tang, W., and Prusov, E.V. (2012). Total synthesis of RNA-polymerase inhibitor ripostatin B and 15-deoxyripostatin A. *Angew. Chem. Int. Ed. Engl.* **51**, 3401–3404.
- Whiting, P.F., Wolff, R.F., Deshpande, S., Di Nisio, M., Duffy, S., Hernandez, A.V., Keurentjes, J.C., Lang, S., Misso, K., Ryder, S., et al. (2015). Cannabinoids for Medical Use: A Systematic Review and Meta-analysis. *JAMA* **313**, 2456–2473.
- Wiley, J.L., Compton, D.R., Dai, D., Lainton, J.A., Phillips, M., Huffman, J.W., and Martin, B.R. (1998). Structure-activity relationships of indole- and pyrrole-derived cannabinoids. *J. Pharmacol. Exp. Ther.* **285**, 995–1004.
- Wollner, H.J., Matchett, J.R., Levine, J., and Loewe, S. (1942). Isolation of a Physiologically Active Tetrahydrocannabinol from Cannabis Sativa Resin. *J. Am. Chem. Soc.* **64**, 26–29.
- Yeates, R.A., Laufen, H., and Leitold, M. (1985). The reaction between organic nitrates and sulphydryl compounds. A possible model system for the activation of organic nitrates. *Mol. Pharmacol.* **28**, 555–559.
- Zoete, V., Cuendet, M.A., Grosdidier, A., and Michelin, O. (2011). SwissParam: a fast force field generation tool for small organic molecules. *J. Comput. Chem.* **32**, 2359–2368.

STAR★METHODS

KEY RESOURCES TABLE

REAGENT or RESOURCE	SOURCE	IDENTIFIER
Antibodies		
HA Epitope Tag Antibody, Alexa Fluor 488 conjugate (16B12)	Thermo Fisher Scientific Inc.	Cat#A-21287; RRID: AB_2535829
Chemicals, Peptides, and Recombinant Proteins		
Polyethylenimine (PEI)	Polysciences	Cat#23966-2
EDTA-free complete protease inhibitor cocktail tablets	Roche	Cat#5056489001
Iodoacetamide	Sigma	Cat#I1149
n-dodecyl-beta-D-maltopyranoside (DDM)	Anatrace	Cat#D310
Cholesterol hemisuccinate (CHS)	Sigma	Cat#C6512
N-[4-(7-diethylamino-4-methyl-3-coumarinyl)phenyl]maleimide (CPM)	Invitrogen	Cat#D10251
TALON IMAC resin	Clontech	Cat#635507
1-Oleoyl-rac-glycerol (monoolein)	Sigma	Cat#M7765
Cholesterol	Sigma	Cat#C8667
CP55,940	Tocris	Cat#0949
SR141716A (Rimonabant)	Tocris	Cat#0923
[³ H]-CP 55,940	NIDA Drug Supply Program	NOCD-092
[³ H]-SR141716A	NIDA Drug Supply Program	NOCD-083
4'-Bromopropiophenone	Aldrich	B79706
2,4-Dichlorophenylhydrazine hydrochloride	Fisher Scientific/Acros	AC166740250
1-Aminopiperidine	Aldrich	A75900
But-3-yn-1-ol	Aldrich	130850
Hünig's base	Aldrich	D125806
Tetrakis(triphenylphosphine)palladium(0)	TCI Chemicals/Aldrich	T1350/216666
Copper(I) iodide	Aldrich	215554
Sodium iodide	Aldrich	383112
Tetrabutylammonium iodide	Aldrich	140775
Silver nitrate	Aldrich	209139
THC	Sigma	Cat#T-005-1ML
[³⁵ S]-GTPγS	PerkinElmer	Cat#NEG030H250UC
Critical Commercial Assays		
HTRF HiRange cAMP Assay Kit	CISBIO	Cat# 62AM6PEC
PathHunter Detection Kit	DiscoveRx	Cat#93-0001
Q5 site directed mutagenesis kit	NEB	Cat#E0554S
Deposited Data		
CB1_AM6538 complex structure	This paper	PDB: 5TGZ
Experimental Models: Cell Lines		
Freestyle 293-F cells	Invitrogen	Cat#R790-07
Phoenix-AMPHO	Allele Biotechnology	Cat#ABP-RCV-10001
CHO-K1	ATCC	CCL-61
CHO-hCB1R PathHunter DiscoveRx	DiscoveRx	Cat#93-0959C2
Experimental Models: Organisms/Strains		
Mice/ C57BL/6J	Jackson Labs	000664
Recombinant DNA		
Human CB ₁ gene	GenScript	N/A
pMSCVpuro vector	Clontech	Cat#634401

(Continued on next page)

Continued

REAGENT or RESOURCE	SOURCE	IDENTIFIER
pcDNA 3.1 (+) vector	Thermo Scientific	V79020
3HA-human CB1 receptor cDNA	Missouri S&T cDNA Resource Center	Cat#CNR010TN01
Sequence-Based Reagents		
Primers for site-direct mutagenesis	This Paper	N/A
F170W_forward:GTGTCATTGG GTCTACAGC	This Paper	N/A
F170A_forward:GTGTCATTGCT GTCTACAGC	This Paper	N/A
F170_reverse:TCCCCAGGAGGTCTG	This Paper	N/A
F174W_forward:CTACAGCTGG ATTGACTTCA	This Paper	N/A
F170A_forward:CTACAGCGCC ATTGACTTC	This Paper	N/A
F174_reverse:ACAAAAATGACACTCCCCAG	This Paper	N/A
F379A_forward:GTGGCTGCATTCTGCAGT	This Paper	N/A
F379W_forward:GTGTGGGCATTCTGCAGT	This Paper	N/A
F379_reverse:CGTCTTAATGAGCTTGTTCATC	This Paper	N/A
Primers for cloning WT CB ₁ to the modified pTT5 vector	This Paper	N/A
pTT5_forward:CTGTATTTCAAGGGCGGCCGCGTCCCT GCCGACCAGGTAACATT	This Paper	N/A
pTT5_reverse:GTGGTGATGGTGGTGATGGTGGTGGGAGGG GAACATGCTCGGAAAGC	This Paper	N/A
Software and Algorithms		
Schrödinger Suite 2015-4	Schrödinger	https://www.schrodinger.com
GROMACS 5.1.2	Abraham et al., 2015	https://www.gromacs.org
SwissParam	Zoete et al., 2011	www.swissparam.ch
XDS	Kabsch, 2010	Xds.mpimf-heidelberg.mpg.de
SCALA	Collaborative Computational Project, Number 4, 1994	www.ccp4.ac.uk/html/scala.html
Phaser	McCoy et al., 2007	https://www.phenix-online.org
Phenix	Adams et al., 2010	https://www.phenix-online.org
Buster	Smart et al., 2012	https://www.globalphasing.com/buster
COOT	Emsley et al., 2010	www.mrc-lmb.cam.ac.uk/personal/pemsley/coot
Prism v.6.0	GraphPad Software Inc.	N/A
Jaguar 9.0	Schrödinger	www.schrodinger.com
ICM	Abagyan and Totrov, 1994	www.molsoft.com
Other		
Solid white 384-well assay plates	VWR	Cat#82051-278 (CS)
Low-volume (20 µL) 384-well assay plates	VWR	Cat#784080
DMEM/F-12 (1:1) cell culture media	Invitrogen	Cat#11330-057
Opti-MEM cell culture media	Invitrogen	Cat#11058-021
FreeStyle 293 Expression Medium	Life Technologies	Cat#12338-026
Phoenix package system	Stanford University	N/A
Penicillin/Streptomycin	Invitrogen	Cat#15140-122
Puromycin	Invitrogen	Cat#A11138-03
Hygromycin B	Life Technologies	Cat#10687-010
Geneticin	Life Technologies	Cat#10131-035
100kDa cutoff concentrators	Sartorius	Cat#VS0642
PD Minitrap G-25 column	GE Healthcare	Cat#28-9180-07
96-well glass sandwich plates for LCP crystallization	NOVA	Cat#NOA90020
Lipofectamine 2000	Thermo Scientific	11668027

CONTACT FOR REAGENT AND RESOURCE SHARING

Further information and requests for reagents may be directed to, and will be fulfilled by the corresponding author Raymond C. Stevens (stevens@shanghaitech.edu.cn).

EXPERIMENTAL MODEL AND SUBJECT DETAILS

Mice

Experimentally naive mice (C57BL/6J) were purchased from Jackson Labs at 9 weeks of age and were housed in groups of five per cage in a specific-pathogen free facility, under a 12-h light-dark cycle with food and water ad libitum. At ~16 weeks of age, mice were euthanized by cervical dislocation prior to cerebellum dissection. A total of four mice were used to generate 4 independent experiments for assessing [³⁵S]GTP γ S binding. All experiments were performed with the approval of the Institutional Animal Care and Use Committee of The Scripps Research Institute, Jupiter, FL and in accordance to NIH guidelines.

METHOD DETAILS

Synthesis and Characterization of AM6538

All reagents and solvents used for chemical synthesis were purchased from Sigma-Aldrich, TCI Chemicals, Fisher Scientific, Acros or Alfa Aesar. The palladium catalysts were purchased from Sigma-Aldrich or TCI Chemicals. ¹H NMR (500 MHz) and ¹³C spectra (125 MHz) were recorded on a Varian Inova spectrometer. Chemical shifts (δ) are reported in parts per million and are referenced to CDCl₃ for 7.26 or 77.7. Multiplicities are indicated as br (broadened), s (singlet), d (doublet), t (triplet) or m (multiplet). Coupling constants (J) are reported in hertz (Hz). Thin layer chromatography (TLC) was performed on Merck-Millipore 210 - 270 μ m TLC silica gel plates, (60 \AA) and coated with a F₂₅₄ fluorescent indicator. Flash column chromatography was performed on a Biotage Isolera Spektra system with UV collections at 254 and 280 nm using Luknova flash columns preloaded with normal phase silica gel (50 μ m). All moisture sensitive reactions were performed under an atmosphere of high-purity argon while using oven-dried glassware. The intermediates and final compounds were characterized using a combination of ¹H NMR, ¹³C NMR and LC/MS techniques. The LC/MS analysis was performed using a Waters MicroMass ZQ system (electrospray ionization mode) equipped with a Waters 2525 binary gradient module, a Waters 2996 photodiode array detector, a Waters 2424 ELS detector, two Waters 515 HPLC pump, a fluidics organizer and a pump control module II. Compounds were analyzed with gradient elution using acetonitrile/water as the mobile phase and an XTerra MS C18 or an XTerra MS C8, 4.6 mm \times 50 mm column (5 μ m). Melting-points were recorded on a Fisher Scientific apparatus. IR spectra were obtained on a PerkinElmer Spectrum One FT-IR spectrometer. Elemental analyses were performed using a PerkinElmer Series II 2400 CHNS analyzer.

4-(4-(1-(2,4-dichlorophenyl)-4-methyl-3-(piperidin-1-ylcarbamoyl)-1H-pyrazol-5-yl)phenyl)but-3-yn-1-yl methanesulfonate (2)

To a stirred solution of 1-(2,4-dichlorophenyl)-5-(4-iodophenyl)-4-methyl-N-(piperidin-1-yl)-1H-pyrazole-3-carboxamide ([Lan et al., 1999](#)) (1, 1.1 g, 2 mmol) in DMF (30 ml), under argon was added but-3-yn-1-yl methanesulfonate ([Tang and Prusov, 2012](#)) (888 mg, 6 mmol), and Hünig's base (1.9 mL 20 mmol). The reaction mixture was degassed by introducing a steady stream of argon into the solution for 5 min and to this was added tetrakis(triphenylphosphine)palladium (0) (231 mg, 10 mol%) and CuI (76 mg, 20 mol%). The resulting mixture was stirred for 3 hr at room temperature. The solvent from the reaction mixture was removed *in vacuo* at 70°C and the residue was dissolved in dichloromethane (100 ml) and washed with deionized water (2 \times ~50 mL). The organic layer was separated, dried over anhydrous MgSO₄, filtered and the filtrate was removed *in vacuo*. The residue obtained was purified by flash column chromatography on silica gel (*n*-hexane/AcOEt = 1/1) to provide **2** as a white solid (511 mg, 45%); m.p 176-178°C; ¹H NMR (500 MHz, CDCl₃-d) δ 7.64 (br. s., 1H, NH), 7.41 (d, J = 1.46 Hz, 1H, ArH), 7.34 (d, J = 8.30 Hz, 2H, ArH), 7.25 - 7.31 (m, 2H, ArH), 7.05 (d, J = 8.30 Hz, 2H, ArH), 4.37 (t, J = 6.84 Hz, 2H, -O-CH₂-), 3.07 (s, 3H, -S(O)₂-CH₃), 2.79 - 2.97 (m, 6H, -CH₂-CH₂- and -N(CH₂CH₂)₂CH₂, 2.37 (s, 3H, HetAr-CH₃), 1.75 (m, 4H, -N(CH₂CH₂)₂CH₂, 1.43 (br. s., 2H, -N(CH₂CH₂)₂CH₂; ¹³C NMR (125 MHz, CDCl₃-d) δ 160.2, 144.7, 143.6, 136.2, 136.1, 133.2, 132.0, 130.8, 130.5, 129.7, 128.8, 128.1, 123.5, 118.5, 85.8, 82.5, 67.4, 57.3, 38.0, 25.7, 23.6, 21.0, 9.6; ES m/z 575.1710 (M⁺+H).

1-(2,4-dichlorophenyl)-5-(4-(4-iodobut-1-ynyl)phenyl)-4-methyl-N-(piperidin-1-yl)-1H-pyrazole-3-carboxamide (3).

To a stirred solution of **2** (500 mg, 0.86 mmol) in anhydrous acetone (50 ml), under argon was added sodium iodide (1.3 g, 8.6 mmol) and tetrabutylammonium iodide (64 mg, 0.17 mmol). The resulting reaction mixture was refluxed overnight. The solvent from the reaction mixture was removed *in vacuo* and the residue was dissolved in dichloromethane (75 ml) and washed with deionized water (2 \times ~50 mL). The organic layer was separated, dried over anhydrous MgSO₄, filtered and the filtrate was removed *in vacuo*. The residue obtained was purified by flash column chromatography on silica gel (*n*-hexane/AcOEt = 7/3) to provide **3** as a white solid (326 mg, 62%); m.p 171-173°C; ¹H NMR (500 MHz, CDCl₃-d) δ 7.65 (s, 1H, NH), 7.43 (d, J = 1.47 Hz, 1H, ArH), 7.38 (d, J = 7.81 Hz, 2H, ArH), 7.27 - 7.33 (m, 2H, ArH), 7.07 (d, J = 8.30 Hz, 2H, ArH), 3.31 (t, J = 7.32 Hz, 2H, I-CH₂), 3.01 (t, J = 7.32 Hz, 2H, -CH₂-CH₂), 2.88 (m, 4H, -N(CH₂CH₂)₂CH₂, 2.39 (s, 3H, HetAr-CH₃), 1.68 - 1.87 (m, 4H, -N(CH₂CH₂)₂CH₂, 1.45 (m, 2H, -N(CH₂CH₂)₂CH₂; ¹³C NMR (125 MHz, CDCl₃-d) δ 160.2, 144.7, 143.7, 136.3, 136.1, 133.2, 132.0, 130.8, 130.6, 129.6,

128.6, 128.1, 123.9, 118.5, 90.3, 81.9, 57.3, 25.7, 24.8, 23.6, 9.6, 1.6; IR (neat) 3308, 2929, 2851, 2787, 2509, 2160, 2031, 1689, 1524, 1486, 1245, 967, 967, 842, 781 cm⁻¹; ES m/z 607.1102 (M⁺+H).

4-(4-(1-(2,4-dichlorophenyl)-4-methyl-3-(piperidin-1-ylcarbamoyl)-1*H*-pyrazol-5-yl)phenyl)but-3-yn-1-yl nitrate (4**, **AM6538**).**

To a stirred solution of **3** (300 mg, 0.5 mmol) taken in anhydrous acetonitrile (30 ml), under argon was added silver nitrate (100 mg, 0.6 mmol). The resulting reaction mixture was heated to 70°C for 1 hr. The contents were cooled to room temperature and the solids were filtered over a celite pad. The filtrate was removed *in vacuo* and the residue was dissolved in dichloromethane (75 ml) and washed with deionized water (2 × ~50 mL). The organic layer was separated, dried over anhydrous MgSO₄, filtered and the filtrate was removed *in vacuo*. The residue obtained was purified by flash column chromatography on silica gel (*n*-hexane/AcOEt = 6/4) to provide **4** (**AM6538**) (Makriyannis and Vemuri, 2016) as a white solid (173 mg, 65%); m.p 178–180°C; ¹H NMR (500 MHz, CDCl₃-d) δ 7.63 (s, 1H, NH), 7.41 (d, J = 1.95 Hz, 1H, ArH), 7.34 (d, J = 8.30 Hz, 2H, ArH), 7.24 - 7.32 (m, 2H, ArH), 7.05 (d, J = 8.30 Hz, 2H, ArH), 4.62 (t, J = 6.59 Hz, 2H, -O-CH₂), 2.81 - 2.91 (m, 6H, -CH₂-CH₂ and -N(CH₂CH₂)₂CH₂), 2.37 (s, 3H, HetAr-CH₃), 1.75 (m, 4H, -N(CH₂-CH₂)₂CH₂, 1.43 (m, 2H, -N(CH₂CH₂)₂CH₂; ¹³C NMR (125 MHz, CDCl₃-d) δ 160.2, 144.7, 143.6, 136.2, 136.1, 133.2, 132.0, 130.8, 130.5, 129.7, 128.8, 128.1, 123.5, 118.5, 85.3, 82.4, 70.4, 57.3, 25.7, 23.6, 18.9, 9.6; IR (neat) 3319, 2935, 2857, 2811, 2502, 2160, 2031, 1976, 1682, 1616, 1528, 1488, 1277, 968, 881, 824, 781 cm⁻¹; ES m/z 542.1627 (M⁺+H); Elemental analysis calculated for C₂₆H₂₅Cl₂N₅O₄: C% 57.57, H% 4.65, N% 12.91; found: C% 57.34, H% 4.46, N% 12.74.

Rational Design of Thermostabilizing Mutations of CB₁

To improve general stability and homogeneity of the detergent-stabilized CB₁, mutations were rationally designed. A 3D homology model of human CB₁ was constructed and refined with ICM (Abagyan and Totrov, 1994) using the X-ray structure of sphingosine 1-phosphate receptor 1 (S1P₁ receptor, PDB: 3V2W) (Hanson et al., 2012) as a template. Best scoring substitutions were visually inspected and evaluated from the evolutionary conservation perspective resulting in a list of proposed substitutions. The predicted substitutions were analyzed for improvement of the receptor monodispersity (as evidenced by SEC traces) and thermal stability (as evidenced by increase in T_m in the CPM assay (Alexandrov et al., 2008).

Protein Engineering for Structure Determination

The sequence of the human CB₁ gene was synthesized by GenScript. The Flavodoxin (PDB: 1I1O, MW 14.9kDa, with Y98W mutation) fusion protein was fused to the third intracellular loop of the human CB₁ gene, using overlapping PCR. The construct has truncations of the CB₁ residues 1-98, 307-331 and 415-472. The resulting CB₁-Flavodoxin chimera sequence was subcloned into a modified mammalian expression pTT5 vector, which contains a haemagglutinin (HA) signal sequence, a FLAG tag and 10 × His tag, followed by a tobacco etch virus (TEV) protease cleavage site, before the N terminus of the chimera sequence. The CB₁ gene was further modified by introducing four rationally designed mutations, Thr210^{3,46}Ala (D'Antona et al., 2006), Glu273^{5,37}Lys, Thr283^{5,47}Val and Arg340^{6,32}Glu, using standard QuickChange PCR.

Protein Expression in Mammalian Expression System

HEK293F cells (Invitrogen) were grown in suspension starting from the densities at 0.2–0.3 × 10⁶ in a humidified incubator with 5% CO₂ at 37°C with a shake speed of 130rpm. Passage cells when the cell density reaches to 1.6–1.8 × 10⁶ cells/ml, about every 2–3 days. CB₁-Flavodoxin construct was transfected and expressed in HEK293F cells (Invitrogen) (Passage number is 12–20) using the FreeStyle™ 293 Expression system (Invitrogen). Briefly, HEK293F cells were seeded on day 0 at 6 × 10⁵ cells/ml in freeStyle 293 expression medium (Invitrogen). On day 2 the transduction was performed at a cell density of 1.0 to 1.2 × 10⁶ cells/ml and the cell viability over 95% using PEI-DNA complexes. Approximately 48 hr post-transfection, cells were harvested by centrifugation at 400 g for 20 min at 4°C.

Protein Purification

Frozen cell pellets were thawed and lysed by repeated washing and centrifugation in the hypotonic buffer of 10 mM HEPES (pH 7.5), 10 mM MgCl₂, 20 mM KCl, and the high osmotic buffer of 10 mM HEPES (pH 7.5), 1.0 M NaCl, 10 mM MgCl₂, 20 mM KCl, with EDTA-free complete protease inhibitor cocktail tablets (Roche). The washed membranes were suspended in hypotonic buffer with 30% glycerol and flash-frozen with liquid nitrogen and stored at –80°C until further use. Purified membranes were thawed at room temperature and incubated with 20 μM AM6538 and inhibitor cocktail at 4°C for 3 hr. The membranes were further incubated with 1.0 mg/ml iodoacetamide (Sigma) for 1 hr. The membranes were solubilized in the buffer containing 50 mM HEPES (pH 7.5), 500 mM NaCl, 1% (w/v) n-dodecyl-beta-D-maltopyranoside (DDM, Anatrace) and 0.2% (w/v) cholesterol hemisuccinate (CHS, Sigma-Aldrich) at 4°C for 2.5–3 hr. The supernatants containing the solubilized CB₁ proteins were isolated by high-speed centrifugation, and then incubated with TALON IMAC resin (Clontech) and 20 mM imidazole, at 4°C overnight. The resin was washed with 15 column volumes of washing buffer I containing 25 mM HEPES (pH 7.5), 500 mM NaCl, 10% (v/v) glycerol, 0.05% (w/v) DDM, 0.01% (w/v) CHS, 30 mM imidazole and 20 μM AM6538, and 5 column volumes of washing buffer II containing 25 mM HEPES (pH 7.5), 500 mM NaCl, 10% (v/v) glycerol, 0.05% (w/v) DDM, 0.01% (w/v) CHS, 50 mM imidazole and 20 μM AM6538. The protein was eluted using 2.5 column volumes of elution buffer containing 25 mM HEPES (pH 7.5), 500 mM NaCl, 10% (v/v) glycerol, 0.02% (w/v) DDM, 0.004% (w/v) CHS, 250 mM imidazole and 10 μM AM6538. A PD MiniTrap G-25 column (GE Healthcare) was used to remove imidazole. The protein was treated overnight with TEV protease to cleave the N-terminal FLAG/His tags from the proteins.

Finally, the purified protein was concentrated to about 50 mg/ml with a 100 kDa cutoff concentrator (Sartorius) and used in crystallization trials. The protein yield and monodispersity were tested by analytical size exclusion chromatography.

Lipidic Cubic Phase Crystallization of CB₁-AM6538 Complex

For the initial crystallization setup, purified CB₁-Flavodoxin in complex with AM6538 was reconstituted into lipidic cubic phase (LCP) by mixing with molten lipid (90% (w/v) monoolein and 10% (w/v) cholesterol) at a protein/lipid ratio of 2:3 (v/v) using a mechanical syringe mixer (Caffrey and Cherezov, 2009). LCP crystallization trials were performed using an NT8-LCP crystallization robot (Formulatrix). 96-well glass sandwich plates were incubated and imaged at 20°C using an automatic incubator/imager (RockImager 1000, Formulatrix). The crystals grew in the condition of 0.1M HEPES pH 7.0-7.4, 100mM (NH₄)₂HPO₄, 25%-32% PEG400, 2-20 mM Ethylenediaminetetraacetic acid disodium salt dehydrate (EDTA) and grew to the full size after 2 wk. The crystals were harvested using micromounts (MiTeGen) and flash-frozen in liquid nitrogen.

Data Collection and Structure Determination

X-ray diffraction data were collected at the Spring-8 beam line 41XU, Hyogo, Japan, using a Pilatus3 6M detector (X-ray wavelength 1.0000 Å). A rastering and data-collection strategy was followed as previously described (Cherezov et al., 2009; Hanson et al., 2012). Data were integrated and scaled using XDS (Kabsch, 2010) and merged using SCALA (Collaborative Computational Project, Number 4, 1994). Initial phase information was obtained by molecular replacement (MR) with Phaser (McCoy et al., 2007) using the receptor portion of LPA₁ (PDB: 4Z34) and Flavodoxin structure (PDB: 111O) as search models. Refinement was performed with Phenix (Adams et al., 2010) and Buster (Smart et al., 2012) followed by manual examination and rebuilding of the refined coordinates in the program COOT (Emsley et al., 2010) using both |2F_o-|F_c| and |F_o-|F_c| maps.

Quantum Mechanical Optimization of AM6538

Optimizing the geometry of AM6538 by quantum-mechanical energy minimization was performed using Jaguar 9.0 (Schrödinger, 2015a). Density functional theory (DFT) with B3LYP functional and basis set 6-31G**++ was used. The conformation in the crystal structure was used as starting point.

Docking Simulations of CB₁ Ligands

Prediction of ligand binding to CB₁ was done with Schrodinger Suite 2015-4. Processing of the protein structure was performed with the Protein Preparation Wizard. Converting of ligands from 2D to 3D structures was performed using LigPrep. Molecular docking was performed by two different methods: for antagonists, rigid protein docking in extra precision was used with Glide 6.9 (Friesner et al., 2004; Friesner et al., 2006; Halgren et al., 2004; Schrödinger, 2015a); for agonists, Induced Fit Docking (Felder and Schrott-Fischer, 1995; Schrödinger, 2015b; Sherman et al., 2006), allowing optimization of residues within 5.0 Å, in extra precision, was used.

Molecular Dynamics Simulation of CB₁ in Complex with AM6538 and Representative Antagonists

Molecular dynamics simulation was performed using GROMACS 5.1.2 (Abraham et al., 2015), using force field CHARMM27 (Feller and MacKerell, 2000; MacKerell et al., 1998; Mackerell et al., 2004). Crystal structures of CB₁ with AM6538 or inverse agonists in the binding pocket (binding mode predicted by molecular docking) was embedded into a pre-equilibrated POPC (1-palmytoyl-2-oleoyl-sn-glycero-3-phosphatidylcholine) lipid bilayer following an online protocol (Kandasamy and Larson, 2006). The topology files of ligands and POPC molecules were generated using online server SwissParam (Zoete et al., 2011). The systems were solvated with water, and chloride ions were added to neutralize the system. Molecular Dynamics simulations were performed in the NPT ensemble, at temperature of 310K and pressure of 1 atm using semi-isotropic coupling. First, each system was balanced position-restrained MD for 10 ns (total energy was stable). Then 50 ns MD simulations with no position restraints were performed to each system for three independent runs, and these trajectories are used for analysis. Ligand RMSD and RMSF values were calculated with non-hydrogen protein atoms superimposed to the starting structure. The central structure was the structure with the smallest RMSD of all protein and ligand atoms from all three trajectories, followed by energy minimization.

Radioligand Binding Assay

Stably transfected, hCB₁ HEK293F cell lines expressing the WT receptor were used for saturation and competition binding assays using [³H]-CP55,940 (0.79 nM, specific activity: 88.3 Ci/mmol, Perkin Elmer) with unlabeled CP55,940 (30 µM) used for nonspecific binding determination. Binding assays were performed at 37°C for 1 hr in the presence of 25 µg protein per well prior to collection of membranes by rapid filtration, washing and scintillation facilitated detection of tritium retained on the membranes according to standard procedures (Janero et al., 2015). Saturation binding assays and subsequent nonlinear hyperbolic curve fitting analysis (Graphpad Prism 6.0) revealed a B_{max} of 10.2 ± 2.6 pmol/mg and Kd = 5.6 ± 2.3 nM. Assays were performed in the same manner for determination of affinity for the crystallization CB₁ construct wherein [³H]-CP55,940 (revealed a B_{max} of 47.2 ± 13.1 pmol/mg and Kd = 37.8 ± 13.9 nM). For wash out experiments at the WT CB₁, membranes were incubated at 37°C for 1 hr in the presence of vehicle (buffer with 1% DMSO), 100 nM rimonabant or 50 nM AM6538. The membranes were then resuspended in assay buffer containing 1% BSA followed by centrifugation 2 times and then washed and collected a third time in assay buffer alone. These membranes were then subject to the saturation binding assay as described above in this section.

WT and Mutant hCB₁-CHO Cell Line Generation for Functional Studies

The 3 × HA (haemagglutinin)-N terminus tagged hCB₁ receptor cDNA was obtained from [cDNA.org](#) and subcloned into a murine stem cell virus for cell line transduction (pMSCV-puro, Clontech). Point mutations were introduced to the N terminus-3xHA-tagged human CB₁ receptor cDNA in MSCV retroviral vector by using Q5® Site-Directed Mutagenesis kit (New England Biolabs) to create mutant CB₁ plasmids (F170A, F170W, F174A, F174W, F379A and F379W). The primers used to make the mutations are given in the Key Resources table. The WT and mutant CB₁ constructs were then packaged into retrovirus via Phoenix package system, and the produced retroviruses were applied to CHO-K1 cells for gene transduction. Stable cell lines were generated following selection with antibiotic (puromycin) selection. Cells were passaged onto 384-well plates for pharmacological characterization. Cells were maintained in DMEM/F-12 media supplemented with 10% fetal bovine serum, 1% penicillin/streptomycin, and 5 µg/mL puromycin (Invitrogen, Waltham, MA).

Functional Analysis Studies

CISBIO cAMP HTRF Assay

Inhibition of forskolin-stimulated cAMP was determined using the CISBIO cAMP Homogeneous Time-Resolved Fluorescence resonance energy transfer (FRET) (HTRF) HiRange assay according to the manufacturer's instructions (Cisbio Assays, Bedford, MA). Cells (5,000 cells/well in low-volume 384 well plates) were cotreated at room temperature for 30 min with 25 µM RO-20-1724 and 20 µM forskolin (Sigma-Aldrich), and hCB₁R ligands at concentrations ranging from 0.03 – 10,000 nM. Cells were then incubated with cAMP-d2 antibody in assay diluent and cryptate solution in lysis buffer for 60 min at room temperature (Cisbio Assays). Fluorescence was measured at 620/665 nm using a Perkin-Elmer EnVision plate reader (Waltham, MA). FRET was calculated as fluorescence at 665 nm/620 nm. Basal cAMP levels were determined from cells incubated in the absence of RO-20-1724, forskolin, and ligand. cAMP levels were determined in cells incubated with RO-20-1724 and forskolin. Compounds were dissolved in DMSO in PBS and diluted to final solvent concentrations of 1% at the times and concentrations indicated. Agonist properties in the assays used for the WT cells used competitive analysis were as follows: EC₅₀ = 7.9 ± 2.0 nM, E_{max} = 3.21 ± 0.39 (fold over baseline, set as 100% CP55,940); THC: EC₅₀ = 160.1 ± 26.0 nM; E_{max} = 1.36 ± 0.05 (fold over baseline, set as 100% THC). N ≥ 3 individual experiments performed in duplicate presented as mean ± SEM.

DiscoverRx βArrestin2 Assay

βArrestin2 recruitment was determined using the CHO-hCB₁R PathHunter assay (DiscoverRx) according to the manufacturer's instructions following a 1.5 hr incubation at 37°C with the indicated concentrations of ligands. All experiments included a vehicle control. Agonist properties in the cell lines were as follows: CP55,940: EC₅₀ = 23.8 ± 4.6 nM, E_{max} = 4.03 ± 0.19 (fold over baseline, set as 100% CP55,940); THC: EC₅₀ = 89.2 ± 38.9 nM; E_{max} = 2.24 ± 0.16 (fold over baseline, set as 100% THC). N ≥ 3 individual experiments performed in duplicate presented as mean ± S. E. M.

[³⁵S]GTPγS Binding to CB₁ in C57 Mouse Cerebellum Membranes

G protein-coupling in mouse brain was measured using a previously published protocol (Bohn et al., 2015; Janero et al., 2015). The cerebellum from C57BL/6 mice (4-7 months old) were homogenized (glass on glass) in homogenization buffer (10 mM Tris-HCl, pH 7.4, 100 mM NaCl, 1 mM EDTA, 1 mM DTT). The homogenate was passed through a 26-gauge needle, centrifuged twice at 20,000 x g for 30 min at 4°C, and resuspended in ice-cold assay buffer (50 mM Tris-HCl pH 7.4, 100 mM NaCl, 5 mM MgCl₂, 1 mM EDTA and 2 µM GDP, 1 mM DTT). For each reaction, 2.5 µg of membrane protein was incubated in assay buffer containing ~0.1 nM [³⁵S]GTPγS and increasing concentrations of test compound in a total volume of 200 µL for 2 hr at room temperature. Test compounds (CP55,904, rimonabant, AM6538, and THC) were first diluted through serial dilutions in DMSO, then with assay buffer to a final DMSO concentration of 1%. Reactions were terminated by filtering membrane-bound and free [³⁵S]GTPγS through GF/B filters using a 96-well plate harvester (Brandel Inc., Gaithersburg, MD) and rinsing with ice-cold dH₂O. Filters were dried overnight, and radioactivity was determined with a microplate scintillation counter. For experiments used to analyze drug competition, agonists and antagonists were incubated with the membranes simultaneously. Agonist properties in the mouse cerebellum: CP55,940: EC₅₀ = 63.0 ± 5.5 nM, E_{max} = 2.40 ± 0.04 (fold over baseline, set as 100% CP55,940); N = 4 individual mouse cerebella preparations performed in duplicate presented as mean ± SEM.

Protein Stability Assays

Protein thermostability was tested by a microscale fluorescent thermal stability assay using the thiol-specific fluorochrome N-[4-(7-diethylamino-4-methyl-3-coumarinyl)phenyl]maleimide (CPM), which reacts with the native cysteines embedded in the protein interior as a sensor for the overall integrity of the folded state. The CPM dye (Invitrogen) was dissolved in DMSO at 4 mg/ml and stored at -80°C. Prior to use the dye stock was diluted 1:20 in buffer 25 mM HEPES, pH 7.5, 150 mM NaCl, 10% glycerol, 0.05% (w/v) DDM and 0.01% (w/v) CHS. The tested protein (~5 µg) was diluted in the same buffer to a final volume of 120 µL. 1 µL of the diluted dye was added and thoroughly mixed with protein. The reaction mixture was incubated at room temperature for 15 min, and subsequently transferred to a sub-micro quartz fluorimeter cuvette (Starna Cells, Inc.) and heated in a controlled way with a ramp rate of 1°C/min over a temperature range from 20–90°C in a Cary Eclipse Fluorescence Spectrophotometer (Agilent Technologies). The excitation wavelength was set at 387 nm, while the emission wavelength was 463 nm. Protein homogeneity was also tested by analytical size-exclusion chromatography (aSEC) using a 1260 Infinity HPLC system (Agilent Technologies).

Affinity Mass Spectrometry Analysis of AM6538

The CB₁ protein co-purified with AM6538 was first desalted using PD MiniTrap G-25 column cartridge to deplete free ligands. Then the protein complex sample (~1 µg) was filtered through 30 kDa MW cutoff ultrafiltration membrane (Sartorius, Germany) by centrifugation at 13,000 g for 10 min at 4°C in the buffer containing 150 mM ammonium acetate, 0.02% (w/v) DDM and 0.004% (w/v) CHS. The protein complexes retained on the ultrafiltration membrane was transferred to a new centrifugal tube. The ligands were dissociated from the complexes with 90% methanol and separated from the denatured protein by centrifugation at 13,000 g for 20 min at 25°C. The supernatant was dried out in speed vacuum, reconstituted in 50% methanol, diluted by 50-fold prior to LC-MS analysis using Agilent 6230 TOF equipped with an Agilent 1260 HPLC system. The compound was eluted with 95% methanol/0.1% formic acid from a Hypersil GOLD C18 column (2.1 mm × 100 mm, 3 µm, Thermo Fisher Scientific, USA) at a flow rate of 0.4 mL/min. Full-scan mass spectra were acquired in the range of 100-1000 m/z on Agilent 6230 TOF with major ESI source settings: voltage 3000 V, gas temperature 350°C, fragmentor 100 V.

QUANTIFICATION AND STATISTICAL ANALYSIS

Concentration-response curves for cAMP and β-arrestin2 are presented as % of CP55,940 or THC at 1 µM, as indicated. Concentration-response curves were fit to a non-linear regression (three parameter) model to determine EC₅₀ and E_{max}, or a Gaddum/Schild EC₅₀ shift global non-linear regression model in Prism (v. 6.0, GraphPad Software Inc., San Diego, CA), as indicated. In order to best fit data to the Gaddum/Schild EC₅₀ shift global non-linear regression, pEC₅₀, pA₂, Hill slope, E_{max}, and E_{min} were shared for all datasets. Schild slope was constrained to unity after determining a competitive antagonism model (*i.e.* Schild slope = 1) was the preferred model for these data.

DATA AND SOFTWARE AVAILABILITY

Data Resources

The accession number for the coordinates and structures factors of CB1_AM6538 reported in this paper is PDB: 5TGZ.

Supplemental Figures

Cell

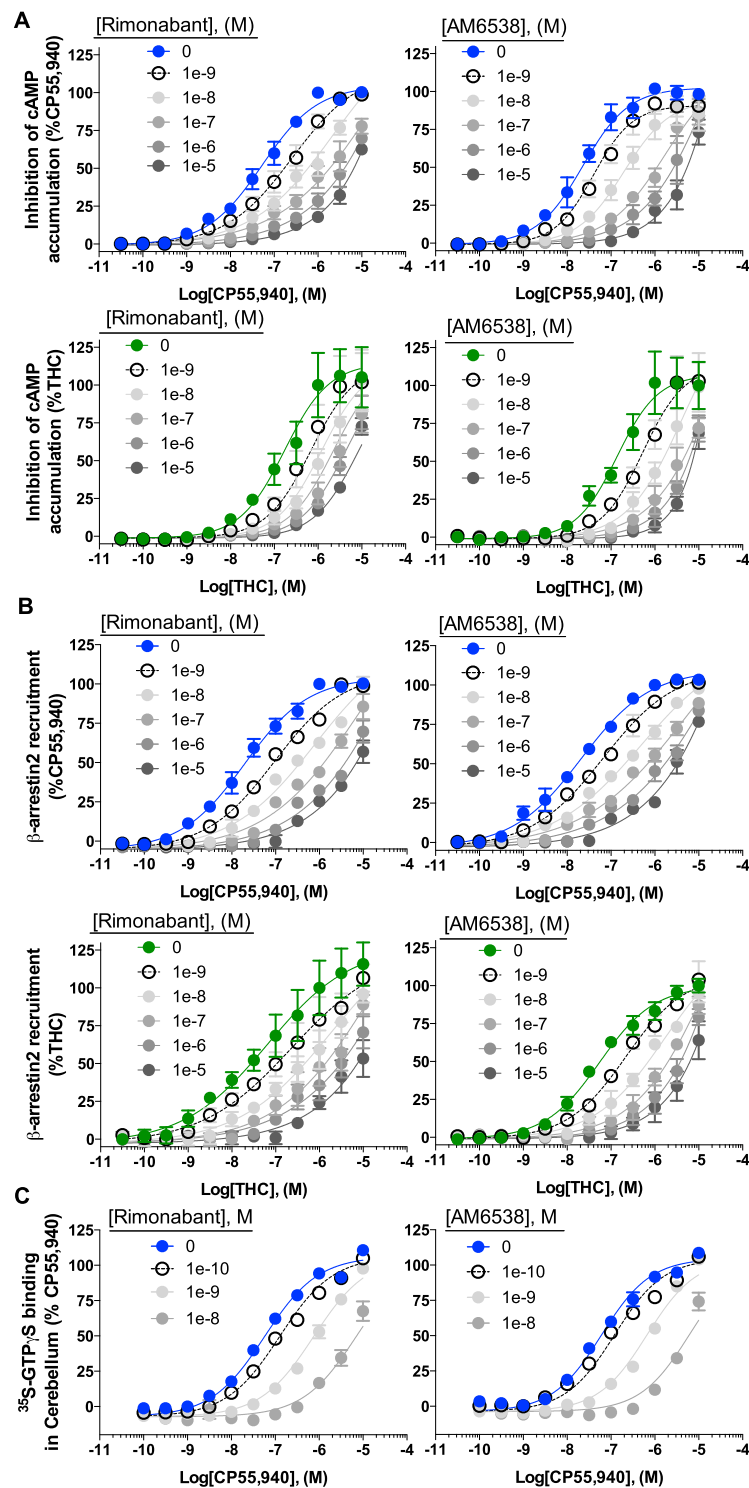


Figure S1. Rimonabant and AM6538 Are Competitive Antagonists of CP55,940 and THC, Related to Figure 2

(A and B) Rimonabant (left) and AM6538 (right) competitively antagonize CP55,940 (top) and THC (bottom)-induced (A) Inhibition of forskolin-stimulated cAMP accumulation in hCB₁-CHO cells and (B) β -arrestin 2-recruitment in hCB₁-CHO DiscoverRx PathHunter cells.

(C) Rimonabant (left) and AM6538 (right) competitively antagonize CP55,940-stimulated [³⁵S]-GTP γ S binding in mouse cerebellum membrane preparations. Data are presented as the mean \pm S. E. M. of 3 or more assays run in duplicate or triplicate. Competitive nonlinear analysis was performed in GraphPad Prism 6.0 and parameters are included in Table S1. Characterization of agonist effects in the cells and cerebellum are provided in the supplemental methods.

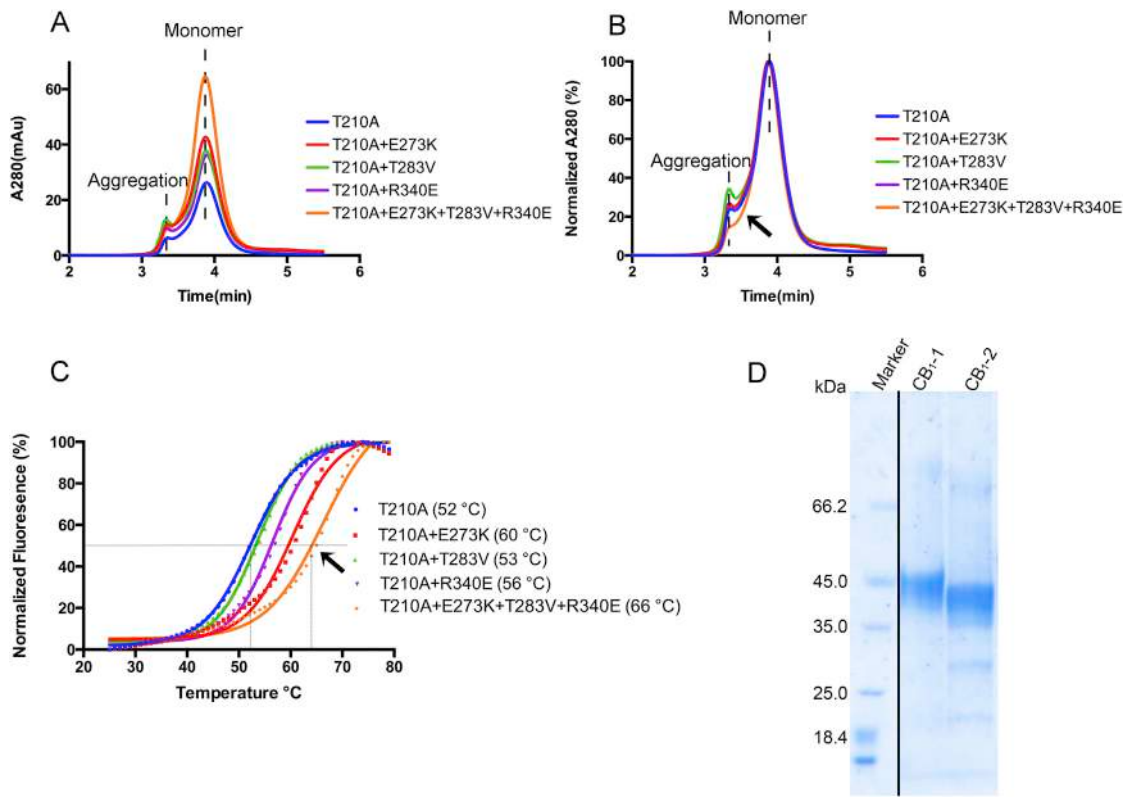


Figure S2. Stability Assay of CB₁ Mutants, Related to Figure 1

(A and B) Analytical size exclusion chromatography (aSEC) of CB₁ mutants testing the effects of mutations and mutation combination on protein homogeneity. (A) The raw data show that the CB₁ mutant containing all four mutations (orange trace) has the highest protein yield. (B) The normalized data show that the combination (orange trace) improves protein homogeneity.

(C) CPM ramping assay of CB₁ mutants testing the effects of mutations and mutation combinations on protein thermostability. The T_m value of the CB₁ mutant containing all four mutations (orange trace) is higher than other mutants, indicating that this mutation combination improves protein thermostability.

(D) Coomassie-stained polyacrylamide gel electrophoresis (PAGE) of the purified crystallization-grade CB₁. CB₁-1: Coomassie-stained PAGE of sample purified by cobalt immobilized-metal affinity chromatography (TALON-IMAC); CB₁-2: Coomassie-stained PAGE of sample after TEV protease digestion. The black line indicates where three intervening lanes from the original gel were removed during figure preparation for clarity of presentation. Three additional lanes following CB1 were omitted as well.

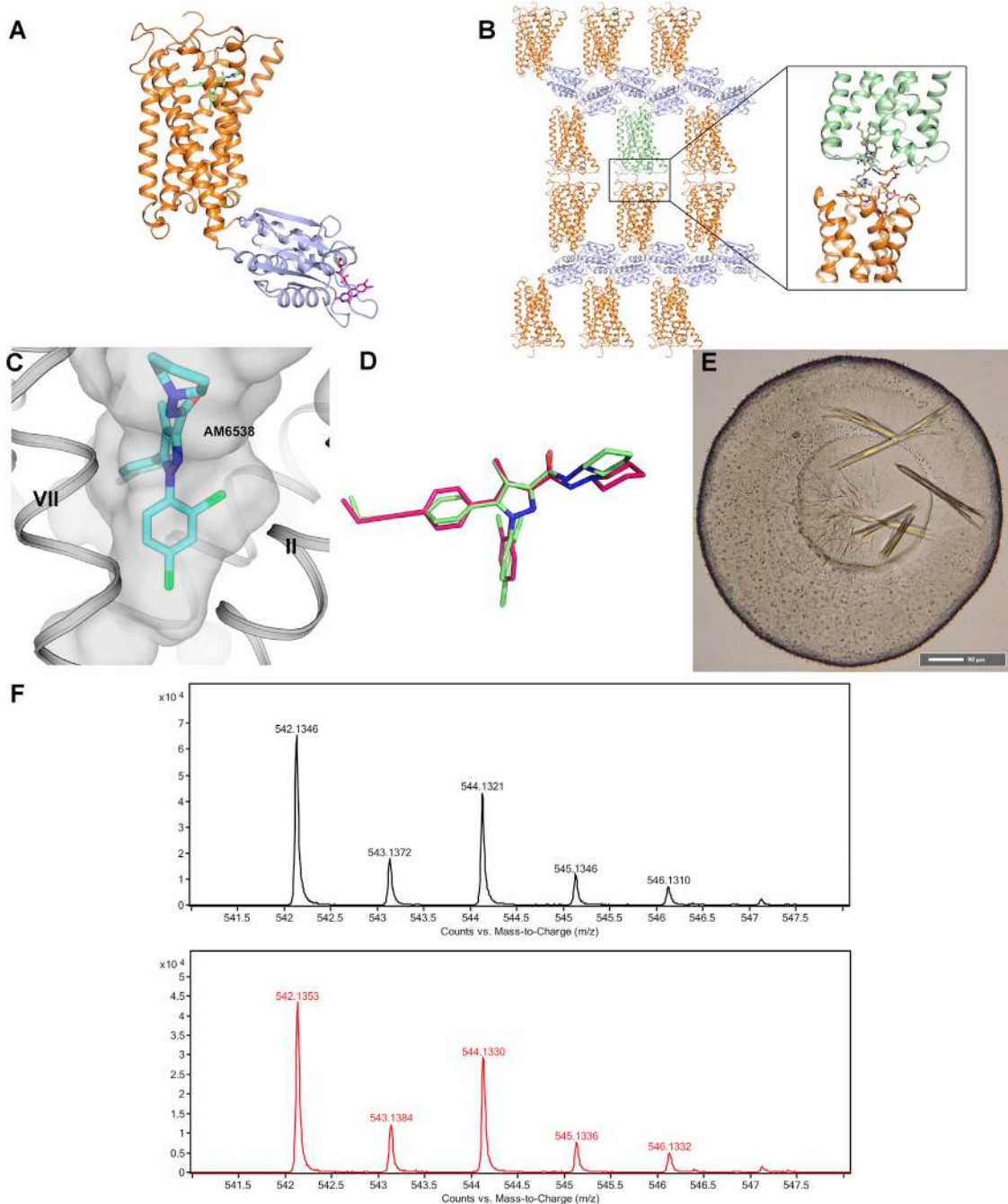
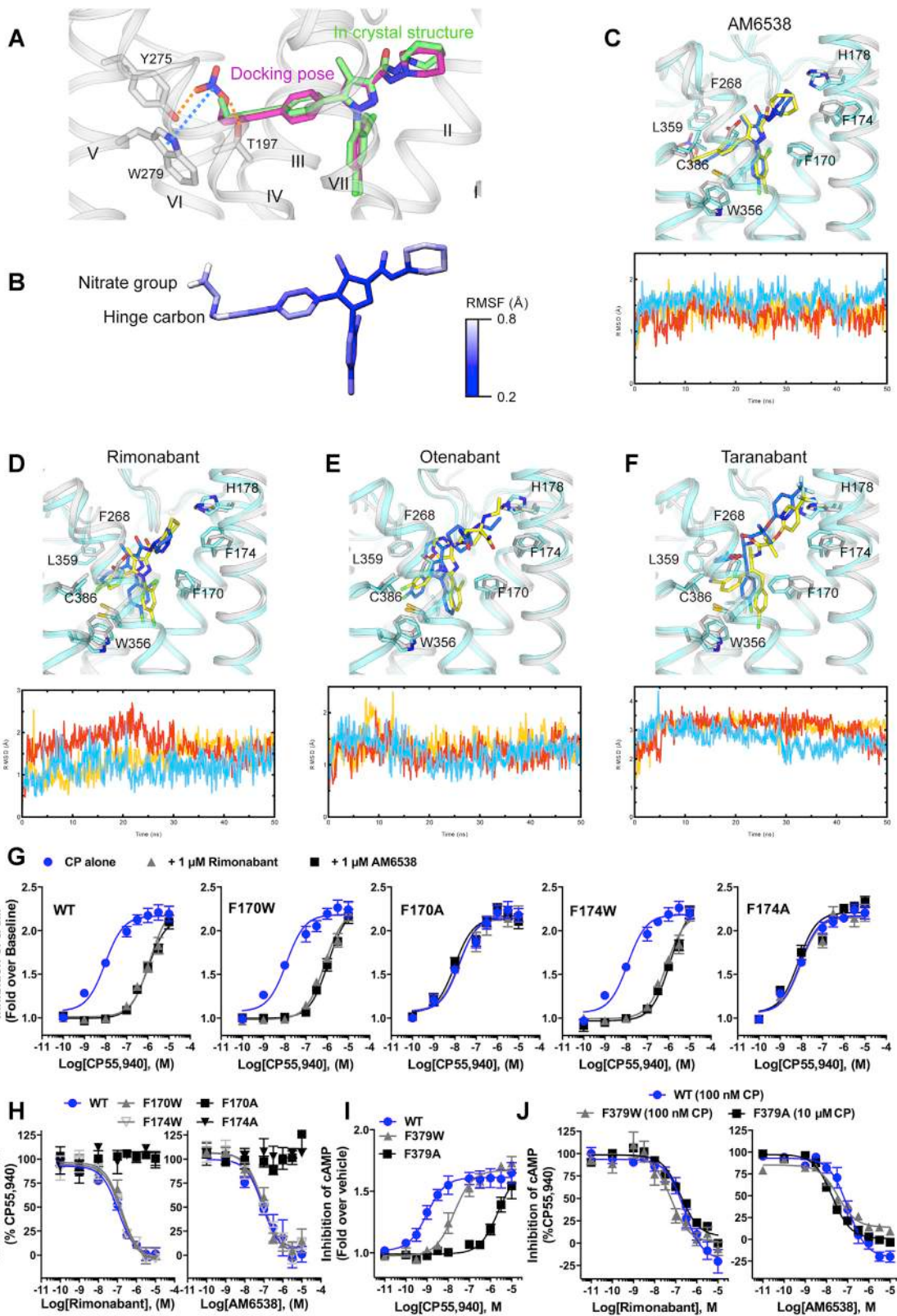


Figure S3. Fusion Protein Engineering and Crystal Packing of CB₁-AM6538 Complex, Related to Figures 1 and 3

- (A) Overall structure of CB₁-AM6538 complex. CB₁ and Flavodoxin are colored in orange and slate, respectively. AM6538 is shown in green stick representation and FMN (the substrate of Flavodoxin) is shown in magenta stick representation.
- (B) Crystal packing of the CB₁-AM6538 complex, N terminus involved in the crystal packing.
- (C) The 2,4-dichlorophenyl ring of AM6538 fits well into the shape of the side-pocket. The receptor is shown in gray cartoon and gray surface, AM6538 is shown in cyan carbons.
- (D) Superposition of AM6538 in crystal structure (green) and local minimum calculated by quantum mechanics (magenta).
- (E) Crystal images for CB₁ in complex with AM6538 (scale bar is 90 μ m).
- (F) The high-resolution mass spectrometry spectra of the pure standard AM6538 (top) and the ligand dissociated from CB₁ complex (bottom). The theoretical m/z for the monoisotopic peak of AM6538 is 542.1356.



(legend on next page)

Figure S4. MD Simulations of the Predicted Antagonists and Mutagenesis Validation of the Docking Predictions, Related to Figures 5 and 6

(A) Docking pose of AM6538 (magenta sticks) and predicted hydrogen bond (orange dashed lines) and π - π interaction (blue dashed lines) in comparison with AM6538 in crystal structure (green sticks).

(B) RMSF of AM6538 in MD simulation.

(C–F) AM6538 (C), rimonabant (D), otenabant (E) and taranabant (F) Central structures in MD (protein is shown in light cyan cartoon; ligands are shown in blue sticks) versus docking poses (protein is shown in white cartoon and ligands are shown in yellow sticks), and ligand RMSD (three independent runs).

(G) Mutations of hCB₁ at Phe170Ala or Phe174Ala disrupts the ability of AM6538 and rimonabant to displace CP55,940 while preserving its functional activity. The corresponding tryptophan mutations have no effect on agonist or antagonist actions.

(H) A loss of antagonist affinity is further demonstrated in competition response curves agonist 100 nM CP55,940.

(I) Mutation of Phe379Trp and Phe379Ala progressively worsen the functional affinity of CP55,940.

(J) When tested against concentrations of CP55,940 that maximally stimulate the receptor, AM6538 and rimonabant maintain their potency as antagonists (100 nM CP55,940 for WT and Phe379Trp and 10 μ M CP55,940 for Phe379Ala; normalization is made per mutant). Data are presented as mean \pm S. E. M. of 3 or more assays performed in duplicate or triplicate.

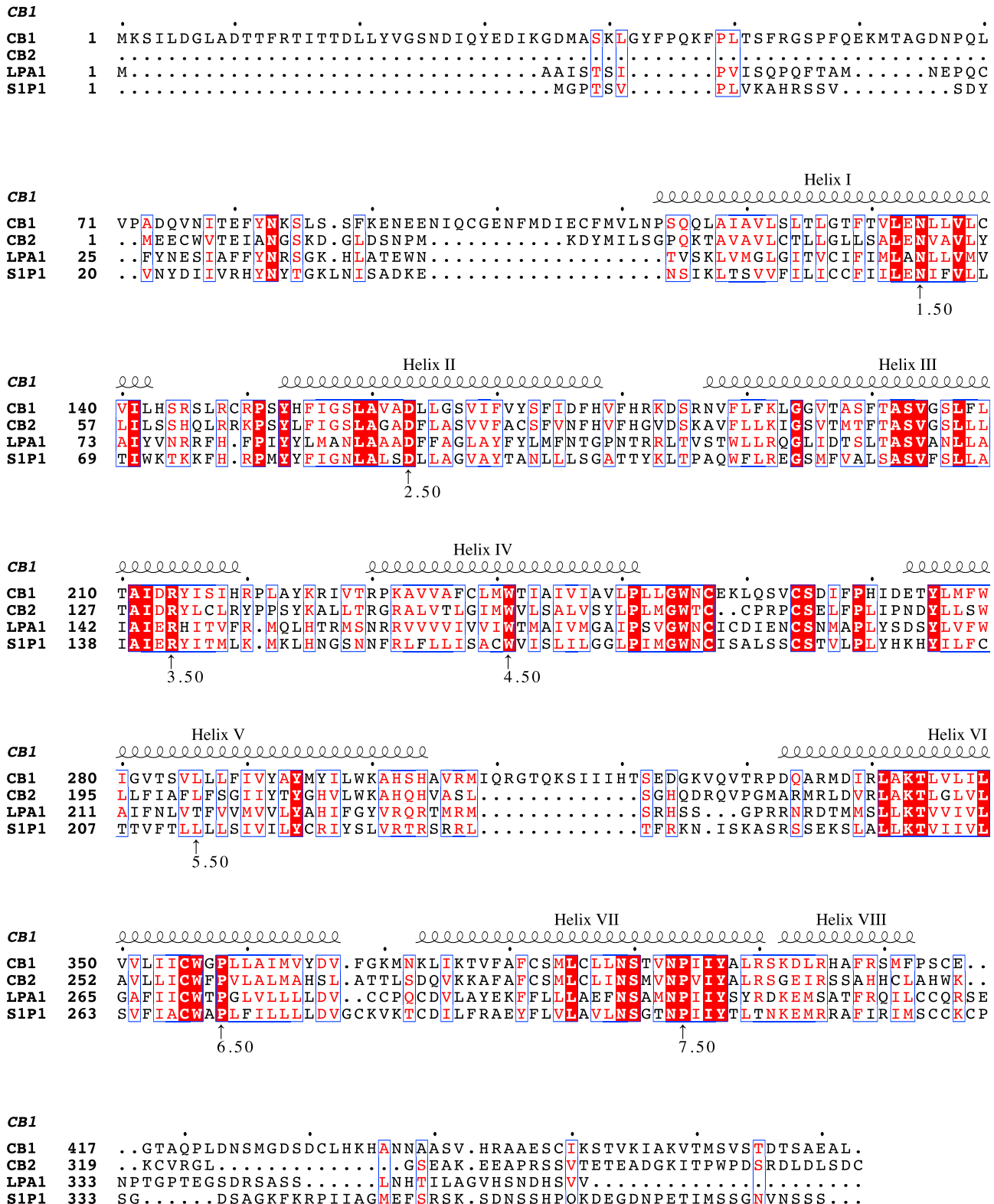


Figure S5. Multiple Sequence Alignment of Human CB₁ with CB₂, LPA₁, and S1P₁ Receptors, Related to Figure 4

Figure S3. Multiple Sequence Alignment of Human CD4 with CD2, LTA, and CCR4 Receptors, Related to Figure 4
Positions that are identical between the receptors are highlighted with a red background. Alignment was done by MAFFT v7.299b (Katoh and Standley, 2013) and the graphics were prepared using ESPript 3.0 server (Robert and Gouet, 2014).

Crystal structures of agonist-bound human cannabinoid receptor CB₁

Tian Hua^{1,2,3}, Kiran Vemuri^{4*}, Spyros P. Nikas^{4*}, Robert B. Laprairie⁵, Yiran Wu¹, Lu Qu^{1,2,3}, Mengchen Pu¹, Anisha Korde⁴, Shan Jiang⁴, Jo-Hao Ho⁵, Gye Won Han⁶, Kang Ding^{1,3,7}, Xuanxuan Li⁸, Haiguang Liu⁸, Michael A. Hanson⁹, Suwen Zhao^{1,7}, Laura M. Bohn⁵, Alexandros Makriyannis⁴, Raymond C. Stevens^{1,6,7} & Zhi-Jie Liu^{1,2,7}

The cannabinoid receptor 1 (CB₁) is the principal target of the psychoactive constituent of marijuana, the partial agonist Δ⁹-tetrahydrocannabinol (Δ⁹-THC)¹. Here we report two agonist-bound crystal structures of human CB₁ in complex with a tetrahydrocannabinol (AM11542) and a hexahydrocannabinol (AM841) at 2.80 Å and 2.95 Å resolution, respectively. The two CB₁-agonist complexes reveal important conformational changes in the overall structure, relative to the antagonist-bound state², including a 53% reduction in the volume of the ligand-binding pocket and an increase in the surface area of the G-protein-binding region. In addition, a ‘twin toggle switch’ of Phe200^{3,36} and Trp356^{6,48} (superscripts denote Ballesteros–Weinstein numbering³) is experimentally observed and appears to be essential for receptor activation. The structures reveal important insights into the activation mechanism of CB₁ and provide a molecular basis for predicting the binding modes of Δ⁹-THC, and endogenous and synthetic cannabinoids. The plasticity of the binding pocket of CB₁ seems to be a common feature among certain class A G-protein-coupled receptors. These findings should inspire the design of chemically diverse ligands with distinct pharmacological properties.

Cannabis sativa L., commonly known as marijuana, has been used for medicinal and recreational purposes across different cultures for more than 5,000 years^{4,5}. The principal *Cannabis* constituent, Δ⁹-THC, exerts its psychotropic effects by activating CB₁, which is also the primary target of the endocannabinoids, anandamide (AEA) and 2-arachidonoyl glycerol (2-AG)^{1,6}. Structural examination of CB₁ in complex with the antagonist AM6538² and taranabant⁷ provides molecular insights into the inactive state of the receptor, yet does not inform us as to how CB₁ elicits its diverse physiological effects.

To facilitate CB₁ crystallization in agonist-bound form, two potent CB₁ agonists, AM11542 and AM841, were designed to introduce a tricyclic terpenoid ring system, the 6aR, 10aR stereochemistry at the junction of the B- and C-rings and the phenolic hydroxyl group at C1, all of which also characterize the Δ⁹-THC tricyclic ring system (Fig. 1a, Methods and Extended Data Fig. 1). The two ligands used in this study differ from Δ⁹-THC by possessing a pivotal 1',1'-gem-dimethylheptyl (DMH) alkyl chain at the C3 position as well as bromo and isothiocyanato groups as ω-substituents for AM11542 and AM841, respectively (Fig. 1a). Having high affinity for CB₁ and binding in a wash-resistant manner to the receptor (Fig. 1a–c), both AM11542 and AM841 are potent, full agonists of CB₁ as determined by their ability to inhibit forskolin-stimulated accumulation of cAMP compared to CP55,940, whereas Δ⁹-THC acts as a partial agonist in this assay (Fig. 1d).

The two agonist-bound CB₁ structures were determined using a thermostabilizing construct as previously described² for CB₁-AM6538

(Extended Data Fig. 2, Extended Data Table 1). The receptor conformations of the AM11542- and AM841-bound complexes are very similar (C_α root mean square deviation (r.m.s.d.) = 0.66 Å), and both ligands overlay well in the same binding pocket (Fig. 2a, Extended Data Fig. 3a). Thus, we focus our discussions mainly on the higher resolution CB₁-AM11542 structure, while mentioning specific differences of the AM841-bound complex where relevant. In contrast to a V-shaped loop in the CB₁-AM6538 structure, the truncated N terminus resides over the ligand-binding pocket where it is not directly involved in agonist binding (Fig. 2b), although it does not preclude the possibility that there may be conformational changes in a full-length N-terminal domain. A cholesterol molecule, which is absent in the antagonist-bound structure, is observed between the cytoplasmic portion of helices II, III and IV in the agonist-bound complexes (Extended Data Fig. 3b). This cholesterol binding cavity is revealed through a rotation of helix II coupled with conformational changes of the side chain of Leu165^{2,52} (superscript denotes Ballesteros–Weinstein numbering³).

The agonist AM11542 adopts an L-shape conformation in the orthosteric-binding pocket, which is much smaller than the more expanded binding domain in the antagonist AM6538-bound structure (Fig. 2b–d). The interactions between AM11542 and CB₁ are mainly hydrophobic and aromatic, consisting of residues from extracellular loop 2 (ECL2), helices III, V, VI and VII (Fig. 3a, d). The tricyclic tetrahydrocannabinol ring system of AM11542 forms π–π interactions with Phe268^{ECL2}, Phe379^{7,35}, Phe189^{3,25} and Phe177^{2,64}, and the phenolic hydroxyl at C1 forms a hydrogen bond with Ser383^{7,39}. In agreement, mutations of Ser383^{7,39} Ala or Phe379^{7,35} Ala greatly reduce CB₁ agonist potency of cannabinoid-like agonists, such as AM11542, AM841 and CP55,940, respectively (Fig. 3c, Extended Data Fig. 4b, Extended Data Table 2). Of note, the hydroxyl group at the C11 position of AM841 forms an additional hydrogen bond with Ile267^{ECL2}.

The alkyl chain of the agonist extends into the long channel formed by helices III, V and VI, undergoing hydrophobic interactions with Leu193^{3,29}, Val196^{3,32}, Tyr275^{5,39}, Leu276^{5,40}, L359^{6,51} and Met363^{6,55} (Fig. 3a, d). In addition, the isothiocyanate moiety of AM841 forms a hydrogen bond with Tyr275^{5,39}. Notably, Leu193^{3,29} Ala and Tyr275^{5,39} Ala mutations markedly decrease the potency of the agonists (Fig. 3c, Extended Data Fig. 4b, Extended Data Table 2). Structure–activity relationship (SAR) studies with classical cannabinoids have shown that the C3 alkyl chain lengths and ω-substitutions modulate ligand affinity. Also, incorporation of a C1'-gem-dimethyl group affects the conformational properties of the alkyl chain and leads to notable enhancement in potency and efficacy^{8–11}. Unlike Δ⁹-THC, which has a shorter alkyl chain (*n*-pentyl), our results show that longer alkyl chains

¹iHuman Institute, ShanghaiTech University, Shanghai 201210, China. ²National Laboratory of Biomacromolecules, Institute of Biophysics, Chinese Academy of Sciences, Beijing 100101, China.

³University of Chinese Academy of Sciences, Beijing 100049, China. ⁴Center for Drug Discovery, Department of Pharmaceutical Sciences; Department of Chemistry and Chemical Biology, Northeastern University, Boston, Massachusetts 02115, USA. ⁵Departments of Molecular Medicine and Neuroscience, The Scripps Research Institute, Jupiter, Florida 33458, USA. ⁶Departments of Biological Sciences and Chemistry, Bridge Institute, University of Southern California, Los Angeles, California 90089, USA. ⁷School of Life Science and Technology, ShanghaiTech University, Shanghai 201210, China. ⁸Complex Systems Division, Beijing Computational Science Research Center, Beijing 100193, China. ⁹GPCR Consortium, San Marcos, California 92078, USA.

*These authors contributed equally to this work.

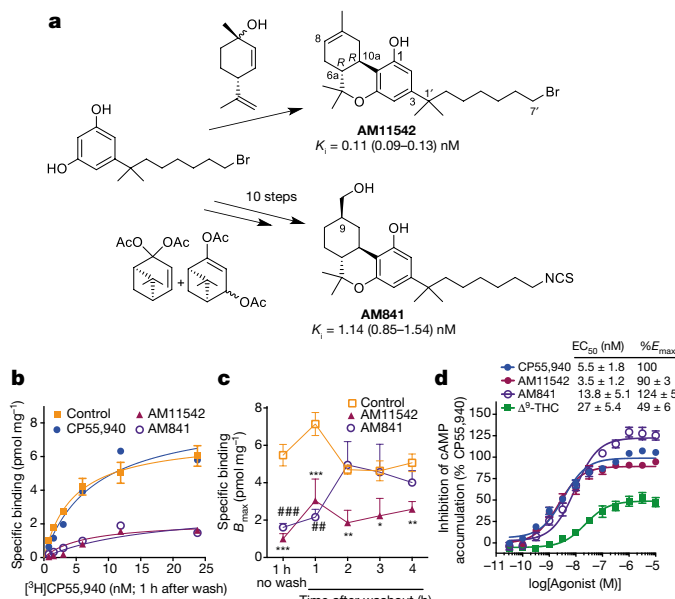


Figure 1 | Synthesis and pharmacological characterization of AM11542 and AM841. **a**, Synthesis of AM11542 and AM841 (Extended Data Fig. 1) with radioligand binding affinity against [³H]CP55,940. K_i , inhibition constant. **b**, Cell membranes were pretreated with CP55,940 (4 nM), AM11542 (1 nM), AM841 (10 nM) or buffer (control) for 1 h, washed, and then subjected to [³H]CP55,940 binding for 1 h. **c**, B_{max} values (maximal binding capacity) were calculated from **b** and in experiments where the incubation time of radioligand was increased following the washing. Pretreatment with either AM11542 or AM841 prevents radioligand binding after 1 h incubation (control: versus AM841: #P < 0.01; versus AM11542 ***P < 0.001), while AM11542 prevents radioligand binding at all later time points tested (control versus AM11542: *P < 0.05, **P < 0.01). Displacement of [³H]CP55,940 binding in the presence of AM11542 (versus control: ***P < 0.001) and AM841 (versus control: #***P < 0.001) are shown for comparison. (Student's *t*-test versus control at each time point; data are mean ± s.e.m.; $n = 3–6$). **d**, Agonist activity measured as the inhibition of forskolin-stimulated cAMP accumulation. Data are mean ± s.e.m. of $n \geq 6$ independent experiments. %E_{max}, percentage of maximum response; EC₅₀, half-maximum effective concentration.

coupled with a C1'-gem-dimethyl group allow extended interactions with CB₁, while the C1'-gem-dimethyl group forms hydrophobic interactions with Phe200^{3,36}, Leu359^{6,51} and Met363^{6,55} (Fig. 3a, d). Taken together, these data provide important insights into the key role of the DMH moiety in activating CB₁.

On the basis of the AM11542-bound CB₁ structure and mutagenesis data¹², we investigated the interactions of representative agonists from three different scaffolds (classical cannabinoids, endocannabinoids and aminoalkylindoles) with CB₁ through docking and molecular dynamics validation (Fig. 3e, f, Extended Data Fig. 5). The predicted binding mode of the classical cannabinoids Δ^9 -THC (Fig. 3e) and HU-210 (Extended Data Fig. 5g) resembles that of AM11542 in the CB₁ crystal structure. HU-211, the enantiomer of HU-210, does not activate CB₁^{13,14} as it exhibits severe clashes when superimposed with its active enantiomer HU-210 (Extended Data Fig. 5i). The endocannabinoids AEA (Fig. 3f) and 2-AG (Extended Data Fig. 5j) adopt a C-shaped conformation and their long tails extend into the long channel. In comparison with other lipid receptors, such as sphingosine-1-phosphate receptor 1 (S1P₁), the alkyl chain of AM11542 and AM841 occupies a similar position as in 'arm 2' of the antagonist AM6538², as well as the alkyl chain of ML056 in the S1P₁ receptor¹⁵ (Fig. 3b), indicating that this could be a conserved binding pocket for alkyl chains within lipid-binding receptors. The structurally distinct aminoalkylindoles WIN 55,212-2 (Extended Data Fig. 5k) and JWH-018 (Extended Data Fig. 5h) occupy the same position in the pocket as AM11542

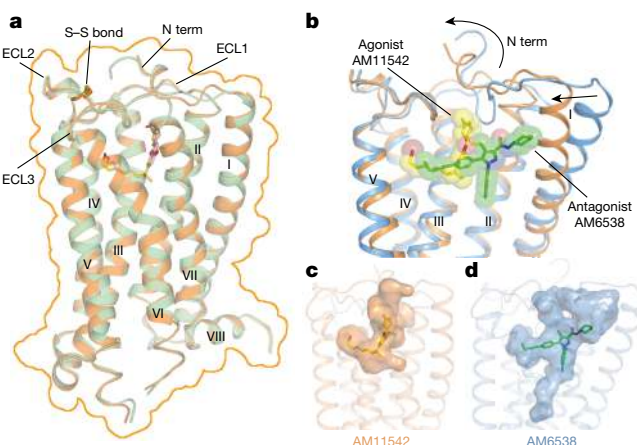


Figure 2 | Overall structures of CB₁-AM11542 and CB₁-AM841 complexes. **a**, Superposition of CB₁-AM11542 and CB₁-AM841 structures with the surface outlined by an orange line. CB₁ is shown in orange and green cartoon with ligands AM11542 (yellow sticks) and AM841 (pink sticks). **b**, Comparison of agonist-bound (orange cartoon) and antagonist-bound (blue cartoon) CB₁ ligand-binding pockets. AM11542 (yellow) and AM6538 (green) are shown in sticks and sphere representations. **c, d**, The shape of AM11542 (c) and AM6538 (d) binding pockets are shown in surface representation.

and AM841, exhibiting major π - π interactions with aromatic residues instead of hydrogen-bond interactions as observed in most classical cannabinoid-CB₁ interactions.

Comparisons between the agonist- and antagonist-bound CB₁ reveal marked structural rearrangements (C_α r.m.s.d. of the overall structure without fusion protein: 3.52 Å; Fig. 4a). Compared with the AM6538-bound CB₁, the notable conformational change occurs in helices I and II. The extracellular part of helix I bends inwards by 6.6 Å and helix II rotates in by about 6.8 Å, respectively in the AM11542-bound structure (Fig. 4b). Similarly, important conformational changes are also observed in the cytoplasmic part of the receptor, in which helix VI moves outwards by about 8 Å (Fig. 4b), resembling the β_2 adrenergic receptor (β_2 AR)-G_s complex¹⁶. This is the largest structural change, especially within the extracellular portion, observed in the solved agonist/antagonist-bound pairs of class A G-protein-coupled receptors (GPCRs) (Extended Data Table 3). Consequently, owing to the inward shifts of helices I/II, and the subsequent inward rotation of the side chains of Phe170^{2,57} and Phe174^{2,61} that occupy the gap pocket² (Fig. 3b), the volume of the ligand-binding pocket shrinks from 822 Å³ in the antagonist-bound structure to 384 Å³ in the agonist-bound complex, representing a 53% reduction (Fig. 2c, d, Extended Data Table 3).

The agonist-induced conformational changes, discussed above, probably trigger the activation and downstream signalling associated with CB₁. From a more granular perspective, CB₁ seems to use an extended molecular toggle switch involving a synergistic conformational change between Phe200^{3,36} and Trp356^{6,48}, which we refer to as the 'twin toggle switch' (Fig. 4c). In the AM6538-bound structure, Phe200^{3,36} points away from the ligand-binding pocket and forms an aromatic stacking interaction with Trp356^{6,48}, which may contribute to stabilization of the receptor in the inactive state (Fig. 4c). While in the AM11542-bound structure, the cooperative rotation of helix III and the side-chain flipping of Phe200^{3,36} lead the phenyl ring to point towards the ligand and form hydrophobic interactions with the C1'-gem-dimethyl group of AM11542 (Fig. 4c). Simultaneously, the outwards rotation of helix VI leads the side chain of Trp356^{6,48} to swing away from the ligands (Fig. 4c), disrupting the π - π stacking of the side chains of Phe200^{3,36} and Trp356^{6,48}. Comparing previously proposed 'toggle switch' of Trp356^{6,48}, the synergistic movement of two residues, Phe200^{3,36} and Trp356^{6,48}, during the activation of receptors has never been observed

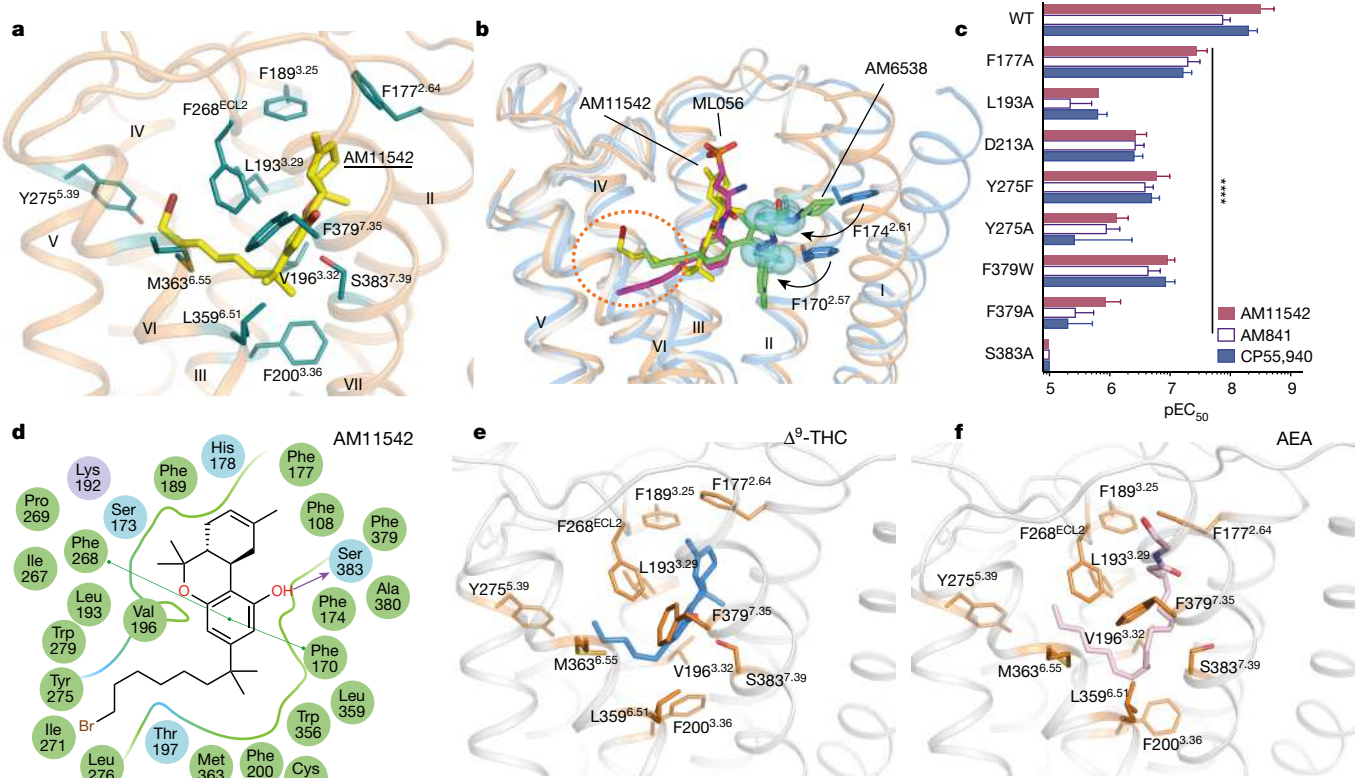


Figure 3 | AM11542 binding pocket analysis and molecular docking of Δ^9 -THC and AEA. **a**, Key residues (deep teal sticks) involved in AM11542 (yellow sticks) binding. **b**, Binding pose comparison of AM11542 (yellow), AM6538 (green) and ML056 (magenta) in their receptors, which are shown in orange, blue and grey cartoon, respectively. Phe170^{2.57} and Phe174^{2.61} in AM11542 and AM6538 complexes are shown in blue sphere and blue sticks, respectively. **c**, Certain mutations on CB₁ significantly decreased potency in the cAMP assay compared to agonist-response at the wild-type (WT) receptor as determined by comparison of negative

logarithm of the EC₅₀ (pEC₅₀) values by two-way analysis of variance (ANOVA) without repeated measures followed by Dunnett's post hoc test (comparing each drug to its effect in the wild type: ****P < 0.0001, data are mean \pm s.e.m., n \geq 3) (Extended Data Table 2). **d**, Summary of receptor interactions of AM11542. Purple ball (positive charged interaction); cyan ball (polar interaction); green ball (hydrophobic interaction); purple arrow (H-bond); green line (π - π stacking). **e**, **f**, The docking pose of Δ^9 -THC (e, blue sticks) and AEA (f, pink sticks).

before and we speculate that this twin toggle switch is related to CB₁ activation, a structural observation that is in agreement with a previous modelling study^{17,18}.

To investigate whether the twin toggle switch concept exists in other receptors, we performed a sequence analysis among class A GPCRs that shows that CB₂ as well as certain chemokine receptors (such as CCR2 and CCR5), possess an aromatic residue at the appropriate position (Phe/Tyr^{3.36}) to synergize with the highly conserved tryptophan on

helix VI (Trp^{6.48}). In addition, the highly conserved E/DRY motif and NPXXY motif are also rearranged in the AM11542 agonist-bound CB₁ structure. The polar network around the DRY motif is disrupted during activation (Fig. 4d). Arg214^{3.50} adopts an extended conformation, the intra-helical salt bridge between Asp213^{3.49} and Arg214^{3.50} as well as the 'ionic lock' between Arg214^{3.50} and Asp338^{6.30} are broken, resulting in rotamer shift of Asp338^{6.30} and movement of helix VI away from helix III (Fig. 4d). Notably, CB₁ shows the largest helix VI bending

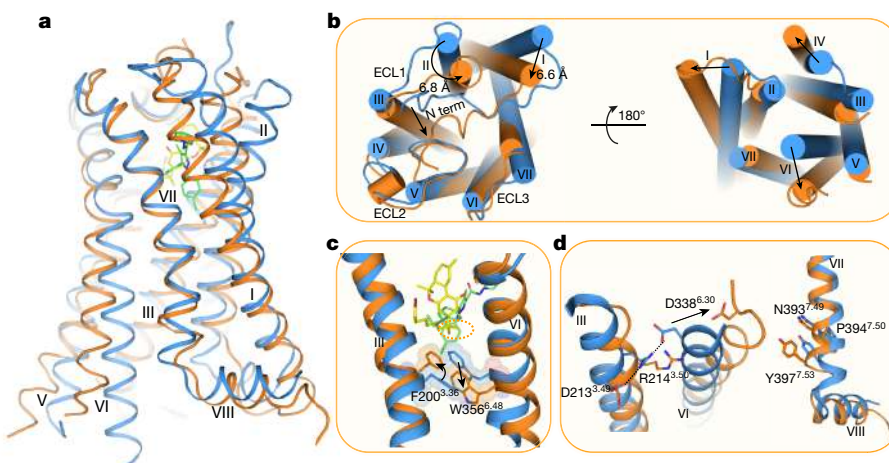


Figure 4 | Structural comparison of agonist- and antagonist-bound CB₁. **a**, Side view of the CB₁-AM11542 complex (receptor as orange and ligand as yellow) and CB₁-AM6538 complex (receptor in blue and ligand as green). **b**, The extracellular (left) and intracellular (right) views of the compared receptors. **c**, The 'twin toggle switch', Phe200^{3.36}/Trp356^{6.48}, is shown in sticks and spheres. Colour scheme as in a. **d**, Rearrangement of DRY (left) and NPXXY motifs (right) in agonist- and antagonist-bound CB₁ structures.

angle among all known agonist-bound (without G protein or G-protein mimics) class A GPCRs (Extended Data Fig. 6b). Similarly, the most important rearrangement around NPXXY region is a partial ‘unwinding’ of helix VII around Tyr397^{7,53} (Fig. 4d).

A notable feature of the CB₁ agonist bound structure is the large (53%) reduction in volume in the ligand-binding pocket between agonist- and antagonist-bound structures, and subsequent volume increase in the intracellular G-protein-binding site. Such plasticity in the orthosteric binding pocket enables CB₁ to respond to a diverse array of ligands with considerably different sizes, shapes and associated functions, consistent with the repertoire of CB₁ to modulate such varied physiological and psychological activities.

To investigate whether a similar feature exists in other receptors, the ligand-binding volume of all agonist- and antagonist-bound structural pairs in class A GPCRs are compared (Extended Data Table 3). Related to the ligand-binding volume change, we analysed the helices movement between antagonist- and agonist-bound structures in extracellular and intracellular halves. In most structural pairs, the extracellular half undergoes small changes while larger conformational changes in the intracellular half occur due to movements of helices VI, V and VII (Extended Data Fig. 6a). As an exception to this minimal trigger, CB₁ has the largest ligand-binding pocket volume change, contributed mainly by the movements of the extracellular half of helices I and II. Large inwards bending (over 4 Å) of helix VI is also observed in the purinergic receptor P2Y₁₂ structure^{19,20} (Extended data Fig. 6a). The balloon-like flexibility of CB₁ in the extracellular region may also occur in other GPCRs. Therefore, while designing GPCR agonists and antagonists using structure-based strategies, multiple, structurally varied receptor models should be considered.

Online Content Methods, along with any additional Extended Data display items and Source Data, are available in the online version of the paper; references unique to these sections appear only in the online paper.

Received 6 April; accepted 15 June 2017.

Published online 5 July 2017.

- Mechoulam, R., Hanuš, L. O., Pertwee, R. & Howlett, A. C. Early phytocannabinoid chemistry to endocannabinoids and beyond. *Nat. Rev. Neurosci.* **15**, 757–764 (2014).
- Hua, T. et al. Crystal structure of the human cannabinoid receptor CB1. *Cell* **167**, 750–762 e714 (2016).
- Ballesteros, J. A. & Weinstein, H. in *Methods in Neurosciences* Vol. 25 (ed. Sealfon Stuart, C.) 366–428 (Academic, 1995).
- Lemberger, L. Potential therapeutic usefulness of marijuana. *Annu. Rev. Pharmacol. Toxicol.* **20**, 151–172 (1980).
- Li, H.-L. An archaeological and historical account of cannabis in China. *Econ. Bot.* **28**, 437–448 (1973).
- Makriyannis, A. 2012 Division of Medicinal Chemistry Award Address. Trekking the cannabinoid road: a personal perspective. *J. Med. Chem.* **57**, 3891–3911 (2014).
- Shao, Z. et al. High-resolution crystal structure of the human CB1 cannabinoid receptor. *Nature* **540**, 602–606 (2016).
- Nikas, S. P. et al. The role of halogen substitution in classical cannabinoids: a CB₁ pharmacophore model. *AAPS J.* **6**, e30 (2004).
- Nikas, S. P. et al. Novel 1',1'-chain substituted hexahydrocannabinols: 9 β -hydroxy-3-(1-hexyl-cyclobut-1-yl)-hexahydrocannabinol (AM2389) a highly potent cannabinoid receptor 1 (CB₁) agonist. *J. Med. Chem.* **53**, 6996–7010 (2010).

- Xie, X. Q., Melvin, L. S. & Makriyannis, A. The conformational properties of the highly selective cannabinoid receptor ligand CP-55,940. *J. Biol. Chem.* **271**, 10640–10647 (1996).
- Makriyannis, A. & Rapaka, R. S. The medicinal chemistry of cannabinoids: an overview. *NIDA Res. Monogr.* **79**, 204–210 (1987).
- Ahn, K. H., Bertalovitz, A. C., Mierke, D. F. & Kendall, D. A. Dual role of the second extracellular loop of the cannabinoid receptor 1: ligand binding and receptor localization. *Mol. Pharmacol.* **76**, 833–842 (2009).
- Feigenbaum, J. J. et al. Nonpsychotropic cannabinoid acts as a functional N-methyl-d-aspartate receptor blocker. *Proc. Natl. Acad. Sci. USA* **86**, 9584–9587 (1989).
- Mechoulam, R. et al. Enantiomeric cannabinoids: stereospecificity of psychotropic activity. *Experientia* **44**, 762–764 (1988).
- Hanson, M. A. et al. Crystal structure of a lipid G protein-coupled receptor. *Science* **335**, 851–855 (2012).
- Rasmussen, S. G. et al. Crystal structure of the β_2 adrenergic receptor–Gs protein complex. *Nature* **477**, 549–555 (2011).
- Singh, R. et al. Activation of the cannabinoid CB1 receptor may involve a W6.48/F3.36 rotamer toggle switch. *J. Pept. Res.* **60**, 357–370 (2002).
- Tiburk, E. K. et al. Structural biology of human cannabinoid receptor-2 helix 6 in membrane-mimetic environments. *Biochem. Biophys. Res. Commun.* **384**, 243–248 (2009).
- Zhang, K. et al. Structure of the human P2Y₁₂ receptor in complex with an antithrombotic drug. *Nature* **509**, 115–118 (2014).
- Zhang, J. et al. Agonist-bound structure of the human P2Y₁₂ receptor. *Nature* **509**, 119–122 (2014).

Supplementary Information is available in the online version of the paper.

Acknowledgements This work was supported by the NSF of China grant 31330019 (Z.-J.L.), the MOST of China grants 2014CB910400 (Z.-J.L.) and 2015CB910104 (Z.-J.L.), NSF of Shanghai 16ZR1448500 grant (S.Z.), Key R&D Program of China grant 2016YCF0905902 (S.Z.), NIH grants R01DA041435 (R.C.S., A.M.), P01DA009158 (A.M., L.M.B.), R37DA023142 (A.M.), NSF grants, Shanghai Municipal Government, ShanghaiTech University and GPCR Consortium. The diffraction data were collected at GM/CA@APS of Argonne National Laboratory, X06SA@SLS of the Paul Scherrer Institute, and BL41XU@ Spring-8 with JASRI proposals 2015B1031 and 2016A2731. We thank M. Wang, C.-Y. Huang, V. Olieric, M. Audet and M.-Y. Lee for their help with data collection, A. Walker for critical review of the manuscript, and F. Sun for high-resolution mass spectrometry analysis.

Author Contributions T.H.: crystallization, data collection, structure determination and analysis; K.V., S.P.N., S.J.: design, synthesis and characterization of ligands; Y.W.: docking, molecular dynamics simulation; L.Q., M.P.: data collection and processing, structure refinement; G.W.H., M.A.H.: structure refinement and data analysis. R.B.L. and J.-H.H.: functional studies, mutations; A.K.: radioligand binding assays; K.D.: structure analysis; X.L. and H.L.: molecular dynamics simulations; S.Z.: supervision of structure and simulation analysis; L.M.B.: design and supervision of functional and kinetic studies; A.M.: supervision on agonist conceptual design, synthesis and characterization; R.C.S.: project conception, data analysis supervision; Z.J.L.: design and supervision of experiments, data analysis; Z.J.L., T.H., R.C.S., A.M., L.M.B. and S.Z. wrote the manuscript with discussions and improvements from M.A.H., K.V., S.P.N. and Y.W.

Author Information Reprints and permissions information is available at www.nature.com/reprints. The authors declare competing financial interests: details are available in the online version of the paper. Readers are welcome to comment on the online version of the paper. Publisher’s note: Springer Nature remains neutral with regard to jurisdictional claims in published maps and institutional affiliations. Correspondence and requests for materials should be addressed to Z.-J.L. (liuzhi@shanghaitech.edu.cn), A.M. (a.makriyannis@northeastern.edu), L.M.B. (lbohn@scripps.edu) or S.Z. (zhaosw@shanghaitech.edu.cn).

Reviewer Information *Nature* thanks G. Kunos and the other anonymous reviewer(s) for their contribution to the peer review of this work.

METHODS

No statistical methods were used to predetermine sample size. However, for mutants in the cAMP accumulation assays, after an $n = 3$ was obtained, an additional power analysis was performed ($\alpha = 0.05$; power = 80%) to determine the n required to have confidence in the values produced; additional curves were added as indicated.

Synthesis of AM11542 and AM841: experimental procedures and spectroscopic data. Experimental procedures for steps a–m (Extended Data Fig. 1) are similar to those we reported earlier for closely related systems^{9,21,22}.

{(6aR,9R,10aR)-3-(8-bromo-2-methyloctan-2-yl)-1-((tert-butylidimethylsilyl)oxy)-6,6-dimethyl-6a,7,8,9,10,10a-hexahydro-6H-benzo[c]chromene-9-carbaldehyde (12). Colourless oil. ^1H NMR (500 MHz, CDCl_3) δ 9.63 (d, $J = 1.5$ Hz, 1H, 9β-CHO), 6.38 (d, $J = 2.0$ Hz, 1H, Ar-H), 6.32 (d, $J = 2.0$ Hz, 1H, Ar-H), 3.52–3.46 (t and m as br d overlapping, t, $J = 6.5$ Hz, 2H, $-\text{CH}_2\text{Br}$, m as br d, $J = 13.5$ Hz, 1H, C-ring), 2.46–2.33 (m, 2H, C-ring), 2.14–2.06 (m, 1H, C-ring), 2.02–1.96 (m, 1H, C-ring), 1.69 (sextet, $J = 6.7$ Hz, 2H, 6'-H), 1.52–1.42 (m, 4H, 2'-H, C-ring), 1.42–1.30 (m and s, overlapping, 5H, $-\text{CH}_2$ - of the side chain and 1.39, s, 6-Me), 1.26–1.10 (m, 10H, $-\text{CH}_2$ - of the side chain, C-ring and $-\text{C}(\text{CH}_3)_2$), 1.09–1.00 (m, s and s, overlapping, 14H as follows: 2H, $-\text{CH}_2$ - of the side chain, 1.08, s, 3H, 6-Me, 1.01, s, 9H, $-\text{Si}(\text{Me})_2\text{CMe}_3$), 0.26 (s, 3H, $-\text{Si}(\text{Me})_2\text{CMe}_3$), 0.15 (s, 3H, $-\text{Si}(\text{Me})_2\text{CMe}_3$). ^{13}C NMR (100 MHz, CDCl_3) δ 203.5, 154.5, 154.2, 149.5, 112.5, 109.5, 108.4, 105.4, 104.0, 45.0, 44.4, 37.3, 35.4, 32.6, 30.2, 29.5, 28.8, 28.6, 27.6, 26.9, 26.8, 25.9, 24.5, 18.8, 18.2, –3.6–4.2. HRMS (m/z): [M + H]⁺ calculated for $\text{C}_{31}\text{H}_{52}\text{O}_3^{79}\text{BrSi}$, 579.2869; found, 579.2862; calculated for $\text{C}_{31}\text{H}_{52}\text{O}_3^{81}\text{BrSi}$, 581.2849; found, 581.2850.

{(6aR,9R,10aR)-3-(8-Bromo-2-methyloctan-2-yl)-1-[(tert-butylidimethylsilyl)oxy]-6,6-dimethyl-6a,7,8,9,10,10a-hexahydro-6H-benzo[c]chromen-9-yl]methanol (13). Colourless viscous oil. ^1H NMR (500 MHz, CDCl_3) δ 6.37 (d, $J = 2.0$ Hz, 1H, Ar-H), 6.30 (d, $J = 2.0$ Hz, 1H, Ar-H), 3.54 (dd, $J = 10.5$ Hz, $J = 5.5$ Hz, half of an AB system, 1H, $-\text{CH}_2\text{OH}$), 3.50–3.43 (dd and t overlapping, especially, 3.48, t, $J = 6.5$, 7'-H, dd, $J = 10.0$ Hz, $J = 6.5$ Hz, half of an AB system, 1H, $-\text{CH}_2\text{OH}$), 3.18–3.16 (m as br d, $J = 13.0$ Hz, 1H, C-ring), 2.40–2.32 (m as td, $J = 11.0$ Hz, $J = 3.0$ Hz, 1H, C-ring), 2.04–1.97 (m, 1H, C-ring), 1.94–1.88 (m, 1H, C-ring), 1.8–1.64 (m, 1H, C-ring, 2H, 6'-H), 1.52–1.44 (m, 3H, 2'-H, C-ring), 1.4–1.3 (m and s overlapping, 5H, $-\text{CH}_2$ - of the side chain, 6-Me, especially 1.25, s, 3H, 6-Me), 1.24–1.1 (m, s, and s overlapping, 10H, $-\text{C}(\text{CH}_3)_2$, $-\text{CH}_2$ - of the side chain, C-ring, especially, 1.20, s, 3H, $-\text{C}(\text{CH}_3)_2$, and 1.19, s, 3H, $-\text{C}(\text{CH}_3)_2$), 1.09–1.02 (s and m overlapping, 5H, 6-Me, $-\text{CH}_2$ - of the side chain, especially, 1.06, s, 3H, 6-Me), 1.0 (s, 9H, $-\text{Si}(\text{Me})_2\text{CMe}_3$), 0.82–0.7 (m, 1H, C-ring), 0.23 (s, 3H, $-\text{Si}(\text{Me})_2\text{CMe}_3$), 0.12 (s, 3H, $-\text{Si}(\text{Me})_2\text{CMe}_3$). ^{13}C NMR (100 MHz, CDCl_3) δ 154.5, 154.3, 149.0, 113.5, 109.7, 108.4, 68.5, 49.6, 45.1, 44.4, 40.5, 37.2, 35.5, 33.2, 32.6, 29.8, 29.5, 28.8, 28.6, 27.6, 27.5, 26.8, 25.9, 24.5, 18.8, 18.2, –3.6–4.3. HRMS (m/z): [M + H]⁺ calculated for $\text{C}_{31}\text{H}_{54}\text{O}_3^{79}\text{BrSi}$, 581.3026; found, 581.3018; calculated for $\text{C}_{31}\text{H}_{54}\text{O}_3^{81}\text{BrSi}$, 583.3005; found, 583.3007.

(6aR,9R,10aR)-3-(8-Bromo-2-methyloctan-2-yl)-9-(hydroxymethyl)-6,6-dimethyl-6a,7,8,9,10,10a-hexahydro-6H-benzo[c]chromen-1-ol (14). To a solution of 13 (210 mg, 0.36 mmol) in anhydrous THF (9 ml) at –40 °C, under an argon atmosphere, was added tetra-*n*-butylammonium fluoride (0.72 ml, 0.72 mmol, 1 M solution in anhydrous THF). The reaction mixture was stirred for 30 min at the same temperature, and then quenched using a saturated aqueous NH_4Cl solution. Extractive isolation with diethyl ether, and purification by flash column chromatography on silica gel (20–50% ethyl acetate in hexane) gave 14 (164 mg, 96% yield) as a white solid. Melting point = 68–70 °C. ^1H NMR (500 MHz, CDCl_3) δ 6.35 (d, $J = 1.0$ Hz, 1H, Ar-H), 6.18 (d, $J = 1.5$ Hz, 1H, Ar-H), 4.75 (br s, 1H, ArOH), 3.61–3.42 (m and t overlapping, 4H, $-\text{CH}_2\text{OH}$, 7'-H, especially, 3.49, t, $J = 6.5$ Hz, 2H, $-\text{CH}_2\text{OH}$), 3.23–3.16 (m as br d, $J = 13.0$ Hz, 1H, C-ring), 2.52–2.44 (m as td, $J = 11.0$ Hz, $J = 2.5$ Hz, 1H, C-ring), 2.02–1.91 (m, 2H, C-ring), 1.82–1.74 (m, 1H, C-ring), 1.72–1.64 (m, 1H, 6'-H), 1.54–1.46 (m, 3H, 2'-H, C-ring), 1.44–1.31 (s and m overlapping, 5H, 6-Me, $-\text{CH}_2$ - of the side chain, especially, 1.39, s, 3H, 6-Me), 1.29–1.15 (s, and m overlapping, 10H, $-\text{C}(\text{CH}_3)_2$, $-\text{CH}_2$ - of the side chain, C-ring, especially, 1.20, s, 6H, $-\text{C}(\text{CH}_3)_2$), 1.10–1.01 (s and m overlapping, 5H, 6-Me, $-\text{CH}_2$ - of the side chain, especially, 1.09, s, 3H, 6-Me), 0.89–0.78 (m as q, $J = 11.5$ Hz, 1H, C-ring). ^{13}C NMR (100 MHz, CDCl_3) δ 154.7, 154.4, 149.7, 109.6, 107.9, 105.4, 68.5, 49.3, 45.2, 44.2, 40.5, 37.2, 34.9, 33.1, 32.6, 29.7, 29.5, 28.7, 28.6, 27.7, 27.4, 26.7, 24.4, 19.0. HRMS (m/z): [M + H]⁺ calculated for $\text{C}_{25}\text{H}_{40}\text{O}_3^{79}\text{Br}$, 467.2161; found, 467.2162; calculated for $\text{C}_{25}\text{H}_{40}\text{O}_3^{81}\text{Br}$, 469.2140; found, 469.2144.

(6aR,9R,10aR)-3-(8-Azido-2-methyloctan-2-yl)-9-(hydroxymethyl)-6,6-dimethyl-6a,7,8,9,10,10a-hexahydro-6H-benzo[c]chromen-1-ol (15). To a stirred solution of 14 (160 mg, 0.34 mmol) in anhydrous $\text{CH}_3\text{Cl}/\text{CH}_3\text{NO}_2$ (1:1 mixture, 6 ml) at room temperature, under an argon atmosphere was added N,N,N',N' -tetramethylguanidinium azide (1.6 g, 10.2 mmol) and stirring was continued for 1 day. On completion, the reaction was quenched with water and diluted with

CH_2Cl_2 . The organic phase was washed with brine, dried over MgSO_4 and concentrated *in vacuo*. Purification by flash column chromatography on silica gel (50–80% diethyl ether in hexanes) gave 15 as a white solid in 84% yield. Melting point = 59–61 °C; IR (neat) 3343 (br, OH), 2931, 2860, 2093 (s, N₃), 1713, 1621, 1537, 1413, 1331, 1268, 1138, 1011, 967, 839 cm^{–1}; ^1H NMR (500 MHz, CDCl_3) 8.635 (d, $J = 1.0$ Hz, 1H, Ar-H), 6.19 (d, $J = 1.5$ Hz, 1H, Ar-H), 4.81 (br s, 1H, AroOH), 3.57–3.47 (m, 2H, $-\text{CH}_2\text{OH}$), 3.23–3.17 (m and t overlapping 3H, C-ring, 7'-H, especially, 3.21, t, $J = 6.5$ Hz, 2H, 7'-H), 2.52–2.44 (m as td, $J = 11.0$ Hz, $J = 2.5$ Hz, 1H, C-ring), 2.02–1.91 (m, 2H, C-ring), 1.82–1.74 (m, 1H, C-ring), 1.56–1.46 (m 5H, 6'-H, 2'-H, C-ring), 1.38 (s, 3H, 6-Me), 1.35–1.26 (m, 2H, $-\text{CH}_2$ - of the side chain), 1.25–1.11 (s and m overlapping, 10H, $-\text{C}(\text{CH}_3)_2$, $-\text{CH}_2$ - of the side chain, C-ring, especially, 1.20, s, 6H, $-\text{C}(\text{CH}_3)_2$), 1.10–1.02 (s and m overlapping, 5H, 6-Me, $-\text{CH}_2$ - of the side chain, especially, 1.09, s, 3H, 6-Me), 0.87–0.78 (m as q, $J = 12$ Hz, 1H, C-ring). ^{13}C NMR (100 MHz, CDCl_3) δ 154.6, 154.5, 149.7, 109.6, 107.8, 105.4, 68.5, 51.5, 49.3, 44.2, 40.5, 37.2, 34.9, 33.1, 29.7, 29.6, 28.8, 28.7, 27.7, 27.4, 26.5, 24.4, 19.0. HRMS (m/z): [M]⁺ calculated for $\text{C}_{25}\text{H}_{40}\text{N}_3\text{O}_3$, 430.3070; found, 430.3065.

(6aR,9R,10aR)-9-(Hydroxymethyl)-3-(8-isothiocyanato-2-methyloctan-2-yl)-6,6-dimethyl-6a,7,8,9,10,10a-hexahydro-6H-benzo[c]chromen-1-ol (AM841). To a solution of 15 (120 mg, 0.28 mmol), in anhydrous THF (5.6 ml) at room temperature, was added triphenyl phosphine (365 mg, 1.4 mmol). Carbon disulfide (0.55 ml, 8.4 mmol) was then added dropwise and the reaction mixture was stirred for an additional 10 h at the same temperature. Upon completion, the reaction mixture was concentrated under reduced pressure and purified by flash column chromatography on silica gel (50–80% diethyl ether in hexanes) to give 95 mg of AM841 as white solid in 76% yield. Melting point = 63–65 °C. IR (neat) 3332 (br, OH), 2931, 2860, 2093 (s, NCS), 1620, 1537, 1451, 1413, 1331, 1269, 1137, 1037, 966, 838 cm^{–1}; ^1H NMR (500 MHz, CDCl_3) 8.635 (d, $J = 1.5$ Hz, 1H, Ar-H), 6.19 (d, $J = 2.0$ Hz, 1H, Ar-H), 4.76 (br s, 1H, ArOH), 3.52 (m, 2H, $-\text{CH}_2\text{OH}$), 3.46 (t, $J = 6.5$ Hz, 2H, 7'-H), 3.22–3.16 (m as d, $J = 13$ Hz, 1H, C-ring), 2.51–2.44 (m as td, $J = 11.0$ Hz, $J = 2.5$ Hz, 1H, C-ring), 2.02–1.91 (m, 2H, C-ring), 1.82–1.74 (m, 1H, C-ring), 1.65–1.56 (m, 2H, 6'-H), 1.54–1.46 (m, 3H, 2'-H, C-ring), 1.39 (s, 3H, 6-Me), 1.37–1.29 (m, 2H, $-\text{CH}_2$ - of the side chain group), 1.26–1.11 (s and m overlapping, 10H, $-\text{C}(\text{CH}_3)_2$, $-\text{CH}_2$ - of the side chain, C-ring, especially, 1.20, s, 6H, $-\text{C}(\text{CH}_3)_2$), 1.10–1.03 (s and m overlapping, 5H, 6-Me, $-\text{CH}_2$ - of the side chain, especially, 1.09, s, 3H, 6-Me), 0.87–0.7 (m as q, $J = 12$ Hz, 1H, C-ring); ^{13}C NMR (100 MHz, CDCl_3) δ 154.6 (ArC-1 or ArC-5), 154.5 (ArC-5 or ArC-1), 130.1 (NCS), 149.6 (tertiary aromatic), 109.7 (tertiary aromatic), 107.8 (ArC-2 or ArC-4), 105.3 (ArC-4 or ArC-2), 68.5 (– CH_2OH), 49.3, 45.0, 44.1, 40.5, 37.2, 35.0, 33.1, 29.8, 29.7, 29.3, 28.7, 28.6, 27.7, 27.4, 26.3, 24.3, 19.0. HRMS (m/z): [M]⁺ calculated for $\text{C}_{26}\text{H}_{40}\text{NO}_3\text{S}$, 446.2729; found, 446.2726.

(–)7'-Bromo-1',1'-dimethylheptyl- Δ^8 -tetrahydrocannabinol (AM11542). Experimental procedures for the synthesis and purification, along with spectroscopic and analytical data were reported earlier from our laboratory⁸.

Purification of CB₁-flavodoxin protein and crystallization in lipidic cubic phase. CB₁-flavodoxin construction, expression and membrane preparation were performed using the same procedure as described before². In brief, the construct has truncations of residues 1–98, 307–331 and 415–472, the flavodoxin (PDB accession 1I1O, molecular mass 14.9 kDa, with Y98W mutation) fusion protein was fused to the truncated third intracellular loop of the human CNR1 (also known as CB1) gene. The resulting CB₁-flavodoxin chimaera sequence was subcloned into a modified mammalian expression vector pTT5 that contains a haemagglutinin (HA) signal sequence, a Flag tag and 10× His tag, followed by a tobacco etch virus (TEV) protease cleavage site, before the N terminus of the chimaera sequence. The CNR1 gene was further modified by introducing four rationally designed mutations²³, Thr210^{3,46}Ala, Glu273^{5,37}Lys, Thr283^{5,47}Val and Arg340^{6,32}Glu, using standard QuickChange PCR. The protein was expressed using the FreeStyle 293 Expression system (Invitrogen) in HEK293F cells for 48 h, and the membrane was washed repeatedly using hypotonic buffer with low and high salt. Notably, the receptor used for crystallization was capable of binding to [³H]CP55,940 and this binding could be replaced by AM11542 ($K_i = 0.29$ (0.17–0.50) nM); AM841 ($K_i = 0.53$ (0.36–0.80) nM) as the wild-type receptor, and cold CP55,940 ($K_i = 2.0$ (1.2–3.5) nM). This CB₁ construct yielded no signalling in signalling assays (not shown), which is probably due to the flavodoxin insert that prevents coupling secondary effectors. However, the individual point mutations did not interfere with agonist activity except for Thr210^{3,46}Ala, which has been previously reported²³. These controls are summarized in Extended Data Fig. 4c and Extended Data Table 2.

Purified membranes were thawed at room temperature and then incubated with 20 μM corresponding ligand (AM11542 or AM841) in the presence of 1.0 mg ml^{–1} iodoacetamide, and EDTA-free protease inhibitor cocktail (Roche) for 30 min at room temperature, and then further incubated at 4 °C for 3 h. The membranes were then solubilized with 50 mM HEPES (pH 7.5), 500 mM NaCl, 1% (w/v)

lauryl maltose neopentyl glycol (LMNG, Anatrace) and 0.2% (w/v) cholesterol hemisuccinate (CHS, Sigma-Aldrich) at 4 °C for 2.5–3.0 h. The supernatants containing the solubilized CB₁ proteins were isolated by high-speed centrifugation, and then incubated with TALON IMAC resin (Clontech) and 20 mM imidazole, at 4 °C overnight. The resin was washed with 15 column volumes of washing buffer I containing 25 mM HEPES (pH 7.5), 500 mM NaCl, 10% (v/v) glycerol, 0.1% (w/v) LMNG, 0.02% (w/v) CHS, 30 mM imidazole and 20 μM AM11542 or AM841, and 5 column volumes of washing buffer II containing 25 mM HEPES (pH 7.5), 500 mM NaCl, 10% (v/v) glycerol, 0.03% (w/v) LMNG, 0.015% (w/v) CHS, 50 mM imidazole and 20 μM AM11542 or AM841. The proteins were eluted by 2.5 column volumes of eluting buffer containing 25 mM HEPES (pH 7.5), 500 mM NaCl, 10% (v/v) glycerol, 0.01% (w/v) LMNG, 0.002% (w/v) CHS, 250 mM imidazole and 20 μM AM11542 or AM841. PD MiniTrap G-25 column (GE Healthcare) was used to remove imidazole. The protein was then treated overnight with TEV protease to cleave the N-terminal Flag/His tags from the proteins. Finally, the purified CB₁ protein together with TEV protease was concentrated to about 35 mg ml⁻¹ with a 100 kDa cutoff concentrator (Sartorius) and used in crystallization trials. The protein yield and monodispersity were tested by analytical size exclusion chromatography.

Protein samples were reconstituted into lipidic cubic phase (LCP) by mixing with molten lipid (90% (w/v) monolein and 10% (w/v) cholesterol) at a protein/lipid ratio of 2.3 (v/v) using a mechanical syringe mixer²⁴. LCP crystallization trials were performed using an NT8-LCP crystallization robot (Formulatrix). 96-well glass sandwich plates were incubated and imaged at 20 °C using an automatic incubator/imager (RockImager 1000, Formulatrix). For the CB₁-AM11542 complex, the crystals grew in conditions of 0.1 M sodium cacodylate trihydrate pH 6.4, 300–350 mM C₄H₄KNaO₆, 30% PEG400 and grew to the full size within 1 week. For the CB₁-AM841 complex, the crystals appeared after 2 days in 0.1 M sodium cacodylate trihydrate pH 6.2, 120 mM C₆H₅Na₃O₇·2H₂O, 30% PEG400 and 100 mM glycine and reached their full size after 1 week. The crystals were harvested using micromounts (MiTeGen) and flash-frozen in liquid nitrogen.

Data collection, structure solution and refinement. X-ray diffraction data were collected at GM/CA-CAT beamline 23ID-B at the Advanced Photon Source (APS), Argonne National Laboratory IL, using an Eiger 16 M detector (X-ray wavelength 1.0000 Å) and at beamline X06SA of the Swiss Light Source. The crystals were exposed with a 10 μm minibeam for 0.2 s and 0.2° oscillation per frame, a rastering system was applied to find the best diffracting parts of single crystals^{25,26}. XDS²⁷ was used for integrating and scaling data from the 16 crystals for the CB₁-AM11542 complex and 10 crystals for the CB₁-AM841 complex. Initial phase information was obtained by molecular replacement with Phaser²⁸ using the receptor portion of CB₁ (PDB code 5TGZ) and flavodoxin structure (PDB code 1I1O) as search models. Refinement was performed with Phenix²⁹ and Buster³⁰ followed by manual examination and rebuilding of the refined coordinates in the program COOT³¹ using both |2F_o| - |F_c| and |F_o| - |F_c| maps.

Radioligand binding assay. Radioligand binding to determine agonist affinity and wash resistant residency was determined as previously described² using [³H]CP55,940 (specific activity: 81.1 Ci mmol⁻¹, NDSP, NIDA) and an excess of CP55,940 to determine nonspecific binding. Specifically for wash out experiments at the wild-type CB₁, membranes were incubated at 37 °C for 1 h in the presence of vehicle (buffer with 1% DMSO), 1 nM AM11542, 10 nM AM841 or 4 nM CP55,940 followed by resuspension in assay buffer containing 1% BSA and incubated at 37 °C for 30 min (to remove non-specifically bound ligand); this was repeated twice to wash away bound ligands before the saturation radioligand binding assay on membranes (37 °C for 1–4 h as indicated). K_i and B_{max} calculations were performed by nonlinear regression analysis using GraphPad Prism 7.0, n = 3–6.

Wild-type and mutant CB₁-CHO cell line generation for functional studies. Cell line generation and maintenance was conducted as described previously² and briefly described here. The N terminus 3 × HA-tagged CB₁ cDNA was obtained from <http://cDNA.org> and subcloned into a mouse stem-cell virus for cell line transduction (pMSCV-puro, Clontech). Point mutations were introduced to the N terminus 3 × HA-tagged CB₁ cDNA in MSCV retroviral vector by using Q5 Site-Directed Mutagenesis kit (New England Biolabs) (F177A, L193A, D213A, Y275A, Y275F, F379A, F379W, S383A). Generation of F379 mutants was described previously². Wild-type and mutant CB₁ constructs were packaged into retrovirus via Phoenix package system (Allele Biotechnology cat. no. ABP-RVC-10001), and the produced retroviruses were applied to CHO-K1 (ATCC cat. no. CCL-61) cells for gene transduction. Cells were maintained in DMEM/F-12 media supplemented with 10% fetal bovine serum, 1% penicillin/streptomycin, and 5 mg ml⁻¹ puromycin (Invitrogen) for stable line selection at 37 °C (5% CO₂ and 95% relative humidity). Cell lines were negative for mycoplasma. See Extended Data Fig. 4a for primers used to make mutant CB₁ receptors.

Quantitative flow cytometry. Validation of cell-surface expression of the HA-tagged wild-type and mutant CB₁ receptors expressed in CHO-K1 cells was obtained by anti-HA antibody staining followed by quantitative flow cytometry and visually confirmed by confocal imaging. In brief, cells were serum-starved 30 min at 37 °C and collected in 5 mM EDTA and fixed with 4% paraformaldehyde for 10 min at 4 °C. Cells were washed twice with PBS and resuspended in PBS containing 1% FBS and 5 mM EDTA. Cells were incubated with anti-HA AlexaFluor488-conjugated antibody (1:1,000) for 30 min at 4 °C, washed twice with PBS and again resuspended in PBS containing 1% FBS and 5 mM EDTA. Fluorescence was recorded using a BD Canto flow cytometer (excitation/emission: 488/525 nm). Approximately 50,000 events were recorded for each cell line. Data are expressed as the percentage of positive-fluorescent cells from 50,000 events recorded (3 × HA-CB₁ CHO wild-type = 65%) and relative to 3 × HA-CB₁ wild-type CHO (100%). Untransfected CHO cells had 0% fluorescence. See Extended Data Fig. 4a for primers used to make mutant CB₁ receptors and surface expression comparisons of all mutants reported herein. See Supplementary Fig. 1 for flow cytometry graphs.

cAMP accumulation assay. Inhibition of forskolin-stimulated cAMP was determined using the CISBIO cAMP Homogeneous Time-Resolved Fluorescence resonance energy transfer (FRET) (HTRF) (Cisbio Assays) as previously described².

Docking and molecular dynamics simulations. Prediction of ligand binding to CB₁ was carried out with Schrödinger Suite 2015-4. Processing of the protein structure was performed with the 'Protein Preparation Wizard'. Converting of ligands from 2D to 3D structures was performed using 'LigPrep'. Rigid protein docking in extra precision was used with Glide 6.9^{32–34} (induced fit docking protocol 2015-4, Glide v.6.4, Primer v.3.7, Schrödinger LLC; <https://www.schrodinger.com/induced-fit>) for molecular docking.

Molecular dynamics simulation was performed using GROMACS 5.1.2³⁵, using force field Amber 14 (AMBER 2017; <http://ambermd.org/>). CB₁ in complex with each agonist in the pocket (binding modes predicted by molecular docking) was embedded into a pre-equilibrated POPC (1-palmytoyl-2-oleoyl-sn-glycerol-3-phosphatidylcholine) lipid bilayer using the membed tool in GROMACS program. The topology files of ligands and POPC molecules were generated using AmberTools in UCSF Chimera program³⁶ version 1.10.2 and converted to GROMACS format with ACPYPE tool³⁷. The systems were solvated with water, sodium ions were added to 0.15 M in water, and chloride ions were added to neutralize the system. Molecular dynamics simulations were performed in the NPT ensemble, at a temperature of 310 K and pressure of 1 atm using semi-isotropic coupling. First, each system was balanced position-restrained MD for 15 ns (total energy was stable). Then 1 μs molecular dynamics simulations with no position restraints were performed to each system for two independent runs, and these trajectories are used for analysis. Ligand r.m.s.d. value was calculated with protein C_α atoms superimposed to the starting structure.

Comparison of agonist- and antagonist-bound class A GPCRs structures. Seventeen crystal structures of seven GPCRs that have both agonist- and antagonist-bound structures were selected from the PDB³⁸. Among them, there are 24, 32 and 21 structures for the β₂-adrenergic receptor, rhodopsin and A_{2A} adenosine receptor, respectively. To pick representative structures of the three GPCRs, their PDB structures were clustered by R package Bio3D³⁹ based on r.m.s.d. differences. The following structures from each cluster were manually picked. Agonist/arrestin-bound structures include CB₁ (this study; PDB code 5XRA), β₂-adrenergic receptor (PDB codes 3SN6, 4LDL), μ-opioid receptor (PDB code 5C1M), M₂ muscarinic receptor (PDB code 4MQS), rhodopsin (PDB codes 2X72, 4ZWJ (arrestin-bound)), A_{2A} adenosine receptor (PDB codes 3QAK, 5G53) and P_{2Y} purinoceptor 12 (PDB code 4PXZ). Antagonist-bound structures include CB₁ (PDB code 5TGZ), β₂-adrenergic receptor (PDB code 3NY8), μ-opioid receptor (PDB code 4DKL), M₂ muscarinic receptor (PDB code 3UON), rhodopsin (PDB code 1U19), A_{2A} adenosine receptor (PDB code 4EIY) and P_{2Y} purinoceptor 12 (PDB code 4NTJ).

Binding pocket volume calculation. These structures were processed by 'Protein Preparation Wizard' in Schrödinger Suite 2015-4 (<https://www.schrodinger.com/protein-preparation-wizard>). The volume of binding pockets was calculated by 'Sitemap' (<https://www.schrodinger.com/sitemap>).

The r.m.s.d. values of extracellular/intracellular transmembrane helices. Seven conserved residues close to the middle point of each helix with Ballesteros-Weinstein numbering 1.50, 2.50, 3.39, 4.50, 5.50, 6.50 and 7.49 were used to divide the seven transmembrane helices into extracellular and intracellular parts. The whole structures of each pair of agonist/antagonist-bound structures were aligned in UCSF Chimera³⁶, then the r.m.s.d. values of C_α atoms in the extracellular and intracellular parts were calculated in UCSF Chimera.

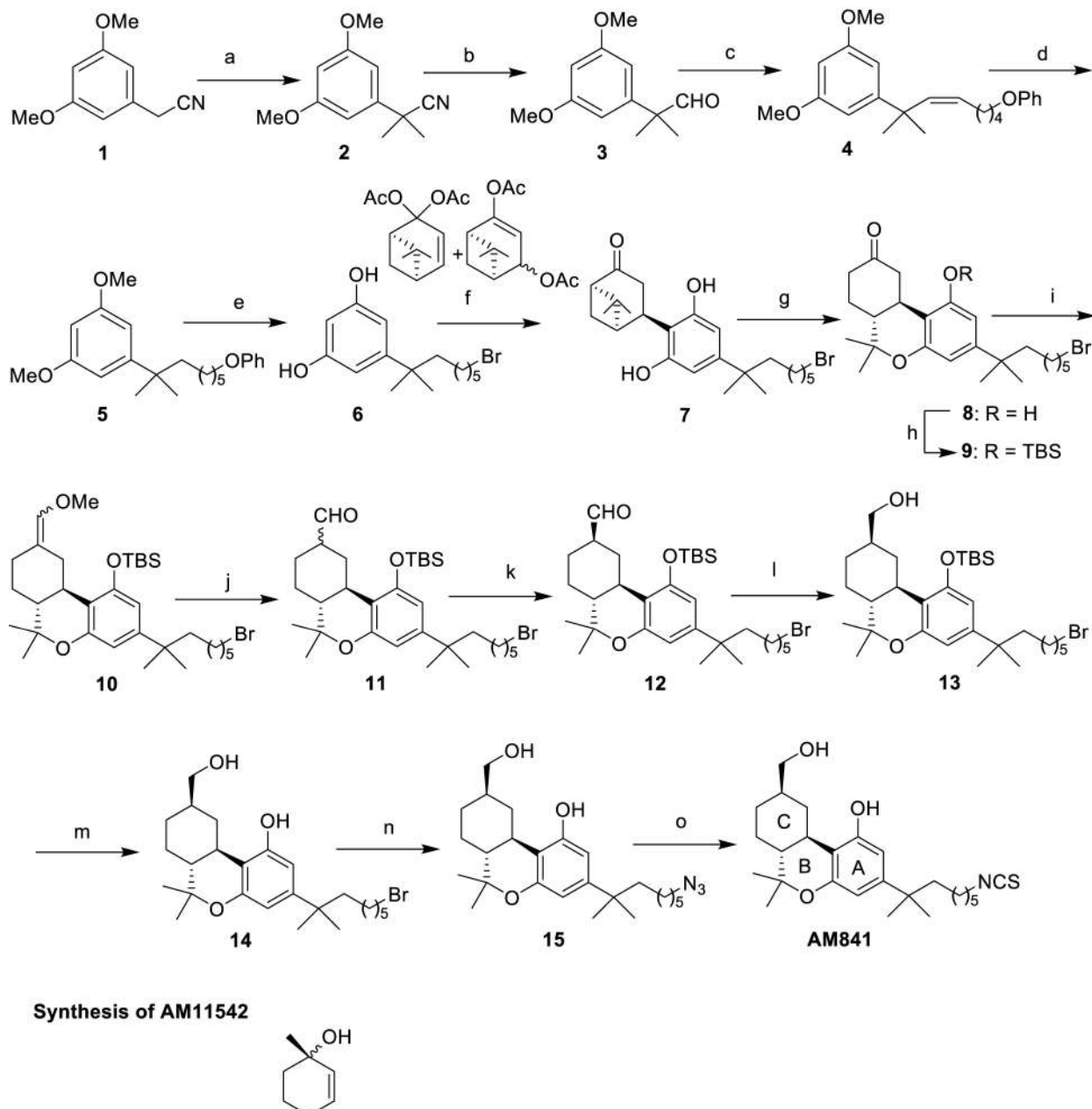
Quantification and statistical analysis. Concentration-response curves expressed as fold over basal, were fit to a nonlinear regression (three parameter) model in

Prism (v7.0, GraphPad Software Inc.). For functional analysis of wild-type and CB₁ mutants, pEC₅₀ and E_{max} values were calculated from nonlinear regression (three parameter) analysis of mean data from independent experiments performed in duplicate. In Fig. 1d, CP55,940 served as an assay control and was assayed in parallel with all compounds; n = 11 for CP55,940, n = 6 for AM11542, n = 5 for AM841 and n = 6 for THC. In Extended Data Table 2, n = 3 independent experiments performed in duplicate for all mutants except F177A (n = 4), T210A (n = 4 for AM841 and CP55,940) and wild type (n = 7 for AM841 and CP55,940; n = 6 for AM11542). Statistical analyses comparing pEC₅₀ between CB₁ wild-type and mutant lines were conducted using two-way ANOVA followed by Dunnett's post hoc test in the Prism software, v.7.0.

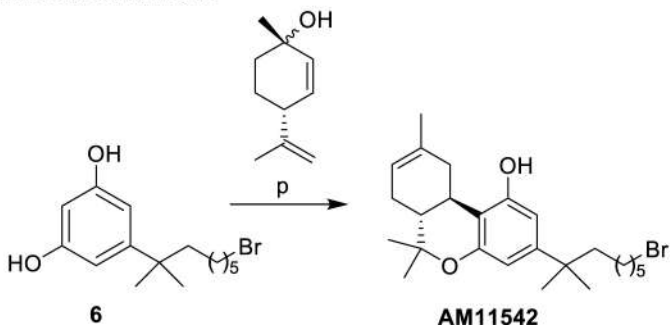
Data availability. Atomic coordinates and structures have been deposited in the Protein Data Bank (PDB) with accession codes 5XRA (CB₁-AM11542) and 5XR8 (CB₁-AM841). All other data are available from the corresponding authors upon reasonable request.

21. Nikas, S. P. et al. A concise methodology for the synthesis of (−)-Δ⁹-tetrahydrocannabinol and (−)-Δ⁹-tetrahydrocannabivarin metabolites and their regiospecifically deuterated analogs. *Tetrahedron* **63**, 8112–8113 (2007).
22. Kulkarni, S. et al. Novel C-ring-hydroxy-substituted controlled deactivation cannabinergic analogues. *J. Med. Chem.* **59**, 6903–6919 (2016).
23. D'Antona, A. M., Ahn, K. H. & Kendall, D. A. Mutations of CB₁ T210 produce active and inactive receptor forms: correlations with ligand affinity, receptor stability, and cellular localization. *Biochemistry* **45**, 5606–5617 (2006).
24. Caffrey, M. & Cherezov, V. Crystallizing membrane proteins using lipidic mesophases. *Nat. Protocols* **4**, 706–731 (2009).
25. Cherezov, V. et al. Rastering strategy for screening and centring of microcrystal samples of human membrane proteins with a sub-10 microm size X-ray synchrotron beam. *J. R. Soc. Interface* **6** (suppl. 5), S587–S597 (2009).
26. Chun, E. et al. Fusion partner toolchest for the stabilization and crystallization of G protein-coupled receptors. *Structure* **20**, 967–976 (2012).
27. Kabsch, W. Xds. *Acta Crystallogr. D* **66**, 125–132 (2010).
28. McCoy, A. J. et al. Phaser crystallographic software. *J. Appl. Crystallogr.* **40**, 658–674 (2007).
29. Adams, P. D. et al. PHENIX: a comprehensive Python-based system for macromolecular structure solution. *Acta Crystallogr. D* **66**, 213–221 (2010).
30. Smart, O. S. et al. Exploiting structure similarity in refinement: automated NCS and target-structure restraints in BUSTER. *Acta Crystallogr. D* **68**, 368–380 (2012).
31. Emsley, P., Lohkamp, B., Scott, W. G. & Cowtan, K. Features and development of Coot. *Acta Crystallogr. D* **66**, 486–501 (2010).
32. Friesner, R. A. et al. Glide: a new approach for rapid, accurate docking and scoring. 1. Method and assessment of docking accuracy. *J. Med. Chem.* **47**, 1739–1749 (2004).
33. Friesner, R. A. et al. Extra precision glide: docking and scoring incorporating a model of hydrophobic enclosure for protein-ligand complexes. *J. Med. Chem.* **49**, 6177–6196 (2006).
34. Halgren, T. A. et al. Glide: a new approach for rapid, accurate docking and scoring. 2. Enrichment factors in database screening. *J. Med. Chem.* **47**, 1750–1759 (2004).
35. Abraham, M. J. et al. GROMACS: High performance molecular simulations through multi-level parallelism from laptops to supercomputers. *SoftwareX* **1–2**, 19–25 (2015).
36. Pettersen, E. F. et al. UCSF Chimera—a visualization system for exploratory research and analysis. *J. Comput. Chem.* **25**, 1605–1612 (2004).
37. Sousa da Silva, A. W. & Vranken, W. F. ACPYPE – AnteChamber PYthon Parser interface. *BMC Res. Notes* **5**, 367 (2012).
38. Berman, H. M. et al. The Protein Data Bank. *Nucleic Acids Res.* **28**, 235–242 (2000).
39. Skjærven, L., Yao, X. Q., Scarabelli, G. & Grant, B. J. Integrating protein structural dynamics and evolutionary analysis with Bio3D. *BMC Bioinformatics* **15**, 399 (2014).

Synthesis of AM841

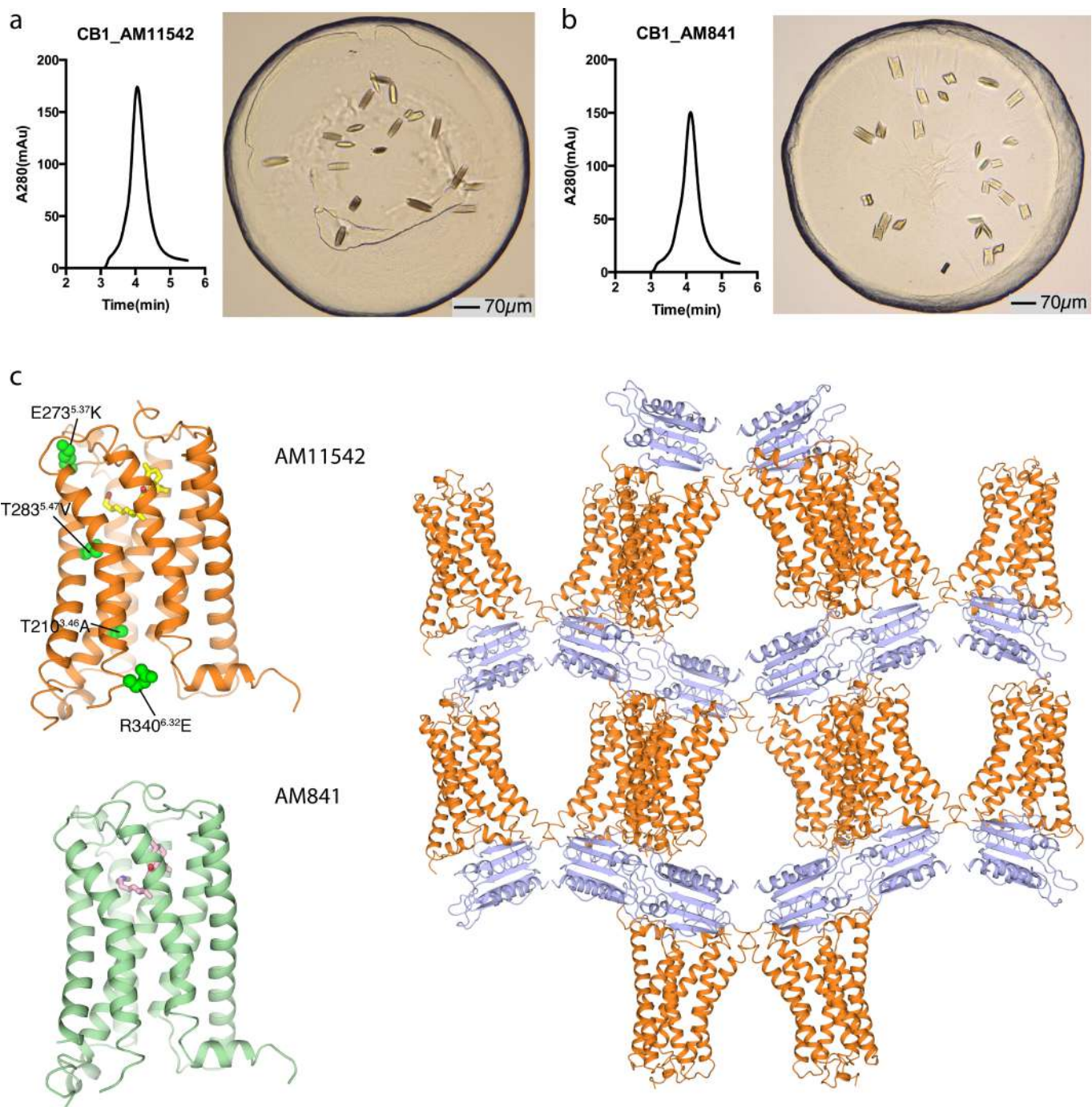


Synthesis of AM11542



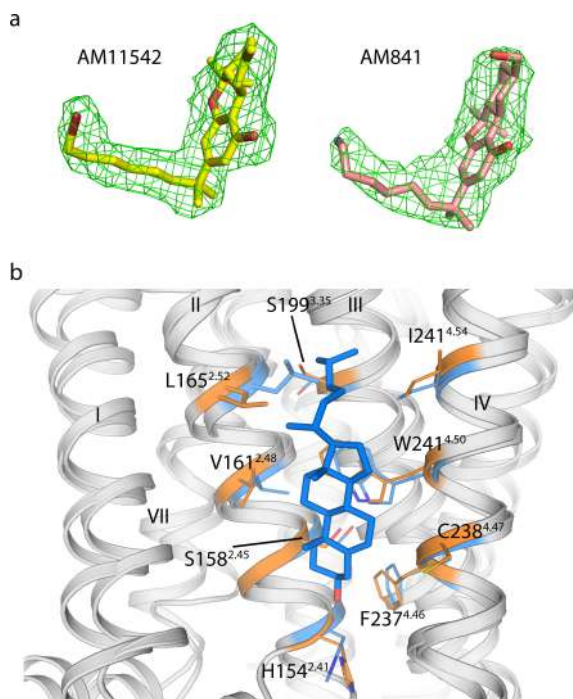
Extended Data Figure 1 | Synthesis of AM841 and AM11542. Reagents and conditions: (a) CH₃I, NaH, DMF, 0 °C to room temperature, 2 h, 95%; (b) DIBAL-H, CH₂Cl₂, -78 °C, 0.5 h, 87%; (c) Br⁻P⁺Ph₃(CH₂)₅OPh, (Me₃Si)₂NK, THF, 0–10 °C, 30 min, then addition to 3, 0 °C to room temperature, 2 h, 96%; (d) H₂, 10% Pd/C, AcOEt, room temperature, 2.5 h, 89%; (e) BBr₃, CH₂Cl₂, -78 °C to room temperature, 6 h, 85%; (f) diacetates, *p*-TSA, CHCl₃, 0 °C to room temperature, 4 days, 64%; (g) TMSOTf, CH₂Cl₂/MeNO₂, 0 °C to room temperature, 3 h, 71%;

(h) TBDMSCl, imidazole, DMAP, DMF, room temperature, 12 h, 85%; (i) Cl⁻Ph₃P⁺CH₂OMe, (Me₃Si)₂NK, THF, 0 °C to room temperature, 1 h, then addition to 9, 0 °C to room temperature, 1.5 h, 73%; (j) Cl₃CCOOH, CH₂Cl₂, room temperature, 50 min, 95%; (k) K₂CO₃, EtOH, room temperature, 3 h, 84%; (l) NaBH₄, EtOH, 0 °C, 30 min, 98%; (m) TBAF, THF, -40 °C, 30 min, 96%; (n) TMG-N₃, CHCl₃/MeNO₂, room temperature, 18 h, 84%; (o) PPh₃, CS₂, THF, room temperature, 10 h, 76%; (p) (+)-cis/trans-p-mentha-2,8-dien-1-ol, *p*-TSA, benzene, reflux 4 h, 65%.

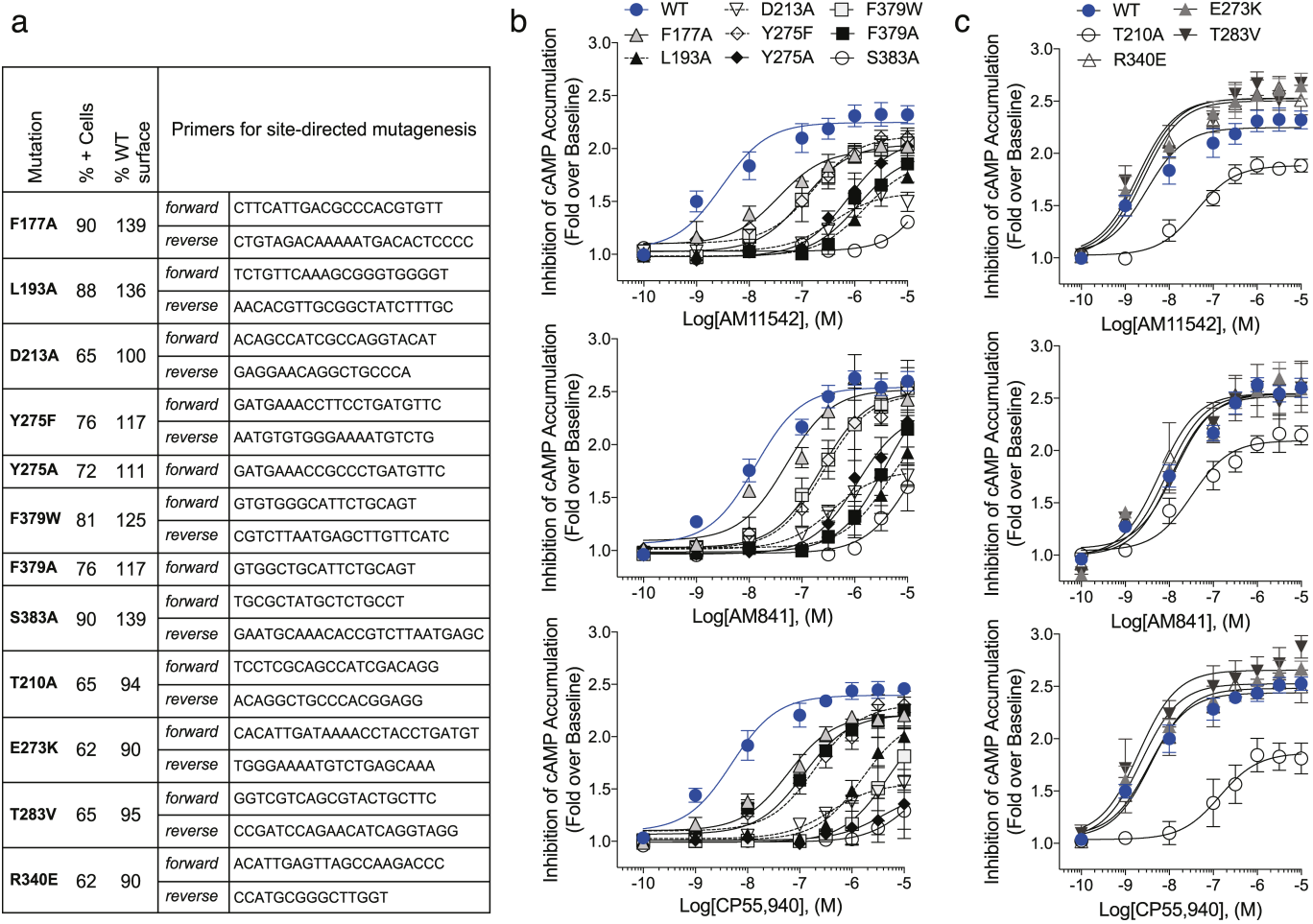


Extended Data Figure 2 | Analytical size exclusion chromatography profile and crystals of CB₁-AM11542/AM841 complex. **a**, Analytical size exclusion chromatography and crystal image of the CB₁-AM11542 complex. Scale bar, 70 μm. **b**, Analytical size exclusion chromatography and crystal image of the CB₁-AM841 complex. Scale bar, 70 μm. **c**, The overall structures of CB₁-AM11542 and CB₁-AM841 complexes and

crystal packing of CB₁-AM11542; receptor is in orange (AM11542)/green (AM841) colour and the flavodoxin fusion protein is in purple-blue colour. The agonists AM11542 (yellow) and AM841 (pink) are shown in sticks representation. The four single mutations T210^{3.46}A, E273^{5.37}K, T283^{5.47}V and R340^{6.32}E are shown as green spheres in the CB₁-AM11542 structure.

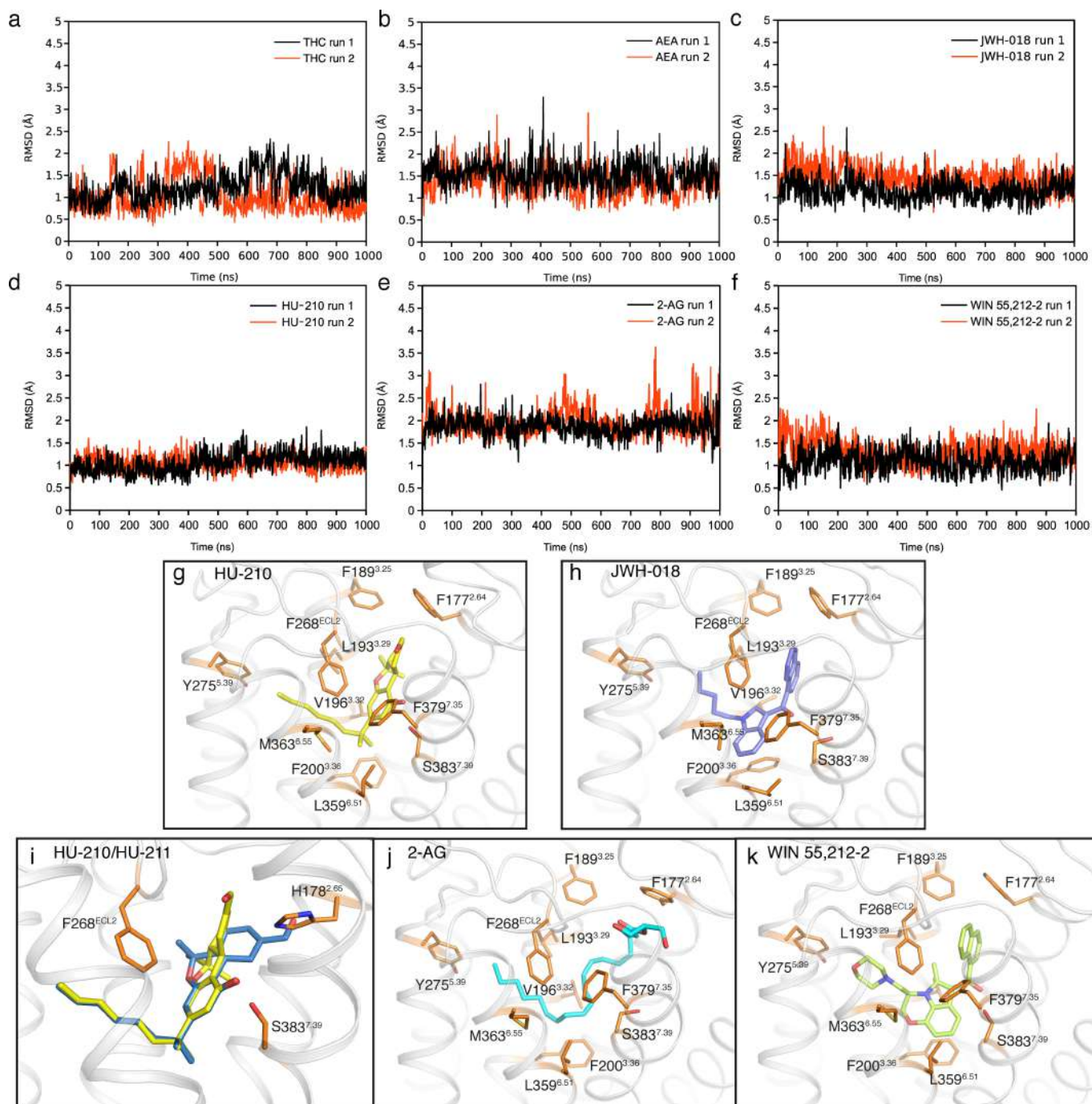


Extended Data Figure 3 | Representative electron density of the CB₁ agonists-bound structures and cholesterol binding sites. **a**, The $|F_o| - |F_c|$ omit maps of AM11542 and AM841 contoured at 3.0σ at 2.80 Å and 2.95 Å, respectively. **b**, The cholesterol binding site in the CB₁-AM11542 structure (orange) with CB₁-AM6538 structure (blue) superposed.



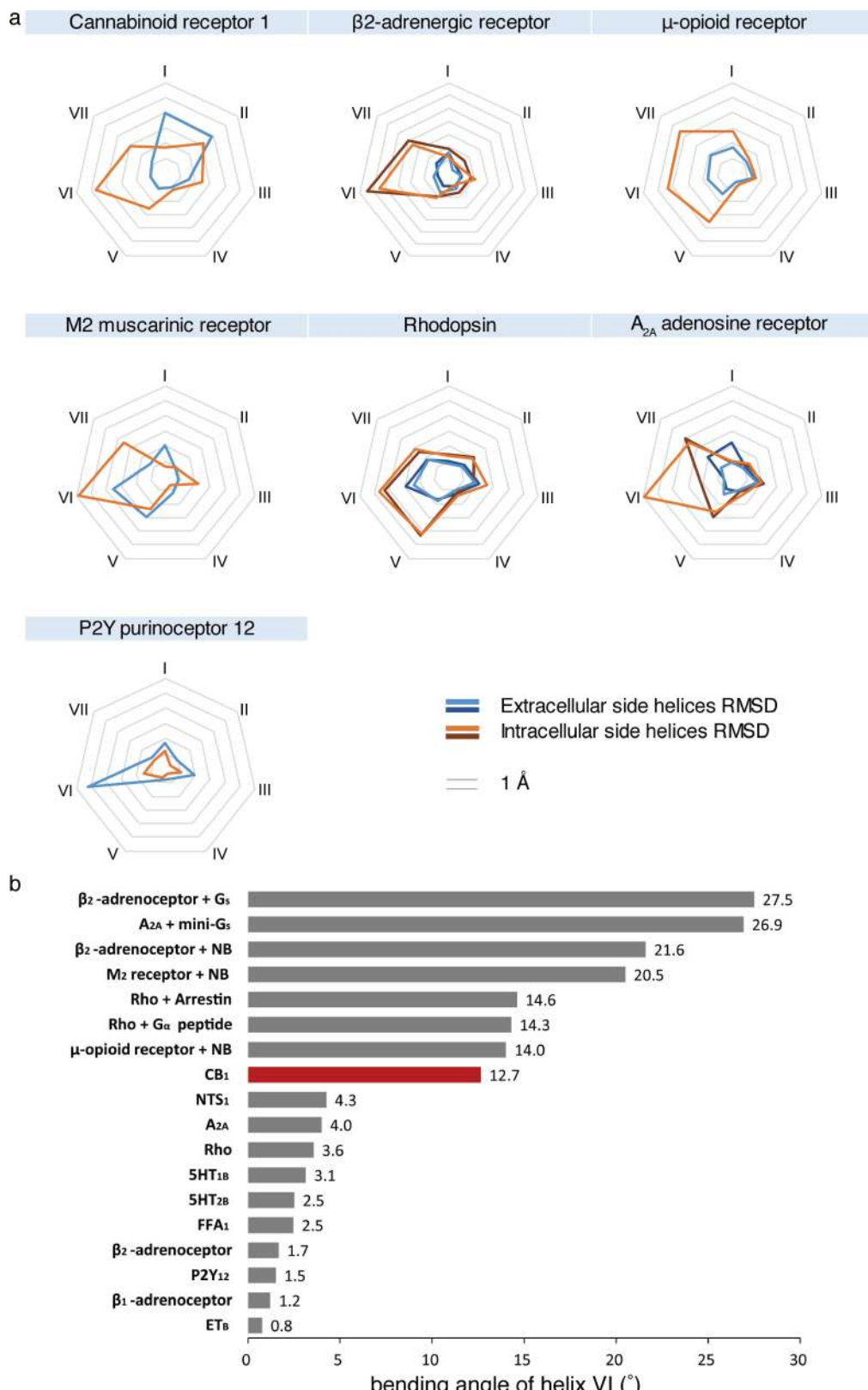
Extended Data Figure 4 | Mutations of the CB₁ receptor and the effects on agonist-induced activity as assessed by the forskolin-stimulated accumulation of cAMP. **a**, Primers used to generate mutations in 3×HA-CB₁ and validation of cell-surface expression of wild-type and mutant CB₁ in CHO-K1 cell lines quantitative flow cytometry. **b**, Dose response studies of agonist (AM11542, AM841 and CP55,940) activity for each mutant

compared to wild type (in blue filled circles) from Fig. 3c. **c**, Assessment of the effect of the individual point mutations that were made to stabilize the receptor, in absence of the flavodoxin insert, on receptor activity. All experiments were repeated at least three times, and error bars denote s.e.m. of duplicate measurements (parameters are in Extended Data Table 2).



Extended Data Figure 5 | Docking poses of different cannabinoid receptor agonists and MD validation. **a-f**, The r.m.s.d. values of ligand heavy atoms show that the docked poses are stable during the 1 μ s molecular dynamics simulations: Δ^9 -THC (**a**), AEA (**b**), JWH-018 (**c**), HU-210 (**d**), 2-AG (**e**), WIN 55,212-2 (**f**). **g, h, j, k**, The poses of

HU-210 (**g**), JWH-018 (**h**), 2-AG (**j**) and WIN 55,212-2 (**k**) are shown. **i**, The superimposition of HU-210 (yellow sticks) and HU-211 (blue sticks) in the binding pocket. The binding pose of HU-210 explains why HU-211, the enantiomer of HU-210, failed to stimulate CB₁ because superimposed HU-211 on HU-210 shows severe clashes with H178^{2.65} in CB₁.



Extended Data Figure 6 | See next page for caption.

Extended Data Figure 6 | Structural conformation changes of solved agonist- and antagonist-bound class A GPCRs. **a**, The pattern of r.m.s.d. values of transmembrane helices between agonist- and antagonist-bound class A GPCR structures. The structures used for analysis are the same as described in Extended Data Table 3. **b**, Measurement of the degree of helix VI bending observed in class A GPCRs structures. All structures were superimposed onto inactive-state β_2 -adrenergic receptor by UCSF Chimera. The direction of helices VI were defined by vectors η_i which starts from the centre of C_α of residues 6.45–6.48 to the centre of C_α of residues 6.29–30–6.32–33. The two vectors η_0 and η_1 of helices VI in the inactive-state and active-state β_2 -adrenergic receptor were selected as reference to form a plane α . The vector η_i of helix VI of other structure

was projected to the plane α as a new vector η'_i . The bending angle of each helix VI was then defined by the angle between η'_i and η_0 . The structures are: ET_B (PDB code 5GLH), β_1 -adrenergic receptor (PDB code 2Y02), P_{2Y}12 (PDB code 4PXZ), β_2 -adrenergic receptor (PDB code 3PDS), FFA1 (PDB code 4PHU), 5HT_{2B} (PDB code 4IB4), 5HT_{1B} (PDB code 4IAR), Rho (PDB code 2HPY), A_{2A} (PDB code 3QAK), NTS₁ (PDB code 4BUO), CB₁ (bound to AM11542; PDB code 5XRA), μ -opioid receptor + nanobody (NB) (PDB code 5C1M), Rho + NB (PDB code 2X72), Rho + arrestin (PDB code 4ZWJ), M2R + NB (PDB code 4MQS), β_2 -adrenergic receptor + NB (PDB code 4LDL), A_{2A} + mini-G_s (PDB code 5G53), β_2 -adrenergic receptor + G_s (PDB code 3SN6).

Extended Data Table 1 | Data collection and structure refinement statistics

	CB1-AM11542 (PDB: 5XRA)	CB1-AM841 (PDB: 5XR8)
Data collection		
Number of crystals	16	10
Space group	P2 ₁ 22 ₁	P2 ₁ 22 ₁
Cell dimensions		
<i>a, b, c</i> (Å)	66.05, 75.87, 138.90	66.83, 73.61, 139.64
Number of reflections measured	102213	84586
Number of unique reflections	16685	13367
Resolution (Å) ^a	37.91-2.80 (2.90-2.80)	49.48-2.95 (3.05-2.95)
<i>R</i> _{merge}	0.101 (0.562)	0.081 (0.490)
Mean <i>I</i> / <i>σI</i>	10.41 (2.07)	11.06 (1.97)
<i>CC</i> _{1/2}	1 (0.62)	1 (0.54)
Completeness (%)	93.50 (90.03)	88.18 (77.30)
Redundancy	6.1 (4.8)	6.3 (3.6)
Refinement		
Resolution (Å)	37.91-2.80	49.48-2.95
No. reflections	16669	13329
<i>R</i> _{work} / <i>R</i> _{free} (%)	23.4/25.2	25.5/27.4
No. atoms		
Protein	3311	3314
Ligand	28 (AM11542)	29 (AM841)
Lipid and other	122	66
Average B factors (Å ²)		
Wilson / Overall	79.6 / 90.0	110.0 / 130.7
CB ₁	82.9	121.6
Flavodoxin	105.9	152.0
Ligand	62.4	93.3
Lipids and other	81.9	106.3
R.m.s. deviations		
Bond lengths (Å)	0.003	0.002
Bond angles (°)	0.732	0.484
Ramachandran Plot Statistics (%)		
Favored regions	97.88	96.02
Allowed regions	2.12	3.98
Disallowed regions	0	0

^aValues in parentheses are for highest-resolution shell.

Extended Data Table 2 | Mutations analysis of changes in pEC₅₀ and E_{max}

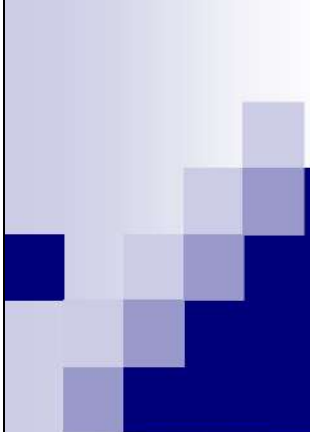
CB ₁	AM11542		AM841		CP55,940	
	pEC ₅₀	E _{max} (Fold)	pEC ₅₀	E _{max} (Fold)	pEC ₅₀	E _{max} (Fold)
WT	8.5 ± 0.21	2.3 ± 0.05	7.9 ± 0.12	2.5 ± 0.04	8.3 ± 0.15	2.3 ± 0.05
F177A	7.4 ± 0.17****	2.0 ± 0.04	7.3 ± 0.20****	2.5 ± 0.08	7.2 ± 0.14****	2.2 ± 0.05
L193A	5.8 ± 0.06****	1.9 ± 0.10	5.4 ± 0.35****	2.3 ± 0.42	5.8 ± 0.15****	2.2 ± 0.12
D213A	6.4 ± 0.18****	1.6 ± 0.05***	6.4 ± 0.14****	1.8 ± 0.05****	6.4 ± 0.14****	1.6 ± 0.04***
Y275A	6.1 ± 0.19****	2.1 ± 0.12	5.9 ± 0.22****	2.3 ± 0.18	5.4 ± 0.95****	1.5 ± 0.40***
Y275F	6.8 ± 0.21****	2.1 ± 0.09	6.6 ± 0.13****	2.5 ± 0.09	6.7 ± 0.13****	2.3 ± 0.07
F379A	5.9 ± 0.25****	2.0 ± 0.15	5.4 ± 0.30****	2.6 ± 0.42	5.3 ± 0.40****	2.2 ± 0.50
F379W	7.0 ± 0.12****	2.0 ± 0.05	6.6 ± 0.20****	2.5 ± 0.13	7.0 ± 0.15****	2.2 ± 0.07
S383A	< 5	1.0 ± 0.02****	< 5	1.6 ± 0.51****	< 5	1.3 ± 0.12***
T210A	7.5 ± 0.32**	1.9 ± 0.07**	7.4 ± 0.22	2.1 ± 0.06****	6.9 ± 0.32***	1.9 ± 0.09***
E273K	8.7 ± 0.14	2.5 ± 0.05*	8.1 ± 0.12	2.5 ± 0.06	8.7 ± 0.09	2.5 ± 0.04
T283V	8.8 ± 0.17	2.5 ± 0.06*	7.9 ± 0.16	2.5 ± 0.07	8.7 ± 0.25	2.7 ± 0.07**
R340E	8.6 ± 0.15	2.5 ± 0.05*	8.1 ± 0.17	2.5 ± 0.09	8.5 ± 0.30	2.5 ± 0.06

Inhibition of forskolin-stimulated cAMP accumulation in wild-type and mutant CB₁ CHO cells. Data are mean pEC₅₀ and E_{max} values ± s.e.m. from fitting concentration–response data to nonlinear regression (3 parameter) analysis; n = 3 independent experiments performed in duplicate for all mutants except F177A (n = 4), T210A (n = 4 for AM841 and CP55,940) and wild type (n = 7 for AM841 and CP55,940; n = 6 for AM11542). Compared to wild type with agonist treatment: *P < 0.05, **P < 0.01, ***P < 0.0001 as determined by two-way ANOVA without repeated measures followed by Dunnett's post hoc test. Statistical analyses were not performed on S383A as the pEC₅₀ values were estimated at >5 μM due to lack of response and non-convergence of the data to nonlinear regression analysis. The last four mutations represent those appearing in the crystal structure CB₁ construct.

Extended Data Table 3 | Binding pocket volume comparison and r.m.s.d. analysis of solved representative agonist- and antagonist-bound pairs of seven class A GPCRs

GPCRs	Agonist-bound Structures	Binding Pocket Volume (Å ³)	Antagonist-bound Structures	Binding Pocket Volume (Å ³)	RMSD (Å) of transmembrane helices	
Cannabinoid receptor 1 (CB ₁)	Agonist (PDB:5XRA)	383.5	Antagonist (PDB:5TGZ)	821.8	E	2.50
	Agonist (PDB:3SN6)	469.7			I	3.07
β2-adrenergic receptor			Inverse agonist (PDB:3NY8)	670.9	E	1.13
	Agonist (PDB:4LDL)	670.9			I	3.40
					E	1.19
					I	2.96
μ-opioid receptor	Agonist (PDB:5C1M)	576.6	Antagonist (PDB:4DKL)	586.5	E	1.49
					I	3.04
M ₂ muscarinic receptor	Agonist (PDB:4MQS)	114.6	Antagonist (PDB:3UON)	320.7	E	1.99
					I	3.17
Rhodopsin	Agonist (PDB:2X72)	342.3			E	1.72
			Antagonist (PDB:1U19)	214.7	I	3.19
	Arrestin (PDB:4ZWJ)	373.8			E	1.56
					I	3.24
A _{2A} adenosine receptor	Agonist (PDB:3QAK)	445.2			E	1.58
			Antagonist (PDB:4EIY)	461.0	I	2.23
	Agonist (PDB:5G53)	288.8			E	1.12
					I	3.28
P2Y purinoceptor 12 (P2Y ₁₂)	Agonist (PDB:4PXZ)	298.8	Antagonist (PDB:4NTJ)	392.7	E	2.13
					I	0.93

E: RMSD of extracellular side helices I: RMSD of intracellular side helices



GROMACS 分子动力学模拟 —综合实例

李继存

北京

2017年8月7日

大纲

- 回顾昨天内容
- 扩展应用到实例
 - 小分子: 多巴胺
 - 蛋白: 4xp1
 - 蛋白-配体: 4xp1-多巴胺

实例1: 多巴胺

- 构型
- GAFF拓扑
- 真空单分子
- 多分子盒子
- 单分子水溶液
- 自由能: 水中的溶剂化能
- 伞形采样: 跨POPC膜PMF

3

实例2: 4xp1

- 处理pdb文件
- 创建amber力场拓扑文件
- 单独模拟
- 水溶液模拟

4

实例3: 4xp1-多巴胺

- 装配复合物
- 组合拓扑
- 添加水/离子
- 预平衡
- 成品模拟
- 分析

5

实例4: MMPBSA

- 理论基础
- 程序使用
 - gmmpbsa
 - g_mmpbsa

6

实例5: 配体牵引

- 类似伞形采样其中一步
- 不同牵引方式的表现
- 根据需要选择牵引方式

7

实例6: 石墨烯上的液滴

- 石墨烯上的乙醇液滴
- OPLS-AA 力场
- 刚性/柔性石墨烯

8

流程

- 创建石墨烯gro与top
- 创建乙醇gro与top
- 创建乙醇液滴,立方/半球/圆柱形
- 将液滴与石墨烯组合
- NVT

9

石墨烯

- 创建石墨烯: GaussView/其他工具
 - 基本单元: 20x12
 - 碳原子数目: 960
- 将石墨烯放入盒子: editconf/手动
 - x, y方向周期性正确
 - 盒子z方向高度4 nm
 - 石墨烯z方向高度0.5 nm
- 获取石墨烯itp文件: x2top

10

乙醇

- 创建乙醇分子结构文件:
GaussView
- 获取乙醇分子拓扑文件: **tppmktop**
- 创建半球形乙醇液滴:
packmol/getConf/VMD
 - 半径: **1 nm**
 - 底面z方向高度: **0.5+0.2 nm**

11

组合

- 组合石墨烯与乙醇液滴, **gro**
- 创建总拓扑文件, **top**
- 创建**mdp**文件
 - 刚性石墨烯
 - 柔性石墨烯
 - **NVT**
- 运行模拟

12

配置msys2

环境变量

/home/【用户名】/.bashrc

```
export PATH=$PATH:/C/GMX/amber14/bin  
export AMBERHOME=/C/GMX/amber14
```

PDB文件基础

下载pdb文件

类似 溶菌酶教程

熟悉pdb文件

阅读 PDB文件格式说明

重点关注

- 链: CHAIN
- 缺失原子: MISSING ATOM
- 配体信息: HET, HETNAM
- 二硫键: SSBOND

处理pdb文件

以 4xp1 为例, 为多巴胺复合物

简单文本处理Notepad2+bash

1. 删除 杂原子: HETATM
2. 删除 连接信息: CONECT
3. 删除 水分子: HETATM HOH
4. 抽取 多巴胺: LDP

多巴胺模拟: 小分子示例

获取构型

1. 从pdb中抽取
2. 网络查询
3. 自己构建

确保构型完整. 若pdb中缺失原子, 务必补充完整

创建GAFF力场拓扑

1. antechamber: 计算电荷并生成mol2文件

电荷可使用两种模型:

1. RESP: 基于量化静电势拟合, 计算较慢, 适用于小分子
2. AM1-BCC: 半经验拟合, 快速, 可处理大分子

示例AM1-BCC电荷模型

```
antechamber -i ldp.pdb -fi pdb -o ldp.mol2 -fo mol2 -pf y -c
```

如果生成的 **ldp.mol2** 文件正常, 则说明命令运行成功. 其他文件可删除.

生成的mol2文件, 有时存在不一致之处, 需要改正

```
ldp.mol2
1 @<TRIPOS>MOLECULE
2 LDP # 分子名称
3 22 22 1 0 0 # 原子数, 键数, 分子数目
4 SMALL
5 bcc
6
7 @<TRIPOS>ATOM
8 # 编号 原子 x y z 分子编
9 1 C7 -9.1900 2.9910 -26.8180 c3
10 2 C1 -10.3400 3.5770 -26.0270 ca
11 ...
```

如果 **ATOM** 部分中的分子编号和名称与前面的不一致, 需要修改至相同, 否则后续步骤会出错.

我们得到的 **ldp.mol2** 中两处的分子编号不一致, 所以要将 **708** 改为 **1**, 如下

```
ldp.mol2
1 @<TRIPOS>MOLECULE
2 LDP # 分子名称
3 22 22 1 0 0 # 原子数, 键数, 分子数目
4 SMALL
5 bcc
6
7 @<TRIPOS>ATOM
8 # 编号 原子 x y z 分子编
9 1 C7 -9.1900 2.9910 -26.8180 c3
10 2 C1 -10.3400 3.5770 -26.0270 ca
11 ...
```

2. parmchk2: 检查GAFF参数并生成缺失参数文件

```
parmchk2 -i ldp.mol2 -f mol2 -o ldp.frcmod
```

3. **sleep**: 生成AMBER参数文件和坐标文件

编写**sleep**需要的输入文件, 文件名任意, 如**leap.in**, 内容如下:

```
leap.in
1 source leaprc.ff14SB
2 source leaprc.gaff
3 loadamberparams ldp.frcmod
4 lig=loadmol2 ldp.mol2
5 check lig
6 saveamberparm lig ldp.prmtop ldp.inpcrd
7 quit
```

运行**sleep**命令

```
sleep -f leap.in
```

现在**ldp**目录内容如下

4. **acpype**: 将AMBER文件转换为GROMACS文件

```
acpype -p ldp.prmtop -x ldp.inpcrd -d
```

现在目录内容如下

我们得到了运行 GROMACS 的坐标文件 **ldp_GMX.gro** 和拓扑文件 **ldp_GMX.top**.

真空单分子

为了验证所得的多巴胺分子的拓扑是否正常, 可以运行单个多巴胺分子的 NVT 模拟. 当然, 如果你经验丰富, 也可以直接模拟更复杂的体系. 但如果出现问题, 排查错误时不易定位.

指定盒子大小

```
gmx editconf -f ldp_GMX.gro -d 1 -o conf.gro
```

准备拓扑文件

将**ldp_GMX.top**更名为默认名**topol.top**

准备mdp文件

分子很简单, 我们不进行预平衡, 直接做NVT模拟.

```
grompp.mdp
1 ;=====
2 ; 运行控制参数
3 ;=====
4 integrator      = md      ; 积分方法, md: 蛙跳; sd: 随机
5 dt              = 1E-3    ; 积分步长(ps), EM不用
6 nsteps          = 10000   ; 最大积分步数, 默认0表示不限制
7
```

```
8 ;=====
9 ; 输出控制参数
10 ;=====
11 nstxout          = 1      ; trr坐标的输出频率(步)
12 nstvout          = 1      ; 速度
13 nstfout          = 1      ; 力
14 nstxout-compressed = 1      ; xtc压缩坐标的输出频率
15 compressed-x-precision = 1000 ; xtc坐标的精度
16
17 nstlog           = 1000 ; 日志文件中能量的输出频率
18 nstenergy         = 1000 ; 能量文件
19 nstcalcenergy     = 100   ; 计算能量的频率, 最好为n.
20
21 ;=====
22 ; 邻区搜索参数
23 ;=====
24 nstlist           = 1      ; 邻区列表更新频率, 0: 用于
25 rlist             = 1      ; 邻区列表的截断距离(nm)
26 cutoff-scheme     = Verlet ; 截断方式(Verlet: 粒子截断
27 ns_type           = grid   ; 邻区搜索方法(grid: 较快;
28
29 pbc               = xyz    ; 周期性比较条件: xyz, xy,
30 periodic-molecules = no     ; 周期性分子: no, yes
31
32 ;=====
33 ; 静电与范德华
34 ;=====
35 rvdw              = .9     ; 范德华截断半径
36 rcoulomb          = .9     ; 静电截断半径
37 vdw-type          = Cut-off ; 范德华计算方法
38 coulombtype       = PME    ; 静电的计算方法
39
40 DispCorr          = No     ; 能量/压力的色散长程校正, no: 无; Er
41
42 ;=====
43 ; 温度耦合
44 ;=====
45 tcoupl             = nose-hoover ; 耦合方法, no: 无; v-res
46 tc-grps            = system    ; 温度耦合组, 可多个
47 tau_t              = 2        ; 耦合时间常数(ps)
48 ref_t              = 298.15   ; 参考温度(K)
49
50 ;=====
51 ; 压力耦合
52 ;=====
53 pcoupl             = No      ; 耦合方法, no: 无, 盒子大小
54 pcoupltype         = Isotropic ; 耦合类型, isotropic: 各向
55                                     ; semiisotropic: x/y方向各
56                                     ; anisotropic: 各向异性, 盒
57                                     ; surface-tension: 表面张力
58 tau-p               = 1        ; 时间常数(ps)
59 compressibility     = 4.5E-5  ; 压缩率(1/bar)
60 ref-p               = 1        ; 参考压力(bar)
61
62 ;=====
63 ; 初始速度
```

```
64 ;=====
65 gen_vel           = yes    ; no: 使用gro文件的值; yes: A
66 gen_temp          = 298.15 ; 随机速度对应的温度
67 gen-seed          = -1     ; 随机数种子; -1: 自动确定
```

执行模拟

```
gmx grompp  
gmx mdrun
```

查看原子运行是否有明显异常

多分子盒子

多巴胺盒子的模拟, 示例如何创建溶剂盒子.

创建溶剂盒子

我们使用前面使用的盒子, 将多巴胺分子插入其中

```
gmx insert-molecules -f conf.gro -ci ldp.pdb -o ldp_box.gro -
```

-nmol 指定要插入的分子数目, 如果要填满, 可设个很大的值

-try 指定每次插入的尝试次数

在我的机器上运行, 插入了74个多巴胺.

得到的构型可能不够好, 如果需要更合理的构型, 可以试试packmol

准备拓扑文件

只须修改多巴胺的数目即可

```
topol.top
1 ...
2 [ molecules ]
3 ; Compound      nmols
4 ldp            75
```

准备mdp文件

NVT使用前面的即可, NPT则修改压力耦合部分pcoupl的值即可

执行模拟

```
gmx grompp -c ldp_box.gro -maxwarn 2
```

可能遇到警告. 明白意思, 为什么, 修正或忽略

```
gmx mdrun
```

运行中可能出错

- 未平衡好, 可先预平衡一下: EM, NVT, NPT

- 时间步长过大, 先改小, 平衡好后再使用大步长
- 刚性水分子无法约束, 先换用柔性水模型

单分子水溶液

创建水溶液

方法多样:

1. gmx solvate
2. gmx insert-molecules
3. packmol
4. 其他软件

```
gmx solvate -cp conf.gro -cs -o ldp_wat.gro
```

准备拓扑文件

我们前面使用的是独立的拓扑文件, 其中没有引用任何其他文件. 对简单体系, 这种文件用起来简单, 但对复杂体系, 容易出问题, 所以我们修改文件这个文件, 将其变为itp文件, 方便引用.

改为itp的方法: 只保留与多巴胺有关的部分

```
ldp.itp
1 [ atomtypes ]
2 ;name      bond_type      mass      charge      ptype      sigma
3   c3        c3            0.00000  0.00000  A          3.39967e
4   ca        ca            0.00000  0.00000  A          3.39967e
5 ...
6
7 [ moleculetype ]
8 ;name          nrexcl
9   ldp           3
10
11 [ atoms ]
12 ;    nr      type      resi      res      atom      cgnr      charge      mas
13     1       c3        1       LDP      C7        1      -0.038100  12.
14     2       ca        1       LDP      C1        2      -0.075300  12.
15 ...
16
17 [ bonds ]
18 ;    ai      aj      funct      r                  k
19     1       2       1      1.5130e-01  2.7070e+05 ;      C7
20     1       10      1      1.5350e-01  2.5363e+05 ;      C7
21 ...
22
23 [ pairs ]
24 ;    ai      aj      funct
25     1       6       1 ;      C7 - C5
26     1       7       1 ;      C7 - C3
27 ...
28
```

```

29 [ angles ]
30 ;   ai      aj      ak      funct    theta          cth
31       1        2        4        1  1.2063e+02  5.3421e+02
32       1        2        5        1  1.2063e+02  5.3421e+02
33 ...
34
35 [ dihedrals ] ; propers
36 ; for gromacs 4.5 or higher, using funct 9
37 ;   i      j      k      l      func    phase      kd
38       1        2        4        7        9  180.00  15.16700
39       1        2        4       14        9  180.00  15.16700
40 ...
41
42 [ dihedrals ] ; impropers
43 ; treated as propers in GROMACS to use correct AMBER an-
44 ;   i      j      k      l      func    phase      kd
45       2        6        5       15        4  180.00  4.60240
46       2        7        4       14        4  180.00  4.60240
47       3        4        7        8        4  180.00  4.60240
48       3        5        6       16        4  180.00  4.60240
49       4        5        2        1        4  180.00  4.60240
50       6        7        3        9        4  180.00  4.60240

```

总的拓扑文件

```

topol.top
1 # include "C:\GMX\GMX5.1.4\share\gromacs\top\amber99sb-
2
3 # include "ldp.itp"
4
5 # include "C:\GMX\GMX5.1.4\share\gromacs\top\amber99sb-
6
7 [ system ]
8 ldp
9
10 [ molecules ]
11 ; Compound      nmols
12 ldp            1
13 SOL            550

```

注意: 由于 `ldp.itp` 中包含 `[atomtypes]` 部分, 在总拓扑中需要注意各个 itp 文件的顺序.

准备mdp文件

执行模拟

溶剂化能

分子在水中的溶剂化能, 也就是水合自由能, 可表征分子的水溶性大小.

自由能计算很重要, 却困难, 而且麻烦. 针对不同体系, 有不同的处理方法:

- 小分子使用较准确的方法: **gmx bar**, 须在不同条件下运行多次模拟
- 蛋白质使用较粗略的方法: **MMPBSA**, 须借助外部程序
- 更实用的分析: 相互作用能, 牵引势能

我们以多巴胺溶剂化能为例, 学习自由能的计算

创建水盒子并充分平衡

使用前面的水盒子, 作为示例, 没有充分平衡好

准备拓扑文件

无须修改

准备mdp文件

自由能计算的关键步骤, mdp文件中涉及到的选项

grompp.mdp	
1	; =====
2	; 自由能计算
3	; =====
4	free-energy = no
5	couple-moltype =
6	
7	sc-power = 1
8	sc-alpha = 0
9	sc-sigma = 0.3
10	sc-r-power = 6
11	sc-coul = no
12	
13	couple-intramol = no
14	
15	couple-lambda0 = vdw-q
16	couple-lambda1 = vdw-q
17	init-lambda-state = -1
18	
19	coul-lambdas =
20	vdw-lambdas =
21	
22	fep-lambdas =
23	mass-lambdas =
24	bonded-lambdas =
25	restraint-lambdas =
26	temperature-lambdas =
27	
28	init-lambda = -1
29	delta-lambda = 0
30	
31	calc-lambda-neighbors = 1
32	init-lambda-weights =
33	

```
34 nstdhdl          = 50
35 dhdl-print-energy = no
36 separate-dhdl-file = yes
37 dhdl-derivatives   = yes
38 dh_hist_size       = 0
39 dh_hist_spacing    = 0.1
```

首先, 我们需要指定要计算哪个分子的自由能, `couple-moltype`, 这需要使用索引文件来指定.

```
gmx make_ndx -f ldp_wat.gro
```

其次, 使用 `integrator = sd`, `pcoupl = Parrinello-Rahman` 否则会警告.

```
gmx grompp
```

执行模拟

理论上, 对每个状态都需要做预平衡, 但对于小分子, 由于比较容易平衡, 所以我们可以使用某一状态的平衡构型(最好是中间状态)直接进行自由能计算即可.

伞形采样

计算多巴胺的跨POPC膜的PMF

创建POPC双层膜

有多种方法:

1. `gmx genconf`: 堆叠
2. packmol: 自定义性好
3. VMD: 根据已平衡好构型扩展
4. CHARMM-GUI: 功能最强
5. 自编脚本
6. LipidBook下载

所得构型必须进行重新平衡, 性质验证后方可进行成品模拟.

我们使用最简单的VMD

`Extensions->Modeling->Membrane Builder`

创建30x30的POPC膜, VMD同时会添加水分子

转为gro文件: `gmx editconf -f 2 2 10`

抽取单个POPC分子, 获取其GAFF拓扑文件, 并整理为itp文件备用

使用外来构型的问题在于, 原子编号顺序与默认的可能不一致

准备拓扑文件和mdp文件

关键在于理解伞形采样的实质: 在反应坐标上取一系列相互间有重叠的点, 对每个点进行外加偏离势作用下的模拟, 对所有点的能量数据使用WHAM(加权直方分析方法)计算PMF

模拟流程:

1. 定义反应坐标
2. 反应坐标取点
3. 外加偏离势模拟
4. WHAM分析计算PMF

其中2是难点, 可根据不同体系采用不同方法, 不必照搬, 只要所得构型满足要求即可.

计算多巴胺跨POPC膜的PMF:

1. 反应坐标: 垂直膜方向, 从一端到另一端
2. 取点方法: 牵引, 非平衡, 虚拟键长
3. 偏离势: 简谐势
4. WHAM: `gmx wham`

使用与其他粒子无相互作用, 位置固定的参考原子, 以其为牵引的参考组

抽取指定坐标的点, 以每个点为初始构型, 设牵引速率为零, 做模拟

使用 `gmx wham` 分析所得数据

4xp1模拟: 蛋白示例

处理pdb文件

检查构型

使用 `spdbv` 补充缺失原子

创建amber力场拓扑

`gmx pdb2gmx`

单独模拟

真空

水溶液模拟

加水: `gmx solvate`

离子: `gmx genion` 或 `gmx insert-molecules`

预平衡: EM, NVT, NPT

4xp1-多巴胺: 蛋白配体示例

基本流程

1. 准备蛋白

自行创建/下载蛋白PDB

PDB数据清洗

pdb2gmx 获取蛋白拓扑文件

2. 准备配体

配体构型文件

配体拓扑文件: GAFF

3. 装配复合物

4. 组合复合物拓扑文件

5. 添加水/离子

6. 预平衡: EM, PR, NVT, NPT

7. 成品模拟 NPT

8. 分析

装配复合物

配体结合位置(蛋白配体相对位置)

- PDB中已有结合位置
- 自行决定结合位置: 模拟, 对接, 经验

组合复合物拓扑文件

手动编写

添加水/离子

- `gmx solvate`
- `gmx insert-molecules`
- `gmx genion`

预平衡: EM, PR, NVT, NPT

成品模拟: NPT

分析

平衡判断: RMSD, RMSF, 二级结构

相互作用: 结合能

蛋白-配体MMPSA结合能

自由能计算方法

- 小分子 准确方法: 自由能微扰(Zwanzig), 接受比例(Bennet, **gmx bar**), 热力学积分(Kirkwood), 非平衡近似(Jarzynski)
- 蛋白 经验方法: MMGBSA, MMPSA

MMPSA

理论基础

$$\Delta G = G_{\text{cmp}} - G_{\text{pro}} - G_{\text{lig}}$$

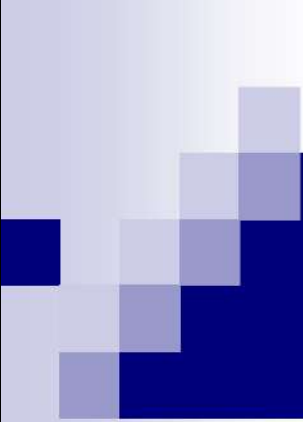
$$\begin{aligned}G &= G_{\text{gas}} + G_{\text{slv}} \\&= [E_{\text{gas}} - TS_{\text{gas}}] + [G_{\text{polar}} + G_{\text{nonpolar}}] \\&= [E_{\text{MM}} - TS_{\text{MM}}] + [G_{\text{PB}} + G_{\text{surface}}] \\&= [E_{\text{MM}} - TS_{\text{MM}}] + [G_{\text{PB}} + \gamma A + b]\end{aligned}$$

可选程序

皆依赖于GROMACS, APBS

比较

程序	语言	编译	系统	效率	能量分解	丙氨酸突变
gmxbpsa	bash, perl	无须	Win/Lin	低	无	支持
g_mmpbsa	C/C++	需要, 也提供二进制版本	Lin	高	有	不支持



GROMACS 分子动力学模拟 —分析进阶

李继存

北京

2017年8月7日

大纲

- 模拟结果分析
 - 轨迹的处理, 创建分组, 选区工具
 - 自带的分析工具
 - 轨迹文件的编程处理
- GROMACS分析工具综合运用
- GROMACS进阶

模拟三部曲

- 前处理

建模 准备输入文件

- 运行

耗时最长,但参与最少

- 后处理

分析,处理输出文件

3

分析

- 可分析性质巨多
- 根据自己体系与关注问题选择
- 大致分结构,能量,动力学
- 结构,热力学,动力学
- 自带工具,组合
- 第三方分析工具
- 自编程序

4

分析流程

- 处理轨迹
- 只需要坐标 xtc
- 还需要速度 trr
- 创建分组 ndx 文件
- 合理使用 select

5

轨迹的处理 trjconv

- PBC: whole mol
- 居中: center
- 叠合: rot+trans

6

“Think like a man of action, act like a man of thought. 如行动者那般思考，如思考者那般行动。— Henri Bergson 亨利·柏格森”

速度不给力？试试国内网站 <https://Jerkwin.coding.me>

评论与问题？请至论坛留言 <https://Jerkwin.herokuapp.com>

GROMACS轨迹周期性边界条件的处理

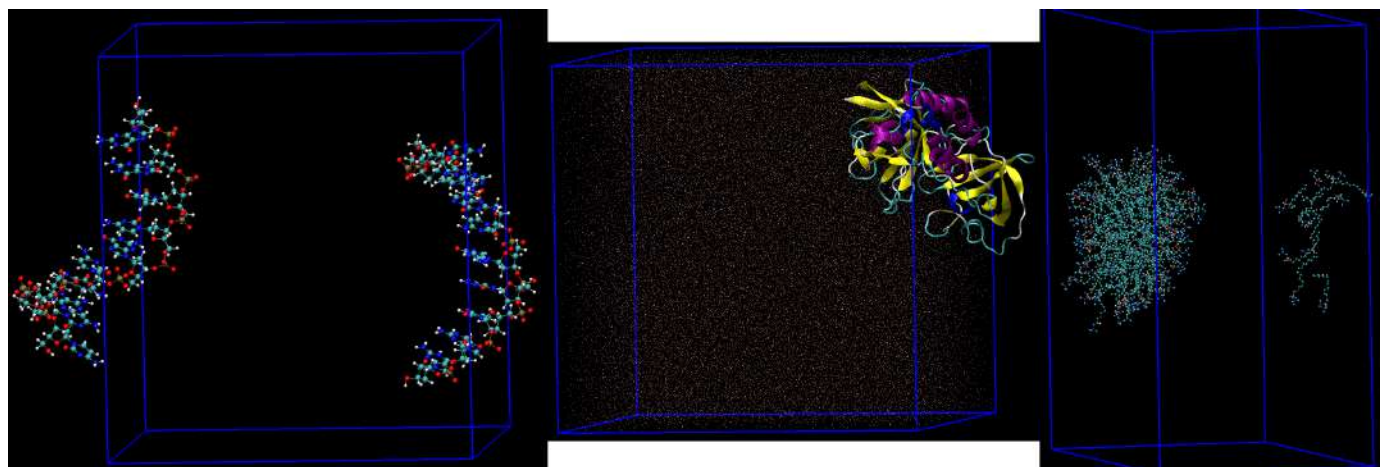
类别: 科 标签: gmx vmd 阅读次数: 1041 版权: (CC) BY-NC-SA

- 2016-05-31 11:22:44 整理: 刘世恩; 补充: 李继存
- 2016-06-01 10:37:24 补充VMD的pbc命令: 赵道辉

使用GROMACS完成模拟后, 有时需要对轨迹的周期性边界条件(PBC)进行处理. 可能的目的主要有两个: 为了观看轨迹时分子保持完整, 不产生断键或过长的键, 同时未解离的复合物保持在一起; 为了对选定的中心分子进行居中, 以便进行后面的分析. GROMACS的大多数分析工具都会自动处理PBC, 不劳自己费心, 如计算距离, 角度, RDF, MSD时, PBC会自动考虑在内, 所以没有必要对轨迹进行预处理. 但对那些分析时需要进行叠合的工具, 如计算RMSD之类, 需要对轨迹进行预处理, 这种情况下就需要小心处理PBC的问题.

GROMACS处理PBC的主要工具是 `gmx trjconv`, 请先仔细阅读其[文档及补充说明](#), 确保理解 `-pbc` 几个选项的功能, 以及 `-center` 的作用. 如果不能明白其中的道理, 在处理轨迹时只是尝试选项的各种组合, 一味地乱试, 很难得到正确的结果.

下面我们以双链DNA体系为例, 具体说明一下如何使用 `gmx trjconv` 来处理复合物体系. 这里所谓的复合物, 指的是体系中有一些分子在模拟过程中会聚集在一起, 并不解离. 比如, 模拟双链DNA时, 如果DNA的两条链始终没有分开(一般是这种情形, 否则的话, 所用的力场可能有问题), 就可以认为它们形成了一个复合物. 我们在观看轨迹时, 不希望看到DNA的两条链在盒子中分离开来, 这时就需要进行PBC的处理了. 模拟蛋白-配体复合物, 或者分子聚集体如胶束时, 有时也会面临的同样的情况.



首先需要明确, 只要在整个模拟过程中复合物没有解离, 我们一定可以通过PBC处理使其处于盒子中间且保持完整; 如果模拟过程中复合物发生了解离, 但解离分子之间的最大距离小于盒子长度的

一半, 我们仍可以通过PBC处理使这些解离的分子处于盒子中, 不在盒子两侧跳来跳去; 如果解离分子之间的最大距离超过了盒子长度的一半, 我们还可以通过PBC处理使每个解离分子保持完整, 但没有办法保证观看轨迹时所有的分子不在盒子两侧之间跳跃. 其中的原因, 想想PBC的定义就能明白.

具体的示例体系是一段双链DNA, 并添加了离子和水(为清晰起见下面的图中忽略了水和离子), DNA中的原子距盒子边界的最小距离为1 nm.

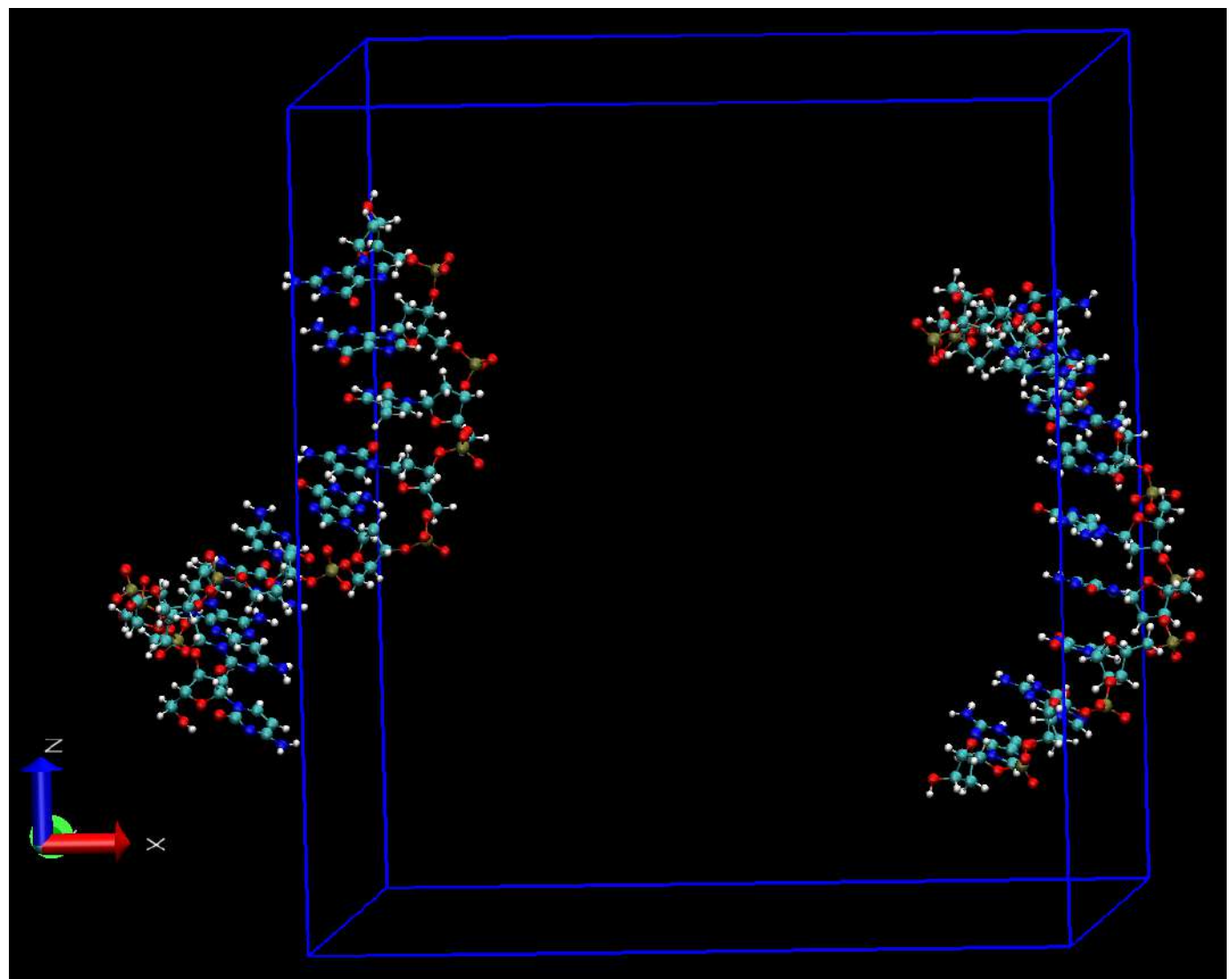
使分子保持完整

模拟完成得到轨迹后, 按照经典的轨迹处理步骤, 先保证体系中每个分子完整:

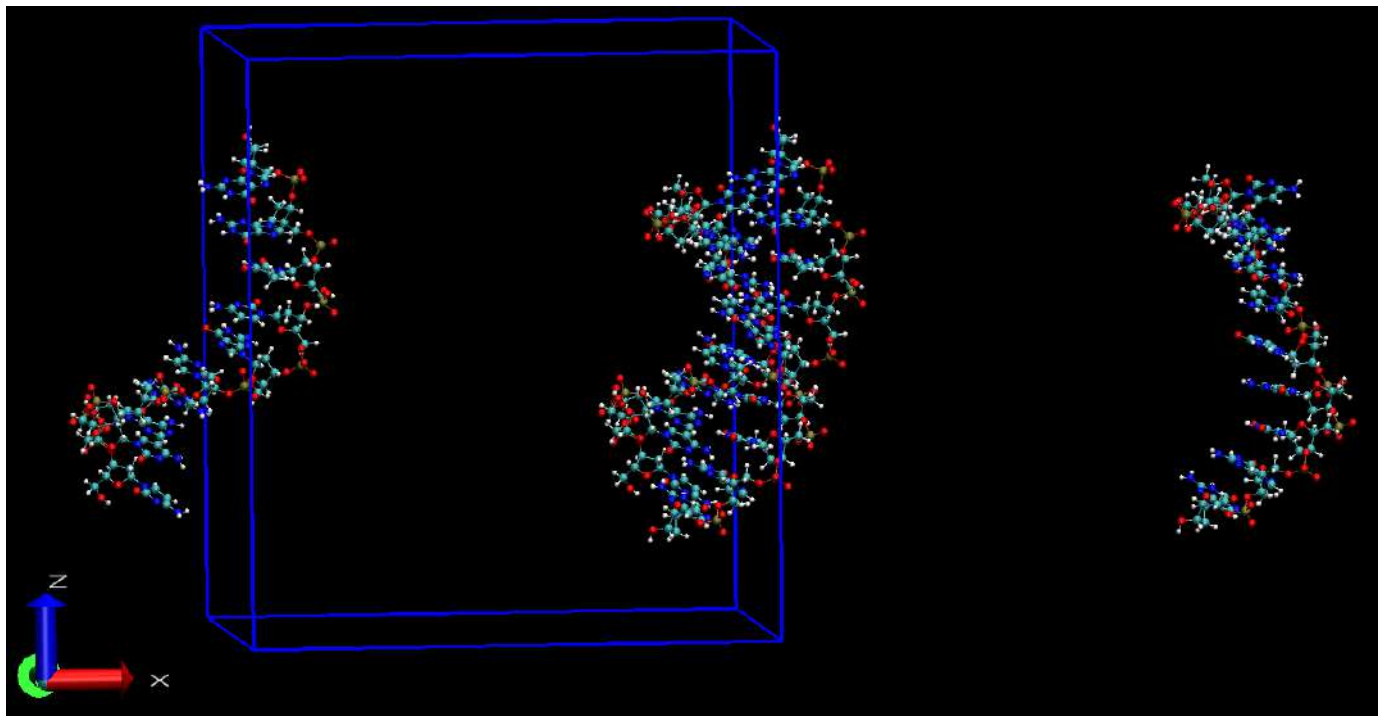
```
gmx trjconv -s npt.tpr -f prod.xtc -o prod_whole.xtc -pbc whole
```

使用VMD观看得到的轨迹 `prod_whole.xtc`, 则发现虽然每个分子都保持了完整, 没有异常的键, 但对很多帧, DNA两条链不在盒子内, 而是分处于盒子两侧, 且X, Y, Z三个方向均出现这种情况. 在播放轨迹时两条链不时地在盒子两侧之间跳跃. 根据经验, 初步认为这是由于PBC处理不当导致的.

为确认这一点, 我们使用VMD查看轨迹中的一帧 `test.pdb`. 在VMD的命令窗口中执行 `pbc box` 显示盒子, 可看到两条链沿X轴方向确实分处于盒子两侧, 且有些原子处于盒子内, 有些处于盒子外.



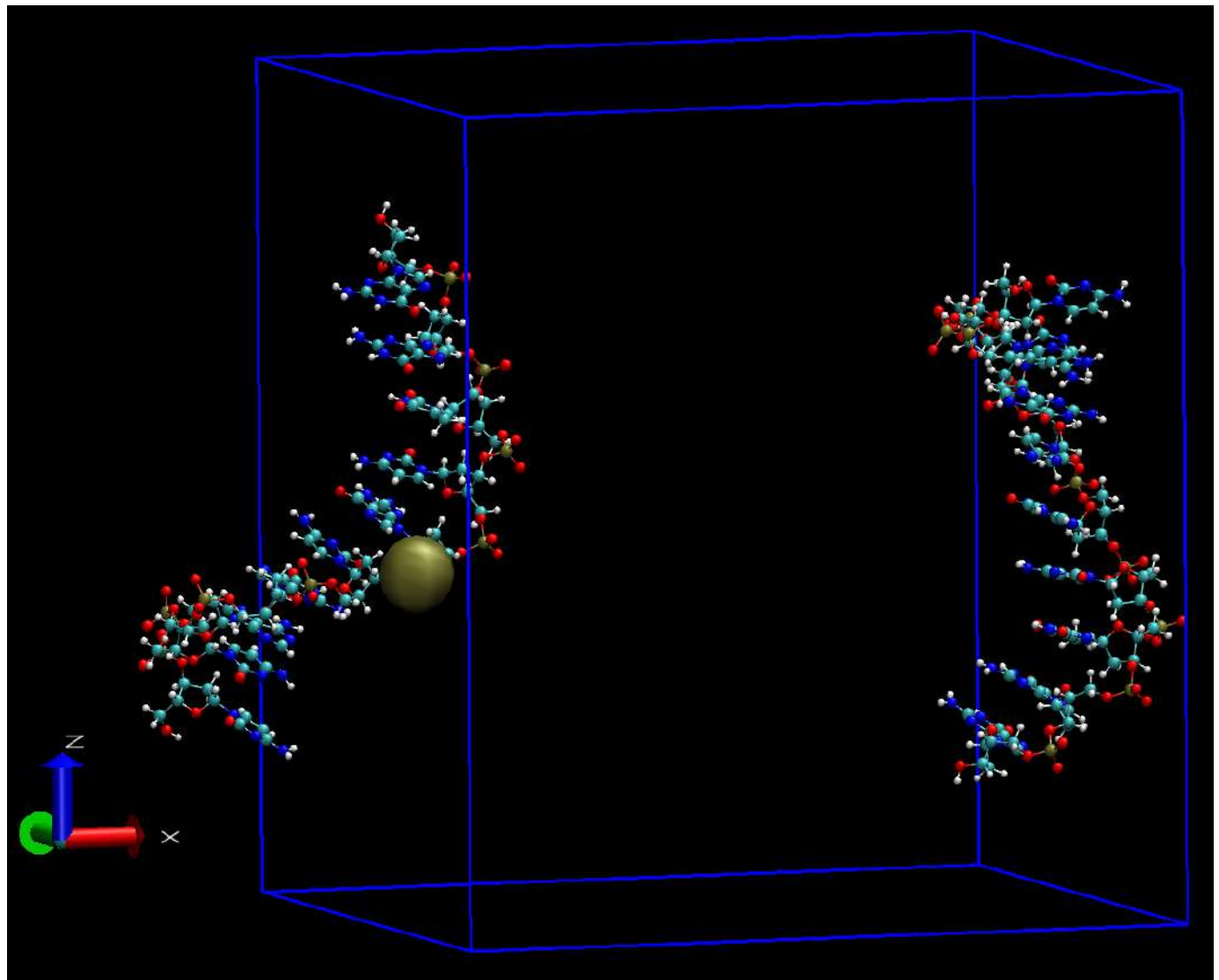
为确认两段DNA并没有分离, 点击 **Graphics** -> **Representations** -> **Periodic**, 选择 **+X** 或 **-X** 体系在X反向的映象, 就可看到两条链处于一起了, 这就说明先前显示的分离确实是由于PBC的原因导致的. 根据上面的说明, 我们一定有办法通过PBC处理使VMD显示正常.



使复合物按中心原子进行居中

对得到的轨迹 **prod_whole.xtc** 进行下一步处理时, 需要选择DNA分子中需要居中的 **一个原子**. 选择的标准是, 如果将DNA以此原子在盒子中居中, DNA中的所有原子均能包含在盒子中. 这里要注意的是, 对我们的这个体系, 不要选择序列最中间配对的两个核苷酸(或其C1')作为中心组, 因为这样的话, 会以这些原子的质心进行居中, 而这些原子已经分离开来, 即便以其质心居中, 仍不能保证所有原子都聚集在一起.

我们选择 **154** 号原子作为中心, 因为它近似处于分子的中心



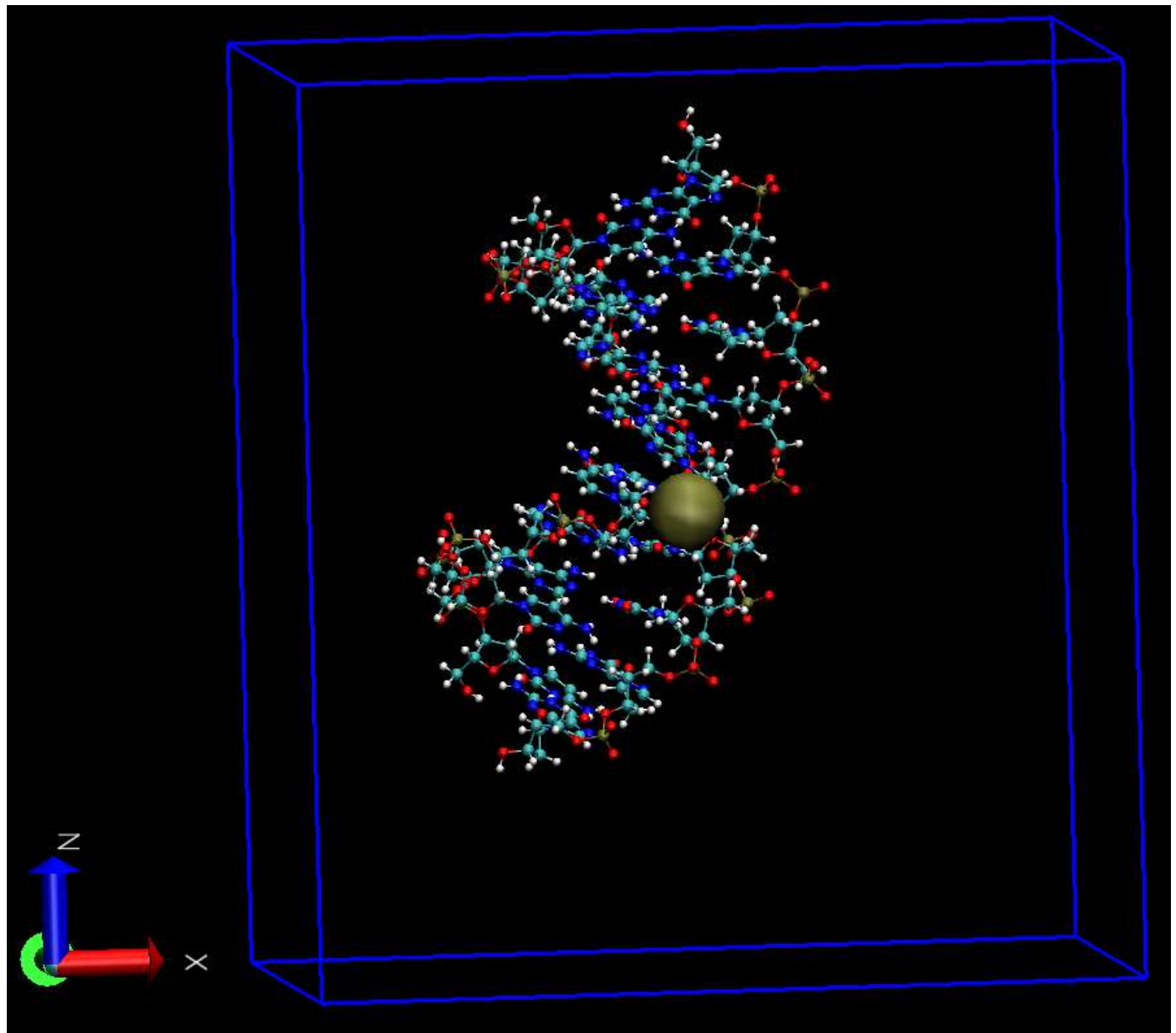
在 **index.ndx** 文件中添加这个中心组

```
[ center ]  
154
```

然后执行下面的命令

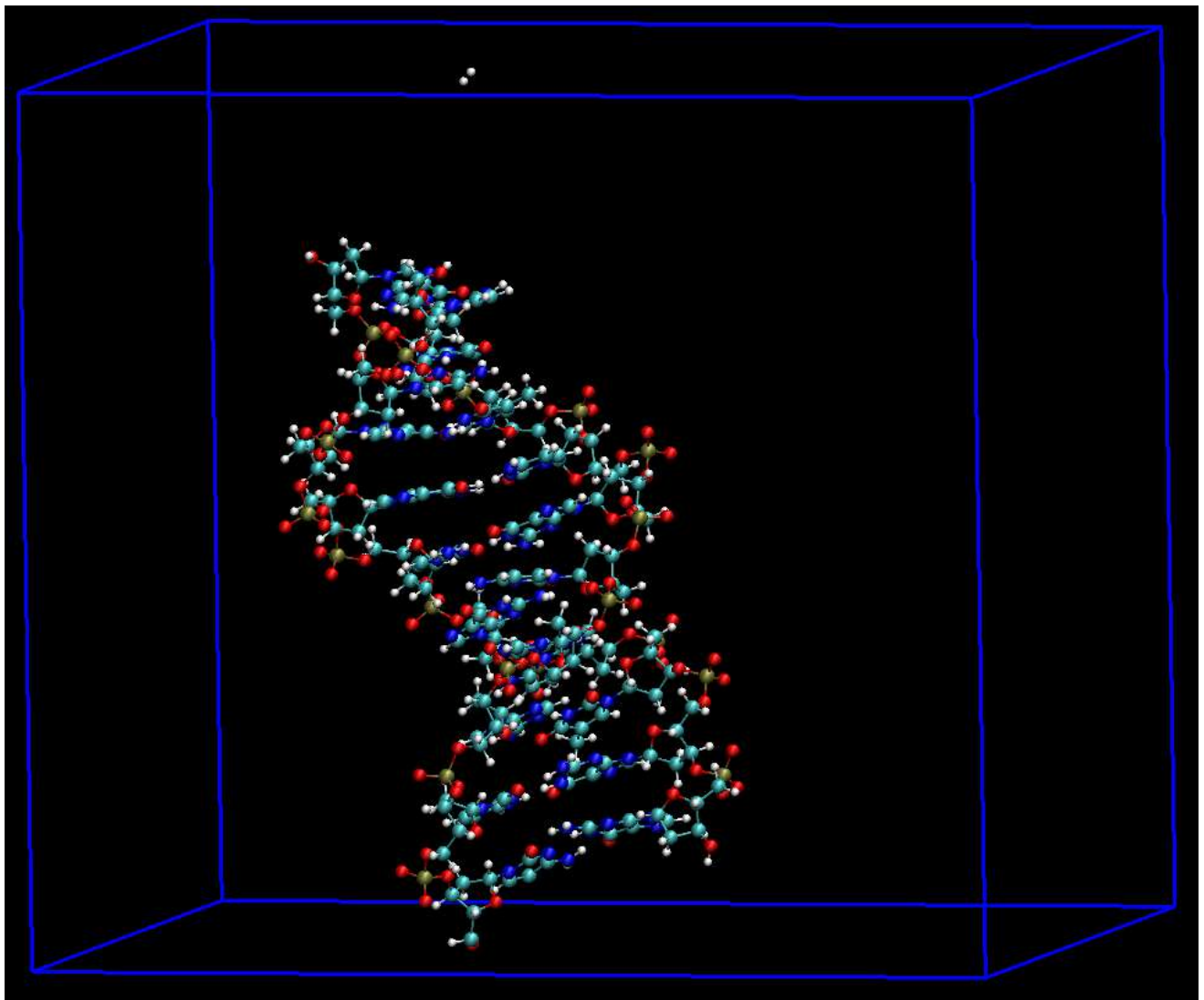
```
gmx trjconv -s npt.tpr -f prod_whole.xtc -n index.ndx -o prod_atom_center.xtc
```

提示时分别选择中心组和DNA即可. **test.pdb** 处理后的构型如下



关于上面命令中 **-pbc** 选项的选取, 则根据不同情况来,

- **atom**: 最通用, 适用于所有情况. 但如果查看得到的轨迹, 发现个别帧仍有部分原子处于盒子外面, 则说明所选的中心原子不合适, 需要重新选择中心原子.



此外, 若复合物距离盒子边缘的距离过小, 也容易出现这种情况, 因此建议准备体系时, 盒子尽量大些, 视个人计算资源而定, 一般可取3-5 nm. 一则处理PBC时方便, 二则可以避免计算能量时引入分子映象间相互作用的误差.

- **res**: 用于生物分子, 因为在这些分子中可以定义残基. 对我们的示例DNA体系, 使用此选项可能比 **atom** 更好.
- **mol**: 只有当复合物中的每个分子在拓扑文件的 [**system**] 中单独定义时, 使用这个选项才有效. 对我们的DNA体系, 由于在拓扑文件中将两条链定义为了一个分子类型, **gmx trjconv** 处理时会将两条链视为同一个分子, 即便分子质心处于盒子中, 其中某条链或者两条链仍可能处于盒子外, 所以使用此选项不能满足要求.

如果需要, 进行叠合处理

如果需要, 可以进一步进行叠合去除平动和转动

```
gmx trjconv -s npt.tpr -f prod_atom_center.xtc -o prod_atom_center_fit.xtc -fi
```

附

如果你想要尝试一下上面作法, 可以[下载用到的文件](#).

另: 使用VMD的**pbc**命令显示完整分子

VMD提供了一个命令, 也可用于对体系的PBC进行处理. 如果只是用于论文作图, 使用这个命令可能比上面的方法更简单.

基本命令是

```
pbc wrap -compound res -all  
pbc box
```

你也可以同时对盒子进行平移, 以将分子显示在盒子中央(注意, 平移是以盒子长度为单位的)

```
pbc wrap -compound res -all -shiftcenterrel {0.0 -0.5 0.0}  
pbc box -shiftcenterrel {0.0 -0.5 0.0}
```

如果溶质分子的原子类型都是1, 你可以使用下面的命令使其在盒子中居中

```
pbc wrap -sel type=1 -all -centersel type=2 -center com
```

更复杂的一个命令

```
pbc wrap -center com -centersel protein -compound fragment -all
```

详细说明请参考其文档

- pbctools
- pbcbox
- pbcwrap
- pbcwrap示例

评论

- 2016-11-07 19:26:04 **franklinly** 太好了, 李老师, 只是这里面“如果你想要尝试一下上面作法, 可以下载用到的文件.”, 下载后发现没有prod.xtc文件。试不了啊, 希望李老师补上, 谢谢。franklinly
- 2016-11-08 08:25:12 **Jerkwin** 有了输入文件, mdrun一下就可以了. 轨迹文件太大, 没法放附件.



◆本文地址: <https://jerkwin.github.io/2016/05/31/GROMACS轨迹周期性边界条件的处理/>, 转载请注明◆

◆评论问题: <https://jerkwin.herokuapp.com/category/3/博客>, 欢迎留言◆

使用组

gmx make_ndx, gmx mk_angndx, gmx select

```
[ Oxygen ]  
1 4 7
```

```
[ Hydrogen ]  
2 3 5 6  
8 9
```

7

`make_ndx`程序可用来选择原子组(要分析的某些特定原子或残基的ID标签)并创建索引文件. GROMACS已经定义了一些默认的组, 对普通分析可能够用了, 但如果你想进行更深入的分析, 如为了在模拟中固定某些特定的组, 或获得某些组的特殊能量信息, 则需要使用`make_ndx`程序来指定这些组.

运行`make_ndx`后, 可使用`r`选择残基, `a`选择原子, `name`对多组进行改名, 还可以使用`|`表示或运算, `&`表示与运算. 下面是几个简单的例子:

- `r 56`: 选择56号残基
- `r 1 36 37`: 选择不连续的残基
- `r 3-45`: 选择3至45号残基, 使用连接符指定残基标号范围
- `r 3-15 | r 23-67`: 选择3至15, 23至67号残基
- `r 3-15 & 4`: 选择3至15号残基的主干链原子, 在索引文件中, 4号组为默认的主干链.
- `r 1-36 & a C N CA`: 使用包含`&`的命令指定只包含骨架原子的残基范围

新建索引组的默认名称(如`r_1_36_37`)很繁琐, 可以使用`name`命令进行修改. 如`name 15 Terminal`可将组`15`的名称改为`Terminal`. 修改后我们可以使用`v`命令查看名称是否修改成功, 使用`q`命令保存修改并退出.

需要注意的一点就是, 对`make_ndx`的选择, 处理是由左向右依次执行的, `&`和`|`没有优先级别之分. 如`r 1-3 | r 5-9 & CA`会先选择1-3, 5-9号残基, 再从中选择CA原子.

8

使用示例

```
There are:      0      OTHER residues
There are:   960      PROTEIN residues
There are:      0      DNA residues
Analysing Protein...

0 System          : 14571 atoms
1 Protein         : 14571 atoms
2 Protein-H       : 7479 atoms
3 C-alpha         : 960 atoms
4 Backbone        : 2880 atoms
5 MainChain       : 3844 atoms
6 MainChain+Cb    : 4730 atoms
7 MainChain+H     : 4744 atoms
8 SideChain       : 9827 atoms
9 SideChain-H     : 3635 atoms

nr : group      !  'name' nr name  'splitch' nr  Enter: list groups
'a': atom       &  'del' nr      'splitres' nr  'l': list residues
't': atom type  |  'keep' nr     'splitat' nr  'h': help
'r': residue    |  'res' nr      'chain' char
"name": group   |  'case': case sensitive      'q': save and quit
```

9

选择残基

命令 r 1 - 355

```
Found 5467 atoms with res.nr. in range 1-355
```

```
10 r_1-355          : 5467 atoms
0 System            : 14571 atoms
1 Protein           : 14571 atoms
2 Protein-H         : 7479 atoms
3 C-alpha           : 960 atoms
4 Backbone          : 2880 atoms
5 MainChain         : 3844 atoms
6 MainChain+Cb      : 4730 atoms
7 MainChain+H       : 4744 atoms
8 SideChain         : 9827 atoms
9 SideChain-H       : 3635 atoms
10 r_1-355          : 5467 atoms
```

10

重命名 交集

命令

```
name 10 SUB_H
```

```
10 & 2
```

```
Copied index group 10 'SUB_H'  
Copied index group 2 'Protein-H'  
Merged two groups with AND: 5467 7479 -> 2783
```

```
11 SUB_H & Protein-H : 2783 atoms
```

11

拆分链

命令 `splitch 1`

```
Found 4 chains  
1: 5467 atoms (1 to 5467)  
2: 5467 atoms (5468 to 10934)  
3: 1816 atoms (10935 to 12750)  
4: 1821 atoms (12751 to 14571)
```

12

拆分组

命令 `splitat 9`

```
0 System      : 14571 atoms
1 Protein     : 14571 atoms
2 Protein-H   : 7479 atoms
3 C-alpha     : 960 atoms
4 Backbone    : 2880 atoms
5 SUB_H_BB    : 1065 atoms
6 SUB_J_BB    : 1065 atoms
7 SUB_M_BB    : 375 atoms
8 SUB_L_BB    : 375 atoms
9 r_886_985   : 40 atoms
10 r_886_985_N_13464 : 1 atoms
11 r_886_985_H_13465 : 1 atoms
...
32 r_886_985_CM_13486 : 1 atoms
33 r_886_985_HM1_13487 : 1 atoms
34 r_886_985_HM2_13488 : 1 atoms
35 r_886_985_HM3_13489 : 1 atoms

...
45 r_886_985_CG_13770 : 1 atoms
46 r_886_985_OD1_13771 : 1 atoms
47 r_886_985_OD2_13772 : 1 atoms
48 r_886_985_C_13773 : 1 atoms
49 r_886_985_O_13774 : 1 atoms
```

13

删除

命令

```
del 9-31
del 13 -21
del 16-17
```

```
0 System      : 14571 atoms
1 Protein     : 14571 atoms
2 Protein-H   : 7479 atoms
3 C-alpha     : 960 atoms
4 Backbone    : 2880 atoms
5 SUB_H_BB    : 1065 atoms
6 SUB_J_BB    : 1065 atoms
7 SUB_M_BB    : 375 atoms
8 SUB_L_BB    : 375 atoms
9 r_886_905_CM_13486 : 1 atoms
10 r_886_905_HM1_13487 : 1 atoms
11 r_886_905_HM2_13488 : 1 atoms
12 r_886_905_HM3_13489 : 1 atoms
13 r_886_905_CG_13770 : 1 atoms
14 r_886_905_OD1_13771 : 1 atoms
15 r_886_905_OD2_13772 : 1 atoms
```

14

选区语法

- 每个分析工具需要的选区数目各不相同,对选区的解读也不一样,但大致意思仍然相同:每个选区最终都归结为一套位置(a set of position),位置可以是一些原子的原子位置,质心,或几何中心.分析工具可使用这些位置进行分析,这样处理时更加灵活.需要注意的是,某些分析工具对允许使用的选区种类可能存在限制.

15

关键词

- 根据整数型性质选择原子的关键词:

- atomnr
- mol (与 molindex 同义)
- molecule (与 molindex 同义)
- molindex
- resid (与 resnr 同义)
- residue (与 resindex 同义)
- resindex
- resnr

(在表达式中使用, 或类似于 atomnr 1 to 5 7 9)

16

关键词

- 根据数值性质选择原子的关键词:

- `beta` (与 `betafactor` 同义)
- `betafactor`
- `charge`
- `distance from POS [cutoff REAL]`
- `distance from POS [cutoff REAL]`
- `mass`
- `mindistance from POS_EXPR [cutoff REAL]`
- `mindistance from POS_EXPR [cutoff REAL]`
- `occupancy`
- `x`
- `y`
- `z`

(在表达式中使用, 或类似于 `occupancy 0.5 to 1`)

17

关键词

- 使用字符串性质选择原子的关键词:

- `altloc`
- `atomname`
- `atomtype`
- `chain`
- `insertcode`
- `name` (与 `atomname` 同义)
- `pdbatomname`
- `pdbname` (与 `pdbatomname` 同义)
- `resname`
- `type` (与 `atomtype` 同义)

(用法类似于 `name PATTERN [PATTERN] ...`)

18

关键词

- 直接选中原子的额外关键词:

- `all`
- `insolidangle center POS span POS_EXPR [cutoff REAL]`
- `none`
- `same KEYWORD as ATOM_EXPR`
- `within REAL of POS_EXPR`

- 直接求值为位置的关键词:

- `cog of ATOM_EXPR [pbc]`
- `com of ATOM_EXPR [pbc]`

(另可参见《位置》小节)

- 额外关键词:

- `merge POSEXPRESS`
- `POSEXPRESS permute P1 ... PN`
- `plus POSEXPRESS`

19

示例

- 选中所有水中的氧原子

`resname SOL and name OW`

- 残基1到5, 以及残基10的质心

`res_com of resnr 1 to 5 10`

- 距一个固定位置超过1 nm的所有原子

`not within 1 of [1.2, 3.1, 2.4]`

- 属于残基LIG并距一个蛋白质0.5 nm以内的所有原子(使用自定义名称)

`"Close to protein" resname LIG and within 0.5 of group "Protein"`

- 至少有一个原子距残基LIG 0.5 nm以内的所有蛋白质残基

`group "Protein" and same residue as within 0.5 of resname LIG`

- 质心距残基总质心介于2和4 nm之间的所有RES残基

`rdist = res_com distance from com of resname RES`

`resname RES and rdist >= 2 and rdist <= 4`

示例

- 包含如C1 C2 C2 C3 C3 C4 ... C8 C9的重复原子的选区

```
name "C[1-8]" merge name "C[2-9]"
```

这可用于`gmx distance`以计算C1-C2, C2-C3等原子之间的距离.

- 具有顺序C2 C1的选区

```
name C1 C2 permute 2 1
```

这可用于`gmx gangle`以得到C2->C1矢量而不是C1->C2矢量.

- 由两个索引组的质心组成的选区

```
com of group 1 plus com of group 2
```

这可用于`gmx distance`以计算这两个质心间的距离.

- 沿x的固定矢量(可在`gmx gangle`中用作参考)

```
[0, 0, 0] plus [1, 0, 0]
```

示例

- 以下示例解释了各种位置类型之间的差异. 这个选区在每个残基选中一个位置, 其中三个原子C[123]中的任意一个满足`x < 2`. 这个位置为所有三个原子的质心. 这是你只写`res_com of`时的默认行为.

```
part_res_com of name C1 C2 C3 and x < 2
```

下面这个选区完成同样的工作, 但位置是整个残基的质心

```
whole_res_com of name C1 C2 C3 and x < 2
```

最后, 下面这个选区选中同样的残基, 但位置是那些严格满足`x < 2`判断的原子的质心

```
dyn_res_com of name C1 C2 C3 and x < 2
```

- 没有`of`关键词时, 默认行为会与以上所述不同, 但除此以外规则是相同的:

```
name C1 C2 C3 and res_com x < 2
```

就像指定了`whole_res_com`一样工作, 并从质心满足`x < 2`的残基中选中那三个原子. 使用

```
name C1 C2 C3 and part_res_com x < 2
```

会基于从C[123]原子计算的质心来选中残基.

分析轨迹

[gmx trjcat](#) - 连接轨迹文件(翻译: 李继存) 原始文档

[gmx trjconv](#) - 转换和操控轨迹文件(翻译: 黄灏) 原始文档

[gmx editconf](#) - 编辑模拟盒子以及写入子组(**subgroups**)(翻译: 严立京) 原始文档

[gmx spatial](#) - 计算空间分布函数(翻译: 刘建川) 原始文档

[gmx traj](#) - 输出轨迹文件中的坐标x, 速度v, 力f, 盒子, 温度和转动能(翻译: 康文斌) 原始文档

[gmx dump](#) - 生成人类可读的二进制文件(翻译: 黄丽红) 原始文档

[gmx make_ndx](#) - 制作索引文件(翻译: 刘恒江) 原始文档

[gmx mk_angndx](#) - 生成用于gmx angle的索引文件(翻译: 白艳艳) 原始文档

[gmx trjorder](#) - 根据到参考组原子的距离对分子排序(翻译: 李培春) 原始文档

[gmx gangle](#) - 计算角度(翻译: 杨宇) 原始文档

[gmx distance](#) - 计算两个位置之间的距离(翻译: 姚闯) 原始文档

[gmx freevolume](#) - 计算自由体积(翻译: 姜山) 原始文档

[gmx sasa](#) - 计算溶剂可及表面积(翻译: 白艳艳) 原始文档

[gmx select](#) - 打印选区的通用信息(翻译: 陈珂) 原始文档

23

分析轨迹: 距离

结构间的距离

[gmx cluster](#) - 对结构进行团簇分析(翻译: 姚闯) 原始文档

[gmx confrms](#) - 叠合两个结构并计算RMSD(翻译: 李耀) 原始文档

[gmx rms](#) - 计算与参考结构之间的RMSD及其矩阵(翻译: 王育伟) 原始文档

[gmx rmsf](#) - 计算平均结构, 原子涨落, 温度因子(翻译: 杨旭云) 原始文档

结构中的距离随时间的变化

[gmx mindist](#) - 计算两组间的最小距离(翻译: 王燕) 原始文档

[gmx mdmat](#) - 计算残基接触映射图(翻译: 陈辰) 原始文档

[gmx polystat](#) - 计算聚合物的静态性质(翻译: 杜星) 原始文档

[gmx rmsdist](#) - 计算-2, -3或-6次平均的原子对距离(翻译: 冯佳伟) 原始文档

24

分析轨迹: 分布性质

[gmx gyrate](#) - 计算蛋白质的回旋半径(翻译: 黄丽红) [原始文档](#)

[gmx msd](#) - 计算均方位移(翻译: 赵丙春) [原始文档](#)

[gmx polystat](#) - 计算聚合物的静态性质(翻译: 杜星) [原始文档](#)

[gmx rdf](#) - 计算径向分布函数(翻译: 严立京) [原始文档](#)

[gmx rotacf](#) - 计算分子的转动相关函数(翻译: 韩广超) [原始文档](#)

[gmx rotmat](#) - 计算叠合到参考结构的旋转矩阵(翻译: 李继存) [原始文档](#)

[gmx sans](#) - 计算小角中子散射谱(翻译: 李耀) [原始文档](#)

[gmx saxs](#) - 计算小角X射线散射谱(翻译: 李继存) [原始文档](#)

[gmx traj](#) - 输出轨迹文件中的坐标x, 速度v, 力f, 盒子, 温度和转动能(翻译: 康文斌) [原始文档](#)

[gmx vanhove](#) - 计算Van Hove位移及相关函数(翻译: 刘恒江) [原始文档](#)

25

分析轨迹: 结构

[gmx anadock](#) - 根据Autodock运行计算团簇结构(翻译: 白艳艳) [原始文档](#)

[gmx bundle](#) - 分析轴束, 例如螺旋(翻译: 王燕) [原始文档](#)

[gmx clustsize](#) - 计算原子团簇的尺寸分布(翻译: 康文斌) [原始文档](#)

[gmx disre](#) - 分析距离限制(翻译: 严立京) [原始文档](#)

[gmx hbond](#) - 计算分析氢键(翻译: 杨旭云) [原始文档](#)

[gmx order](#) - 计算碳末端每个原子的序参量(翻译: 张爱) [原始文档](#)

[gmx principal](#) - 计算一组原子的惯性主轴(翻译: 李继存) [原始文档](#)

[gmx rdf](#) - 计算径向分布函数(翻译: 严立京) [原始文档](#)

[gmx saltbr](#) - 计算盐桥(翻译: 罗健) [原始文档](#)

[gmx sorient](#) - 分析溶质周围的溶剂取向(翻译: 李继存) [原始文档](#)

[gmx spol](#) - 分析溶质周围溶剂的偶极取向及极化(翻译: 李继存) [原始文档](#)

20

分析轨迹: 动力学性质

[gmx bar](#) - 利用Bennett接受比率方法计算自由能差的估计值(翻译: 陈珂) [原始文档](#)

[gmx current](#) - 计算介电常数和电流自相关函数(翻译: 刘恒江) [原始文档](#)

[gmx dos](#) - 分析态密度及相关性质(翻译: 韩广超) [原始文档](#)

[gmx dyecoupl](#) - 从轨迹中抽取染料动力学(翻译: 李继存) [原始文档](#)

[gmx principal](#) - 计算一组原子的惯性主轴(翻译: 李继存) [原始文档](#)

[gmx tcaf](#) - 计算液体的粘度(翻译: 肖慧芳) [原始文档](#)

[gmx traj](#) - 输出轨迹文件中的坐标x, 速度v, 力f, 盒子, 温度和转动能(翻译: 康文斌) [原始文档](#)

[gmx vanhove](#) - 计算Van Hove位移及相关函数(翻译: 刘恒江) [原始文档](#)

[gmx velacc](#) - 计算速度自相关函数(翻译: 刘建川) [原始文档](#)

27

分析轨迹: 静电性质

[gmx current](#) - 计算介电常数和电流自相关函数(翻译: 刘恒江) [原始文档](#)

[gmx dielectric](#) - 计算频率相关的介电常数(翻译: 白艳艳) [原始文档](#)

[gmx dipoles](#) - 计算总偶极及其涨落(翻译: 曹锟) [原始文档](#)

[gmx potential](#) - 计算盒子内的静电势(翻译: 陈珂) [原始文档](#)

[gmx spol](#) - 分析溶质周围溶剂的偶极取向及极化(翻译: 李继存) [原始文档](#)

[gmx genion](#) - 在能量有利位置加入单原子离子(翻译: 李继存) [原始文档](#)

28

分析轨迹: 蛋白质相关

[gmx do_dssp](#) - 指定二级结构并计算溶剂可及表面积(翻译: 杨旭云) [原始文档](#)

[gmx chi](#) - 计算chi和其他二面角的所有信息(翻译: 黄炎) [原始文档](#)

[gmx helix](#) - 计算 α 螺旋结构的基本性质(翻译: 李卫星) [原始文档](#)

[gmx helixorient](#) - 计算螺旋内的局部螺距/弯曲/旋转/取向(翻译: 陈辰) [原始文档](#)

[gmx rama](#) - 计算Ramachandran图(翻译: 杜星) [原始文档](#)

[gmx wheel](#) - 绘制螺旋轮图(翻译: 李继存) [原始文档](#)

29

分析轨迹: 界面

[gmx bundle](#) - 分析轴束, 例如螺旋(翻译: 王燕) [原始文档](#)

[gmx density](#) - 计算体系的密度(翻译: 阮洋) [原始文档](#)

[gmx densmap](#) - 计算二维的平面或轴径向密度映射图(翻译: 姚闯) [原始文档](#)

[gmx densorder](#) - 计算表面涨落(翻译: 李卫星) [原始文档](#)

[gmx h2order](#) - 计算水分子的取向(翻译: 嘉晔, 严立京) [原始文档](#)

[gmx hydorder](#) - 计算给定原子周围的四面体参数(翻译: 王浩博) [原始文档](#)

[gmx order](#) - 计算碳末端每个原子的序参量(翻译: 张爱) [原始文档](#)

[gmx potential](#) - 计算盒子内的静电势(翻译: 陈珂) [原始文档](#)

30

轨迹的读取处理

- **xdrfile:** C, Fortran, Python

[http://www.gromacs.org/Developer_Zone/
Programming_Guide/XTC_Library](http://www.gromacs.org/Developer_Zone/Programming_Guide/XTC_Library)

- **Gro2mat:** MatLab

<http://opig.stats.ox.ac.uk/resources>

- **MDtraj:** python 轨迹转换

<http://mdtraj.org/>

- **MDAnalysis:** Python多种轨迹格式

<http://www.mdanalysis.org/>

31

简单分析工具

- 能量性质: gmx energy

- 距离/角度: gmx

distance/gangle

- RDF: gmx rdf -cn

- rmsd/rmsf: gmx rms

- MSD 扩散系数: gmx msd

32

复杂分析与模拟

- 无法使用已有工具一步完成
 - 组合已有工具
 - 自己编写工具
 - 建议二者结合
- 借助脚本语言
- 提高效率, 不受限

33

思路

- 明确问题
- 搜寻工具
- 组合工具
- 处理数据, 汇报结果
- 先拿几帧轨迹做测试
- 运用到整条轨迹

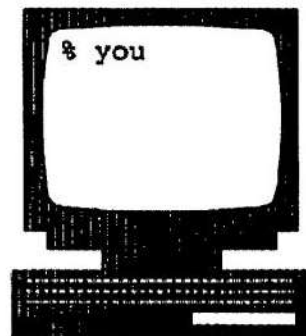
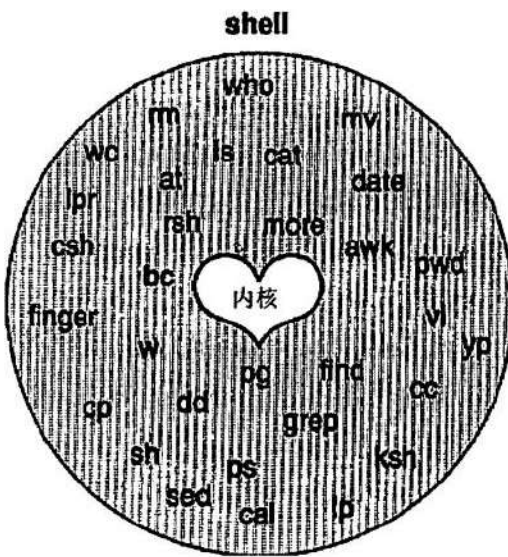
34

bash 脚本

- 基础命令
- 正则表达式/通配符
- 文本处理 <http://ahei.info/text-processing.htm>

35

内核 shell 用户界面



36

基础命令

bash

man

clear

sleep

nohup

xargs

ls

cp

rcp

rm

mv

pwd

mkdir

chmod

basename

echo

touch

cat

more

head

tail

grep

cut

paste

join

sort

uniq

wc

split

bc

awk
sed

37

awk

awk – 扫描模式并处理语言

awk [-fprogram-file] [-Fc] [prog] [parameters] [filename...]

awk 扫描每个输入文件名指定的文件，以查找与 prog 指定的模式组中任一模式匹配的行。

范例 A-4

```
1 awk '{print $1, $2}' file
2 awk '/John/{print $3, $4}' file
3 awk -F: '{print $3}' /etc/passwd
4 date | awk '{print $6}'
```

说明

1. 打印文件 file 中各行的头两个字段，文件中的字段以空白符分隔。
2. 找到模式 found 后，打印所在行的第 3 个和第 4 个字段。
3. 把冒号作为字段分隔符，打印文件/etc/passwd 的第 3 个字段。
4. 把 date 命令的输出结果发给 awk，由 awk 打印出结果的第 6 个字段。

38

basename

basename – 提取给定目录名中的部分路径名

```
basename string [ suffix ]  
dirname string
```

basename 从字符串 string 中删除以正斜杠/结尾的前缀，以及字符串 string 中可能包含的指定后缀 suffix，然后将结果打印在标准输出上。

范例 A-6

```
1 basename /usr/local/bin  
2 scriptname="basename $0"
```

说明

1. 删除前缀/usr/local/，结果为 bin。
2. 仅将脚本的名称，\$0，赋值给变量 scriptname。

39

bash

bash – GNU Bourne Again shell

```
bash [options] [file[arguments]]  
sh [options] [file[arguments]]
```

bash 版权信息为 Copyright © 1989, 1991 by the Free Software Foundation, Inc. bash 是一个与 sh 兼容的命令语言解释器，它从标准输入或文件中读取并执行命令。bash 同时还结合了来自 Korn shell 和 C shell(ksh 和 csh)的有用的特性。

40

bc

bc – 处理高精度的算术运算

```
bc [ -c ] [ -l ] [ filename... ]
```

bc 是一个交互式的语言处理程序，处理类似于 C 语言的对象，但能提供高精度的算术运算。bc 先从所有指定文件中读取输入，处理完之后，接着从标准输入读取。

范例 A-7

```
1 bc << EOF
scale=3
4.5 + 5.6 / 3
EOF
Output : 6.366
```

说明

1. 这是一个 here 文档。从第一个 EOF 到结尾处那个 EOF 之间的输入被传给 bc 命令。

scale 用于指定小数点后的位数。计算结果被显示在屏幕上。

41

cat

cat – 连接文件并显示

```
cat [ -bnsuvet ] filename...
```

cat 按顺序读入指定的每个文件，把它们的内容写到标准输出。如果未指定输入文件，或指定了参数-，cat 就从标准输入文件读取输入。

范例 A-9

```
1 cat /etc/passwd
2 cat -n file1 file2 >> file3
```

说明

1. 显示文件/etc/passwd 的内容。
2. 连接文件 file1 和 file2，并将结果追加到文件 file3 中。开关-n 使得每一行都被标上行号。

42

chmod

chmod – 改变文件的权限模式

```
chmod [ -fR ] mode filename...
chmod [ugo ]{ + | - | = }[ rwxlsStTugo] filename...
```

chmod 用于修改或设置文件的模式。文件的模式规定了文件的访问权限等属性。模式可以是绝对的或链接的。

范例 A-10

```
1 chmod +x script.file
2 chmod u+x,g-x file
3 chmod 755 *
```

说明

1. 打开属主、属组和其他用户对文件 script.file 的执行权限。
2. 打开属主对文件 file 的执行权限，同时取消属组用户的执行权限。
3. 为当前工作路径下所有文件打开属主用户的读、写和执行权限、属组用户的读和执行权限，以及其他用户的读和执行权限。所给的参数是一个八进制值(111 101 101)，相当于：

```
rwxr-xr-x
```

clear

clear – 清空终端屏幕

cp

cp – 复制文件

```
cp [ -i ] [ -p ] [ -r ] [ filename ... ] target
```

cp 命令将文件 filename 复制到 target, target 可以是一个文件或目录。filename 和 target 这两个参数不能相同。如果 target 不是目录, target 前面就只能指定一个文件; 如果 target 是个目录, 就可以指定多个文件。如果 target 不存在, cp 就创建一个名为 target 的文件。如果 target 存在并且不是目录, 它的内容就会被覆盖。如果 target 是一个目录, 指定的文件就被复制到该目录下。

范例 A-15

```
1 cp file1 file2  
2 cp chapter1 book  
3 cp -r desktop /usr/bin/tester
```

说明

1. 把文件 file1 的内容复制到文件 file2。
2. 把文件 chapter1 的内容复制到目录 book 下。复制到目录 book 的文件保留了原来的名字 chapter1。
3. 逐层将整个 desktop 目录复制到 /usr/bin/tester。

→5

cut

cut – 删减文件各行中的指定字段或字符

```
cut -c list [ filename ... ]  
cut -f list [ -d c ] [ -s ] [ filename ... ]
```

cut 命令从文件的各行中截除某一(或某几)列或字符; 如果未指定文件, cut 便对标准输入进行操作。选项-d 指定字段分隔符。默认的字段分隔符是制表符。

范例 A-17

```
1. cut -d: -f1,3 /etc/passwd  
2. cut -d: -f1-5 /etc/passwd  
3. cut -c1-3,8-12 /etc/passwd  
4. date | cut -c1-3
```

说明

1. 以冒号作为字段分隔符, 显示文件 /etc/passwd 的第 1、3 字段。
2. 以冒号作为字段分隔符, 显示文件 /etc/passwd 的第 1~5 字段。
3. 截除文件 /etc/passwd 中各行的第 1~3、8~12 个字符, 并显示在屏幕上。
4. 将 date 命令的输出结果作为输入传给 cut。打印结果的头 3 个字符。

→6

echo

echo – 回显参数

```
echo [ argument ] ...
echo [ -n ] [ argument ]
```

echo 命令把传给它的参数写到标准输出上，用空格分隔各参数，并且在输出的末尾加上一个换行符。

针对 System V 系统的 echo 命令选项：

\b	退格
\c	取消输出结果末尾的换行符
\f	换页
\n	换行
\r	回车
\t	制表符
\v	纵向制表符
\\\	反斜杠
\0n	n 为 1、2 或 3，八进制值

47

grep

grep – 在文件中查找模式

```
grep [ -bchilnsvw ] limited-regular-expression [ filename ... ]
```

grep 在文件中查找指定模式，并且打印出包含该模式的所有行。grep 使用正则表达式元字符来匹配模式。egrep 使用的则是扩展的元字符集。

范例 A-32

```
1 grep Tom file1 file2 file3
2 grep -in '^tom savage' *
```

说明

1. grep 显示文件 file1、file2 和 file3 中所有包含模式 Tom 的行。
2. grep 显示当前工作目录下的文件中包含 tom savage 的所有行，并且给出各自的行号。这条 grep 命令忽略大小写，但要求 tom savage 必须出现在行首。

48

head

head – 输出文件的前 10 行

```
head [-c N[bkm]] [-n N] [-qv] [--bytes=N[bkm]] [--lines=N] [--quiet]
      [--silent] [--verbose] [--help] [--version] [file...]
head [-Nbcklmqv] [file...]
```

head 在标准输出上显示文件的前十行。多于一个文件时，在每行前面加上文件名。如果没有文件或文件为-，则从标准输入读。

49

ls

ls – 列出目录内容

```
ls [ -abcCdfFgillLmnopqrRstux1 ] [ names ]
```

对于每个目录参数，ls 列出该目录的内容；对于每个文件参数，ls 打印该文件的名称和所需的其他信息。默认情况下，输出结果按字母顺序排序。如果未给定参数，ls 列出当前目录的内容。

范例 A-37

```
1 ls -alF
2 ls -d a*
3 ls -i
```

说明

1. -a 列出隐藏文件(即那些名称以句点开头的文件)。-l 以长格式列出文件的属性。-F 在目录文件名末尾加上斜杠，在可执行脚本名末尾加上星号(*)，在符号链接文件的名字后面加上符号@。

2. 如果开关-d 的参数是某个目录，则只显示该目录的名称，而不显示内容。

3. 开关-i 指示 ls 在每个文件名前面给出该文件的 i 节点号。

50

man

man – 在线手册的格式设计与显示

```
man [-acdfhktwW] [-m system] [-p string] [-C config_file] [-M path]
      [-P pager] [-S section_list] [section] name...
```

51

mkdir

mkdir – 创建目录

```
mkdir [ -p ] dirname ...
```

52

more

more – 浏览或逐页查看文本文件

```
more [ -cdflsruuw ] [ -lines ] [ +linenumber ] [ +/pattern ] [ filename ... ]
page [ -cdflsruuw ] [ -lines ] [ +linenumber ] [ +/pattern ] [ filename ... ]
```

more 是一个过滤器，它在终端上显示文本文件的内容，每次一屏。通常，more 每显示一屏就暂停，同时在屏幕底端打印—More-。

53

mv

mv – 移动或更名文件

```
mv [ -f ] [ -i ] filename1 [ filename2 ... ] target
```

mv 命令将源文件移动到目标文件。源文件和目标文件不能重名。如果 target 不是目录，它前面就只能指定一个文件。如果 target 是目录，就能指定多个文件。如果 target 不存在，mv 就创建一个名为 target 的文件。如果 target 已存在并且不是目录，它的内容将被覆盖。如果 target 是目录，mv 就将源文件(一个或多个)移到该目录下。

范例 A-38

```
1 mv file1 newname
2 mv -i test1 test2 train
```

说明

1. 将文件 file1 更名为 newname。如果 newname 已存在，其内容将被覆盖。
2. 将文件 test1 和 test2 移动到目录 train。开关-i 指定使用交互模式，即在移动文件前进行询问。

54

nohup

nohup – 使命令不响应挂起和退出信号

```
/usr/bin/nohup command [ arguments ]
```

nohup 有 3 个不同的版本。在 C shell 里，nohup 是一个内置命令，在 Bourne shell 中则是可执行文件/usr/bin/nohup。Bourne shell 版的 nohup 执行命令，使其不受 HUP(挂起)信号和 TERM(终止)信号的影响。标准输出如果是终端，就会被重定向到文件 nohup.out。标准错误输出随标准输出一起被重定向。命令的优先级被加 5。从 shell 调用 nohup 时应该加上 &，以防止它响应中断和来自下一用户的输入。

范例 A-39

```
nohup lookup &
```

说明

lookup 程序将在后台运行，而且即使用户退出系统，也会持续运行直至完成。lookup 产生的所有输出都被写到当前目录下一个叫做 nohup.out 的文件中。

55

paste

paste – 合并多个文件中的相同行或同一文件连续行

```
paste filename1 filename2...
paste -d list filename1 filename2...
paste -s [ -d list ] filename1 filename2...
```

paste 连接给定的 filename1、filename2 等输入文件中相应的行。它把每个文件视为表的一列或多列，将它们横向粘贴在一起。

范例 A-40

```
1  ls | paste - - -
2  paste -s -d"\t\n" testfile1 testfile2
3  paste file1 file2
```

说明

1. 分 3 列将文件列出，列之间用制表符连接。
2. 将两行合成一行，用制表符和换行符作为分隔符，即头两行用制表符连接，接下来的两行用换行符连接，再往下的两行又用制表符连接，以此类推。开关-s 使得文件 testfile1 中的行贴在前头，后面才是 testfile2 中的行。
3. 将文件 file1 里的行加到文件 file2 的行后。二者用制表符连接，看起来就像表的两列。

pwd

pwd – 显示当前工作目录名

57

rcp

rcp – 远程文件复制

```
rcp [ -p ] filename1 filename2  
rcp [ -pr ] filename...directory
```

rcp 命令按下列格式在机器之间复制文件：

```
remotehostname:path  
user@hostname:file  
user@hostname.domainname:file
```

范例 A-43

```
1 rcp dolphin:filename /tmp/newfilename  
2 rcp filename broncos:newfilename
```

说明

1. 从远程机器 dolphin 将 filename 复制到本机的/tmp/newfilename。
2. 从本机复制 filename 到远程机器 broncos，并将其命名成 newfilename。

58

rm

rm – 从目录删除文件

```
rm [-f] [-i] filename...
rm -r [-f] [-i] dirname...[filename...]
```

如果对文件有写权限, rm 就能删除一个或多个文件在目录中的对应记录。如果 filename 是一个符号链接, rm 会删除该链接, 但链接指向的文件或目录不会被删除。用户要删除符号链接不必对它有写权限, 只要具有对链接所在目录的写权限就行。

范例 A-46

```
1 rm file1 file2
2 rm -i *
3 rm -rf dir
```

说明

1. 从目录中删除文件 file1 和 file2。
2. 删除当前工作目录下的所有文件, 但是事先询问是否删除。
3. 逐层删除 dir 下的所有文件和目录, 忽略报错消息。

59

sed

sed – 精简的编辑器

```
sed [-n] [-e script] [-f sfilename] [filename ...]
```

sed 把指定的文件 filename(默认为标准输入)复制到标准输出, 文件的内容已被 sed 依据命令或脚本编辑过。sed 不改变原文件。

范例 A-49

```
1 sed 's/Elizabeth/Lizzy/g' file
2 sed '/Dork/d' file
3 sed -n '15,20p' file
```

说明

1. 用 Lizzy 替换文件 file 中出现的所有 Elizabeth, 并将结果显示在终端屏幕上。
2. 删除所有包含 Dork 的行并在屏幕上打印剩余的行。
3. 只打印第 15~20 行。

60

sleep

sleep – 挂起一定的秒数后执行

```
sleep time
```

sleep 挂起 time 指定的秒数后执行。它用来在一段时间后执行一个命令。

范例 A-50

```
1 (sleep 105; command) &
2 (In Script)
while true
do
    command
    sleep 60
done
```

说明

1. 在 105 秒后，执行命令。提示符会立即出现。
2. 进入循环：执行命令并在再次进入循环前暂停一分钟。

61

sort

sort – 排序和/或合并文件

```
sort [ -cmu ] [ -ooutput ] [ -T directory ] [ -ykmem ]
      [ -dfiMnr ] [ -btx ] [ +pos1 [ -pos2 ] ] [ filename... ]
```

sort 命令将所有命名文件里的行进行排序(ASCII 码)，并把结果写入标准输出。比较是基于从各输入行抽取的一个或多个排序键进行的。默认情况下，有一个排序键，即整个输入行，并且按机器排序序列里的字典排序法进行排列。

范例 A-51

```
1 sort filename
2
3 sort -u filename
4 sort -r filename
5 sort -1 2 filename
6 sort -2n filename
7 sort -t: +2n -3 filename
8 sort -f filename
9 sort -b +1 filename
```

topSage.co

说明

1. 按字母顺序将行排序。
2. 排序输出重复的条目。
3. 逆序排序。
4. 排序从第一个字段(字段用空白符分隔并从 0 开始计算)开始，在第二个字段结束，而不是一直排序到行尾。
5. 按数值将第三个字段排序。
6. 按数值从第三个字段开始排序，并在第四个字段停止，把冒号当作字段分隔符(-t)。
7. 排序合并大小写字母。
8. 排序从第一个字段开始，删除前导空白符。

split

split – 将文件分片

```
split [ -n ] [ filename [ name ] ]
```

split 命令读取文件 filename 并将其分成大小为 n 行的一组小文件作为输出。第一个输出文件在文件名后追加 aa，然后以词典顺序追加直到 zz(最多 676 个文件)。name 的最大长度比文件系统所允许的最大文件名长度小 2 个字符。参见 statvfs。如果没有指定名称，则默认为使用 x(输出文件则为 xaa, xab 等)。

范例 A-52

```
1 split -500 filea  
2 split -1000 fileb out
```

说明

1. 将文件 filea 分成 500 行大小的文件，依次命名为 xaa, xab, xac 并以此类推。
2. 将文件 fileb 分成 1000 行大小的文件，依次命名为 out.aa, out.ab 并以此类推。

63

tail

tail – 显示文件尾

```
tail +[ -number [ lbc ] [ f ] [ filename ] ]  
tail +[ -number [ l ] [ rf ] [ filename ] ]
```

在 number 前加上一个加号，则 tail 将从文件第 number 行开始显示内容，显示内容可以是代码段、行或字符串。如果在 number 前加连字号，则 tail 将从文件尾开始计数。

范例 A-55

```
1 tail +50 filex  
2 tail -20 filex  
3 tail filex
```

说明

1. 从第 50 行开始显示 filex 文件的内容。
2. 显示 filex 文件的最后 20 行。
3. 显示 filex 文件的最后 10 行。

64

touch

touch – 更新文件的访问时间和/或修改时间

```
touch [ -amc ] [ mmddhhmm [ yy ] ] filename...
```

touch 更新参数指定的各文件的访问时间和修改时间。如果指定的文件不存在，touch 就会创建它。如果未指定时间，touch 将使用当前时间。

范例 A-61

```
touch a b c
```

说明

创建 a、b 和 c 这 3 个文件。如果三者中某个已存在，则更新其修改时间戳。

65

uniq

uniq – 报告文件中的重复行

```
uniq [ [ -u ] [ -d ] [ -c ] [ +n ] [ -n ] ] [ input [ output ] ]
```

uniq 命令读取输入文件，并比较相邻行。正常情况下，重复行的第二个副本及之后的副本都被删除，剩余的内容则被写到标准输出。任何时候，输入和输出必须不同。

范例 A-67

```
1 uniq file1 file2  
2 uniq -d -2 file3
```

说明

1. 删除文件 file1 中的重复行，将结果写入文件 file2。
2. 显示从第 3 个字段开始内容相同的重复行。

66

WC

WC – 统计行数、词数和字符数

```
wc [ -lwc ] [ filename ... ]
```

wc 命令用于计算文件中的行数、词数和字符数，如果未指定文件，则对标准输入进行统计。词指的是用空格、制表符或换行符分隔的字符串。

范例 A-69

```
1  wc filex  
2  who | wc -l  
3  wc -l filex
```

说明

1. 打印文件 filex 中行、词和字符的数目。
2. 用管道将 who 命令的输出发送到 wc，显示计算得到的行数。
3. 打印文件 filex 中行的数目。

67

xargs

xargs – 构造参数列表并执行命令

```
xargs [ flags ] [ command [ initial-arguments ] ]
```

xargs 命令允许将文件的内容传递给命令行，并动态地构造命令行。

范例 A-70

```
1  ls $1 | xargs -i -t mv $1/{} $2/{}  
2  ls | xargs -p -l rm -rf
```

说明

1. 把目录\$1 下的所有文件移到目录\$2 下，并且在执行每条 mv 命令前先回显它。
2. 逐一提示(-p)用户要删除哪个文件，然后再删除它。

68

Bash脚本

- 基本命令与一些语句组合在一起
- 自动完成某些工作

69

一般

表 2-4 Bash shell 的语法和结构

shbang 行	<p>“shbang”行是脚本的第一行，它通知内核使用哪种 shell 解释脚本中的行。shbang 行由一个#!后跟 shell 的完整路径组成，后面还可跟上各种选项以控制 Shell 的运行方式。</p> <p>例：</p> <pre>#!/bin/bash</pre>
注释	<p>注释由一个符号# 后跟一些描述性的说明组成，他们可以从行的任意位置开始，在行的末尾结束。</p> <p>例：</p> <pre># This is a comment</pre>
通配符	<p>shell 中有些字符的意义比较特殊，它们被称作是 shell 元字符或通配符。这些字符既非数字也非字母。例如，*、?和[]号常用于文件名扩展，<、>、2>、>>和 则用于标准 I/O 重定向和管道。为防止这些字符被 shell 解释，它们必须被引用。</p> <p>例：</p> <pre>rm *; ls ??; cat file[1-3]; echo "How are you?"</pre>
显示输出	<p>echo 命令用于向屏幕显示输出。通配符必须使用反斜杠和配对引号进行转义。</p> <p>例：</p> <pre>echo "How are you?"</pre>

70

变量

局部变量	局部变量的作用域被限定在当前 shell 中。当一个脚本执行结束，它们不再可用。也就是说，它们超出了作用域。内置函数 <code>declare</code> 也可以用来定义局部变量。可以创建局部变量并为其赋值。 例： <pre>variable_name=value declare variable_name=value name="John Doe" x=5</pre>
全局变量	全局变量又称环境变量，它们由内置的 <code>export</code> 命令创建。它们为当前运行的 shell 及由此 shell 派生的所有子进程创建。当脚本结束，该全局变量超出作用域。 带-x 选项的内置函数 <code>declare</code> 也用于设置环境变量并将其作为输出。 例： <pre>export VARIABLE_NAME=value declare -x VARIABLE_NAME=value export PATH=/bin:/usr/bin:.</pre>

71

输入

提取 变量值	使用美元符号可以从变量中提取数值。 例： <pre>echo \$variable_name echo \$name echo \$PATH</pre>
读取 用户输入	用户可能会要求输入， <code>read</code> 命令用于从用户输入中读取一行。如果 <code>read</code> 命令有多个参数，则会将输入的这一行分解为多个单词，每个单词赋给一个命名变量。 例： <pre>echo "What is your name?" read name read name1 name2 ...</pre>

72

参数数组

参数	<p>可以从命令行传递参数给脚本。位置参数用于在脚本中得到它们的值。</p> <p>例:</p> <p>命令行: \$ scriptname arg1 arg2 arg3 ...</p> <p>在脚本里:</p> <table><tr><td>echo \$1 \$2 \$3</td><td>位置参数</td></tr><tr><td>echo \$*</td><td>所有位置参数</td></tr><tr><td>echo \$#</td><td>位置参数的个数</td></tr></table>	echo \$1 \$2 \$3	位置参数	echo \$*	所有位置参数	echo \$#	位置参数的个数
echo \$1 \$2 \$3	位置参数						
echo \$*	所有位置参数						
echo \$#	位置参数的个数						
数组	<p>Bourne shell 利用位置参数创建词表。除了使用位置参数, Bash shell 还支持一种数组语法, 因此其元素是通过从 0 开始的下标来访问的。Bash shell 数组使用 declare -a 命令进行创建。</p> <p>例:</p> <pre>set apples pears peaches (positional parameters) echo \$1 \$2 \$3 declare -a array_name=(word1 word2 word3 ...) declare -a fruit=(apples pears plums) echo \${fruit[0]}</pre>						

命令替换

命令替换	<p>与 C shell、TC shell 以及 Bourne shell 类似, UNIX/Linux 命令的输出可以被赋给一个变量, 或者通过使用反引号引用命令, 在一个字符串中使用该命令的输出。Bash shell 还提供了一种新的语法: 无需反引号, 只将命令包含在由美元符号开始的一对圆括号中即可。</p> <p>例:</p> <pre>variable_name=`command` variable_name=\$(command) echo \$variable_name echo "Today is `date`" echo "Today is \$(date)"</pre>
------	---

运算

运算符	与 C 语言运算符类似, Bash shell 使用内置的 test 命令运算符测试数字和字符串。 例: <table><tr><td>等式运算符</td><td>逻辑运算符</td></tr><tr><td><code>==</code> 等于</td><td><code>&&</code> 与</td></tr><tr><td><code>!=</code> 不等于</td><td><code> </code> 或</td></tr><tr><td></td><td><code>!</code> 非</td></tr><tr><td>关系运算符</td><td></td></tr><tr><td><code>></code></td><td>大于</td></tr><tr><td><code>>=</code></td><td>大于等于</td></tr><tr><td><code><</code></td><td>小于</td></tr><tr><td><code><=</code></td><td>小于等于</td></tr></table>	等式运算符	逻辑运算符	<code>==</code> 等于	<code>&&</code> 与	<code>!=</code> 不等于	<code> </code> 或		<code>!</code> 非	关系运算符		<code>></code>	大于	<code>>=</code>	大于等于	<code><</code>	小于	<code><=</code>	小于等于
等式运算符	逻辑运算符																		
<code>==</code> 等于	<code>&&</code> 与																		
<code>!=</code> 不等于	<code> </code> 或																		
	<code>!</code> 非																		
关系运算符																			
<code>></code>	大于																		
<code>>=</code>	大于等于																		
<code><</code>	小于																		
<code><=</code>	小于等于																		
算术运算	Bash shell 支持整型运算。declare -i 命令将声明一个新的整型变量。为保持向后兼容, Korn shell 的 typeset 命令以后仍然可以使用。通过这种方式声明的变量可以进行整型运算。否则, 算术运算将使用(0)语法(let 命令)。 例:																		
算术运算 (续)	<code>declare -i variable_name</code> 用于 bash <code>typeset -i variable_name</code> 用于保持与 ksh 的兼容 <code>((n=5 + 5))</code> <code>echo \$n</code>																		

条件

条件语句	if 结构后跟着一个由圆括号括起来的表达式。这个运算符与 C 运算符类似, 关键字 then 放在闭括号之后。if 必须由 fi 结束。新的测试命令([])用于条件表达式的模式匹配。为和 Bourne shell 向后兼容, 旧的测试命令[]仍旧可用。case 命令与 if/else 的功能等价。 例:
------	---

```

if 结构
if command
then
    block of statements
fi

if [[ expression ]]
then
    block of statements
fi

if (( numeric expression ))
then
    block of statements
else
    block of statements
fi

```

```

if/else 结构
if command
then
    block of statements
else
    block of statements
fi

if [[ expression ]]
then
    block of statements
else
    block of statements
fi

if (( numeric expression ))
then
    block of statements
else
    block of statements
fi

```

77

```

if/else/elseif 结构
if command
then
    block of statements
elif command
then
    block of statements
else if command
then
    block of statements
else
    block of statements
fi

```

```

if [[ expression ]]
then
    block of statements
elif [[ expression ]]
then
    block of statements
else if [[ expression ]]
then
    block of statements
else
    block of statements
fi

if (( numeric expression ))
then
    block of statements
elif (( numeric expression ))
then
    block of statements
else if (( numeric expression ))
then
    block of statements
else
    block of statements
fi

```

78

```

case 结构
case variable_name in
    pattern1)
        statements
        ;;
    pattern2)
        statements
        ;;
    pattern3)
        ;;
esac

case "$color" in
    blue)
        echo $color is blue
        ;;
    green)
        echo $color is green
        ;;
    red|orange)
        echo $color is red or orange
        ;;
    *) echo "Not a match"
        ;;
esac

```

79

循环

循环语句

有 4 种类型的循环: `while`、`until`、`for` 与 `select`。

`while` 循环后跟一个用方括号括起来的表达式, 关键字 `do`, 一个语句段, 最后以关键字 `done` 结束。只要表达式为真, `do` 和 `done` 之间的语句就会执行。综合测试运算符`[[]]`是 Bash 的一个新运算符, 为保持与 Bourne shell 的向后兼容, 旧式的测试运算符`[]`仍然可以用来对条件表达式求值。

`until` 循环和 `while` 循环类似, 不同的是, 只要表达式为假, 循环体就会执行。

`for` 循环用于在一列词中进行遍历, 处理一个词然后将其移开, 接着处理下一个词。当词表中所有的词都被处理后, 循环结束。`for` 循环后跟一个变量名, 关键字 `in`, 一系列词, 然后是一个语句段, 最后以关键字 `done` 结束。

`select` 循环常常提供一条提示信息和含多个选项的菜单, 用户从中选择项, 这个输入将被存储在内置的特定变量 `REPLY` 中。`select` 循环通常与 `case` 命令一起使用。

循环控制命令为 `break` 和 `continue`。`break` 命令允许在到达末尾之前退出循环; `continue` 命令允许在到达末尾之前返回至循环表达式。

80

while command do block of statements done		for variable in word_list do block of statements done
while [[string expression]] do block of statements done		----- for color in red green blue do echo \$color done
while ((numeric expression)) do block of statements done	until command do block of statements done	----- select variable in word_list do block of statements done
	----- until [[string expression]] do block of statements done	
	----- until ((numeric expression)) do block of statements done	

81

函数

函数允许您定义一段 shell 代码并对其命名。它有两种格式，一种来自 Bourne shell，一种是 Bash shell 版本，使用 function 关键字。

例：

```
function_name() {  
    block of code  
}
```

```
function function name {  
    block of code  
}  
-----  
function lister {  
    echo Your present working directory is `pwd`  
    echo Your files are:  
    ls  
}
```

82

分析工具综合运用

- 石墨烯表面上不同高度处水分子的速度大小分布
- 距蛋白一定范围内的氢键
- 溶剂分子的平均滞留时间

83

思路

- 明确问题
- 搜寻工具
- 组合工具
- 处理数据,汇报结果
- 先拿几帧轨迹做测试
- 运用到整条轨迹

84

“大多数人宁愿死去，也不愿思考。-事实上他们也确实到死都没有思考。 —罗素”

速度不给力？试试国内网站 <https://Jerkwin.coding.me>

评论与问题？请至论坛留言 <https://Jerkwin.herokuapp.com>

统计轨迹中分子速度大小沿某一个方向的分布

类别: 科 标签: awk gmx 阅读次数: 183 版权: (CC) BY-NC-SA

- 2017年03月29日 09:25:09

写过一个简单的awk脚本, 用来统计轨迹中水分子的质心速度大小沿坐标的变化情况, 目的是可以用来拟合计算粘度. 具体的计算方法可参考:

A Comparison Of The Value Of Viscosity For Several Water Models Using Poiseuille Flow In A Nano-channel

A. P. Marksteijin, Remco Hartkamp, S. Luding, J. Westerweel; J. Chem. Phys. 136(13):134104, 2012; 10.1063/1.3697977

脚本只能处理gro格式的轨迹, 效率不是很高, 但基本能用. 放在这里, 存个档, 也供需要的人参考吧.

zvx.bsh

```

1  awk ' BEGIN {
2      mo=16; mh=1; M=mo+2*mh      # 定义原子质量
3      Ntot=10                      # 定义要计算的帧数
4      Zmin=3; Zmax=26; dZ=0.2    # 定义计算区间, 分格间距
5      Nfrm=0; N=int((Zmax-Zmin)/dZ)
6      for(i=0; i<=N; i++) { Z[i]=Zmin+i*dZ; Vx[i]=0; Nwat[i]=0 }
7  }
8
9  NF==1 { Nfrm++ }
10 NF>6 && $2~/OW/ {      # 根据 OW 原子统计
11     z = mo*$(NF-3); vx = mo*$(NF-2) # O 的z坐标, x方向速度
12     getline; z += mh*$(NF-3); vx += mh*$(NF-2) # H1的
13     getline; z += mh*$(NF-3); vx += mh*$(NF-2) # H2的
14
15     z /= M; vx /= M      # 质心坐标和速度
16     i=int((z-Zmin)/dZ)
17     Nwat[i]++; Vx[i] += vx
18     if(Nfrm>Ntot) exit
19 }
20 END {
21     print "# Z: [\"Zmin\":\"Zmax\":\"dZ\"]      Frames: " Nfrm
22     for(i=0; i<=N; i++) if(Nwat[i]>0) printf "%f %f\n", Z[i], Vx[i]/Nwat[i]
23 }
24 ' File.gro >Z-Vx.xvg

```

“你若不想做，总能找到借口；你若想做，总会找到方法。 —— 阿拉伯谚语”

速度不给力？试试国内网站 <https://Jerkwin.coding.me>

评论与问题？请至论坛留言 <https://Jerkwin.herokuapp.com>

GROMACS分析教程：氢键分析

类别: 科 标签: gmx vmd 氢键 阅读次数: 432 版权: (CC) BY-NC-SA

• 2017-01-09 16:56:34

卢天给过一个VMD的tcl脚本，用于计算不同z位置水能形成的平均氢键数。但轨迹大了以后，VMD的tcl脚本分析起来有点吃力，且得到的结果与GROMACS的默认氢键标准存在差距。这里我以此为例，展示下如何组合GROMACS自带的工具进行复杂一点的分析，并且利用gmx trjconv的外挂脚本功能让分析自动化。示例所用GROMACS版本为5.1.4。

运行模拟

示例文件用的是GROMACS自带的spc216.gro，只不过沿z方向将盒子扩大了一些，留出一定的真空层。运行NVT模拟。

```
gmx grompp  
gmx mdrun
```

预处理轨迹

得到轨迹后，先对轨迹进行预处理

```
gmx trjconv -f traj_comp.xtc -pbc whole -o traj_pbc.xtc
```

选择0，对整个体系进行PBC校正，保证分子完整。如果需要，根据情况进行其他特殊处理。

分析单帧构型

在对整个轨迹进行分析前，先选择一帧构型测试命令和脚本的正确性，这样可以节约时间。

```
gmx trjconv -f traj_pbc.xtc -o traj.gro -dump 0 -sep
```

选择0，输出整个体系，得到traj0.gro。

选择需要的原子组

我们的最终目的是分析不同高度层内水分子所成的平均氢键数目，要使用的命令是gmx hbond。使用这个命令分析氢键时，需要指定两个组，它们可以相同也可以不同。如果相同，分析的是本组分子之间形成的氢键；如果不同，分析的则是两组分子之间形成的氢键。

对于我们的目的而言，我们需要两个组，组1 Wsel是某高度层内的水分子，组2 Wexc是排除Wsel后的其余水分子。这样我们就可以计算组1之间的氢键数目N(Wsel-Wsel)，组1和组2之间的氢键数目N(Wsel-Wexc)，而Wsel中的水分子所成的平均氢键数目 Nhb = (2*N(Wsel-Wsel)+N(Wsel-Wexc)

) $N(water)$. $N(Wsel-Wsel)$ 之前的因子2是因为 **gmx hbond** 报告同组分子所成的氢键数目时会排除重复, 而我们不需要这样做.

选择不同高度层内的分子, 选择方式有几种策略, 或者根据氧原子的位置, 或者根据分子的质心位置, 几何中心位置, 或者根据任意原子位置等, 具体的语法看参考 **gmx select** 的语法及用法.

选中一定高度层内的水分子, 最简单的策略是根据氧原子的位置, 先选中符合条件的氧原子, 然后扩展到与氧原子所属分子相同的原子. 下面是的语句选择z坐标位于3到3.2之间的水分子以及其余水分子:

```
"Wsel" same mol as (name OW and (3<z and z<3.2))  
"Wexc" not same mol as (name OW and (3<z and z<3.2))
```

如果利用质心条件的话, 可以使用下面的语句

```
resname SOL and (3<res_com z and res_com z<3.2)  
或 resname SOL and (res_com z 3 to 3.2)
```

如果要同时选择Wsel和Wexc的话, 最好先定义一个变量, 这样写起来简洁, 执行起来效率也更高

```
Wsel = resname SOL and (res_com z 3 to 3.2); "Wsel" Wsel; "Wexc" not Wsel
```

最终, 我们可以使用下面的命令获得 **gmx hbond** 所需要的分组及其原子数目

```
gmx select -f traj0.gro -s -select 'Wsel = resname SOL and (res_com z 3 to 3.2'
```

traj0.xvg 最后一行的第二列是 Wsel 中的原子数目, 其 1/3 就是我们所需要的 $N(water)$; **traj0.ndx** 中保存了我们需要的两个分组.

对原子组进行分析

获得了原子组的索引文件, 就可以用它进行氢键数目分析了.

```
gmx hbond -f traj0.gro -n traj0.ndx -num traj0.xvg
```

运行上面的命令时会提示选择两个分组, 手动选择不利于自动化, 我们可以利用echo命令和管道来替代手动选择

```
echo 0 0 | gmx hbond -f traj0.gro -n traj0.ndx -num traj0_00.xvg  
echo 0 1 | gmx hbond -f traj0.gro -n traj0.ndx -num traj0_01.xvg
```

traj0_00.xvg 最后一行的第二列是我们需要的 $N(Wsel-Wsel)$, **traj0_01.xvg** 最后一行的第二列则是我们需要的 $N(Wsel-Wexc)$.

整理报告分析结果

有了这两个数据, 以及前面的水分子数目, 我们就可以计算出每个水分子所成的平均氢键数目了. 当然还是需要用脚本来自动计算, 这样后面才能实现自动化.

```
Nsel=$(tail -n 1 traj0.xvg)  
N00=$( tail -n 1 traj0_00.xvg)  
N01=$( tail -n 1 traj0_01.xvg)  
echo $Nsel $N00 $N01 | awk '{print; print $1, (2*$5+$8)/($2/3) >>"HB.xvg"}'
```

上面的脚本先获取每个文件的最后一行, 然后使用管道将其传awk, awk计算出所需要的值并保存到HB.xvg中.

通用单帧构型分析脚本

将前面的命令写到一个bash脚本中, 就可以自动执行上面的分析了

```
hb.bsh
1 i=0
2
3 file=traj$i
4 gmx select -f $file.gro -s -select 'Wsel = resname SOL and (res_com z > 3
5
6 echo 0 0 | gmx hbond -f $file.gro -n $file.ndx -num ${file}_00.xvg
7 echo 0 1 | gmx hbond -f $file.gro -n $file.ndx -num ${file}_01.xvg
8
9 Nsel=$(tail -n 1 $file.xvg)
10 N00=$( tail -n 1 ${file}_00.xvg)
11 N01=$( tail -n 1 ${file}_01.xvg)
12
13 echo $Nsel $N00 $N01 | awk '{print; print $1, (2*$5+$8)/($2/3) }' >>"HB.xvg"
14
15 rm -rf $file.gro $file.xvg $file.ndx ${file}_00.xvg ${file}_01.xvg
```

我们在最前面定义了帧号, 这样脚本就很容易用于其他帧了, 只要改变帧号对应的变量*i*就可以了. 脚本的最后我们删除了用到的中间文件, 这样既可以避免重复运行GROMACS工具时因备份文件太多而导致的错误, 也可以让我们的目录更清爽.

分析整条轨迹

既然已经可以对一帧构型进行分析, 并完成了一个通用的分析脚本, 那么将脚本用于多个构型就比较简单了. 最直接的方式就是先使用gmx trjconv输出所有的构型, 然后循环处理每帧构型. 比如我们有帧号为0到100的多个构型文件, 那么在bash中可以使用

```
hb.bsh
1 for i in {0..100}; do
2   file=traj$i
3   gmx select -f $file.gro <略> -os $file.xvg -on $file.ndx
4
5   echo 0 0 | gmx hbond -f $file.gro -n $file.ndx -num ${file}_00.xvg
6   echo 0 1 | gmx hbond -f $file.gro -n $file.ndx -num ${file}_01.xvg
7
8   Nsel=$(tail -n 1 $file.xvg)
9   N00=$( tail -n 1 ${file}_00.xvg)
10  N01=$( tail -n 1 ${file}_01.xvg)
11
12  echo $Nsel $N00 $N01 | awk '{print; print $1, (2*$5+$8)/($2/3) }' >>"HB.xvg"
13
14  rm -rf $file.gro $file.xvg $file.ndx ${file}_00.xvg ${file}_01.xvg
```



这种方式的缺点在于需要先输出一大堆构型文件, 当处理的帧数很多时, 就凌乱了. 好在 **gmx trjconv** 支持一个外挂脚本的选项, **-exec "命令"**, 可以在输出每一帧后对此帧构型执行指定的命令, 脚本或程序, 且以帧号作为命令行参数. 举例来说, 如果选项为 **-exec "cmd"**, 那么对输出每帧构型后对其执行的命令就是 **cmd 帧号**. 利用这一功能, 我们就不再需要自己写循环了, 只要将我们上面的脚本改为以帧号为输入参数就可以了

hb.bsh

```
1 i=$1
2 file=traj$i
3 <下同>
```

这样我们直接使用

```
gmx trjconv -f traj_pbc.xtc -o traj.gro -sep -exec "bash hb.bsh"
```

就可以自动对整条轨迹进行分析, 得到所需要的数据了. 对我们的测试轨迹, 得到的平均数目为3.5左右, 符合预期.

总结说明

- **gmx trjconv** 的 **-sep** 选项只支持gro或pdb格式, 不支持二进制格式构型文件.
- 这种组合GROMACS已有工具, 以及简单数据处理小脚本的分析方式不需要自己编写代码处理轨迹, PBC, 分析等问题, 只需要一些代码处理输出输入文件, 流程具有通用性, 但难度远小于自己从头写代码处理轨迹.
- 这种处理方法在分析时每次只处理一帧构型, 对于需要多帧构型才能计算的物理量就不适用了. 在那种情况下, 只能先输出所有的信息, 再统一处理了.
- 这种方式每次只处理一帧构型, 效率不是太高, 但对机器的要求低, 不像VMD那样要先载入整条轨迹, 需要很大内存.
- 如果你对于效率很在意, 那么可以采用并行的方式进行处理: 先输出所有的构型文件, 使用脚本并行处理左右构型文件, 最后再将这些文件的结果合并. 至于如何并行处理, 这里就不再细说了, 可参考我以前的两篇博文[Bash脚本实现批量作业并行化, GNU Parallel](#).
- 如果你想试验一下这种处理方式, 那可以试着完成我前面提出的一个问题, 蛋白口袋或纳米通道内水分子的个数统计. 当然, 这些口袋或通道都是柔性的, 否则的话, 就没有必要这么处理了.

附: 类似功能的VMD tcl脚本

使用VMD的tcl脚本进行分析时, 思路也是类似的. 但值得注意的是, VMD的默认氢键标准与GROMACS不同, 这是因为目前存在多种判断氢键的标准. 简言之, VMD的3.5埃-40度标准大致和GROMACS的标准一致. 此外, VMD还没有考虑PBC的问题. 详情可见前一篇博文[GROMACS的默认氢键标准](#).

```

1 #mol delete all
2 #mol new conf.gro traj_pbc.xtc
3
4 set sel "same resid as resname SOL and z 30 to 32 "
5 set Zset "z 30 to 32 and x 4 to 14 and y 4 to 14"
6 set Wsel [atomselect top "same resid as name OW and $Zset"]
7 set Wexc [atomselect top "same resid as name OW and not($Zset)"]
8
9 set Nfrm 100
10 set Rcut 3.5
11 set Angle 40.
12
13 puts "#Frm #Wsel #Wexc #sel-sel #sel-exc #exc-sel #HB/Wat"
14
15 for {set i 0} {$i<=$Nfrm} {incr i} {
16   $Wsel frame $i
17   $Wsel update
18   $Wexc frame $i
19   $Wexc update
20
21   set Nsel [expr [$Wsel num]/3.]
22   set Nexc [expr [$Wexc num]/3.]
23
24   set NSS [llength [lindex [measure hbonds $Rcut $Angle $Wsel] 0]]
25   set NSE [llength [lindex [measure hbonds $Rcut $Angle $Wsel $Wexc] 0]]
26   set NES [llength [lindex [measure hbonds $Rcut $Angle $Wexc $Wsel] 0]]
27
28   puts "$i      $Nsel $Nexc      $NSS $NSE $NES      [expr (2.*$NSS+$NSE+$NES)
29 }

```



◆本文地址: <https://jerkwin.github.io/2017/01/09/GROMACS分析教程-氢键分析/>, 转载请注明◆

◆评论问题: <https://jerkwin.herokuapp.com/category/3/博客>, 欢迎留言◆

“虽有嘉肴，弗食，不知其旨也；虽有至道，弗学，不知其善也。是故，学然后知不足，教然后知困。知不足，然后能自反也；知困，然后能自强也。故曰：教学相长也。—《礼记·学记》”

速度不给力？试试国内网站 <https://Jerkwin.coding.me>
评论与问题？请至论坛留言 <https://Jerkwin.herokuapp.com>

GROMACS分析教程：使用g_select计算平均滞留时间

类别: 科 标签: gmx 阅读次数: 721 版权: (CC) BY-NC-SA

- 2016-03-11 21:18:39 初稿
- 2016-03-22 14:28:06 补充 程刚 的方法
- 2016-03-27 22:02:21 补注

理论考虑

分子动力学模拟的分析是动力学的精髓部分，要依据模拟的假设和目的去分析所得到的数据，看是否支持自己的假设，进而得到更多的洞察。没有假设和目的就去盲目地做模拟，是不可取的。由于各人所作体系不同，对于分析没有通用的套路，你需要多参考文献才好。

虽然GROMACS自带了很多分析工具，可能仍不能满足你的需要，这时候就需要你自己写代码对轨迹进行分析了。对此，我的建议如下：

1. 如果可能，请尽量使用GROMACS自带的工具完成分析过程，必要时可以组合多个分析工具达到目的。虽然这种做法处理时间可能稍长，但无须写代码，适合普通用户使用。但这种做法需要你对GROMACS自带的工具有比较详尽的了解，知晓各个工具的功能，并能根据自己的目的进行恰当地组合。
2. 即便需要自己写代码分析轨迹，仍然建议先利用GROMACS自带的工具对轨迹进行初步处理，如利用 `gmx trjconv` 转换轨迹格式，处理居中，PBC问题；利用 `gmx select` 获取特定原子的索引；利用 `gmx trjconv` 或 `gmx traj` 抽取特定索引原子的信息等。因为无论做哪种分析，都要牵涉到这些问题的处理，而自己写代码实现这些功能虽然不是很可能，但相当麻烦，而且执行效率也没有使用GROMACS自带工具高。这样得到需要的原子坐标后，我们就可以把注意力集中到自己需要分析方面，节省了时间和精力。
3. 如果为了提高处理轨迹的效率或其他原因，你不得不自行处理轨迹，建议你使用 `xtc` 格式。这种压缩格式只包含坐标，文件小，当只需要分析坐标时，使用它可大大提高效率。但如果你同时需要坐标和速度甚至受力，那你就只能使用 `trr` 格式了。
4. 具体如何使用C, Fortran或MatLab来处理 `xtc` 或 `trr` 格式的轨迹，请参考博文。
5. 如果熟悉，VMD的tcl脚本也可用于分析轨迹，缺点是速度慢，且对文件大小有限制。

具体示例

下面我们模拟TIP3P水中的一个甲烷CH₄分子, 以计算CH₄第一溶剂化层中水分子的平均滞留时间为例, 来对分析过程进行具体地说明.

下载[示例文件](#), 解压后得4个文件, `conf.gro`, `gromppmdp`, `index.ndx`, `topol.top`. 值得注意的是, `index.ndx`文件使用`gmx make_ndx`添加了每种原子的索引号, 这是为了便于后面的分析.

体系中包含一个CH₄分子(OPLS-AA力场)和241个TIP3P水分子



Fig.1

下面我们来运行模拟

```
grompp -maxwarn 2  
mdrun
```

作为示例, 我们只运行了20 ps, 得到了轨迹文件 `traj.xtc`.

要计算CH₄分子第一溶剂化层中水分子的平均滞留时间, 我们首先需要知道第一溶剂化层的厚度, 为此, 我们可以计算CH₄分子和水分子二者质心之间的径向分布函数RDF

```
g_rdf -f -n -rdf mol_com  
> 2 3
```

得到如下图形

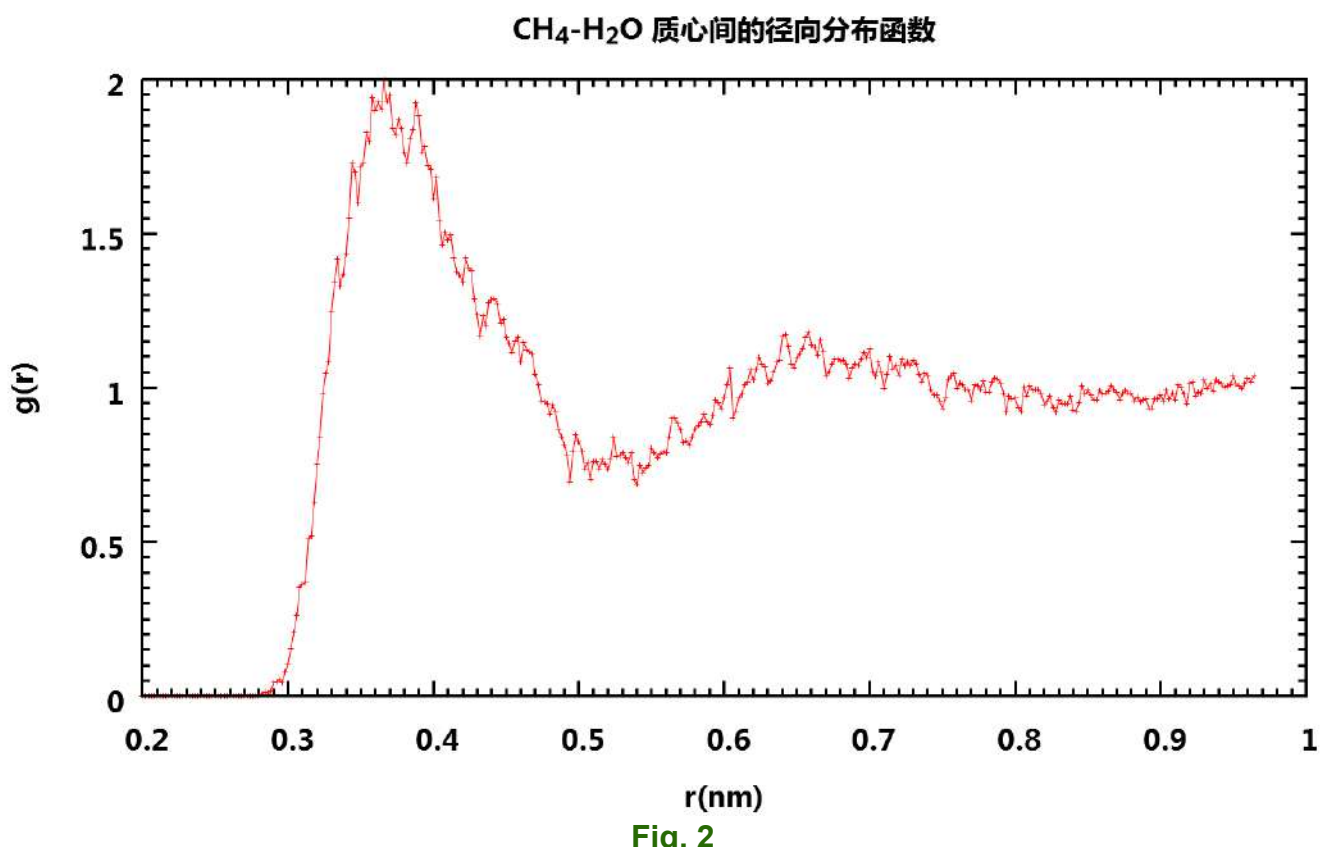


Fig. 2

可以看到,由于模拟时间较短,得到的RDF并不是十分光滑(延长模拟时间就可以得到更漂亮的图形),但我们仍然可以看出第一溶剂化层的厚度大约是0.5 nm. 也就是说,我们在计算平均滞留时间时,只考虑其质心处于CH4质心0.5 nm 范围内的水分子.

【2016-03-27 补注】上面关于第一溶剂化层厚度的说法不严谨. 文献上一般以RDF的第一个峰值作为第一溶剂化层的厚度, 所以根据上图应该是0.36 nm左右, 下面分析中应该使用这个数值.

我们使用 `g_select` 工具来获取每个水分子的是否处于CH4第一溶剂化层中的信息.

```
g_select -f -n -os -oc -oi -om -on selFrm.ndx -selrpos mol_com  
>"1st shell" resname SOL and name OW and within 0.5 of resname CH4
```

在上面的命令中我们为 `-on` 选项指定了输出文件, 以防止默认的输出文件 `index.ndx` 与前面我们使用的 `index.ndx` 文件冲突. 有关 `g_select` 的使用说明请参考[其说明文档](#)和[GROMACS选区\(selection\)语法及用法](#).

我们得到如下文件

- `size.xvg`: 每一时刻第一溶剂化层中原子的个数
- `cfrac.xvg`: 每一时刻第一溶剂化层中原子的覆盖比例
- `index.dat`: 每一时刻第一溶剂化层中原子的个数及其编号
- `mask.dat`: 每一时刻分子是否处于第一溶剂化层中的掩码, 0: 不处于, 1: 处于
- `selFrm.ndx`: 每一时刻第一溶剂化层中原子的索引组

请打开这些文件进行查看, 了解其含义.

我们只要对 `mask.dat` 进行分析处理就可以计算平均滞留时间了. 这可以使用下面的bash脚本完成

bash

```
1 file=mask.dat  
2 ftrs=${file%.*}_trs.dat  
3 ffrq=${file%.*}_frq.dat  
4  
5 awk ' BEGIN {  
6   getline  
7   while($1=="#") getline  
8   Ncol=NF  
9   close(FILENAME)  
10  
11  for(i=2; i<=Ncol; i++) {  
12    while(getline<FILENAME) if(NF==Ncol) printf "%s", $i  
13    print ""  
14    close(FILENAME)  
15  }  
16 }' $file > $ftrs  
17  
18 awk -v file=$file '  
19 BEGIN{ Navg=0; Tavg=0  
20   getline <file
```

```

21 while($1=="#") getline <file; dt=$1
22 getline <file; dt=$1-dt
23 close(file)
24 }
25
26 { gsub(/0+/, " ")
27 Ntxt=split($0, txt)
28 for(i=1; i<=Ntxt; i++) {
29   T=length(txt[i])
30   print T
31   Navg++; Tavg += T
32 }
33 }
34 END{ print "# Avaraged Residence Time(ps)=", Tavg*dt/Navg}
35 '$ftrs >$ffrq

```

得到的平均滞留时间为0.807243 ps. 当然, 实际情况中你需要运行更长的模拟来确认得到的数据是否收敛. 水分子滞留时间的分布图如下

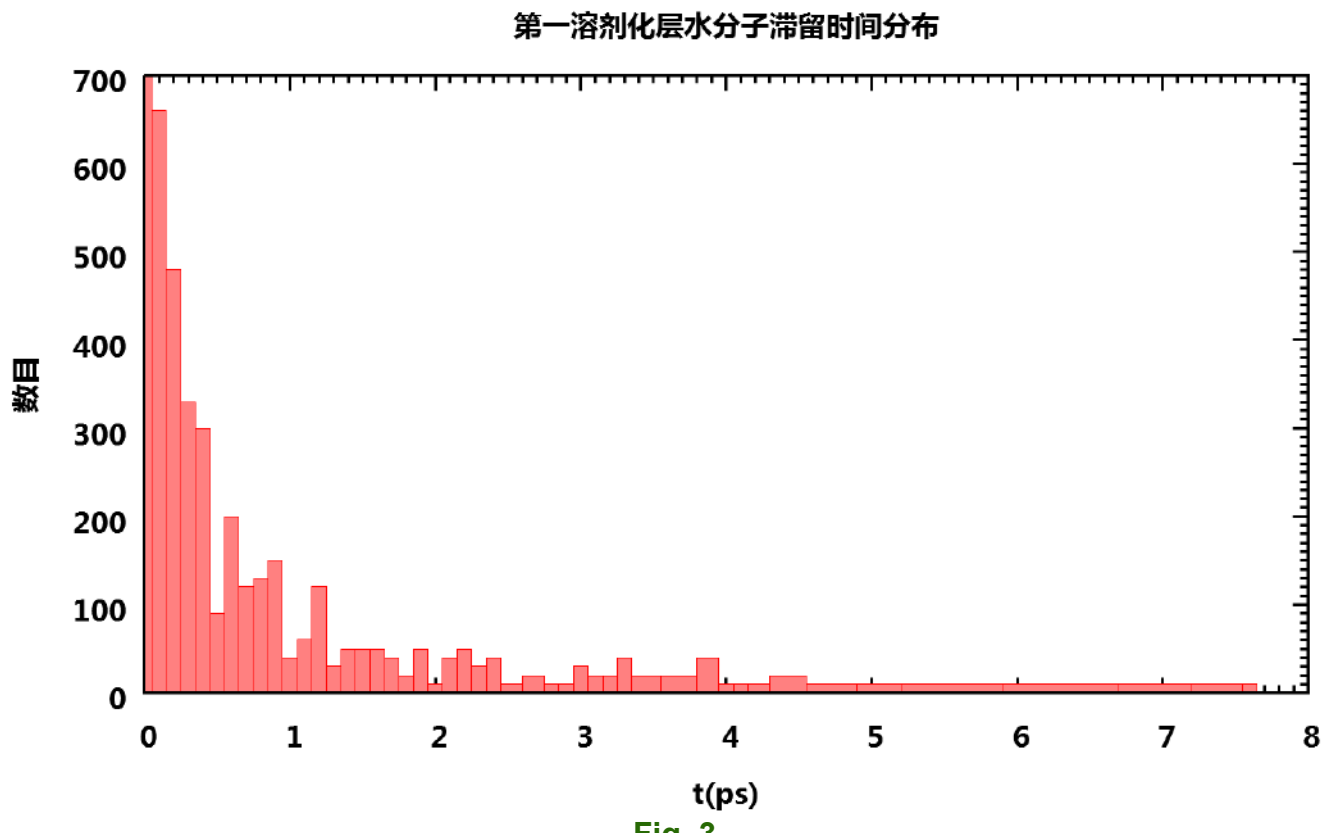


Fig. 3

对更大的体系, 更长的模拟时间, 上面的简单脚本可能执行时间很长. 这主要是因为在第一步中对 `mask.dat` 进行行列互换时, 如果文件太大就要花费很长的时间. 一种更高效些的方法是使用中间文件, 方法如下

bash

```

1 awk -v ftrs=$ftrs ' BEGIN{ Nmax=2000; N=0
2   system("rm -rf _row-* " ftrs " && cat <> " ftrs)
3 }
4 $1!="#" {

```

```

5   N++
6   Frow=_row-`sprintf("%04d",N)
7   $1=""` sub(/^\s*/,"")` gsub(" ", "\n", $0)
8   print $0 >Frow
9   close(Frow)
10  if(N>Nmax) {
11    N=0
12    system("ls _row-* | sort | xargs paste -d \047\047 "ftrs" >_trsRow")
13    system("rm -rf _row-* && mv _trsRow "ftrs")
14  }
15 }
16 END{
17   system("ls _row-* | sort | xargs paste -d \047\047 "ftrs" >_trsRow")
18   system("rm -rf _row-* && mv _trsRow "ftrs")
19 }
20 '$file

```

更高效的方法, 就只能换用其他编译型语言或MatLab等软件了.

我们可以利用程序并借助文件获取每一时刻所选原子的坐标, 只需要根据对每一帧指定不同的索引组即可. 获取前100帧的示例代码如下

bash

```

1 file=selFrm.gro
2 echo -n ""> $file
3
4 dt=0.002
5 for i in {0..100}; do
6   t=$(echo "$dt*$i" | bc)
7   echo $i | trjconv -f -n selFrm.ndx -dump $t -o _tmp.gro 2>/dev/null
8   cat _tmp.gro >>$file
9   rm -rf _tmp.gro
10 done

```

当然这种每次处理一帧的方法运行起来很慢, 但可惜的是GROMACS的分析工具中并没有提供解决方案, 如果需要更快地抽取出构型, 那就只能自己写代码了. 此外, 这样直接得到的构型由于PBC的原因可能看起来不连续, 为此, 你可能需要先使用对轨迹进行居中, PBC处理, 然后再使用上面的方法获取坐标.

网络资料

1. 如何计算平均滞留时间(residence time)
2. trajectory output from g_select?
3. gmx dipoles with dynamic indices (gromacs 5.0.x)
4. extract coordinates of selected atoms
5. Windows Cmd终端Ctrl D不起作用的解决方法
6. Equivalent to ^D (in bash) for cmd.exe?

7. LINUX SHELL 行列转换、倒序

程刚: 基于GROMACS和MatLab计算平均滞留时间

一、计算原理

可参考文献 Phys. Chem. Chem. Phys., 2012, 14, 16536-16543

划定一定的区域，定义为系统计算空间，比如距离聚合物膜0.5 nm的空间。假设体系里有N个分子，每个分子在系统计算空间的平均滞留时间都不同，对体系的N个分子全部进行平均，就得到了平均滞留时间。下面以计算水分子的平均滞留时间为例。

假设统计的轨迹共n帧，共计x ns，统计轨迹时间x ns应该远大于水分子的滞留时间。以第1号水分子为例，统计这n帧轨迹中第1号水分子在系统计算空间内出现的总时间，再除以第1号水分子进出此空间的次数，就得到了第1号分子的平均滞留时间，记为T(1)。然后对所有的水分子的平均滞留时间进行平均，记为Tavg=sum(T)/n，其中sum为加和函数，n为出现在系统计算空间的总分子数（即排除所有未曾出现在系统计算空间内的分子）。

二、计算过程

1. 采用GROMACS软件对轨迹进行处理

```
g_select -f md.xtc -s md.tpr -n index.ndx -om M_1.dat -select 'name OW and wit
```

系统计算空间为距离M基团0.195 nm的空间；其中md.xtc文件为轨迹，共计n帧；index.ndx索引文件中应该提前设定好待分析的组和OW原子；产生的M_1.dat文件是二进制的二维数据表，第一列为轨迹时间，后面每列为每个OW原子在每个轨迹时间点上在系统计算空间内的出现情况（1代表出现，0代表不出现）。

2. 采用MatLab软件处理dat文件

使用下面的MatLab代码处理得到的M_1.dat文件，注意文件名要匹配。程序运行结束后，Tavg为所求。

李继存注：此代码效率较低，数据量太大时可能出现问题，请优化使用。

matlab

```
1 function ResTime  
2     clc; clear all;  
3  
4     global Ntime Natom  
5  
6     dt=2; % 时间间隔  
7     mat=load('S03_1.dat'); % mask数据文件  
8  
9     [Ntime,Ncol]=size(mat); %  
10    mat=mat(1:Ntime,2:Ncol); %  
11  
12    Natom=Ncol-1;  
13    T=zeros(1,Natom); % 某一列的滞留时间
```

```

14 Tnum=zeros(1,Natom); % 未连续出现的次数统计
15 Ttot=zeros(1,Natom); % 某一列的总和, 出现的总时间
16
17 for i=1:Natom
18     Ttot(i)=sum(mat(:,i));
19     if(Ttot(i)~=0)
20         for j=1:Ntime-1
21             if mat(j+1,i)~=mat(j,i)
22                 Tnum(i)=Tnum(i)+0.5;
23             end
24         end
25         T(i)=double(Ttot(i)/ceil(Tnum(i)));
26     end
27 end
28
29 Tavg=sum(T)*dt/length(find(Ttot>0))

```

评论

- 2016-10-20 11:40:17 **wlzzl** 第一个脚本运行总是错误，是复制下来格式不对吗？
- 2016-10-21 12:46:48 **Jerkwin** 说清楚，是哪个脚本，错误提示是什么？
- 2016-10-24 20:01:30 **wlzzl** 就是第一个利用mask.dat求驻留时间的脚本，awk指令的最后那个单引号，没有跟大括号在同一行，运行时总是报错，也不知什么原因。
- 2016-10-25 15:10:25 **Jerkwin** 系统的原因吧，可能和换行符什么的有关
- 2016-10-24 19:45:37 **wlzzl** 谢谢了，翻看了书，已经解决。
- 2016-11-02 15:29:48 **live** 想问下，利用第一个脚本文件算出的滞留时间和文献差异大吗？我算出来差异有点大。
- 2016-11-02 21:12:52 **Jerkwin** 这种方法有其本身的缺点，计算得到的值和使用的时间步长有关。更好的方法你可以参考文献。
- 2017-02-26 16:07:46 **Topin** 李老师，5.0+版Gromacs, gmx select里-olt项输出的lifetime.xvg文件就是滞留时间分布数据吧？
- 2017-02-26 19:05:25 **Jerkwin** 有人说是，但是我没有测试过，不清楚到底是不是。你可以测试一下，如果确定了，请告诉我一声，以便我更新下文章。

随意赞赏	
------	--

NOW THIS IS NOT THE END.
IT IS NOT EVEN THE BEGINNING OF THE END.
But it is, perhaps,
**THE END OF THE
BEGINNING.**

© www.famouscelebrityquotes.org

- WINSTON CHURCHILL



谢谢!

